Dissertation Anna Maria Hofmann

Amphiphilic polyethers via oxyanionic polymerization: From liposomes to liquid crystals

JOHANNES GUTENBERG UNIVERSITÄT MAINZ

Amphiphilic polyethers via oxyanionic polymerization: From liposomes to liquid crystals

Dissertation zur Erlangung des Grades
"Doktor der Naturwissenschaften"
im Promotionsfach Makromolekulare Chemie

am Fachbereich Chemie, Pharmazie und Geowissenschaften
der Johannes Gutenberg-Universität in Mainz

Anna Maria Hofmann
geboren in Gießen

Mainz, Oktober 2011

Dekan:

Prodekan:

1. Berichterstatter:

2. Berichterstatter:

Tag der mündlichen Prüfung: 23.11.2011

Hiermit versichere ich gemäß § 10 Abs. 3d der Promotionsordnung vom 24.07.2007, dass ich die als Dissertation vorgelegte Arbeit selbst angefertigt und alle benutzten Hilfsmittel (Literatur, Apparaturen, Material) in der Arbeit angegeben habe.

Die als Dissertation vorgelegte Arbeit wurde in der Zeit vom September 2008 bis Oktober 2011 am Institut für Organische Chemie der Johannes Gutenberg-Universität Mainz im Arbeitskreis von Univ.-Prof. Dr. Holger Frey angefertigt.

In Dankbarkeit

für meine Eltern

„Die Wissenschaft fängt eigentlich erst da an interessant zu werden, wo sie aufhört."

Justus von Liebig (1803-1873)

Danksagung (Acknowledgments)

Table of contents

Motivation and objectives

Motivation and objectives

Over the last century, polymer synthesis via anionic polymerization has evolved from an academic curiosity to a major subject in various areas of macromolecular chemistry and materials science with application in industrial processes. The living anionic polymerization, showing no transfer and termination reactions under appropriate reaction conditions, allows precise control not only over molecular weights but also over the incorporation of monomers, initiating and terminating agents. Especially the development of numerous epoxide monomers offering diverse functionalities, i.e, multiple hydroxy, amino, thiol and allyl groups, via orthogonal protective group chemistry gave rise to a variety of materials. Furthermore, the combination of these monomers with various functional initiating and terminating systems increases the complexity of the molecular structures that are accessible via anionic polymerization techniques. Thus, novel complex but well-defined molecular architectures, such as stars, spheres or brushes, can be prepared in facile synthetic approaches.

During the last decades, poly(ethylene glycol)s (PEG) lipids have attracted increased attention due to their ability to sterically stabilize drug carrier such as liposomes in cell culture and *in vivo* applications (Lasic et al. *Science* 1995). These so-called stealth-liposomes have been evolved as a potent delivery system in a variety of cancer therapies, resulting in the clinical approval of different liposomal formulations containing amphiphilic PEG. Despite numerous exceptional characteristics of PEG-modified lipids, such as biocompatibility, high water solubility and effective shielding properties, one disadvantage of the well-known and widely used PEGylation strategies is the lack of additional functional groups in the polymer chain, which could be used for further derivatization. To covalently bind PEG to lipids, targeting groups or markers, active linkers have to be introduced by functional initiation or termination of the anionic ring-opening polymerization (ROP) of ethylene oxide (EO) or by additional modification of the terminal hydroxyl group. In contrast to linear PEG, hyperbranched polyglycerol offers possibilities for further functionalization due to its polyfunctionality and exhibits a high aqueous solubility.

The objective of the current thesis is the preparation of complex amphiphilic polyethers bearing multiple functional groups by anionic ring-opening polymerization of different epoxide monomers. The combination of linear and hyperbranched polymerization techniques, using functional lipophilic initiators, allows the synthesis of multifunctional polyether lipids. Following this approach, a variety of amphiphilic stealth-type polymer lipids with systematically varied

structures can be obtained. In detail, the ring-opening polymerization of ethylene oxide (EO), glycidol and glycidyl derivatives, such as ethoxyethyl glycidyl ether (EEGE) and isopropylidene glyceryl glycidyl ether (IGG), initiated with lipophilic alcohols has been employed for the preparation of amphiphilic, multifunctional polyethers with unusual molecular architectures.

Surface modification of liposomes with the novel polymer lipids might improve their medical potential by increasing their stability in cell culture as well as *in vivo* and by specific targeting.

In the first chapter, the basic science, current developments and future perspectives in the field of stealth liposome research are reviewed. Furthermore, the synthetic pathways for new functional polyether lipids via oxyanionic ring-opening polymerization and their biomedical application for the preparation of long circulating liposomes are presented. The encapsulation and targeted transport of siRNA in liposomes coated with the novel amphiphilic polyethers emphasize the potential of these stealth-type lipids as an effective drug carrier system.

The characterization of the physical behavior of the synthetic polyether lipids, for instance the self-assembly at the water-air interface in Langmuir-Blodgett films and in interaction with lipid monolayers, are shown as well as the formation of non-conventional liquid crystalline phases of cholesterol-initiated polyether structures depending on molecular weights and architectures.

Graphical abstract

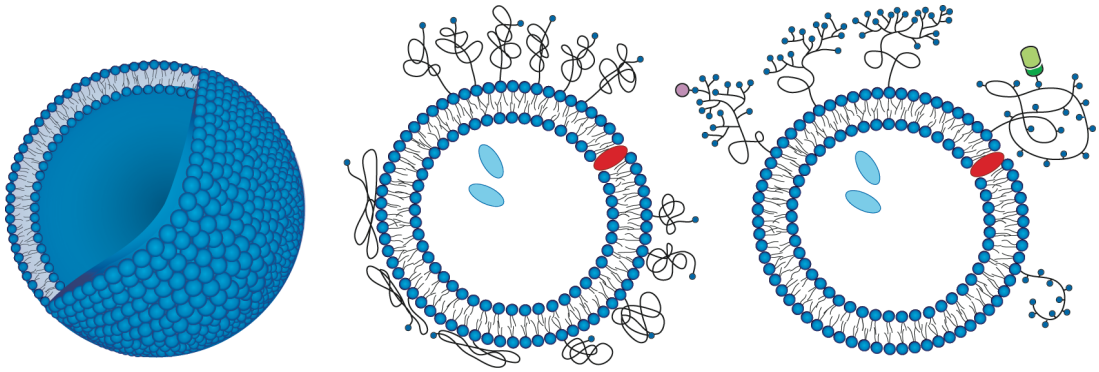

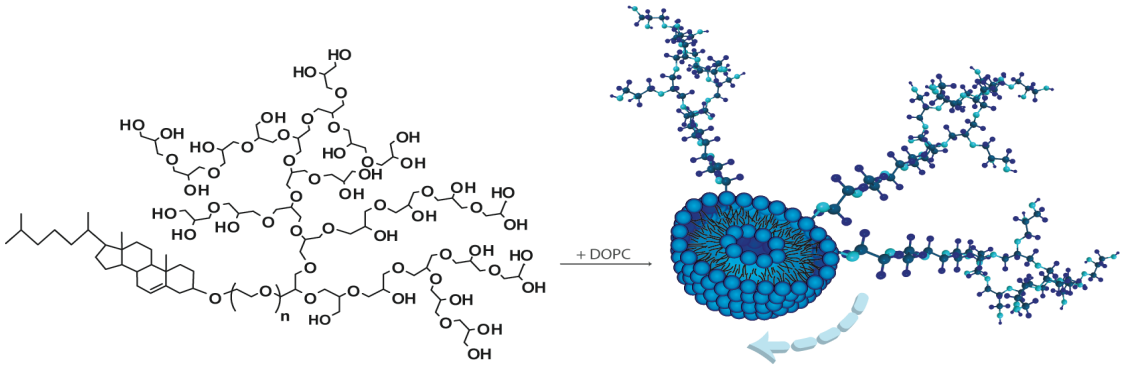

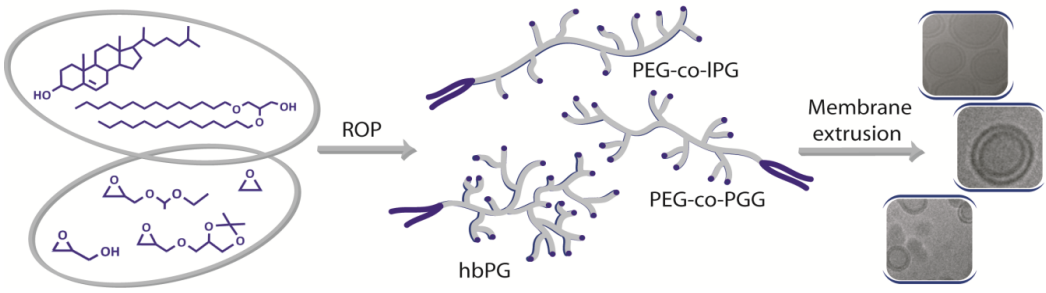

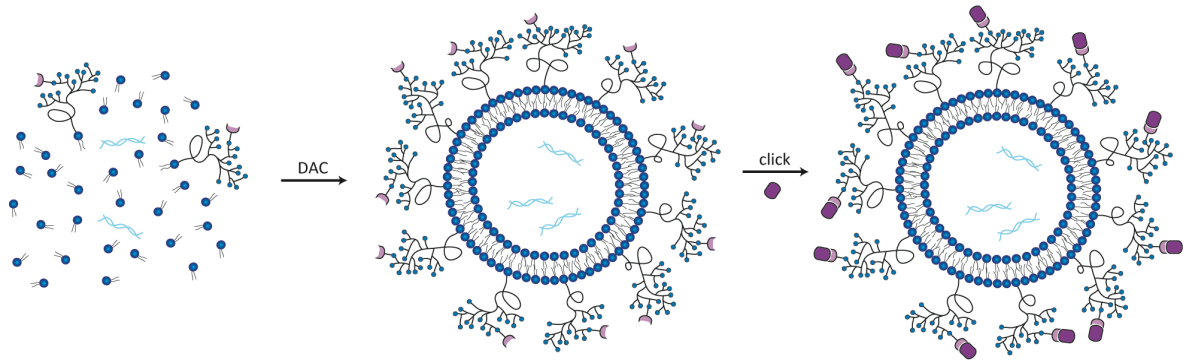

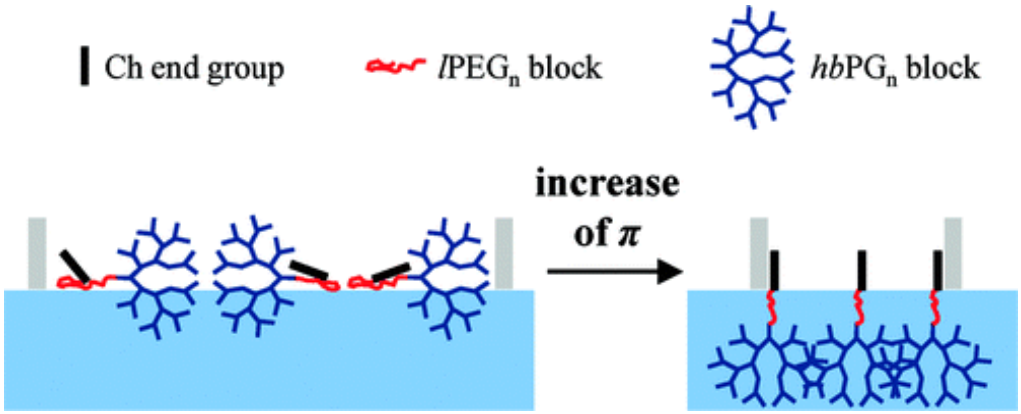

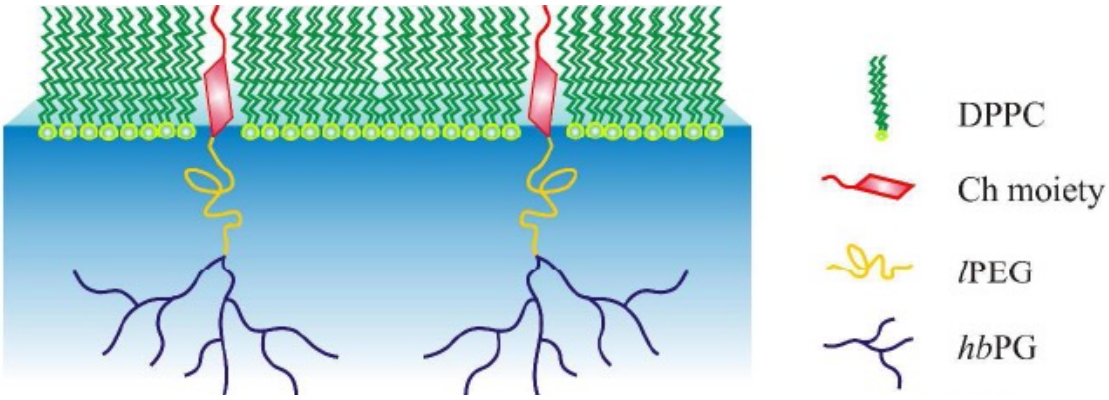

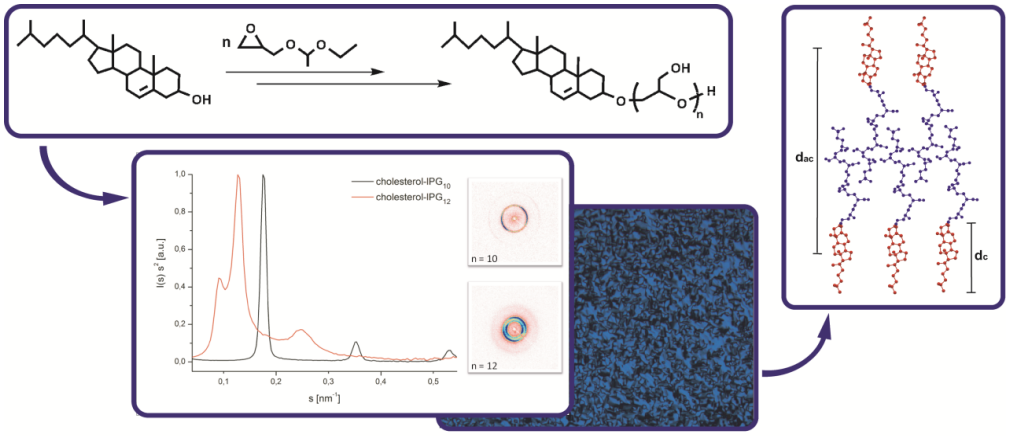

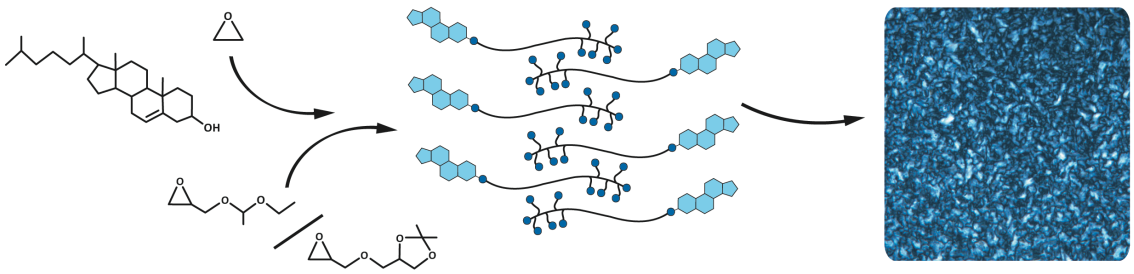

Abstract

Abstract

During the last decades amphiphilic polyether structures have attracted increased attention due to their ability of self-assembly in a multitude of patterns. Thus, polyether modified lipids have been used to prepare sterically stabilized (stealth) liposomes for drug delivery systems. **Chapter 1** gives a comprehensive overview of the state of the art in the field of liposome research. The combination of linear and hyperbranched polymerization techniques for the ring-opening anionic polymerization of different epoxide monomers, using functional initiators allows the synthesis of multifunctional polyether lipids. Following this approach, a variety of amphiphilic stealth-type polymer lipids with systematically varied structures have been obtained. The resulting synthetic polyether lipids have been used for the solubilization of multiwalled carbon nanotubes, for the preparation of functional stealth liposomes and siRNA-loaded liposomes, for the investigation of Langmuir and Langmuir-Blodgett films as well as for studies of their self-assembly in liquid crystalline phases. Besides the basic synthesis pathways for the new functional copolymer lipids via oxyanionic polymerization (**Chapter 2.1** and **Chapter 2.2**), the eventual biomedical application in the field of stealth lipids for long circulating liposomes (**Chapter 2.1** and **Chapter 2.2**) and for the encapsulation and transport of siRNA (**Chapter 2.3**) as well as the characterization of their physical behavior, for instance in Langmuir-Blodgett films (**Chapter 3.1**), in interaction with lipid monolayers (**Chapter 3.2**) and in non-conventional liquid crystalline phases (**Chapter 4.1** and **Chapter 4.2**), are presented in the following paragraphs.

Chapter 2.1: Hyperbranched polyglycerol-based lipids via oxyanionic polymerization: Toward multifunctional stealth liposomes

The synthesis of novel polyfunctional linear-hyperbranched polyether lipids for liposome preparation is achieved via a straightforward two-step protocol using oxyanionic ring-opening polymerization of different epoxide monomers. Biocompatible linear-hyperbranched block copolymers consisting of poly(ethylene glycol) (PEG) and hyperbranched polyglycerol (*hb*PG) were prepared from PEG-*b*-poly(glyceryl glycidyl ether) (PGG) precursor block copolymers, which can be obtained via sequential anionic polymerization of ethylene oxide (EO) and isopropylidene glyceryl glycidyl ether (IGG). After deprotection of the PIGG block and partial

deprotonation of the PGG block, hypergrafting of glycidol onto the alkoxide initiating sites is achieved via a slow monomer addition protocol.

In order to anchor the copolymers in liposomal membranes, lipophilic initiators were used that tolerate the strongly basic oxyanionic polymerization and acidic acetal cleavage conditions, which exclude application of commonly used phospholipids. Thus, we employed commercially available cholesterol and three different 1,2-bis-*n*-alkyl glyceryl ethers with varying lengths of the aliphatic chains as initiators for the polymerization of ethylene oxide and isopropylidene glyceryl glycidyl ether. MALDI-ToF mass spectrometry supported complete incorporation of the respective initiators. All lipophilic initiators employed lead to incorporation of the resulting copolymers in liposomal formulations, since cholesterol and 1,2-bis-*n*-alkyl glyceryl ethers are not only components of biological membranes but also have been used to link PEG to liposomes in previous works.

The controlled polymerization conditions allowed the preparation of copolymer lipids with accurate degrees of polymerization, varying the lengths of both blocks while keeping polydispersity low. Adjusting the length of the PEG block permits tailoring of the shielding properties of the polyether lipid. Due to the composition of the PEG-*b*-*hb*PG block copolymers consisting of mere polyether structures, potentially toxic moieties or initiators are avoided, i.e., maximum biocompatibility is achieved.

The linear-hyperbranched polyether lipids are incorporated as the polyfunctional shell in liposome formulations together with 1,2-dioleoyl-*sn*-glycero-3-phosphocholine (DOPC) under sterile conditions. The resulting liposomes were subsequently characterized via dynamic light scattering (DLS) and small angle neutron scattering (SANS) as well as transmission electron microscopy (TEM), demonstrating the formation of unilamellar liposomes.

Chapter 2.2: Rapid access to polyfunctional lipids with complex architecture via anionic ring-opening polymerization

The synthesis of novel multifunctional lipids with diverse hydrophilic polyether-based architectures via facile one- or two-pot approaches was achieved by versatile polymerization strategies. In this manner hyperbranched polyglycerol lipids were prepared via cholesterol- or

1,2-bis-*n*-alkyl glyceryl ether-initiated oxyanionic ring-opening polymerization of protected glycidyl ethers and glycidol, respectively.

In addition to these polyglycerol-lipids, two series of multifunctional PEGs as the hydrophilic part of the lipid have been synthesized, which can be compared to conventional stealth lipids but bear an adjustable amount of hydroxyl functions within the PEG backbone. These lipids can be readily obtained by random copolymerization of ethylene oxide and protected glycidyl ethers such as EEGE and IGG initiated with lipophilic alcohols. Since the use of lipophilic initiators directly leads to amphiphilic structures, i.e., lipids, further derivatization steps or other linkages, like esters, amides etc. can be avoided and maximum biocompatibility is maintained. The degree of polymerization and functionalization was determined via ^{1}H NMR spectroscopy integrating the methyl groups of the initiator, the acetal protecting groups of the comonomer and the polyether backbone. The random distribution of the comonomer units within the PEG backbone was evidenced via ^{13}C NMR analysis, more precisely by investigation of the triad sequence distribution, which indicates a statistical incorporation of the monomers within the polymer chain. The series of cholesterol- or 1,2-bis-*n*-alkyl glyceryl ether-initiated random PEG-*r*PG or PEG-PGG copolymers and hyperbranched polyglycerols could be attached to labeling or targeting moieties via esterification. In addition, the introduction of allyl and alkyne groups opened new ways for derivatization via thiolene coupling or click chemistry. Thus, the introduction of dyes such as rhodamine B was possible.

Liposomes consisting of these novel lipids with different molecular architectures were prepared via membrane extrusion method and are visualized by transmission electron microscopy (TEM) and cryo TEM.

Chapter 2.3: Preparation of PEG-PG liposomes via dual asymmetric centrifugation for efficient encapsulation and targeted delivery of siRNA

Liposomal formulations of siRNA with amphiphilic polyether-modified lipids based on poly(ethylene glycol)-polyglycerol block copolymers (PEG-*b*-PG) have been prepared using the dual asymmetric centrifugation (DAC). This new technique combines rapid and sterile liposome preparation with very high entrapping efficiencies.

The successful incorporation of cholesteryl-PEG-*b*-PG block copolymers with different molecular weights and structural architectures into liposomes has been evidenced by the preparation of formulations with polyethers bearing clickable alkyne functions. Cycloaddition reactions with azide-functionalized fluorescent dyes on the surface of the preformed liposomes and subsequent fluorescent analysis showed full incorporation of the PEG-*b*-PG lipids into the liposomal membranes. The preparation of liposomes coated with clickable, multifunctional PEG-*b*-PG block copolymers using DAC and the sensitive fluorescent analysis allows the handling of very small batch sizes of about 60 mg. Investigation of liposome sizes via dynamic light scattering (DLS) and fluorescence measurements revealed improved stabilization of the formulations during storage over months. Furthermore, the encapsulation of siRNA molecules into the PEG-*b*-PG coated liposomes has been determined employing fluorescence labeled siRNA.

Following another synthetic approach including click chemistry, further functionalization of the liposomes via covalent attachment of molecules such as azide-functionalized folate has been carried out. Thus, the liposomal delivery of the entrapped siRNA molecules might be improved by specific targeting resulting in enhanced receptor-mediated endocytosis of the liposomal carrier. In the recent study, the calcein uptake in epithelial carcinoma cells (KB cells) has been investigated by flow cytometry.

Chapter 3.1: Langmuir and Langmuir-Blodgett films of multifunctional, amphiphilic polyethers with cholesterol moieties

The surface activity of a series of cholesterol-initiated polyethers with systematically varied linear and branched structures has been investigated by Langmuir trough measurements. The amphiphilic homopolymers and diblock copolymers were composed of a hydrophobic cholesterol group and either one or two hydrophilic blocks such as *l*PG, PGG, *hb*PG, or PEG. Langmuir films of multifunctional, hydrophilic polyethers containing a hydrophobic cholesterol group were studied by surface pressure-mean molecular area (π-*mmA*) measurements and Brewster angle microscopy (BAM) and revealed that already marginal variations in the molecular structures had pronounced consequences for their behavior at the air-water interface.

For the first time the behavior of well-defined polymers with hyperbranched blocks has been investigated at the air-water interface. Surface pressure measurements of linear and hyperbranched polyglycerol homopolymers showed the absence of surface activity at the air-water interface due to a strong tendency to dissolve in the water subphase after spreading from a chloroform solution (in clear contrast to PEG). Surprisingly, this behavior changed drastically, when only one cholesterol moiety was covalently linked to *l*PG and *hb*PG. For the other cholesterol-initiated homopolymers, the Langmuir isotherms proved also the existence of stable Langmuir films at the air-water interface. All amphiphilic polymers showed a reduction of the collapse surface pressure of the monolayer compared to the corresponding value of the monolayer of pure cholesterol. Typical hierarchically ordered morphologies of the LB films on hydrophilic substrates were observed for all cholesterol-initiated polymers. The polymers under investigation promise high potential for biomedical applications, since they contain many binding motives to phospholipid bilayers of cell membranes.

Chapter 3.2: Strong interactions between DPPC and a cholesteryl moiety covalently bound to a linear-hyperbranched polyether diblock copolymer

Membranes acting as cell walls of biological cells are basically composed of lipid bilayers and proteins embedded within the lipid matrix. Biological membranes are of particular relevance in the field of drug delivery and targeting, where it is attempted to deliver active species into cells by penetrating these membranes. In order to study the capability of penetration of synthetic molecules into cell membranes, simplified models are often employed. Typical examples in this context are Langmuir monolayers of phospholipids at the air-water interface, which represent a half leaflet analogue of biological membranes. Due to the simple preparation and characterization of Langmuir films, they are used to study the interactions between membrane components, protein interactions with the lipid matrix, and the penetrability for synthetic molecules.

Interactions of the phospholipid 1,2-dipalmitoyl-*sn*-glycero-3-phosphocholine (DPPC) with an amphiphilic diblock copolymer composed of poly(ethylene glycol)-*b*-polyglycerol (PEG-*b*-*hb*PG) initiated with cholesterol are studied at the air-water interface by surface pressure-mean molecular area (π-*mmA*) measurements of mixed Langmuir films and adsorption measurements of ChP to DPPC monolayers at different initial surface pressure values π_0. ChP is composed of a

single hydrophobic cholesteryl (Ch) moiety covalently bound to a hydrophilic linear poly(ethylene glycol) (PEG) block and a hydrophilic hyperbranched polyglycerol (*hb*PG) block. Langmuir isotherms and compression moduli of the mixed Langmuir films of different molar ratios reveal distinct interactions between DPPC and ChP during compression. In adsorption measurements a strong affinity of ChP to DPPC is observed after injection into the water subphase. Atomic force microscopy (AFM) investigations for LB films of DPPC/ChP mixtures of different molar ratios transferred onto hydrophilic silicon substrates confirm attractive interactions between these compounds, since large domains characteristic for macroscopic phase separation do not occur unless the PEG block of ChP crystallizes.

Chapter 4.1: Mesogen-initiated linear polyglycerol isomers: The ordering effect of a single cholesterol unit on "sticky" isotropic chains

Self-assembly in thermotropic phases is long known for cholesterol-derived compounds. In fact, the first observation of liquid crystalline organization was made for cholesteryl benzoates and cholesteryl acetates. The functionalization of polymers with cholesterol or other mesogenic moieties is a common strategy for the preparation of novel types of liquid crystalline polymers (LC).

Unusual liquid crystalline polymers consisting of the single mesogenic cholesterol unit and linear polyglycerol (PG) and poly(glyceryl glycerol) (PGG) chains were synthesized and their thermal properties have been investigated. Incorporation of the mesogenic moiety has been achieved using cholesterol directly as an initiator for the oxyanionic ring-opening polymerization of ethoxyethyl glycidyl ether (EEGE) or isopropylidene glyceryl glycidyl ether (IGG). The controlled oxyanionic polymerization conditions permits the synthesis of LC polymers with varying molecular weights and low polydispersities.

The resulting linear polyglycerols showed liquid crystalline order in an extremely broad temperature range. Polarized optical microscopy (POM) and small angle X-ray scattering (SAXS) experiments revealed self-assembly of the linear, cholesterol-initiated polyglycerols in layered phases with varying layer thicknesses depending on the chain lengths of the respective polymer up to a degree of polymerization (DP_n) of 26. This demonstrates the strong structure-directing effect of the single cholesterol unit, forcing an isotropic liquid, highly polar polymer structure into an ordered mesophase state.

The formation of LC phases in cholesterol-initiated polyglycerols is controlled by three main parameters: (i) by the ratio between the hydrophobic mesogen at the chain end and the hydrophilic polyether moiety; (ii) by the molecular architecture of the respective monomer, i.e., linear glycerol moieties or branched glyceryl glycerol units, (iii) by the hydroxyl functionalities at the polymer chain, contributing to the hydrophilicity and the generation of strong intermolecular interactions. Since linear polyglycerols and poly(glyceryl glycerol ether)s show no crystallization and the amphiphilic character is more distinct in these polymers due to the multiple hydroxyl groups at the polyether backbone, highly stable LC order is observed in comparison to the structurally related cholesterol-PEGs. The formation of LC phases depends on one hand on the amphiphilicity of the polymers, but on the other hand is limited by steric constraints, poly(glyceryl glycerol ether)s with comparable molecular weights showed no liquid crystalline order.

Chapter 4.2: Introduction of a PEG-spacer block in amphiphilic polyether-polyol block copolymers permits formation of ordered structures

In the field of cholesterol-related compounds the phase behavior of hydrophilic polyethers such like poly(ethylene glycol) (PEG) and linear polyglycerol attached to cholesterol-moieties has been studied with regard to the influence of the degree of polymerization, hydrophilicity of the polymer chain and its crystallization onto the formation of liquid crystalline (LC) structures.
The LC behavior of a series of complex double-hydrophilic polyether block copolymers comprising both polar ethylene glycol and glyceryl units is described that bear one single apolar cholesterol moiety. The synthesis of the materials consisting of poly(ethylene glycol)-*block*-polyglycerols (PEG-*b*-*l*PG) and of poly(ethylene glycol)-*block*-poly(glyceryl glycidyl ether) (PEG-*b*-PGG) was carried out via cholesterol-initiated ring-opening oxyanionic polymerization (ROP) of ethylene oxide (EO) and ethoxyethyl glycidyl ether (EEGE) or isopropylidene glyceryl glycidyl ether (IGG). Complete incorporation of the mesogenic unit in the complex molecular structure of the polyether block copolymers was achieved by direct use of cholesterol as an initiator for the polymerization. Varying chain lengths, different molecular architectures and amphiphilic or predominantly lipophilic materials have been prepared in order to elucidate the formation of the resulting LC phases, relying on differential scanning calorimetry (DSC), polarized optical microscopy (POM) and small angle X-ray scattering (SAXS).

Chapter 1: Introduction

Chapter 1:

Introduction: Polyether-modified liposomes

Anna Maria Hofmann[1] and Holger Frey*,[1]

1 Institute of Organic Chemistry, Johannes Gutenberg-Universität, Duesbergweg 10-14, Mainz, Germany

To be submitted to: Advances in Polymer Science.

1.1 Introduction

Almost all cancer therapies require the application of aggressive xenobiotics in high doses over long time periods, which generally leads to serious side effects. Therefore, the efficacy of chemotherapies is strongly restricted by the systemic toxicity of the anticancer agents. Thus, research on effective drug-delivery systems that are able to minimize the undesired adverse reaction on healthy organs, tissues and cells is a major challenge in the field of modern medicine. Providing a high concentration of the active pharmaceutical ingredient at the site of action and preventing its accumulation in healthy tissue by a specific drug carrier reduces the overall systemic dose and strongly improves the therapy progress.

Liposomes, consisting of one or more self-assembled bilayers of natural or synthetic lipids enclosing an aqueous compartment have attracted increased attention as pharmaceutical carriers over the last decades due to their unique properties, such as constant release of a pharmaceutical agent and improved pharmacokinetics.[1-5] The structural similarity of the liposome structure and biological membranes is due to the use of natural phospholipids, which can be easily metabolized in the body and provide excellent biocompatibility. In general, mixtures of phospholipids and cholesterols obtained from egg and soy are employed for the preparation of liposomal formulations. Furthermore, the vesicles formed can entrap hydrophilic drugs in the aqueous interior as well as lipophilic drugs in the membrane. The encapsulation of pharmaceutical agents in liposomes significantly enhances their therapeutic indices by

reduction of the distribution volume and by increase of the drug concentration delivered to a tumor. The liposome inhibits an early degradation or metabolism of the drug in blood plasma and can stabilize liposome drug formulations due to the high impermeability of hydrophilic and amphiphilic molecules through the vesicle membrane.

Although the first observation of the formation of bilayered vesicles by phospholipids in aqueous solution has been published about 40 years ago,[6] the scientific interest in the field of liposomal research remains high (Figure 1). In summary, almost 10 000 papers including over 900 reviews have been published concerning liposomes between 2006 and 2010.

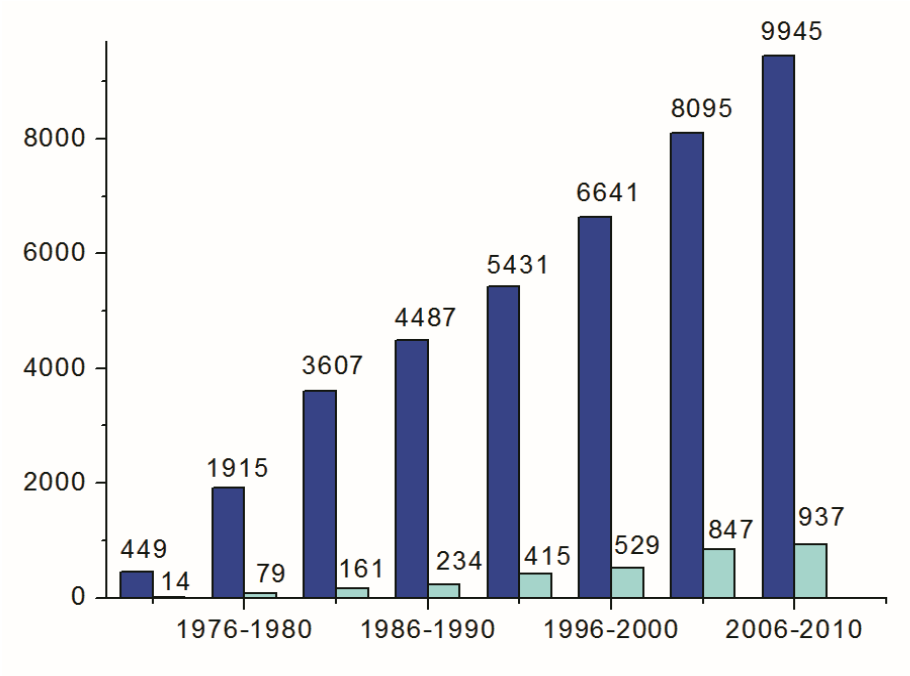

Figure 1. Increase of the number of publications concerning liposomes. Blue: total amount of papers published in the field of liposomes, cyan: total amount of reviews. Data obtained from PubMed.

The present book chapter will deliver insight into the broad field of liposome research, outlines some basic characteristics and presents the progress from first promising investigations to the approval of liposome application as drug carrier systems in cancer therapy. The interdisciplinary field of synthesis and characterization of sterically stabilized liposomes by the incorporation of polymers, especially polyethers such as poly(ethylene glycol) (PEG), in liposomal formulations will be highlighted.

1.2 From conventional to long-circulating liposomes

Bilayered vesicles based on phospholipids, referred to as conventional liposomes, can passively target tissues with discontinuous endothelium such as liver, spleen and bone marrow. Intravenously injected liposomes are rapidly opsonized by serum proteins and removed from the blood stream by cells of the mononuclear phagocyte system (MPS). Thus, half-life times of conventional liposomes in body fluids of only 20 minutes have been observed.[7] Binding of opsonins to the surface of foreign molecules or particles and ingestion by macrophages are the main processes of blood clearance for components larger than the renal threshold limit. Cells of the MPS, typically Kupffer cells or macrophages of the liver, are able to eliminate unprotected nanoparticles, such as conventional liposomes from the blood circulation within seconds after intravenous administration.[8-10] During this process, the interaction of liposomes with the serum proteins, so-called opsonins, is a critical parameter. Binding of opsonins onto the liposomal membrane enhances the clearance of the vesicles from circulation by cells of the MPS. The specific recognition of liposomes and their eventual removal is induced by cellular receptors that do not recognize the foreign substances themselves but opsonins attached to their surface.[11-16]

Generally, opsonins are any blood serum components that are involved in the removal of foreign molecules or particles from the blood stream. Although the precise mechanisms of MPS-related blood clearance is not fully understood, different complement and complement-related proteins have been shown to be involved in the phagocytic recognition and elimination of liposomes including opsonins such as C3, C4 and C5 immunoglobulins as well as other blood serum proteins such as laminin, albumin, fibronectin, α2-macroglobulin, C-reactive protein, type I collagen and lipoproteins.[9, 17-21] In the process of opsonization, the number and type of proteins that adhere to the liposomal surface vary largely with the physicochemical characteristics of the liposomes such as size, surface charge and lipid composition.[22-24] Most of the studies regarding the influence of proteins on the MPS uptake have been carried out *in vivo* animal experiments. For example, inherited and induced C3 deficient animal models have shown to be more often infected by phagocytosis-controlled diseases.[25]

While the first contact of opsonins with foreign particles in the blood stream is caused by random Brownian motion, the binding of the proteins depends on several attractive forces such as van der Waals, ionic, electrostatic or dipole interactions.[8] After the attachment of opsonins

onto the particle surface, cells of the MPS are able to recognize and bind the liposomes themselves. One possible explanation for the recognition and binding of opsonized particles by macrophages is the conformational change of the opsonins from an inactive to an active form induced by its binding to the particle surface. Besides this receptor-dependant differentiation between inactive opsonins in the blood stream and activated surface bonded proteins, phagocytes are able to attach unspecifically to adsorbed serum proteins.[9, 21] However, the attachment of macrophages to activated or adsorbed opsonins results in the phagocytosis of the liposome by mononuclear phagocytes, including endocytosis and controlled degradation by secreted oxidative enzymes, i.e., superoxides, oxyhalides, nitric oxide and hydrogen peroxide.[8,26]

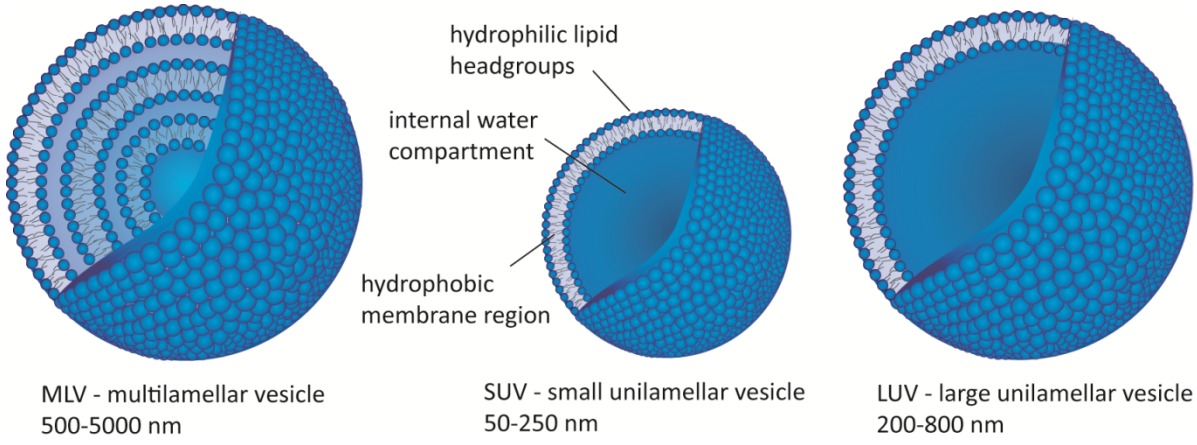

Figure 2. Schematic diagrams of multilamellar vesicles (MLV), small unilamellar vesicles (SUV) and large unilamellar vesicles (LUV). Encapsulation of hydrophilic drugs can be achieved in the internal water compartment or in case of hydrophobic drugs in the hydrophobic membrane region.

Insufficient degradation of the liposomes in this process leads to a rapid sequestration of the drug carriers in organs of the mononuclear phagocyte system. The accumulation of conventional liposomes in cells of the MPS can be exploited in targeting antibiotics in treatment of intracellular infections residing in the MPS. The therapy effect is strongly improved by grafting of ligands, e.g., tuftsin, to the liposomal membrane that specifically bind to MPS cells and furthermore enhance their activity. Following this approach, liposomal delivery systems for anti-Leishmania drugs and immunomodulators to liver and lung macrophages have been developed, resulting in increased therapeutic indices of these agents against Leishmania

infections and metastatic tumor growth, respectively.[27-31]

If the target site is beyond the mononuclear phagocyte system, the removal of liposomes from the blood circulation by macrophages is one of the main disadvantages for conventional liposomes. Drug carrier systems have to be present in the blood stream long enough to reach the site of action and deliver the pharmaceutical agent in sufficient concentration. Since the attachment of serum proteins to liposomal membranes strongly depends on the size, surface charge and lipid composition of the liposome, first attempts to prolong blood circulation times have been achieved by variation of the physicochemical characteristics of the vesicles. Thus, the prematurely release of drugs introduced by interactions of the liposomes with low and high density lipoproteins (LDL and HDL), is reduced in cholesterol-rich liposomal formulations.[32] The incorporation of cholesterol in the membrane results in increased packing density, which decreases bilayer fluidity and transfer of phospholipids to HDL. In a different approach, higher stabilities of liposomes in plasma are achieved by the use of rigid gel-phase phosphatidyl cholines (PC) or sphingomyelins with satured fatty acids compared to analogous lipids with unsatured chains.[33-38] Via manipulation of liposome size, blood circulation times can be prolonged. Thus, small unilamellar vesicles (SUV) with diameters around 100 nm inhibit longer *in vivo* half-life than large multilamellar liposomes (MLV) with sizes of 500-5000 nm (Figure 2).[3, 12, 22, 33, 39, 40]

1.3 Sterically stabilized liposomes: Poly(ethylene glycol) shell

Besides these different methods for the preparation of long-circulating colloidal carriers, the coating of the liposomal surface with biocompatible polymers initially using poly(ethylene glycol) (PEG) and subsequently other selected flexible, hydrophilic polymers results in sterically stabilized, so-called stealth liposomes with longer *in vivo* half-lifes.[41-50] The formation of a protective layer around the drug carrier leads to reduced blood clearance and changes in tissue distribution, mainly due to lower opsonization and consequential lower uptake by the cells of the mononuclear phagocyte system. Thus, PEG-coated liposomes remain in the blood circulation for extended periods with half-lifes of 40 hours up to 5 days.[51] Besides reduced clearance from the blood stream, PEG liposomes show improved biodistribution characteristics, i.e., the main section of the administered doses allocates in the blood while a relatively low percentage of only 10-15% deposits in the liver.

1.4 Synthesis of poly(ethylene glycol) lipids

The surface modification of liposomes with poly(ethylene glycol) chains, the PEGylation, can be achieved using different approaches.

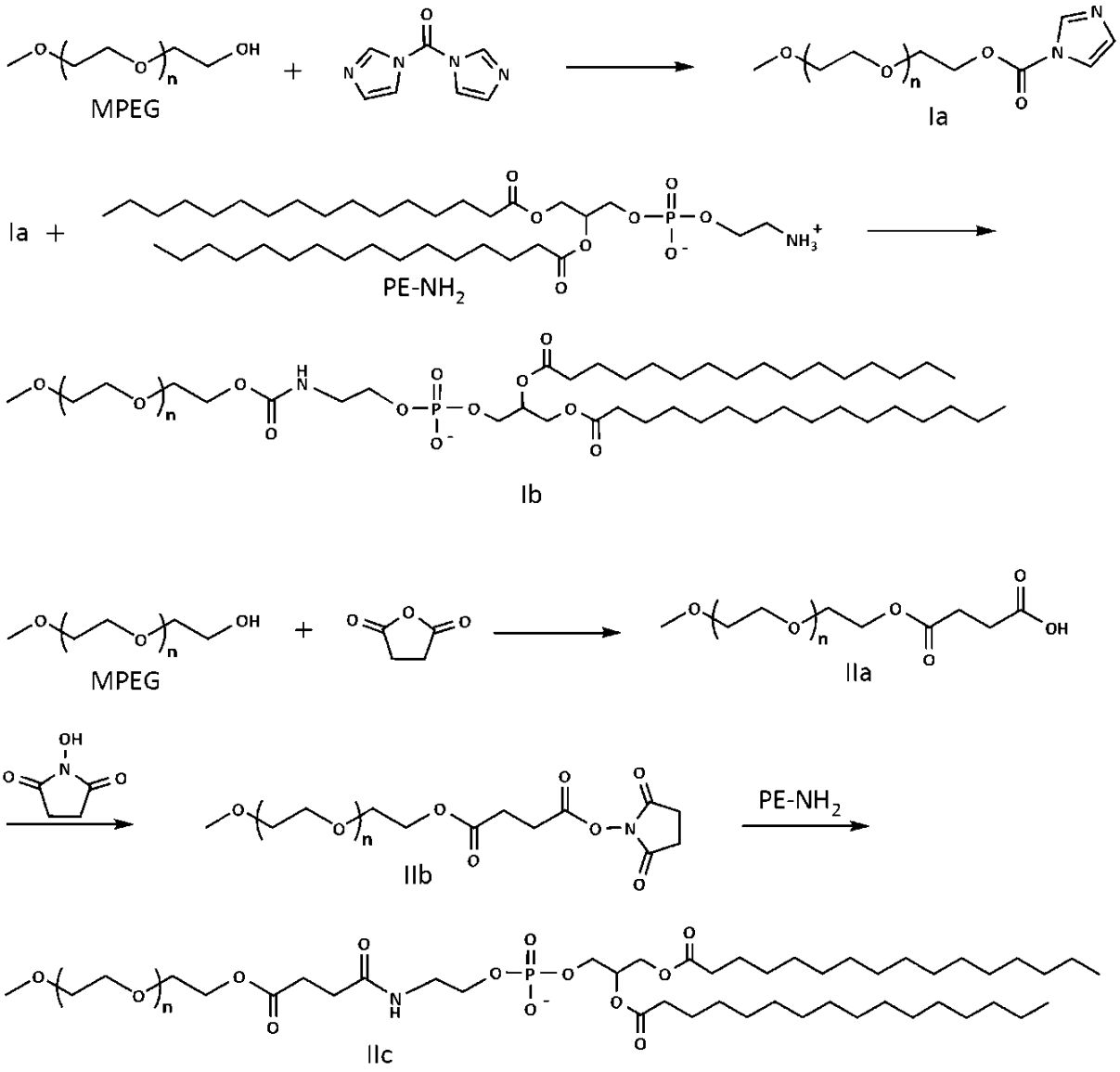

Figure 3. Reaction schemes of different coupling reactions for the preparation of poly(ethylene glycol)-modified phospholipids via carbamate (I) and amide (II) bonds.

Since mere physical adsorption is less stable than covalent attachment to lipids of the liposomal membrane, sterically stabilized particles are generally prepared by the incorporation of suitable polymer-modified lipids in liposome formulations. Among several approaches for the synthesis of polymer-lipid conjugates, the use of amino-functionalized lipids, i.e., phosphatidyl

ethanolamine (PE) reacting with coupling agents and poly(ethylene glycol) monomethyl ether (MPEG) is most frequently used (Figure 3).[52, 53]

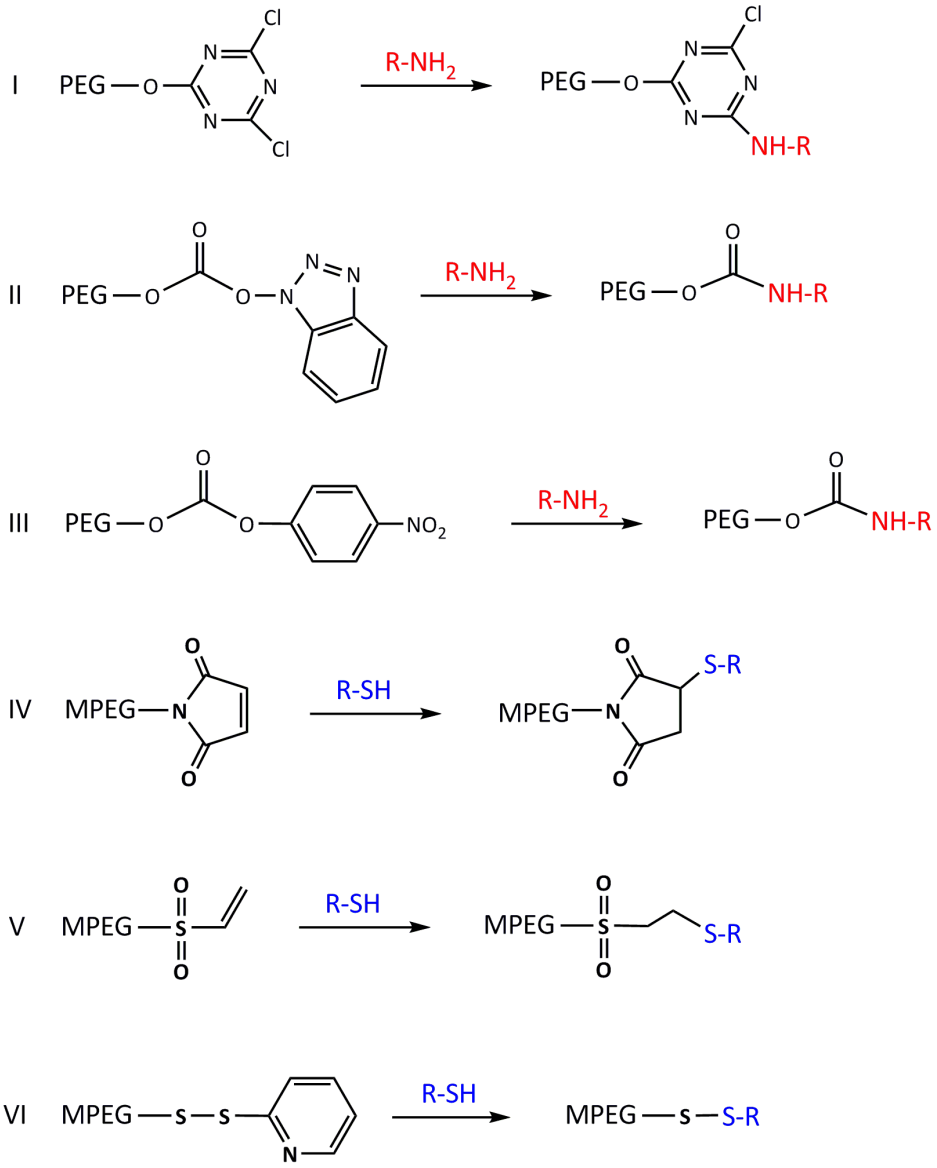

Figure 4. Reaction schemes for amine-reactive PEGs: PEG dichlorotriazine (I), PEG benzotriazole carbonate (II), PEG *p*-nitrophenyl carbonate (III) and thiol reactive PEGs: PEG maleimide (IV), PEG vinyl sulfone (V) and PEG orthopyridyl disulfide (VI).

Covalent coupling is achieved by the formation of carbamate bonds via reaction of carbonyl with amino groups (Figure 3, reaction I). Amide bonds are generated by the reaction of activated carboxyl groups and amino groups (Figure 3, reaction II). The reaction of pyridyldithiols and thiols results in disulfide bonds, while the reaction between maleimides and

thiols give thioether bonds (Figure 4). Besides the synthesis of polymer-lipid conjugates, these general coupling reactions can be employed for the covalent attachment of ligands, such as labeling or targeting moieties directly onto the liposomal surface via reaction with lipids or onto a spacer via reaction with polymer-modified lipids.[4,54,55]

Although the synthesis of amphiphilic materials based on hydrophilic initiators for the oxyanionic ring-opening polymerization of ethylene oxide (EO) is widely known in the preparation of non-ionic surfactants consisting of short-chained poly(ethylene glycol)s, the common preparation of PEG-lipids for liposomal formulations is based on various coupling reactions. While these syntheses include multiple reaction and purifying steps, the direct incorporation of the lipid in the polymer structure via its use as an initiator has been rarely presented in this field of research.[56-58] One main drawback of this preparation method is the limitation to chemically robust, hydrophobic initiating systems such as long-chained alkyl alcohols, bis-*n*-alkyl glycerols or cholesterols (Figure 5). Lipids containing base-labile ester groups including phospholipids are rapidly hydrolyzed under the strongly basic conditions of the anionic polymerization.

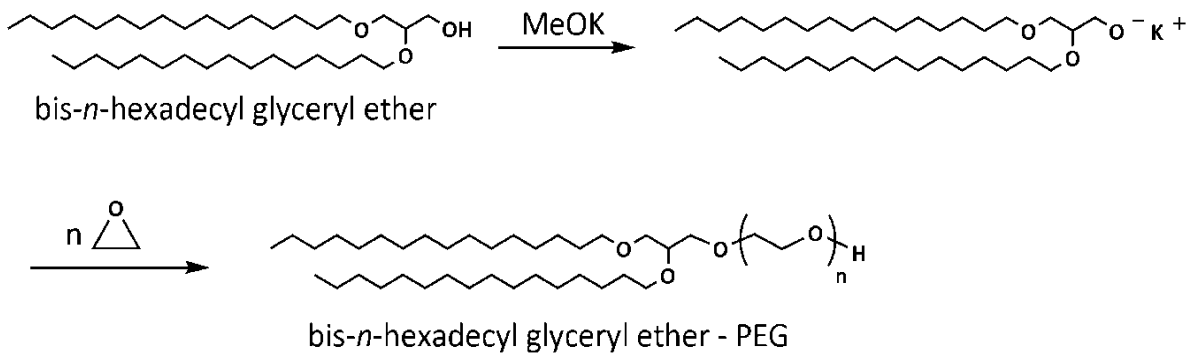

Figure 5. Reaction scheme of the oxyanionic ring-opening polymerization of ethylene oxide using bis-*n*-hexadecyl glycerol and potassium methanolate as initiating system.

1.5 PEG liposomes longevity: Opsonization vs. liposomal aggregation

In numerous publications, the stealth effect of PEG grafted to the liposomal membrane has been investigated regarding the reduced recognition by opsonins.[41-45, 48, 59-61] Nevertheless, the understanding of the fate of long-circulating liposomes in the blood stream is crucial in order to optimize their pharmacologic properties. The capability of PEGylated liposomes to escape the

phagocytic cells of the MPS has been shown to be one main reason for the longevity of this type of drug carrier system.[46, 62] The initial step in the elimination of foreign particles from the blood stream is the attachment of serum proteins to their surface, because the cells of the MPS do not recognize the liposomes themselves, but proteins at the surface. Therefore, the crucial task for long-circulating liposomes is in an ideal case the elimination or more likely the suppression of opsonization by serum components. Although mechanistic details of the opsonization process are not fully understood yet, several publications show the faster attachment of opsonins onto the surface of hydrophobic particles compared to hydrophilic particles. *In vitro* and *in vivo* studies of the surface hydrophilicity has been identified as one main parameter for the interaction with serum proteins.[45, 63] In addition, opsonization also depends on the surface charge of the liposome. In this context, *in vitro* studies demonstrated that particles with surface charges undergo opsonization much faster than the analogous neutral liposomes.[64] Following this approach, grafting of hydrophilic polymer chains onto the liposomal membrane is one method to inhibit the attachment of opsonins via hydrophobic or electrostatic interactions.

The steric shielding effect of the hydrophilic mobile layer formed by PEG chains reducing the rate of adsorption of serum proteins has been demonstrated via multiple techniques, including aqueous two-phase partition.[13, 65] A biphasic aqueous system of dextran and PEG has been developed in order to investigate surface properties and opsonization of liposomes. Depending on various factors such as size, lipid composition and adsorbed components, liposomes diffuse into the PEG-rich top phase or the dextran-rich lower phase. Covalent attachment of PEG chains onto the liposomal membrane leads to partition of the vesicles into the top phase, whereas equivalent conventional liposomes without polymer coating partition to the interface and the bottom phase. Plasma proteins distribute to the dextran-rich bottom phase. Incubation of conventional liposomes in plasma results in partition to the bottom phase, indicating similar surface properties as plasma itself and therefore instantaneous adsorption of proteins onto the liposomal surface. In contrast to these findings, incubation of PEGylated liposomes in plasma results only in a slow change of distribution due to a reduced and gradual protein absorption.

In a different approach the adsorption of serum proteins has been investigated via measurement of the fluorescence of fluorescein isothiocyanate-labeled proteins adhered to lipid-coated glass surfaces.[66] Monolayers of dipalmitoyl phosphatidyl ethanolamine with different amounts of PEGylated phosphatidyl ethanolamine were deposited by the Langmuir-

Blodgett method and incubated with different proteins.[67] The inhibition of protein absorption onto PEG-grafted lipid surfaces increases with higher PEG content. Following this approach, the shielding effect of PEG on the adsorption of bovine serum albumin, laminin and fibronectin as well as erythrocytes, lymphocytes and macrophages has been demonstrated. In the range of 0-0.5 mol% of PEG-grafted lipids, the percentage of erythrocyte and lymphocyte adhesion is in good agreement with the amount of uncovered surface area. With increasing PEG content the attachment of proteins decreases. This concentration dependence of the stealth effect is most distinct at low PEG concentrations of less than 1 mol%, while further increase in the PEG content (1-5 mol%) only slightly reduced the amount of proteins adsorbed. Besides the polymer concentration, the molecular weight of the PEG moiety covalently bound to the lipid surface strongly affects protein adhesion. For instance the steric shielding effect of PEG with molecular weights under 2000 g/mol is lower compared to PEG of 3000 and 5000 g/mol.

A similar investigation of protein adsorption onto lipid surfaces with varying amount of PEG chains has been carried out using surface plasmon resonance.[68] The incorporation of small concentrations of PEGylated lipids into membranes strongly alters interbilayer interactions as well as protein adsorption. Thus, the attachment of three different proteins, namely human serum albumin (HSA), human fibrinogen and bovine pancreatic trypsin inhibitor (BPTI) have been shown to decrease with increasing PEG concentration (0-10 mol%). The protein characteristics such as size, shape and charge proved no significant influence on the shielding effect. Hence, the very small globular BPTI with a molecular weight of 6000 g/mol, small rodlike HSA (M_w: 66 200 g/mol) and large rodlike fibrinogen (M_w: 340 000 g/mol) revealed similar concentration dependence, indicating a nonspecific stealth effect of the PEG moieties.

In another study, the quenching of liposomal fluorescent labels, such as nitrobenzoxadiazole (NBD) or fluorescein with proteins, i.e., rhodamine-ovalbumin (Rh-OVA) or anti-fluorescein antibody has been investigated.[69] In detail, the interaction of ovalbumin with the liposomal surface allows excitation energy transfer from the liposome-associated NBD to rhodamine moiety resulting in a decrease of NBD fluorescence at 530 nm, while the fluorescence intensity of the rhodamine attached to the ovalbumin increases. Conventional liposomes without PEG-modification as well as dextran-modified liposomes (M_w: 6000 g/mol, 1 mol%) showed decreasing NBD fluorescence. In contrast, grafting of poly(ethylene glycol) with a molecular weight of 5000 g/mol to the liposomal surface (1 mol%) impedes fluorescence quenching in NBD-liposomes, suggesting inhibited protein absorption at the vesicle surface. This study

supports the theory that not only the hydrophilicity of the polymer coating determines the stealth effect, but also the flexibility of the polymer chains. Thus, liposome-grafted dextran with a rigid polymer backbone offers less hindrance of liposome-protein interactions than hydrophilic and flexible poly(ethylene glycol) chains.

Since the above mentioned reports present rather indirect techniques in order to investigate liposome-protein interactions, more recent studies were carried out using characterization methods such as protein assay, SDS-PAGE (sodium dodecyl poly(acryl amide) gel electrophoresis) and Western Blotting. A number of these reports have aimed at the specificity of liposome-protein interactions and its contribution to enhanced blood circulation times of stealth liposomes.[70-72] In a general procedure, conventional or stealth liposomes with varying lipid composition and different molecular weights of the polymers were incubated with plasma or various protein solutions followed by separation of the bulk serum proteins by passing liposomes over gel filtration columns. Proteins extracted from column-recovered liposomes were characterized for instance by SDS gel electrophoresis using poly(acryl amide) gels and Western blotting.

Although liposome-protein interactions and opsonization were thought to play a crucial role in the clearance process of liposomal drug carrier systems, the mechanism has not been fully understood yet. Ambiguous results concerning the stealth effect of neutral, positively and negatively charged liposomes have been presented with respect to the absorption of fibrinogen and other serum proteins. Furthermore, recent studies suggest that PEG coated onto liposomes does not reduce plasma protein adsorption.[73, 74] In fact, opsonization of PEG liposomes containing phosphatidyl serine resulted in a significantly decreased uptake by cultured bone marrow macrophages. In a postulated mechanism, the bound serum proteins themselves operate as a nonspecific stealth layer that prevents interactions of the liposomes and the macrophage cells and results in prolonged *in vivo* blood circulation times of the PEG liposomes.[73]

Alternatively, the enhanced lifetime of PEG liposomes might be caused by reduced liposome-liposome aggregation resulting in prolonged circulation times of single and small particles of about 100 nm in diameter in the blood stream.[75] In this case the interaction of vesicles with Fc receptors or complement proteins might be prevented by altered liposome aggregation due to the incorporation of PEG moieties into the liposomal formulation. This indicates a directly

inhibited cell uptake and subsequent rapid elimination due to large particle sizes.[39, 71, 76] Supporting this theory, the presence of poly(ethylene glycol) chains on the surface of distearoyl phosphatidyl choline (DSPC) liposomes has been shown to provide a strong interbilayer repulsion, reducing vesicle aggregation due to lowered van der Waals forces.[77] X-ray analysis confirmed the extension of liposome-bound PEG chains with a molecular weight of 1900 g/mol of about 5.0 nm from the membrane surface. Moreover, the repulsive properties observed for this DSPC liposomes containing 4 mol% of PEG-modified lipids correlates with the extended *in vivo* blood circulation times, suggesting the steric stabilization as the main explanation for the stealth effect. Supporting this mechanism, previous studies demonstrated the capability of the polyether chains to inhibit fusion of dioleoyl phosphatidyl ethanolamine or respectively didodecyl phosphate bilayers containing surface-grafted PEG.[78, 79] Analyzing electron density profiles, the distance of membranes containing DSPC and distearoyl phosphatidyl ethanolamine-PEG (DSPE-PEG) increases with increasing PEG-concentration and molecular weight of the polymer chains. Thus, PEG chains with molecular weights of 350, 750, 2000 and 5000 g/mol extended about 1.0, 2.8, 6.0 and 10.0 nm, respectively, from the lipid bilayer surface.[80] Freeze-fracture electron microscopy and quasielastic light scattering (QELS) analyses support this theory, demonstrating the rapid coalescence and aggregation of 100 mol% DSPC liposomes in particles exceeding 100 nm in diameter.[75] However, liposomes prepared with analogous extrusion methods containing PEG-modified lipids showed no aggregation due to reduced surface-surface interactions. In a similar study, the variation of *in vivo* blood circulation times of DSPC liposomes as a function of aggregation has been investigated.[81] The aggregation of liposomes to larger structures indeed enhanced uptake by macrophages and cells of the MPS. Especially vesicles of liposomal formulations containing cholesterol fuse and aggregate after preparation. Thus, the incorporation of surface-grafted PEG on cholesterol-containing liposomes strongly prevents liposome-liposome interactions resulting in prolonged circulation lifetimes of the drug carriers.[82]

While long-circulating PEG liposomes have been intensively studied, are widely used in numerous biomedical *in vitro* and *in vivo* investigations and even are part of already approved and employed medical therapies, the detailed mechanisms which provide significantly increased blood circulation times remain unclear. The minimized adsorption of serum proteins to the liposomal surface due to the shielding effect of PEG chains reduces the recognition of the vesicles by macrophages and other cells of the mononuclear phagocytic system. Hence, the

effective elimination of the stealth liposomes from the blood stream is suppressed. On the other hand, a number of reports demonstrated that despite opsonization of the PEGylated liposomes prolonged circulation lifetimes are achieved, suggesting reduced liposome-liposome aggregation as the main reason causing the stealth effect.

1.6 PEG liposomes: configurations, molecular weight and circulation times

Liposome-protein as well as liposome-liposome interactions strongly depend on the chemical and physical properties of the polymer chains grafted onto the liposome surface. Therefore also circulation times of the drug carrier systems change with variation of the molecular weight and the amount of PEGylated stealth lipid incorporated in the liposomal formulation. In PEG-modified liposomes, the surface characteristics of the vesicle are mainly defined by the properties of polymer chains, but are also influenced by the lipid anchor employed in order to covalently attach the polymer onto the liposomal surface and the composition of the co-lipids.

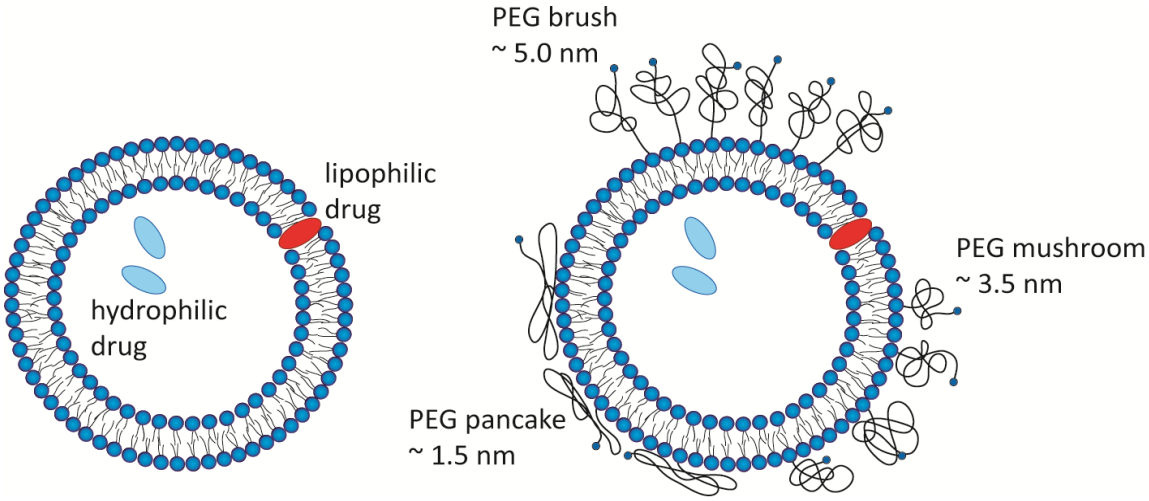

Figure 6. Schematic diagram of a conventional liposome (left) and a PEG-modified liposome (right) with different polymer configurations depending on molecular weight and grafting density of the PEG chains.

The amount of exposed or uncovered areas of poly(ethylene glycol)-modified surfaces is determined by the grafting density and the degree of polymerization of the polymer. Different regimes or configurations are proposed for polymers end-grafted onto lipid bilayer surfaces with varying percentages and molar masses. Thus, the surface area covered by the hydrophilic

and flexible PEG chains as well as the conformation of the chains can be described using different model calculations. With increasing amount of polymer grafted to the surface, the distance between two chains decreases. Thus, at a low percentage of PEG lipids the distance between the chains is larger than the size of the individual coil, so that the polymer chains do not interact. The resulting conformation, which due to additional interactions is equivalent to the bulk confirmation, is called the "mushroom regime".[83-85] If the chains are grafted so densely that strong overlap of adjacent polymer coils occurs, stretching of the chains is induced. The equilibrium expansion of the chains in the so-called brush regime is driven by the osmotic pressure and limited by the elastic force that is determined by the conformational entropy of the chains. Hence, the layer thickness of the grafted polymer can be described as a proportional function of the molar mass and increases with the grafting density. In the pancake model the polymer chains extend about 1.5 nm from the lipid surface, in the mushroom regime the polymer layer thickness is about 3.5 nm while the expansion of the polymer chains in the brush regime due to the intermolecular interactions is the largest with a layer thickness of about 5.0 nm (Figure 6).

In general, the preparation of liposomes, containing PEG moieties of molecular weights of less than 2000 g/mol with a fraction of the stealth lipid not exceeding 0.5 mol%, results in vesicles bearing uncovered surface areas. In these particles the inhibition of protein adhesion is lower than in particles with higher surface coverage. Furthermore, the reduced thickness of polymer layer by shorter chain polymers also reduces the effective suppression of protein and cell adhesion. The incorporation of poly(ethylene glycol) chains with higher degree of polymerization and increased grafting densities above 0.5 mol% decreases cell adhesion and liposome aggregation with estimated decreases of uncovered areas. Theoretical modeling as well as experimental data obtained from surface force measurements and scattering experiments suggest that the molecular origin of PEG liposome stability in the blood circulation is caused by the extended conformation of the flexible, hydrophilic polymer chains and steric repulsion induced by the stretched chains. This effect can be referred to the polymer chains physical properties, i.e., high water solubility, large excluded volume and high degree of conformational entropy.[45, 53, 77, 86] Thus, liposome-liposome interactions are avoided reducing the aggregation of the drug carriers into large structures that are more likely to be recognized and removed from the blood stream. Furthermore, interactions with plasma proteins and phagocytic cells are reduced resulting in decreased liposome clearance via MPS uptake. Thus,

liposomes with PEG-corona provide several advantages, such as strongly improved blood circulation times, reduced aggregation of the PEGylated vesicles and improved stability of the liposomal formulations.[1, 46, 81, 87]

1.7 Sterically stabilized liposomes: Beyond PEG

Among numerous polymers, poly(ethylene glycol) remains the best examined polymer employed for the preparation of long-circulating liposomes due to its unique properties, such as good biocompatibility, decreased to non-existing toxicity, low immunogenicity, easy accessibility, chemical inertness, excellent solubility in water and in organic solvents as well as low cost.[55, 88-94] However, an increasing number of studies have demonstrated the shielding effect of various other hydrophilic polymers or PEG-containing block copolymers consisting of poly(ethylene glycol) and poly(propylene oxide) (PPO), known as poloxamers and poloxamines (Figure 7).[95, 96] These polymers combine various characteristics that are crucial for their use as a protective layer in drug carrier systems and generally consist of hydrophilic and typically very flexible polymer chains and lipophilic anchor groups. In order to reduce undesired electrostatic interactions and to increase the shielding effect, the polymers are mostly charge neutral nonionic surfactants. The stealth effect of lipid-modified polysaccharides such as mannan, pullulan, amylopectin and dextran has been demonstrated.[97] In recent studies, long-circulating liposomes based on poly(vinyl alcohol) (PVA) and poly(acrylic acid) (PAA) have been prepared that showed enhanced blood lifetimes and improved physical stabilities comparable to PEG liposomes.[98-100] Furthermore, the effect of the surface-modification of liposomes with mixtures of PEG and PVA has been studied, revealing reduced clearance from the blood stream and improved biodistribution characteristics.[101] According to the authors of the study, the incorporation of small percentages of PVA (20000 g/mol, 1 mol%) into PEG liposomes (2000 g/mol, 4 mol%) improved the *in vivo* disposition characteristics, suggesting lower accumulation of the vesicles in the liver due to reduced opsonization by serum proteins. Alternatively, the preparation of stealth liposomes based on amphiphilic poly(acryl amide) and poly(vinyl pyrrolidone) has been achieved via end functionalization of the polymers with long-chained acyl groups.[102] Inclusion of these polymers into the liposomal membrane has been shown to enhance liposome circulation *in vivo* and decrease liposome accumulation in the liver. In fact, the shielding effect depends not only on the molar mass of the polymer, but also on the length of the acyl moiety. The anchoring of a high molecular weight polymer of 6000-

8000 g/mol into the lipid bilayer by a relatively short alkyl chain (C_{12}), offering only weak interaction with the colipids of the liposomal membrane, is less stable and more likely to be released due to the polymeric chain motion. Thus, the efficacy of the protective coating increases with the length of the lipophilic anchor group and decreases for higher molecular weight polymers.

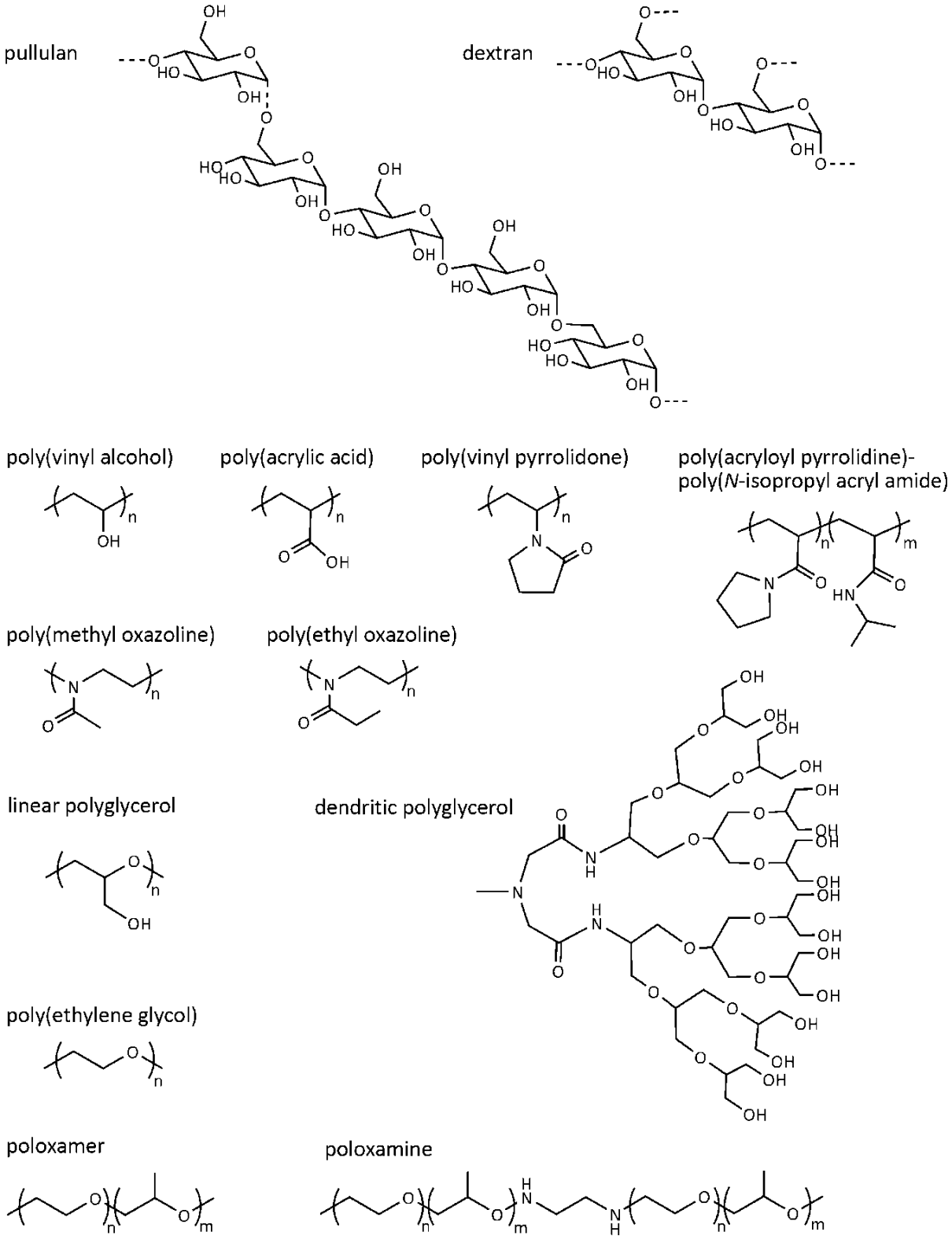

Figure 7. Molecular structures of different polymers for liposome preparation including polysaccharides (pullulan, dextran), vinyl polymers (poly(vinyl alcohol), poly(acrylic acid), poly(vinyl pyrrolidone), poly(acryloyl pyrrolidine)-*b*-poly(*N*-isopropyl acryl amide)), poly(oxazoline)s and polyethers (linear and dendritic polyglycerol, poly(ethylene glycol),

poly(ethylene glycol)-*b*-poly(propylene oxide)).

Thermoresponsive poly(acryl amide) copolymers, i.e., poly(acryloyl pyrrolidine)-*b*-poly(*N*-isopropyl acryl amide, with lower critical solution temperatures (LCST) near the physiological temperature have been synthesized.[103] Calcein-loaded dioleoyl phosphatidyl ethanolamine (DOPE) liposomes modified with these copolymers showed triggered calcein-release by the hydrophilic-to-hydrophobic change of the copolymer chains.

Biodegradable L-amino acid-based polymer-lipid conjugates proved to exert an effective steric protection for liposomes upon covalent attachment to the lipid bilayer surface.[104] Again, the crucial importance of the anchor molecule incorporating the polymer into the liposomal membrane has been emphasized. For the preparation of liposomes with water soluble polypeptides, i.e., poly(hydroxyethyl-L-glutamine) (PHEG) the conjugation to dioctadecyl amine offered sufficient attachment to the lipid bilayer. The poly(amino acid)-lipids are expected to be intracellularly degraded via proteolytic enzymes that are present at pathological target sites such as tumors and inflammations. Thus, the protective polymer layer remained stable during liposome circulation until arrival at the pathological target sites. Plasma concentration-time profiles and uptake by liver and spleen revealed the effective stealth effect of PHEG with molecular weights of 4000 and 5000 g/mol comparable to the capacity of PEG-DSPE (2000 g/mol) to prolong circulation times.

In another report, the blood clearance and tissue distribution of long-circulating liposomes bearing 5 mol% of lipid-conjugates of distearoyl phosphatidyl ethanolamine (DSPE) and poly(2-methyl-2-oxazoline) and poly(2-ethyl-2-oxazoline) with a degree of polymerization of 50 have been investigated.[105] Both polymers enhanced blood circulation times and lowered uptake into liver and spleen equal to the effect of comparable poly(ethylene glycol)-modifications.

Besides poly(ethylene glycol), a number of other polyethers have been investigated regarding their shielding effect in order to obtain liposomes with longer circulation times *in vivo*. For instance, oligomers of linear polyglycerols (*l*PG) have been coupled with dipalmitoyl-phosphatidyl anchor groups via phosphatidylation of the respective polyglycerols by phospholipase D.[106, 107] Prolongation of the *in vivo* circulation times strongly depends on the percentage and molecular weight of the polymer content of the liposomal formulation. While small oligomers such as tetraglycerol required incorporation rates of 8 mol% in

DSPC/cholesterol (1:1) liposomes, an effective shielding of octaglycerol has been observed with a percentage of only 4 mol%. Interestingly, the longest circulation times have been achieved using rather small polyglycerols with molecular weight of about 700 g/mol and a fraction of 6 mol% of the stealth lipid. Related investigations with PEG liposomes have been carried out using polymers with molar masses of 1000 up to 5000 g/mol.

In a similar study, the preparation of long-circulating liposomes coated with branched polyglycerol dendrons have been presented.[108] These branched oligoglycerols have been originally developed to solubilize hydrophobic molecules for biomedical applications.[109-111] The physicochemical properties as well as the pharmacokinetic *in vivo* profile of the dendritic oligoglycerol liposomes in rats have been characterized.[108] According to these investigations, branched polyglycerol dendrons with 12 monomer units provide a similar shielding towards liposomes as PEG with a molecular weight of 2000 g/mol, but in addition to that showed better encapsulation efficiency of doxorubicin (DOX) as well as a better accessibility to specific ligands. The layer thickness of polymer coating in PEG liposomes influences the reduced serum protein adsorption and uptake by the cells of the MPS. Thus, long-circulating liposomes inhibit a steric barrier of PEG chains typically stretched 3-4 nm outwards from the lipid bilayer surface.[112] Studies of branched PG-modified liposomes proved fixed aqueous layer thicknesses of approximately 2 nm similar to the theoretical value of the stable conformation in PG dendrons of 2.1 nm. Despite the thinner protective layer of the PG liposomes, the protein adsorption determined via protein assays is significantly reduced.

1.8 Sterically stabilized liposomes: PEG-PG copolymers

Among the various promising polymers tested for the preparation of long-circulating liposomes, up to now, only PEG has been approved for clinical use in liposomal formulations.

However, one main disadvantage of poly(ethylene glycol) is the lack of additional functional groups at the polymer chain, which could be used for the covalent attachment of labeling or targeting moieties. The incorporation of any functionality demands functional initiation or termination of the anionic ring-opening polymerization (ROP) of ethylene oxide or additional modification of the terminal OH-group, which often requires multiple reaction steps.[113] In recent reports, the well known and widely used PEGylation strategy for the preparation of long-circulating liposomes has been combined with the polyfunctionality of polyglycerol (PG).[56, 57]

The biocompatibility and low cytotoxicity of linear and hyperbranched polyglycerol (*l*PG and *hb*PG) is similarly low as in the case of PEG.[114-117] However, in addition such compounds offer multiple possibilities for further functionalization due to the high number of hydroxyl groups and may exhibit an even higher water solubility. Versatile PEG-PG copolymers have been synthesized varying in architecture, amount of functionalities and molecular weights. The preparation of complex polyethers, such as linear-dendrimer or linear-hyperbranched structures, bearing multiple functional groups is often based on multistep approaches.[118-122] In order to reduce the synthetic effort and cost, the incorporation of the lipophilic anchor group into the polymer structure has been carried out via the use of lipophilic initiators for the combined oxyanionic polymerization of different epoxide monomers.[56, 57, 123-125]

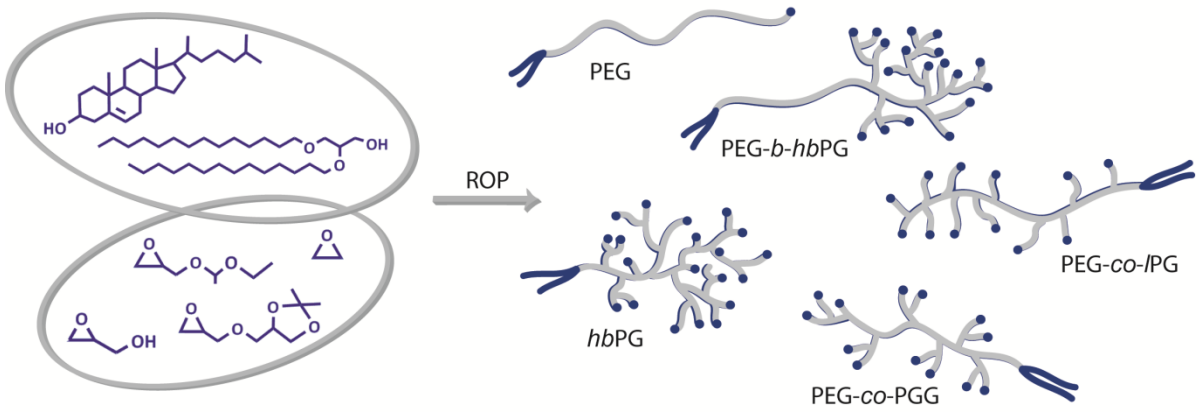

Figure 8. Schematic structures of PEG-PG lipids synthesized via combined ring-opening polymerization of epoxide monomers, such as ethylene oxide (EO), glycidol, ethoxyethyl glycidyl ether (EEGE) and isopropylidene glycidyl glyceryl ether (IGG).

In detail, commercially available cholesterol and long-chained bisalkyl glyceryl ethers have been employed to achieve effective incorporation of the amphiphilic polymers into the liposomal membranes. Both initiators are stable against the strongly basic reaction conditions during the oxyanionic polymerization and acidic reaction conditions that are applied for the protective group cleavage, excluding the use of base labile phospholipids. Besides simplification of the synthetic approach, the covalent attachment of lipids during the controlled anionic polymerization process results in amphiphilic polymers with merely aliphatic polyether structures. Thus, the incorporation of potentially toxic linkage moieties is avoided and the biocompatibility of the polymer-lipid conjugates is maximized. Variation of the molecular

architecture of the polyether lipids has been achieved via the combination of ethylene oxide (EO) with different glycidyl derivatives such as ethoxyethyl glycidyl ether (EEGE), isopropylidene glycidyl glyceryl ether (IGG) and glycidol (Figure 8).[120-122]

Following this approach, a rapid access strategy for polyfunctional lipids via ROP has been achieved, yielding amphiphilic homopolymers, i.e., PEG lipids and hbPG lipids, linear-hyperbranched PEG-*b*-*hb*PG block copolymers and random PEG-*co*-*l*PG as well as PEG-*co*-PGG copolymers. The reaction sequence for the synthesis of cholesterol-initiated PEG-*co*-PGG via random copolymerization of EO and IGG and subsequent removal of the protective groups is shown in Figure 9. In the series of PEG-PG copolymers and PG homopolymers, full incorporation of the lipid and the respective monomers into the molecular structure has been evidenced via matrix assisted laser desorption and ionization time-of-flight (MALDI-ToF) and nuclear magnetic resonance (NMR) measurements. The controlled oxyanionic polymerization conditions and the use of lipophilic initiators allowed for rapid access to complex amphiphilic polyethers with low polydispersity. Furthermore, the facile covalent attachment of ligands and labeling molecules due to the polyfunctionality of the PG moieties and the chemical inertness of the polymers has been confirmed via model reactions of clickable rhodamine B moieties.

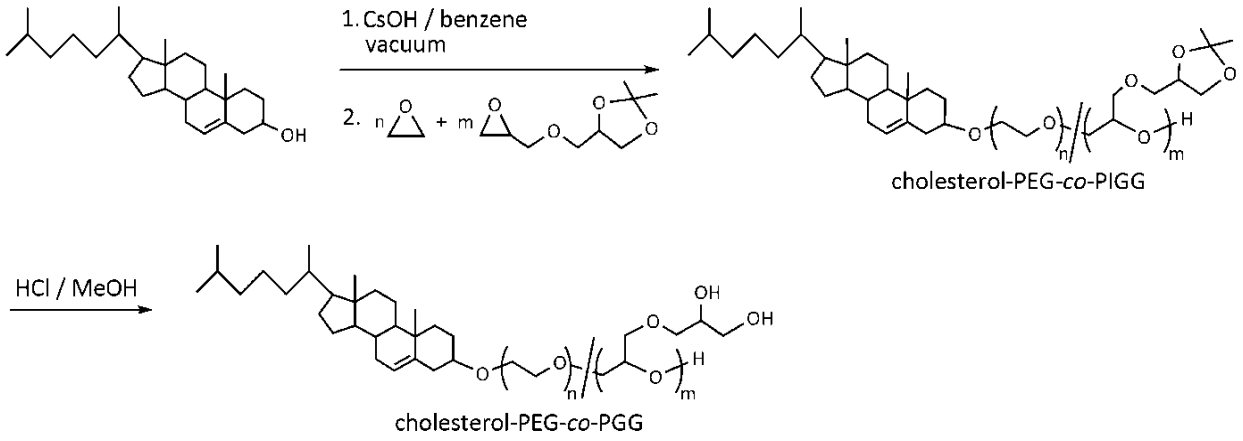

Figure 9. Reaction sequence for the synthesis of cholesterol-initiated PEG-*co*-PGG via random copolymerization of EO and IGG.

Surface modification of dioleoyl glycerol phosphocholine (DOPC) liposomes with all types of PEG-PG copolymers has been realized via the thin film hydration or extrusion method. Transmission electron microscopy (TEM) and cryo TEM as well as dynamic light scattering (DLS)

and small angle neutron scattering (SANS) experiments demonstrated the effective anchoring of the polyethers by cholesterol or long-chained bisalkyl glyceryl ethers.

Although the potential improvement of liposomal formulations and the pharmacokinetic properties of the PEG-PG liposomes have to be investigated, these polymer lipids present a promising novel type of liposome coating (Figure 10). According to earlier studies on PEG and oligo-PG as well as branched PG, the grafting of PEG-PG copolymers onto the lipid surface of liposomes might improve their medical potential by increasing their stability in *in vivo* circulation and reduces the interaction with proteins, cells and surfaces.[3, 108]

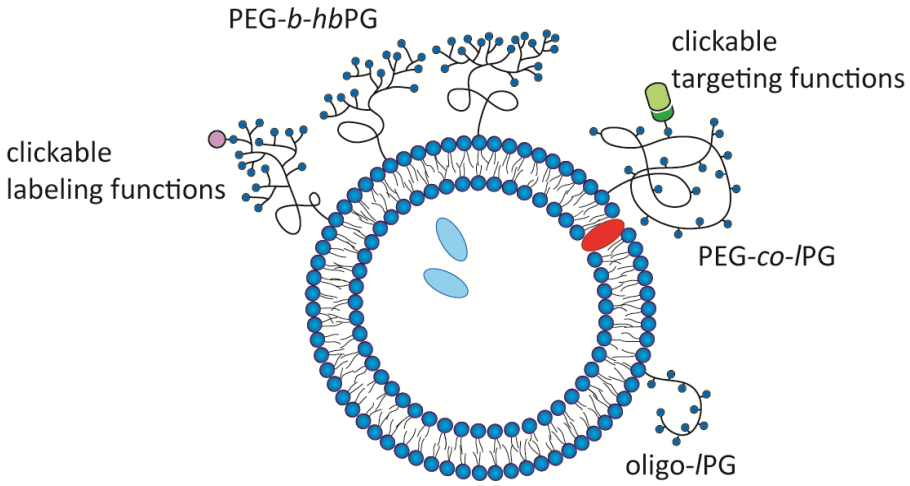

Figure 10. Schematic illustration of liposomes modified with different architectures of multifunctional PEG-PG copolymers (linear-hyperbranched block copolymers and random copolymers) or PG homopolymers with clickable labeling as well as targeting moieties.

1.9 Passive and active targeting / EPR effect

The successful approval and application of PEG-coated liposomes in cancer treatment is based on their improved pharmacokinetic properties and tissue distribution of the drug encapsulated in the lipid vesicles. This includes prolonged blood circulation times and increased accumulation of the liposomes as well as high concentrations of the released drug at the site of action. Thus, the efficacy of cancer therapies can be significantly improved by reducing the doses of aggressive xenobiotics in healthy tissue, lowering the systemic toxicity and therefore serious side effects. Due to passive targeting via enhanced permeability and retention (EPR) of long-circulating drug carrier systems at the tumor site, stealth liposomes are able to fulfill these

criteria. The morphologic anomaly of solid tumors and also infection and inflammation sites, in detail the presence of fenestrated vasculature, permits accumulation of long-circulating drug carrier systems.[126-129] Due to the rapid growth of tumor tissue, angiogenesis is defected, resulting in highly permeable blood vessels of the tumor. Furthermore, the impaired lymphatic drainage is ineffective in transport and removal of nano-size particles. Therefore, liposomes are not only able to reach the target site, but also remain there long enough in order to release the pharmaceutical agent into the tumor cells after endocytosis and degradation of the lipid vesicle. These factors significantly increase the therapeutic indices of chemotherapeutic agents in liposomal formulations.[48, 130]

Although the passive targeting of long-circulating polymer-coated liposomes allows medical treatment of solid tumors with xenobiotics and reduces their systemic toxicity, small tumors as well as metastases remain unaffected due to their lacking or reduced EPR effect.

In order to specifically address tumor tissue and increase selective cellular binding and therefore endocytosis of the drug carrier, targeting moieties have been attached onto the liposomal surface.[131] Especially for PEG-coated liposomes, nonspecific liposome-cell interactions that are crucial for the initial steps of cell uptake, are limited due to the steric barrier providing the necessary long *in vivo* circulating times. Thus, receptor-mediated endocytosis of liposomes modified with respective targeting ligands represents a promising alternative mechanism of cell adsorption. The crucial task in the effective targeting of tumors is the identification of specific receptors that are not only present but over-expressed on the surface of tumor cells, providing numerous reaction sites for the liposome-bound ligands, such that the interaction with healthy tissue is limited. Nevertheless, a high affinity of the targeting moiety towards the receptor should not reduce blood circulation times of the drug carrier. Furthermore, covalent attachment of the ligand at the liposome should allow an unhindered ligand-receptor binding, resulting in the uptake of the liposome into the target cell and the effective release of the pharmaceutical agent in high concentrations. A number of different structures such as antibodies, proteins, peptides and other small molecules have been investigated in this respect, demonstrating their targeting efficiency.[131]

Since non-specific interactions between cell surfaces and PEG-coated liposomes are reduced due to the sterical shielding of the polyether chains, uptake of the drug carrier into the cells is hindered. Thus, receptor-mediated endocytosis of stealth liposomes is a promising strategy to

improve cellular uptake and to increase the drug concentration at the target site. One of the most prominent examples for receptor-mediated delivery of xenobiotics involves the transferrin receptor (TfR) that is over-expressed on the surface of various types of tumors cells.[132, 133] The respective ligand, transferrin, is an iron carrying glycoprotein that binds to TfR in its iron-loaded state, leading to the internalization of the complex via clathrin-coated pits. In the acidic conditions of the endosome the iron ions are released into the cytoplasm while Tf/TfR complex is recycled back to the plasma membrane and unloaded Tf is released. Thus, the attachment of Tf or Tf-antibodies is employed in order to deliver anti-cancer drugs into the cytoplasm of tumor cells via TfR-mediated endocytosis. Despite the high affinity of the Tf ligand towards the ubiquitous receptor with a dissociation constant of around $K_d = 40$ nM, Tf-modulated PEG liposomes demonstrated prolonged blood circulation times and accumulation at the tumor site due to the EPR effect.

In numerous studies, the targeting efficiency of ligands based on small molecules, in particular folic acid (Figure 10) has been investigated.[131, 134-138]

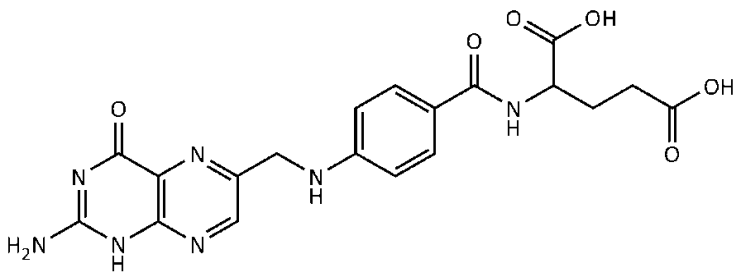

Figure 10. Molecular structure of folic acid used as a ligand for the specific targeting of tumors over-expressing folate receptors on their cell surfaces.

Regular cellular transport of folate is mediated by the reduced folate carrier with a relatively low dissociation constant in the µM range. In comparison to that, the affinity for folate of the folate receptor (FR) is significantly increased. Furthermore, the high-affinity FR is present on the cell surfaces of various types of human tumors, i.e., ovarian cancer cells while cell surfaces of healthy tissue generally lack the FR.[139] Thus, specific targeting of PEG liposomes via folate receptor-mediated endocytosis has been achieved by the covalent attachment of folic acid onto lipids or onto PEG spacer moieties. In order to avoid steric hindrance of the ligand-receptor interaction by the polymer moiety, long PEG_{75} chains with molecular weights above 3000 g/mol are employed in most studies (Figure 11).

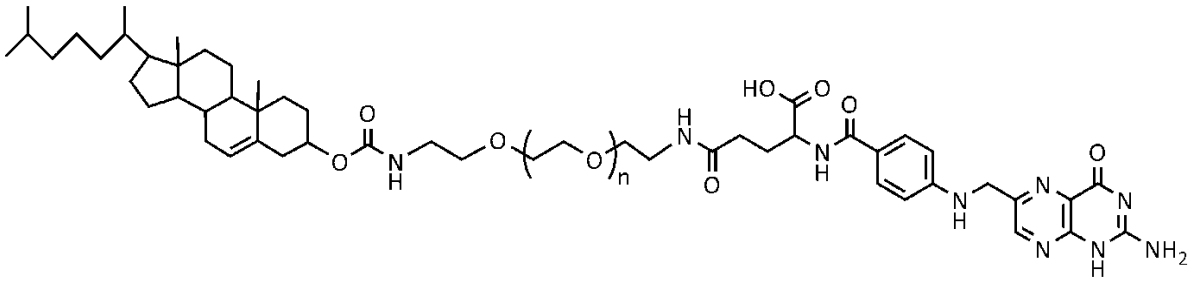

Figure 11. Molecular structure of cholesterol-PEG folate.

Long-circulating liposomes modified with cholesterol-PEG folate or phosphatidyl-PEG folate have been shown to inherit fast internalization and surface recycling rates in cancer cells.[140] Thus, high doses of anticancer agents can be delivered to the site of action due to accumulation of liposomes into the tumor tissue via the EPR effect and rapid internalization via FR-mediated endocytosis.

1.10 Sterically stabilized liposomes in clinical applications

The improvement of pharmacokinetics and biodistribution of chemotherapeutics encapsulated in long-circulating liposomes has resulted in numerous clinical investigations and the approval of different formulations.[4, 131]

In particular, PEGylated liposomal formulations including the drug doxorubicin (DOX) has been studied extensively. The anthracycline antibiotic doxorubicin is a hydroxylated derivative of the natural product daunomycin (Figure 12). The medical applications are commonly focused on the treatment of leukemia, lymphoma as well as cancers in lung, ovaries and breast. The systemic doses of DOX is mainly limited due to its acute and cumulative cardiotoxicity, which has been improved by its encapsulation in liposomes as well as stealth (PEG) liposomes.[141] The enhanced accumulation of the liposomes and the decreased cardiotoxicity strongly improved the therapeutic index of DOX, resulting in revised treatments of ovarian and breast cancer.[142-144] Furthermore, in patient studies with the PEGylated liposomal formulations of doxorubicin (Doxil) for the treatment of HIV-associated Kaposi's sarcoma, the efficacy of the therapy exceeds other methods due to improved pharmacokinetics based on the EPR effect. Thus, Doxil has been the first stealth liposome based drug approved for clinical use in the USA and Europe for the treatment of recurrent ovarian and breast cancer as well as Kaposi's sarcoma.[145-148]

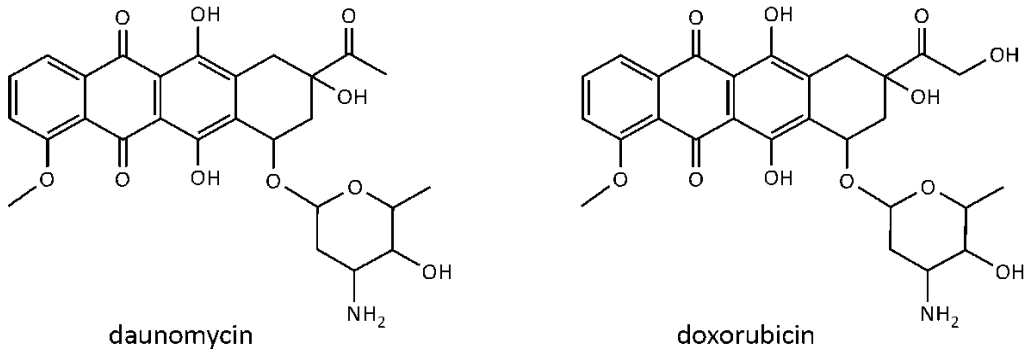

Figure 12. Chemical structures of the anthracyclines daunomycin and its 14-hydroxy derivative doxorubicin.

Table 1. Drugs in conventional and PEGylated liposomal formulations approved for clinical use.

Formulation	Drug	Product name	Company	Indication
conventional liposomes	amphotericin	Ambisome	Astellas Pharma	fungal infections in immuno-compromised patients visceral leishmaniasis
	cytosine arabinoside (cytarabine)	DepoCyt	Skye Pharma	lymphomatous meningitis
	daunomycin	DaunoXome	Gilead	Kaposi's sarcoma
	doxorubicin	Myocet/Evacet	Elan	recurrent breast cancer
	vincristine	Marqibo	Hana Biosciences	non-Hodgkin's lymphoma
PEG liposomes	doxorubicin	Doxil/Caelyx	Alza Johnson&Johnson Schering Plough	Kaposi's sarcoma recurrent breast cancer ovarian cancer multiple myeloma
	cisplatin	Lipoplatin	Regulon	several cancer types
	belotecan	Camtobell	Alza Johnson&Johnson	small cell lung cancer

Intensive research on liposomal formulations composed of neutral or negatively charged phospholipids and cholesterol allowed clinical studies with different active compounds

encapsulated.

Especially in the field of cancer treatment, clinical trials focused on conventional and long-circulating liposomes coated with poly(ethylene glycol) chains have resulted in a number of effective therapies with different pharmaceutical agents, such as the fungicide amphotericin or different xenobiotics, i.e., daunomycin, doxorubicin, cisplatin and so on. A series of liposomal drug formulations for a range of indications have been approved for the clinical use and are available on the market (Table 1).

1.11 Conclusion

Since the first observation of liposomal structures roughly 40 years ago, they have developed to effective drug delivery systems with numerous unique properties. In particular, the incorporation of synthetic polymers such as poly(ethylene glycol) (PEG) improved performances of liposomal formulations. The formation of a protective layer around the drug carrier leads to reduced blood clearance and changes in tissue distribution, mainly due to longer blood circulation times and enhanced accumulation and retention (EPR) at the tumor site. Based on its capability to significantly improve therapeutic indices, biodistributions and pharmacokinetics of various drugs, liposomal drug delivery remains a promising instrument especially in cancer treatment.

Thus, a multitude of clinical investigations have been and are focused on the encapsulation of xenobiotics or other drugs in PEG liposomes reducing systemic toxicity and side reactions. Furthermore, PEG-coated liposomes have been approved for clinical treatment of different diseases including recurrent ovarian and breast cancer as well as HIV-related Kaposi's sarcoma. Nevertheless, the synthesis and characterization of novel polymers offering similar stealth properties as PEG but additional features like biodegradability, polyfunctionality or clickable targeting and labeling moieties remain one key task in the field of liposome research. In this respect, amphiphilic polymeric structures based on poly(ethylene glycol) and polyglycerol represent a promising class of novel multifunctional polyether lipids. Especially the development of effective targeting of sterically stabilized liposomes that allow the specific application of drugs in sufficient concentrations to the site of action is one of the main goals. In the growing field of liposome research, liposomal formulations have been emerged for various therapeutic and imaging applications including the encapsulation of hemoglobin, peptides,

proteins, magnetic particles, DNA and siRNA.

With regard to the advantages and multiple possibilities of liposomal drug delivery, novel liposome-based therapies and diagnostic techniques will be developed and approved to clinical use in the near future.

Since this introduction has been prepared as a review article for Advances in Polymer Science, some of the materials and studies presented in the previous chapter have been objectives of the current thesis and will be discussed in detail in the following chapters.

Abbreviations

BPTI	bovine pancreatic trypsin inhibitor
DLS	dynamic light scattering
DOX	doxorubicin
DPPE	dipalmitoyl phosphatidyl ethanolamine
DSPC	distearoyl phosphatidyl choline
EEGE	ethoxyethyl glycidyl ether
EO	ethylene oxide
EPR	enhanced permeability and retention
FR	Folate receptor
*hb*PG	hyperbranched polyglycerol
HDL	high density lipoprotein
HSA	human serum albumin
IGG	isopropylidene glycidyl glyceryl ether
LDL	low density lipoprotein
*l*PG	linear polyglycerol
LUV	large unilamellar vesicle
MALDI-ToF	matrix assisted laser desorption and ionization time-of-flight
MLV	multilamellar large vesicle
MPEG	poly(ethylene glycol) monomethyl ether
MPS	mononuclear phagocytic system
NBD	nitrobenzoxadiazole
NMR	nuclear magnetic resonance
PAA	poly(acrylic acid)
PC	phosphatidyl choline
PE	phosphatidyl ethanolamine
PEG	poly(ethylene glycol)
PHEG	poly(hydroxyethyl-L-glutamine)
PPO	poly(propylene oxide)
PVA	poly(vinyl alcohol)
Rh-OVA	Rhodamine-ovalbumin
ROP	ring-opening polymerization
SANS	small angle neutron scattering
SDS-PAGE	sodium dodecyl poly(acryl amid) gel electrophoresis
SUV	small unilamellar vesicle
TEM	transmission electron microscopy
Tf	transferrin
TfR	transferrin receptor

References

(1) Lasic, D. D.; Papahadadjopoulos, D. *Science* **1995**, *267*, 1275-1276.

(2) Allen, T. M.; Cullis, P. R. *Science* **2004**, *303*, 1818-1822.

(3) Immordino, M. L.; Dosio, F.; Cattel, L. *Int. J. Nanomed.* **2006**, *1*, 297-315.

(4) Torchilin, V. P. *Nat. Rev. Drug Discovery* **2005**, *4*, 145-160.

(5) Petros, R. A.; DeSimone, J. M. *Nat. Rev. Drug Discov.*, *9*, 615-627.

(6) Sessa, G.; Weissmann, G. *J. Lipid Res.* **1968**, *9*, 310-318.

(7) Martin, F.; Boulikas, T. *Gene Ther. Mol. Biol.* **1998**, *1*, 173-214.

(8) Owens, D. E.; Peppas, N. A. *Int. J. Pharm.* **2006**, *307*, 93-102.

(9) Frank, M.; Fries, L. *Immunol. Today* **1991**, *12*, 322-326.

(10) Gref, R.; Minamitake, Y.; Peracchia, M. T.; Trubetskoy, V.; Torchilin, V.; Langer, R. *Science* **1994**, *263*, 1600-1603.

(11) Scherphof, G. L.; Kamps, J. A. A. M. *Adv. Drug Deliv. Rev.* **1998**, *32*, 81-97.

(12) Ishida, T.; Harashima, H.; Kiwada1, H. *Bioscience Reports* **2002**, *22*, 197-224.

(13) Yan, X.; Scherphof, G. L.; Kamps, J. A. A. M. *J Liposome Res.* **2005**, *15*, 109-139.

(14) Devine, D. V.; Marjan, J. M. *Crit. Rev. Ther. Drug. Carrier Syst.* **1997**, *14*, 105-131.

(15) Semple, A.; Chonn, A.; Cullis, P. R. *Adv. Drug Deliv. Rev.* **1998**, *32*, 3-13.

(16) Moghimi, S. M.; Patel, H. M. *Adv. Drug Deliv. Rev.* **1998**, *32*, 45-60.

(17) Patel, H. M. *Crit. Rev. Ther. Drug Carrier Syst.* **1992**, *9*, 39-90.

(18) Rodrigueza, W. V.; Phillips, M. C.; Williams, K. J. *Adv. Drug Deliv. Rev.* **1998**, *32*, 31-43.

(19) Funato, K.; Yoda, R.; Kiwada, H. *Biochim. Biophys. Acta* **1992**, *1103*, 198-204.

(20) Szebeni, J.; Baranyi, L.; Savay, S.; Milosevits, J.; Bodo, M.; Bunger, R.; Alving, C. R. *Methods Enzymol.* **2003**, *373*, 136-154.

(21) *The complement system*; Johnson, R. J., Ed.; Elsevier Academic Press: Amsterdam, 2004.

(22) Harashima, H.; Sakata, K.; Funato, K.; Kiwada, H. *Pharm. Res.* **1994**, *11*, 402-406.

(23) Chonn, A.; Cullis, P. R.; Devine, D. V. *J. Immunol.* **1991**, *146*, 4234-4241.

(24) Lee, K. D.; Hong, K.; Papahadjopoulos, D. *Biochim. Biophys. Acta* **1992**, *1103*, 185-197.

(25) Singer, L.; Colten, H. R.; Wetsel, R. A. *Pathobiology* **1994**, *62*, 14-28.

(26) *Innate and adaptive immunity: the immune response to foreign materials*; Mitchell, R. N., Ed.; Elsevier Academic Press: Amsterdam, 2004.

(27) Agrawal, A. K.; Gupta, C. M. *Adv Drug Deliv Rev.* **2000**, *41*, 135-146.

(28) Basu, M. K.; Lala, S. *Curr Mol Med.* **2004**, *4*, 681-689.

(29) Ribeiro, R. R.; Moura, P. E.; Pimentel, M. V.; Sampaio, M. W.; Silva, M. S.; Schettini, A. D.; Alves, F. C.; Melo, A. F.; Tafuri, L. W.; Demicheli, C.; Melo, N. M.; Frezard, F.; Michalick, S. M. *Antimicrob. Agents Chemother.* **2008**, *52*, 2564-2572.

(30) Torrado, J. J.; Espada, R.; Ballesteros, P. M.; Torrado-Santiago, S. *J. Pharm. Sci.* **2008**, *97*, 2405-2425.

(31) Zucca, M.; Savoia, D. *Open Med Chem J.* **2011**, *5*, 4-10.

(32) Damen, J.; Regts, J.; Scherphof, G. L. *Biochim. Biophys. Acta* **1981**, *665*, 538-545.

(33) Gregoriadis, G.; Senior, J. *FEBS Lett.* **1980**, *119*, 43-46.

(34) Senior, J.; Gregoriadis, G. *FEBS Lett.* **1982**, *145*, 109-114.

(35) Proffitt, R. T.; Williams, L. E.; Presant, C. A.; Tin, G. W.; Uliana, J. A.; Gamble, R. C.; Baldeschwieler, J. D. *Science* **1983**, *220*, 502-505.

(36) Allen, T. M.; Everest, J. M. *J. Pharmacol. Exp. Ther.* **1983**, *226*, 539-544.

(37) Abra, R. M.; Hunt, C. A. *Res. Comm. Chem. Pathol. Pharmacol.* **1982**, *36*, 17-31.

(38) Senior, J.; Crawley, J. C. W.; Gregoriadis, G. *Biochim. Biophys. Acta* **1985**, *839*, 1-8.

(39) Mayer, L. D.; Tai, L. C.; Ko, D. S.; Masin, D.; Ginsberg, R. S.; Cullis, P. R.; Bally, M. B. *Cancer Res.* **1989**, *49*, 5922-5930.

(40) Mayer, L. D.; Nayar, R.; Thies, R. L.; Boman, N. L.; Cullis, P. R.; Bally, M. B. *Cancer Chemother. Pharmacol.* **1993**, *33*, 17-24.

(41) Klibanov, A. L.; Maruyama, K.; Torchilin, V. P.; Huang, L. *FEBS Lett.* **1990**, *268*, 235-238.

(42) Lasic, D. D.; Martin, F. J.; Gabizon, A.; Huang, S. K.; Papahadjopoulos, D. *Biochim. Biophys. Act.* **1991**, *1070*, 187-192.

(43) Lasic, D. D.; Needham, D. *Chem. Rev.* **1995**, *95*, 2601-2628.

(44) Needham, D.; Hristova, K.; McIntosh, T. J.; Dewhirst, M.; Wu, N.; Lasic, D. D. *J. Liposome Res.* **1992**, *2*, 411-430.

(45) Woodle, M. C.; Lasic, D. D. *Biochim. Biophys. Acta, Biomembr.* **1992**, *1113*, 171-199.

(46) Blume, G.; Cevc, G. *Biochim. Biophys. Acta, Biomembr.* **1990**, *1029*, 91-97.

(47) Allen, T. M.; Hansen, C.; Martin, F.; Redemann, C.; Yau-Young, A. *Biochim. Biophys. Acta, Biomembr.* **1991**, *1066*, 29-36.

(48) Papahadjopoulos, D.; Allen, T. M.; Gabizon, A.; Mayhew, E.; Matthay, K.; Huang, S. K.; Lee, K. D.; Woodle, M. C.; Lasic, D. D.; Redemann, C. *Proc. Natl. Acad. Sci. USA* **1991**, *88*, 11460-11464.

(49) Gabizon, A. A.; Barenholz, Y.; Bialer, M. *Pharm. Res.* **1993**, *10*, 703-708.

(50) Maruyama, K.; Yuda, T.; Okamoto, A.; Kojima, S.; Suginaka, A.; Iwatsuru, M. *Biochim. Biophys. Acta* **1992**, *1128*, 44-49.

(51) Stathopoulos, G. P.; Boulikas, T.; Vougiouka, M.; Deliconstantinos, G.; Rigatos, S.; Darli, E.; Viliotous, V.; Stathopoulos, J. G. *Oncol. Rep.* **2005**, *13*, 589-595.

(52) Zalipsky, S. *Bioconjugate Chem.* **1995**, *6*, 150-165.

(53) Allen, C.; Dos Santos, N.; Gallagher, R.; Chiu, G. N. C.; Shu, Y.; Li, W. M.; Johnstone, S. A.; Janoff, A. S.; Mayer, L. D.; Webb, M. S.; Bally, M. B. *Biosci. Rep.* **2002**, *22*, 225-250.

(54) Torchilin, V. P. *AAPS J.* **2007**, *9*, E128-E147.

(55) Roberts, M. J.; Bentley, M. D.; Harris, J. M. *Adv Drug Deliv Rev.* **2002**, *54*, 459-476.

(56) Hofmann, A. M.; Wurm, F.; Frey, H. *Macromolecules* **2011**.

(57) Hofmann, A. M.; Wurm, F.; Hühn, E.; Nawroth, T.; Langguth, P.; Frey, H. *Biomacromolecules* **2010**, 568-574.

(58) Reuter, S.; Hofmann, A. M.; Busse, K.; Frey, H.; Kressler, J. *Langmuir* **2011**, *27*, 1978-1989.

(59) Gabizon, A.; Papahadjopoulos, D. *Biochim. Biophys. Acta* **1992**, *1103*, 94-100.

(60) Blume, G.; Cevc, G. *Biochim. Biophys. Acta* **1993**, *1146*, 157-168.

(61) Banerjee, R. *J. Biomater. Appl.* **2001**, *16*, 3-21.

(62) Blume, G.; Cevc, G. *J. Liposome Res.* **1992**, *2*, 355-368.

(63) Carstensen, H.; Müller, R. H.; Müller, B. W. *Clin. Nutr.* **1992**, *11*, 289-297.

(64) Roser, M.; Fischer, D.; Kissel, T. *Eur. J. Pharm. Biopharm.* **1998**, *46*, 255-263.

(65) Senior, J.; Delgado, C.; Fisher, D.; Tilcock, C.; Gregoriadis, G. *Biochim. Biophys. Act.* **1991**, *1062*, 77-82.

(66) Du, H.; Chandaroy, P.; Hui, S. W. *Biochim. Biophys. Acta* **1997**, *1326*, 236-248.

(67) Hui, S. W.; Viswanathan, R.; Zasadzinski, J. A.; Israelachvili, J. N. *Biophys. J.* **1995**, *68*, 171-178.

(68) Efremova, N. V.; Bondurant, B.; O'Brie, D. F.; Leckband, D. E. *Biochemistry* **2000**, *39*, 3441-3451.

(69) Torchilin, V. P.; Omelyanenko, V. G.; Papisov, M. I.; Bogdanov, A. A.; Trubetskoy, V. S.; Herron, J. N.; Gentry, C. A. *Biochim. Biophys. Act.* **1994**, *1195*, 11-20.

(70) Cullis, P. R.; Chonn, A.; Semple, S. C. *Adv. Drug Deliv. Rev.* **1998**, *32*, 3-17.

(71) Price, M. E.; Cornelius, R. M.; Brash, J. L. *Biochim. Biophys. Acta* **2001**, *1512*, 191-205.

(72) Harvie, P.; Desormeaux, A.; Bergeron, M. C.; Tremblay, M.; Beauchamp, D.; Poulin, L.; Bergeron, M. G. *Antimicrob. Agents Chemother.* **1996**, *40*, 225-229.

(73) Johnstone, S. A.; Masin, D.; Mayer, L.; Bally, M. B. *Biochim. Biophys. Acta* **2001**, *1513*, 25-37.

(74) Moghimi, S. M.; Szebeni, J. *Prog. Lipid Res.* **2003**, *42*, 463-478.

(75) Santos, N. D.; Allen, C.; Doppen, A.-M.; Anantha, M.; Cox, K. A. K.; Gallagher, R. C.; Karlsson, G.; Edwards, K.; Kenner, G.; Samuels, L.; Webb, M. S.; Bally, M. B. *Biochim. Biophys. Acta* **2007**, *1768*, 1367-1377

(76) Blunk, T.; Hochstrasser, D. F.; Sanchez, J. C.; Müller, B. W.; Müller, R. H. *Electrophoresis* **1993**, *14*, 1382-1387.

(77) Needham, D.; McIntosh, T. J.; Lasic, D. D. *Biochim. Biophys. Acta, Biomembr.* **1992**, *1108*, 40-48.

(78) Kirpotin, D.; Hong, K.; Mullah, N.; Papahadjopoulos, D.; Zalipsky, S. *FEBS Lett.* **1996**, *388*, 115-118.

(79) Rupert, L. A.; Engberts, J. B.; Hoekstra, D. *Biochemistry* **1988**, *27*, 8232-8239.

(80) Kenworthy, A. K.; Hristova, K.; Needham, D.; McIntosh, T. J. *Biophys. J.* **1995**, *68*, 1921-1936.

(81) Ahl, P. L.; Bhatia, S. K.; Meers, P.; Roberts, P.; Stevens, R.; Dause, R.; Perkins, W. R.; Janoff, A. S. *Biochim. Biophys. Acta, Biomembr.* **1997**, *1329*, 370-382.

(82) Edwards, K.; Johnsson, M.; Karlsson, G.; Silvander, M. *Biophys. J.* **1997**, *73*, 258-266.

(83) Alexander, S. *J. Phys.* **1977**, *38*, 983-987.

(84) *Stabilization of colloidal dispersions by grafted polymers*; Borisov, O.; Auroy, P.; Auvray, L., Eds. London, 1995.

(85) de Gennes, P. G. *Macromolecules* **1981**, *13*, 1069-1075.

(86) Needham, D.; Kim, D. H. *Colloids Surf., B* **2000**, *18*, 183-195.

(87) Allen, T. M.; Hansen, C. *Biochim. Biophys. Acta, Biomembr.* **1991**, *1068*, 133-141.

(88) Powell, G. M. In *Handbook of water soluble gums and resins*; Davidson, R. L., Ed. McGraw-Hill, 1980.

(89) Dreborg, S.; Akerblom, E. B. *Crit Rev Ther Drug Carrier Syst.* **1990**, *6*, 315-65.

(90) Harris, J. M. *Poly(ethylene glycol) chemistry: biotechnical and biomedical applications*; Plenum Press., 1992.

(91) Abuchowski, A.; Es, T. v.; Palczuk, N. C.; Davis, F. F. *J. Biol. Chem.* **1977**, *252*, 3578-3581.

(92) *Safety of poly(ethylene glycol) and poly(ethylene glycol) derivatives*; Working, P. K.; Newman, M. S.; Johnson, J., Eds.; ACS Books: Washington, DC, 1997.

(93) Pasut, G.; Veronese, F. M. *Prog. Polym. Sci.* **2007**, *32*, 933-961.

(94) Veronese, F. M.; Pasut, G. *Drug Discov Today.* **2005**, *10*, 1451-1458.

(95) Torchilin, V. P.; Trubetskoy, V. S. *Adv. Drug Deliv. Rev.* **1995**, *16*, 141-155.

(96) Woodle, M. C. *Adv. Drug Deliv. Rev.* **1998**, *32*, 139-152.

(97) Sihorkar, V.; Vyas, S. P. *J. Pharm. Pharm. Sci.* **2001**, *4*, 138-158.

(98) Takeuchi, H.; Yamamoto, H.; Toyoda, T.; Toyobuku, H.; Hino, T.; Kawashima, Y. *Int. J. Pharm.* **1998**, *164*, 103-111.

(99) Takeuchi, H.; Kojima, H.; Yamamoto, H.; Kawashima, Y. *J. Control. Rel.* **2000**, *68*, 195-205.

(100) Takeuchi, H.; Kojima, H.; Yamamoto, H.; Kawashima, Y. *J. Control. Rel.* **2001**, *75*, 83-91.

(101) Tamer Shehata, K.-i. O., Kazutaka Higakia and Toshikiro Kimura *Int. J. Pharm.* **2008**, *359*, 272-279.

(102) Torchillin, V. P.; Shtilman, M. I.; Trubetskoy, V. S.; Whiteman, K.; Milsten, A. M. *Biochim. Biophys. Acta* **1994**, *1195*, 181-184.

(103) Kono, K.; Nakai, R.; Morimoto, K.; Takagishi, T. *Biochim. Biophys. Acta* **1999**, *1416*, 239-250.

(104) Metselaar, J. M.; Bruin, P.; Boer, L. W. T. d.; Vinger, T. D.; Snel, C.; Oussoren, C.; Wauben, M. N. M.; Crommelin, D. J. A.; Storm, G.; Hennink, W. E. *Bioconjugate Chem.* **2003**, *14*, 1156-1164.

(105) Woodle, M. C.; Engbers, C. M.; Zalipsky, S. *Bioconjug. Chem.* **1994**, *5*, 493-496.

(106) Maruyama, K.; Okuizumi, S.; Ishida, O.; Yamauchi, H.; Kikuchi, H.; Iwatsuru, M. *Int. J. Pharm.* **1994**, *111*, 103-107.

(107) Yang, S. F.; Free, S.; Benson, A. *J. Biol. Chem.* **1967**, *242*, 477-484.

(108) Ishiharaa, A.; Yamauchia, M.; Kusanoa, H.; Mimuraa, Y.; Nakakuraa, M.; Kamiyab, M.; Katagirib, A.; Kawanob, M.; Nemotob, H.; Suzawac, T.; Yamasakid, M. *Int. J. Pharm.* **2010**, *391*, 237-243.

(109) Nemoto, H.; Kikunishi, J.; Yanagiya, S.; Kawano, T.; Yamada, M.; Harashima, H.; Kiwada, H.; Shibuya, M. *Bioorg. Med. Chem. Lett.* **1999**, 205-208.

(110) Yamaguchi, H.; Suzawa, T.; Araki, T.; Kamiya, M.; Nemoto, H.; Yamasaki, M. *Biochim. Biophys. Acta* **2008**, *1780*, 680-686.

(111) Nemoto, H.; Araki, T.; Kamiya, M.; Kawamura, T.; Hino, T. *Eur. J. Org. Chem.* **2007**, *18*, 3003-3011.

(112) Sadzuka, Y.; Sugiyama, L.; Tsuruda, T.; Sonobe, T. *Int. J. Pharm.* **2006**, *312*, 83-89.

(113) Thompson, M. S.; Vadala, T. P.; Vadala, M. L.; Lin, Y.; Riffle, J. S. *Polymer* **2008**, *49*, 345-373.

(114) Wilms, D.; Stiriba, S.-E.; Frey, H. *Acc. Chem. Res.* **2010**, *43*, 129-141.

(115) Kainthan, R. K.; Janzen, J.; Levin, E.; Devine, D. V.; Brooks, D. E. *Biomacromolecules* **2006**, *7*, 703-709.

(116) Kainthan, R. K.; Janzen, J.; Kizhakkedathu, J. N.; Devine, D. V.; Brooks, D. E. *Biomaterials* **2008**, *29*, 1693-1704.

(117) Calderón, M.; Quadir, M. A.; Sharma, S. K.; Haag, R. *Adv. Mater.*, *22*, 190-218.

(118) Nguyen, P. M.; Hammond, P. T. *Langmuir* **2006**, *22*, 7825.

(119) Gitsov, I.; Wooley, K. L.; Hawker, C. J.; Ivanova, P. T.; Fréchet, J. M. J. *Macromolecules* **1993**, *26*, 5621.

(120) Istratov, V.; Kautz, H.; Kim, Y.-K.; Schubert, R.; Frey, H. *Tetrahedron* **2003**, *59*, 4017-4024.

(121) Demina, T.; Grozdova, I.; Krylova, O.; Zhirnov, A.; Istratov, V.; Frey, H.; Kautz, H.; Melik-Nubarov, N. *Biochemistry* **2005**, *44*, 4042-4054.

(122) Barriau, E.; Marcos, A. G.; Kautz, H.; Frey, H. *Macromol. Rapid Commun.* **2005**, *26*, 862.

(123) Wurm, F.; Klos, J.; Räder, H. J.; Frey, H. *J. Am. Chem. Soc.* **2009**, *131*, 7954-7955.

(124) Wurm, F.; Nieberle, J.; Frey, H. *Macromolecules* **2008**, *41*, 1909-1911.

(125) Wurm, F.; Nieberle, J.; Frey, H. *Macromolecules* **2008**, *41*, 1184-1188.

(126) Roberts, W. G.; Palade, G. E. *Cancer Res.* **1997**, *57*, 765-772.

(127) Dvorak, H.; Nagy, J.; Dvorak, J.; Dvorak, A. *Am. J. Pathol.* **1988**, *133*, 95-109.

(128) Matsumura, Y.; Maeda, H. *Cancer Res.* **1986**, *46*, 6387-6392.

(129) Thanou, M.; Duncan, R. *Curr Opin Investig Drugs* **2003**, *4*, 701-709.

(130) Gabizon, A. *J. Liposome Res.* **2003**, *13*, 17-20.

(131) Wang, M.; Thanou, M. *Pharm. Res.* **2010**, *62*, 90-99.

(132) Jones, A. T.; Gumbleton, M.; Duncan, R. *Adv. Drug Deliv. Rev.* **2003**, *55*, 1353-1357.

(133) Widera, A.; Norouziyan, F.; Shen, W.-C. *Adv. Drug Deliv. Rev.* **2003**, *55*, 1439-1466.

(134) Lee, R. J.; Low, P. S. *J. Biol. Chem.* **1994**, *269*, 3198-3204.

(135) Wang, X.; Li, J.; Wang, Y.; Cho, K. J.; Kim, G.; Gjyrezi, A.; Koenig, L.; Giannakakou, P.; Shin, H. J. C.; Tighiouart, M.; Nie, S.; Chen, Z.; Shin, D. M. *ACS Nano* **2009**, *3*, 3165-3174.

(136) Goren, D.; Horowitz, A. T.; Tzemach, D.; Tarshish, M.; Zalipsky, S.; Gabizon, A. *Clin. Cancer Res.* **2000**, 1949-1957.

(137) Pan, X.; Lee, R. J. *Expert Opin. Drug Deliv.* **2004**, 7-17.

(138) Lu, Y.; Low, P. S. *Adv. Drug Deliv. Rev.* **2002**, *54*, 675-693.

(139) Weitman, S. D.; Lark, R. H.; Coney, L. R.; Fort, D. W.; Frasca, V.; Zurawski, V. R. J.; Kamen, B. A. *Cancer Res* **1992**, *52*, 3396-3401.

(140) Paulos, C. M.; Reddy, J. A.; Leamon, C. P.; Turk, M. J.; Low, P. S. *Mol. Pharm.* **2004**, *66*, 1406-1414.

(141) Treat, J.; Greenspan, A.; Forst, D. *J. Natl. Cancer Inst.* **1990**, *82*, 1706-1710.

(142) Straubinger, R. M.; Lopez, N. G.; Debs, R. J.; Hong, K.; Papahadjopoulos, D. *Cancer Res.* **1988**, *48*, 5237-5245.

(143) Robert, N. J.; Vogel, C. L.; Henderson, I. C. *Semin. Oncol.* **2004**, *31*, 106-146.

(144) Hamilton, A.; Biganzoli, L.; Coleman, R. *Ann. Oncol.* **2002**, *13*, 910-918.

(145) Rose, P. G. *Oncologist* **2005**, *10*, 205-214.

(146) Krown, S. E.; Northfelt, D. W.; Osoba, D. *Semin. Oncol.* **2004**, *31*, 36-52.

(147) Perez, A. T.; Domenech, G. H.; Frankel, C.; Vogel, C. L. *Cancer Invest.* **2002**, *20*, 22-29.

(148) O'Shaughnessy, J. A. *Clin. Breast Cancer* **2003**, *4*, 318-328.

Chapter 2.1: Hyperbranched polyglycerol-based lipids via oxyanionic polymerization: Toward multifunctional stealth liposomes

Chapter 2.1:

Hyperbranched polyglycerol-based lipids via oxyanionic polymerization: Toward multifunctional stealth liposomes

Anna Maria Hofmann,[1] Frederik Wurm,[1] Eva Hühn,[2] Thomas Nawroth,[2] Peter Langguth,[2] and Holger Frey*,[1]

1 Institute of Organic Chemistry, Johannes Gutenberg-Universität, Duesbergweg 10-14, Mainz, Germany

2 Institute of Pharmacy and Biochemistry, Johannes Gutenberg-Universität, Staudingerweg 5, Mainz, Germany.

Published in Biomacromolecules, 2010, 11 (3), 568-574.

Abstract

We describe the synthesis of linear-hyperbranched lipids for liposome preparation based on linear poly(ethylene glycol) (PEG) and hyperbranched polyglycerol (PG). Molecular weights were adjusted to values around 3000 g/mol with varying degrees of polymerization of the linear and the branched segments in analogy to PEG-based stealth lipids; polydispersities were generally low and below 1.3. The hydrophobic anchors were introduced into the lipid structures as initiators for the anionic polymerization of ethylene oxide and are either based on cholesterol or on different aliphatic glyceryl ethers. Complete incorporation of the apolar initiators was evidenced by MALDI-ToF analysis at all stages of the reaction. The linear-hyperbranched polyether lipid is incorporated as the polyfunctional shell in liposome formulations together with 1,2-dioleoyl-*sn*-glycero-3-phosphocholine (DOPC). The resulting liposomes were subsequently characterized via dynamic light scattering (DLS) and small angle neutron scattering (SANS) as well as transmission electron microscopy (TEM), demonstrating the formation of unilamellar liposomes in the size range of 40 to 50 nm.

Keywords

liposome, stealth-effect, poly(ethylene oxide), polyglycerol, block copolymers, lipids

Introduction

In the field of drug-delivery systems, liposomes represent an advanced technology to transport therapeutic drugs to the site of action and reduce harmful toxic effects on healthy tissues. Vesicles based on phospholipids can passively target tissues with discontinuous endothelium such as liver, spleen, and bone marrow. If the target site is beyond the mononuclear phagocyte system (MPS), the removal of liposomes from the blood circulation by macrophages after binding of opsonins to the vesicle surface is one of the main disadvantages for conventional liposomal drug delivery systems.[1]

Grafting of poly(ethylene glycol) (PEG) on the surface of colloidal carriers results in the so-called "stealth liposomes". This strategy has been shown to prevent the adsorption of certain serum components due to the physical properties of the PEG-chains, such as high water solubility, large excluded volume, and high degree of conformational entropy.[2–5] Thus, liposomes with PEG-corona provide several advantages, such as strongly reduced mononuclear phagocyte system (MPS) uptake, prolonged blood circulation time, reduced aggregation of the PEGylated vesicles and improved stability of the liposomal formulations.[1,6–9]

Research on such stealth liposomes has resulted in a large number of approved and employed formulations, especially in the field of cancer treatment, due to their passive targeting effect. The morphologic anomaly of solid tumors permits accumulation of long-circulating drug carrier systems (enhanced permeability and retention (EPR) effect).[10,11]

One disadvantage of these well known and widely used PEGylation strategies is the lack of additional functional groups in the polymer chain attached to the lipid structures, which could be used for further derivatization. To covalently bind PEG to lipids, targeting groups or markers with different active functionalities have to be introduced by functional initiation or termination of the anionic ring-opening polymerization (ROP) of ethylene oxide or by additional modification of the terminal OH group.[12] In addition to PEG that has been applied in a large number of liposomal formulations in medical treatments for almost two decades, hyperbranched polyglycerol (*hb*PG) shows excellent biocompatibility comparable to PEG,[13–16]

but, in addition, offers possibilities for further functionalization due to its polyfunctionality and exhibits an even higher water-solubility. Surface modification of liposomes with block copolymers based on PEG-*hb*PG might improve their medical potential by increasing their stability in interactions with tissues, cells, and surfaces due to the bulky hyperbranched shield, by specific targeting of nanoparticles as well as by the preservation of loading agent content during storage. Based on multistep approaches, numerous linear polymers with dendrimer blocks have been synthesized. However, to date, only a few works have described the preparation of linear-hyperbranched block structures.[17–24]

In this article, we describe the generation of a new type of liposomes bearing lipids based on linear-hyperbranched polyether block copolymers (see Figure 1).

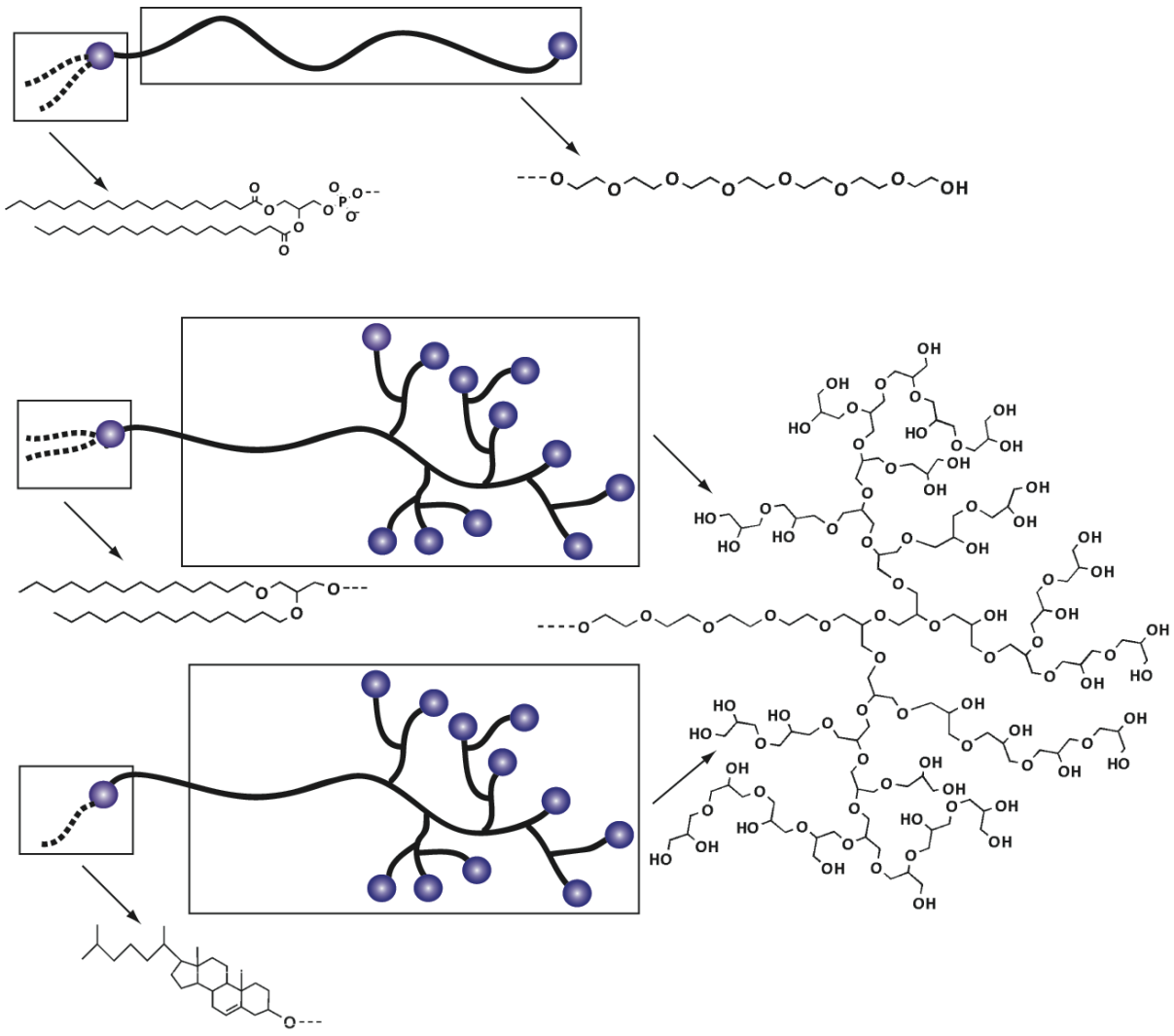

Figure 1. Schematic and chemical structures of a common PEG-lipid (top) and PEG-*hb*PG-lipids based on 1,2-bis-*n*-tetradecyl glyceryl ether (middle) and cholesterol (bottom).

The combined oxyanionic polymerization of different epoxide monomers[25–27] and the use of lipophilic initiators permits the controlled synthesis of lipids with complex polyether structure and low polydispersity (<1.3). Due to the composition of the PEG-*hb*PG block copolymers consisting of mere polyether structures, potentially toxic moieties or initiators are avoided, that is, maximum biocompatibility is achieved.

The novel amphiphilic structures have been introduced into liposome formulations with 1,2-dioleoyl-*sn*-glycero-3-phosphocholine (DOPC), and the resulting liposome structures have been characterized via dynamic light scattering (DLS) and small angle neutron scattering (SANS) as well as transmission electron microscopy (TEM).

Experimental section

Instrumentation. ^{1}H nuclear magnetic resonance (NMR) spectra were recorded using a Bruker AC 300 spectrometer operated at 300 MHz, employing $CDCl_3$ and DMSO-d_6 (dimethyl sulfoxide) as solvents. ^{13}C NMR spectra (referenced internally to solvent signals) were recorded at 100.15 MHz.

FT-IR spectra were recorded on a Nicolet SDXC FT-IR spectrometer equipped with an ATR unit.

SEC measurements were carried out in dimethylformamide (DMF) containing 1 g/L of lithium bromide. An Agilent 1100 Series GPC setup (gel permeation chromatography) was used as an integrated instrument, including a PSS HEMA column (106/105/104 g/mol) and a UV (254 nm) and RI detector. Calibration was achieved using poly(ethylene glycol) standards provided by Polymer Standards Service. The eluent was used at 50 °C and at a flow rate of 1 mL/min.

Matrix-assisted laser desorption and ionization time-of-flight (MALDI-ToF) measurements were performed on a Shimadzu Axima CFR MALDI-ToF mass spectrometer equipped with a nitrogen laser delivering 3 ns laser pulses at 337 nm. Sinapinic acid (SA, 3,5-dimethoxy-4-hydroxy-cinnamic acid) or R-cyano-3-hydroxycinnamic acid (CHCA) were used as matrices. Samples were prepared by dissolving the polymer in methanol at a concentration of 10 g/L. A 10 μL aliquot of this solution was added to 10 μL of a 10 g/L solution of the matrix and 1 μL of a solution of potassium trifluoro acetate (KTFA; 0.1 M in methanol as cationization agent). A 1 μL aliquot of the mixture was applied to a multistage target, methanol evaporated, and a thin matrix/analyte

film was created. The samples were measured in positive ion and in reflection mode of the spectrometer.

All electron microscopy measurements were performed using a transmission electron microscope (FEI, XM12) with an acceleration voltage of 120 kV.

Small angle neutron scattering (SANS) experiments were performed at the Institute Laue-Langevin (ILL) in Grenoble using the D11 instrument. Three sample/detector distances (1.2, 8.0, and 34.0 m) with the neutron wavelength λ = 6 Å were selected to cover an effective *q* range (between 1.63 × 10-3 $Å^{-1}$ and 5.06 × 10-1 $Å^{-1}$). Standard corrections, cell subtraction, and normalization to absolute scattering units were performed using ILL SANS routines. Dynamic light scattering (DLS) measurements were performed on a ProSpecD 501 photon correlation spectrometer (Nanomed) with a HeNe laser (5.1 mW) at a scattering angle of 170° with ALV-correlator and ALV DLS software 3.0.

Reagents. All reagents and solvents were purchased from Acros and used as received, unless otherwise mentioned. Cholesterol was purchased from Fluka and stored at 4 °C. DOPC was purchased from Sigma-Aldrich. Dry solvents stored over molecular sieves were purchased from Fluka. Deuterated $CDCl_3$ and DMSO-d_6 were purchased from Deutero GmbH, dried, and stored over molecular sieves.

Isopropylidene glyceryl glycidyl ether (IGG) was prepared as described in literature,[25] dried over CaH_2, and freshly distilled before use. ^{1}H NMR (300 MHz, $CDCl_3$): δ (ppm) 4.3 (m, 1H, CH acetal), 4.07 (m, 1H), 3.88-3.39 (m, 6H), 3.17 (m, 1H), 2.81 (t, 1H, CH_2 epoxide), 1.44 (s, 3H, CH_3), 1.38 (s, 3H, CH_3). Glycidol (99% Acros) was purified by distillation from CaH_2 directly prior to use.

Synthesis: Polymerizations. (a) Cholesterol was placed in a Schlenk flask and dry tetrahydrofuran (THF) was added via cryo transfer. A solution of potassium naphthalide in THF was added with a syringe and the mixture was stirred at room temperature for 30 min to generate the potassium alkoxide (degree of deprotonation, 90%). Ethylene oxide was cryo transferred first to a graduated ampule and then to the Schlenk flask containing the initiator solution. The mixture was allowed to warm up to room temperature, heated to 60 °C, and polymerization was performed for 12 h at 60 °C in vacuo. Subsequently, the flask was filled with argon, a sample was removed for NMR- and SEC characterization, the appropriate amount of IGG was added with a syringe, and the reaction mixture was heated to 60 °C for an additional

12 h. After removal of another sample the acetal protecting groups of the PIGG block were removed by addition of methanol, water, and acidic ion-exchange resin, stirring for 12 h at room temperature. Filtration and subsequent precipitation into cold diethyl ether resulted in the pure block copolymer that was dried in vacuo.

(b) For the polymerization of ethylene oxide and isopropylidene glyceryl glycidyl ether using 1,2-bis-*n*-alkyl glyceryl ether (cf. nos. 5-9, Table 1) the initiator was deprotonated (90%) with cesium hydroxide.[28,29] Azeotropic removal of the emerging water with benzene gave the dry cesium alkoxide, which was dissolved in dry benzene and added to a Schlenk flask filled with ethylene oxide diluted in THF. The cholesterol-initiated polymerization could be accomplished in analogous manner to the previous procedure using potassium methylate (cf. nos. 1-3, Table 1).

Linear polymers 1,2-bis-n-tetradecyl glyceryl ether-poly-(ethylene oxide). ^{1}H NMR (300 MHz, DMSO-d_6): δ (ppm) 3.78-3.27 (polyether backbone, CH_2O, CHO), 1.44 (br, CH_2CH_2O), 1.23 (br, CH_2), 0.85 (br, CH_3).

Linear block copolymers 1,2-bis-n-tetradecyl glyceryl ether-poly(ethylene oxide)-block-poly(isopropylidene glyceryl glycidyl ether). ^{1}H NMR (300 MHz, DMSO-d_6): δ (ppm) 4.15 (m, CHO acetal), 3.97 (m, CH_2O acetal), 3.78-3.22 (polyether backbone; CH_2O, CHO initiator), 1.44 (br, CH_2CH_2O initiator), 1.31-1.26 (br, CH_3 acetal), 1.23 (br, CH_2 initiator), 0.85 (br, CH_3 initiator). DP_n of PIGG was determined by comparison of methyl and methylene signals of the initiator with the signals for the PIGG block at a chemical shift of 4.15 ppm.

Deprotection to linear block copolymers. *1,2-Bis-n-tetradecyl glyceryl ether-poly(ethylene oxide)-block-poly(glyceryl glycidyl ether).* ^{1}H NMR (300 MHz, DMSO-d_6): δ (ppm) 4.54 (br, OH), 3.78-3.22 (polyether backbone; CH_2O, CHO initiator), 1.44 (br, CH_2CH_2O initiator), 1.23 (br, CH_2 initiator), 0.85 (br, CH_3 initiator).

Hypergrafting of *hb*PG-block. The macroinitiator was placed in a Schlenk flask and dissolved in THF (20 wt %). Subsequently, the appropriate amount of potassium naphthalide dissolved in THF was added and stirred for 30 min at room temperature to achieve 20% of deprotonation of the hydroxyl groups at the PGG block. After removal of the solvent in vacuo the macroinitiator was dissolved in dry diethylene glycol dimethyl ether (diglyme) (20 wt %), heated to 90 °C and a 20 wt % solution of glycidol in diglyme was added slowly with a syringe pump. The reaction was

terminated by addition of an excess of methanol and an acidic cation exchange resin. The crude product was filtrated and precipitated into cold diethyl ether. The resulting material was assimilated in methanol and dried in vacuo.

Linear-hyperbranched block copolymers 1,2-Bis-n-tetradecyl glyceryl ether-poly(ethylene oxide)-block-hyperbranched polyglycerol. ^{1}H NMR (300 MHz, DMSO-d_6): δ (ppm) 4.77-4.43 (br, OH, different signals due to hyperbranched PG), 3.77-3.22 (polyether backbone; CH_2O, CHO initiator), 1.44 (br, CH_2CH_2O initiator), 1.23 (br, CH_2 initiator), 0.85 (br, CH_3 initiator).

Liposome preparation. Liposomes consisting of DOPC and the amphiphilic PEG-*hb*PG block copolymers were prepared by the thin film hydration method under sterile conditions (clean bench). A solution of DOPC in chloroform (100 g/L) and the respective copolymer in methanol (10 g/L) were blended at a molar ratio of 98:2 and the organic solvents were removed under reduced pressure. The lipid film was hydrated with tris(hydroxymethyl)-aminomethane/citrate (tris3citrate) buffer (50 mM, pH 7.2) for liposomes characterized via neutron scattering or tris(hydroxymethyl)-aminomethane/Lu-(carboxymethylimino) bis(ethylenenitrilo)tetraacetic acid (Tris2Lu-DTPA) buffer (250 mM, pH 7.2) for liposomes analyzed by TEM to a final lipid concentration of 40 g/L. The mixture was vortexed to yield multilamellar liposomes (MLV) and briefly sonicated for 6 min under nitrogen atmosphere at 20 °C using a tip-sonifier (Bransonic, B12, 30 W/ml), which gave a suspension of small unilamellar vesicles (SUV). The liposomal suspension was then centrifuged (1300 g, 1 min) to separate SUVs from titanium and stored at 4 °C in sterile vials with Teflon/silicon seals (Chromacol).

Results and discussion

Synthesis of amphiphilic linear-hyperbranched block copolymers. Biocompatible linear-hyperbranched block copolymers consisting of PEG and *hb*PG were prepared from PEG-*b*-poly(glyceryl glycidyl ether) (PGG) precursor block copolymers, which can be obtained via sequential anionic polymerization of ethylene oxide (EO) and isopropylidene glyceryl glycidyl ether (IGG).[25,26] After deprotection of the PIGG block and partial deprotonation of the PGG block, hypergrafting of glycidol onto the alkoxide initiating sites is achieved via a slow monomer addition protocol. This approach afforded a series of narrow polydispersity (M_w / M_n < 1.3) linear-hyperbranched block structures with different chain lengths and block compositions in

which the polyfunctionality or rather the amount of hydroxyl groups of the resulting polymer was controlled by the degree of polymerization (DP_n) of glycidol.

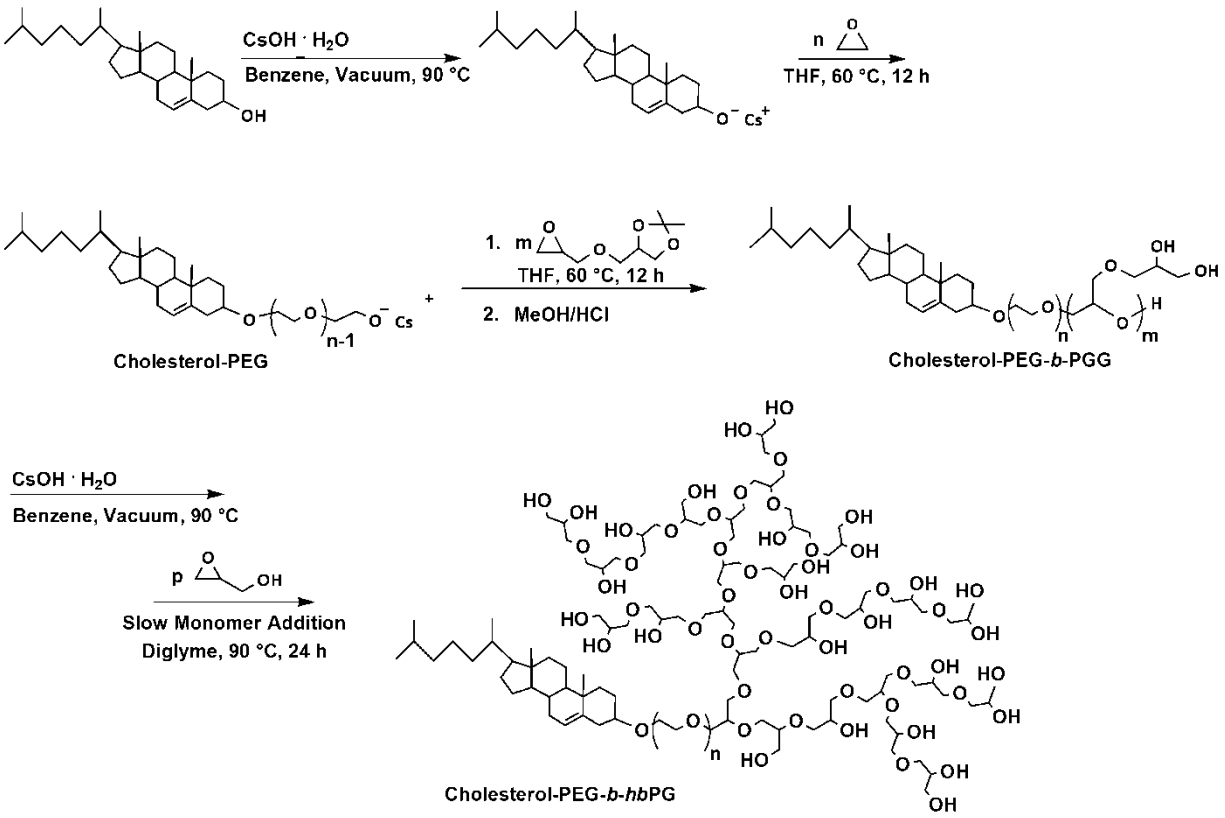

Figure 2. Reaction sequence for the synthesis of cholesterol-initiated PEG-*hb*PG block copolymer lipids.

To anchor the copolymers in liposomal membranes, we used lipophilic initiators that tolerate the strongly basic oxyanionic polymerization and acidic acetal cleavage conditions, which exclude application of commonly used phospholipids. In this manner we employed commercially available cholesterol and three different 1,2-bis-*n*-alkyl glyceryl ethers with varying lengths of the aliphatic chains (1,2-bis-*n*-tetradecyl glyceryl ether; 1,2-bis-*n*-hexadecyl glyceryl ether; 1,2-bis-*n*-octadecyl glyceryl ether) as initiators for the polymerization of ethylene oxide and isopropylidene glyceryl glycidyl ether (Figures 2 and 3). The 1,2-bis-*n*-alkyl glyceryl ether can be obtained from etherification of 1-benzyl glyceryl ether with the respective alkyl bromide and subsequent removal of the benzyl protective group via catalytic hydrogenation.[30,31] All lipophilic initiators employed lead to incorporation of the resulting copolymers in liposomal formulations. This is in line with expectations because cholesterol and

1,2-bis-*n*-alkyl glyceryl ethers are not only components of biological membranes, but have also been used to link PEG to liposomes in previous works.[32,33]

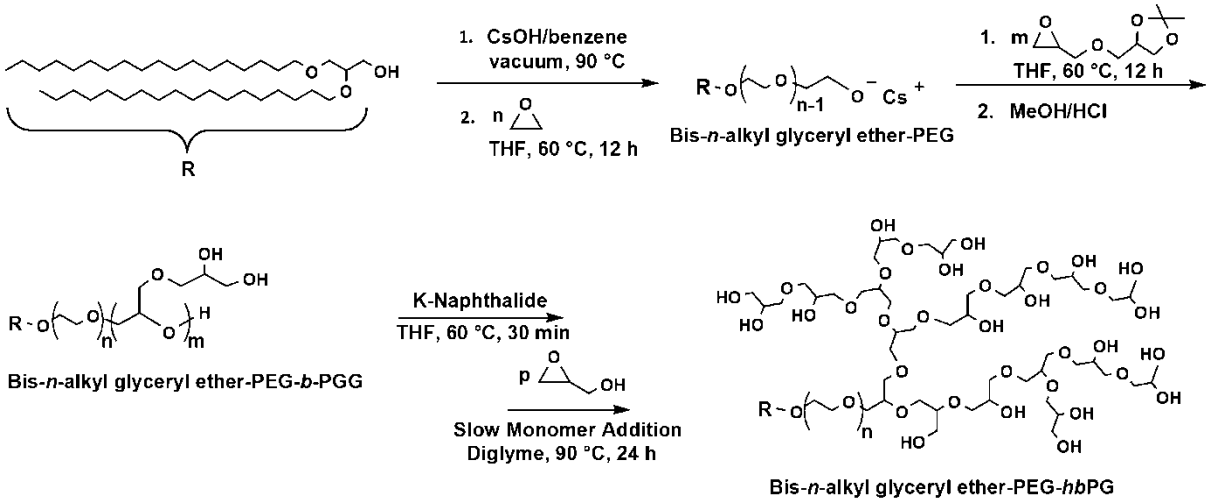

Figure 3. Reaction sequence for the synthesis of 1,2-bis-*n*-alkyl glyceryl ether-initiated PEG-*hb*PG block copolymer lipids.

In liposomes containing PEG the elongation of blood circulation times, respectively, the decrease of MPS uptake have been shown to depend not only on the amount of grafted polymer on the surface of the vesicle but also on the length of the PEG chains.[1,34,35] In view of these studies, the molecular weights of the PEG-*hb*PG block copolymers were adjusted to an overall molecular weight of 3000 g/mol to achieve sufficient protection of the liposome by a steric barrier as well as strong anchoring in the liposomal membrane. Molecular weights of linear and hyperbranched blocks were systematically varied, and narrow molecular weight distributions were obtained in all cases. By variation of the PEG-chain length, the distance between the shielding *hb*PG-block from the liposomal membrane can be adjusted very accurately. Moreover, the linear PEG block has shown very good results in protecting liposomes from binding of opsonins and other serum binding proteins and is therefore widely used not only in numerous *in vivo* studies, but also in therapeutic formulations. The characterization data of all copolymer lipids are listed in Table 1.

Based on previous works by our group, the initial syntheses were performed with CsOH as deprotonating agent leading to higher molecular weights with respect to the theoretical values due to low solubility of the respective cesium alkoxide in benzene and thus to reduced initiator/monomer ratios. Using cholesterol as an initiator, the application of potassium as a

counterion was necessary to achieve a suspension of the initiator that could be quantitatively transferred to the monomer solution in THF. Even better control over the initiator/monomer ratio was guaranteed by suspending cholesterol in THF, subsequent deprotonation with potassium naphthalide, and cryo transfer of ethylene oxide to the initiator solution.

Table 1. Characterization data of amphiphilic linear-hyperbranched block copolymers.

No.	Polymer	Initiator	M_n (th)	M_n[a]	M_n[b]	PDI[b]
1	PEG_9-*hb*PG_{30}	cholesterol[c]	2700	3000	2400	1.22
2	PEG_{22}-*hb*PG_{26}	cholesterol[c]	2700	3300	1800	1.08
3	PEG_{30}-*hb*PG_{24}	cholesterol[c]	2200	3500	2300	1.10
4	PEG_{23}-*hb*PG_{20}	cholesterol[d]	2800	2900	2700	1.22
5	PEG_{32}-*hb*PG_{21}	bistetradecyl glyceryl ether[e]	3200	3400	2000	1.29
6	PEG_{34}-*hb*PG_{16}	bistetradecyl glyceryl ether[e]	2900	3200	2500	1.05
7	PEG_{35}-*hb*PG_{25}	bishexadecyl glyceryl ether[e]	2500	3900	1500	1.10
8	PEG_{20}-*hb*PG_{20}	bisoctadecyl glyceryl ether[e]	3000	3000	1200	1.08
9	PEG_{40}-*hb*PG_{34}	bisoctadecyl glyceryl ether[e]	3100	4800	3800	1.06

[a] *M*n determined via ^{1}H NMR spectroscopy. [b] M_n and M_w determined via SEC-RI in DMF with poly(ethylene oxide) standards. [c] MeOK used as initiator. [d] Potassium naphthalide used as initiator. [e] CsOH used as initiator.

However, all of these strategies allowed good control over molecular weights and resulted in low polydispersities (M_w / M_n < 1.3) of the PEG-*hb*PG block copolymers. Comparison of the molecular weights determined via SEC in DMF using PEG standards and the molecular weights obtained from ^{1}H NMR spectroscopy (see Table 1) showed a general underestimation by SEC that can be attributed to the strong influence of the branched, globular PG block on the hydrodynamic radius of the copolymers.

Figure 4 shows the SEC traces of the PEG block initiated with cholesterol, the linear PEG-P(IGG) block copolymer before and after removal of the acetal protecting groups and the resulting

linear-hyperbranched PEG-*hb*PG block copolymer after hypergrafting of glycidol, demonstrating the narrow and monomodal weight distributions at all stages during the synthesis.

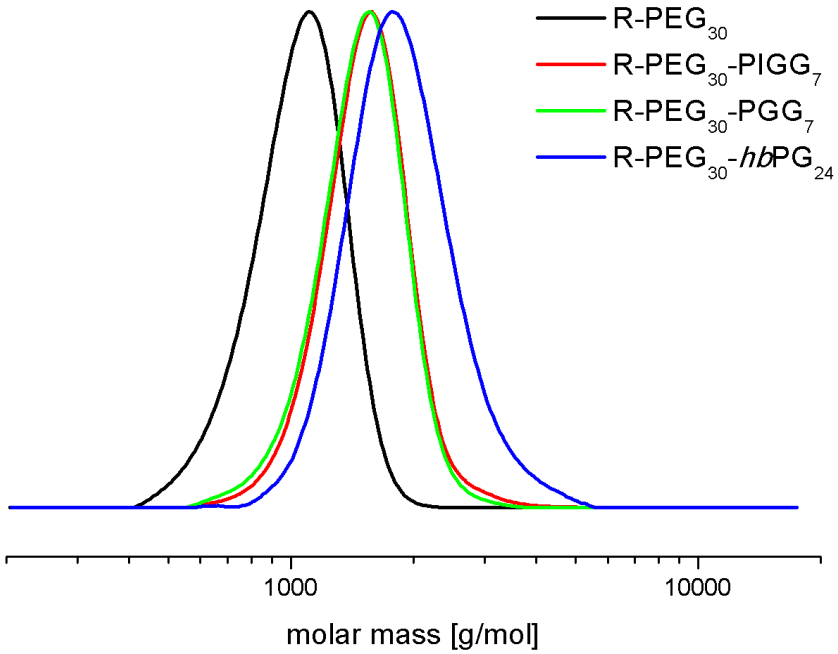

Figure 4. SEC molecular weight distribution (RI detection, PEG standards) of the linear PEG block initiated with cholesterol (R), the linear PEG-P(IGG) block copolymer, the linear PEG-PGG block copolymer after removal of the acetal protecting groups and the final linear-hyperbranched PEG-*hb*PG block copolymer (cf. entry no. 3, Table 1).

Quantitative initiation with the respective initiator and the incorporation of both monomer units in every polymer chain has been verified by MALDI-ToF spectrometry (see Figure 5).
Because the determination of molecular weights via SEC leads to underestimated values, the absolute molecular weights were calculated from ^{1}H NMR integration of the resonances for the methyl and methylene protons (1.23 ppm (CH_2), 0.85 ppm (CH_3), 1,2-bis-*n*-alkyl glyceryl ether as initiator) or the methyl protons (0.63 ppm (CH_3), cholesterol as initiator) with the polyether signals (3.78-3.27 ppm).

The DP*n* of PIGG was determined by comparison of methyl and methylene signals of the initiator with the signals for the PIGG block at a chemical shift of 4.15 ppm. As an example, the ^{1}H NMR spectra of PEG_{32}-*hb*PG_{21} (cf. no. 5, Table 1) initiated with 1,2-bis-*n*-tetradecyl glyceryl ether are shown in Figure 6.

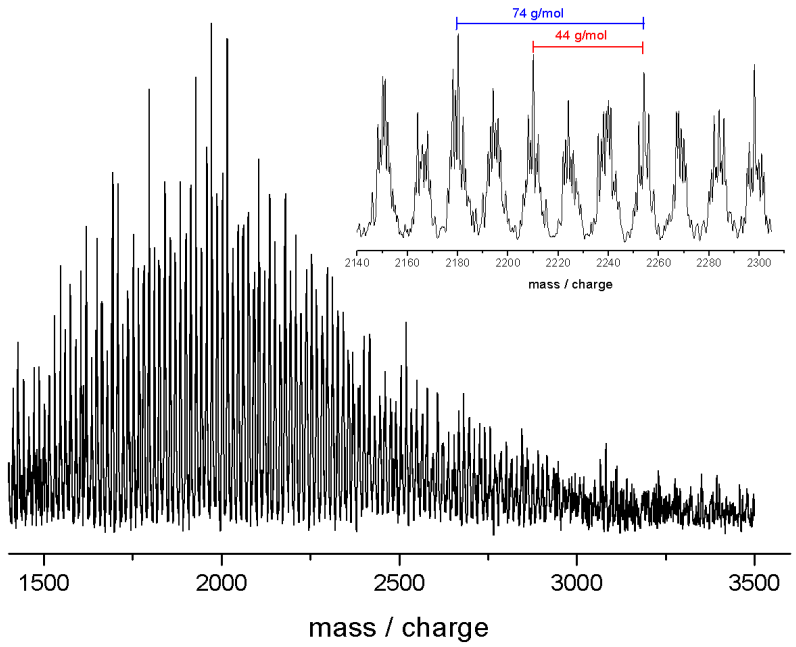

Figure 5. MALDI-ToF spectrum of a linear-hyperbranched PEG-*hb*PG block copolymer (cf. no. 3, Table 1) with cholesterol as initiator, using potassium trifluoro-acetate as an additive.

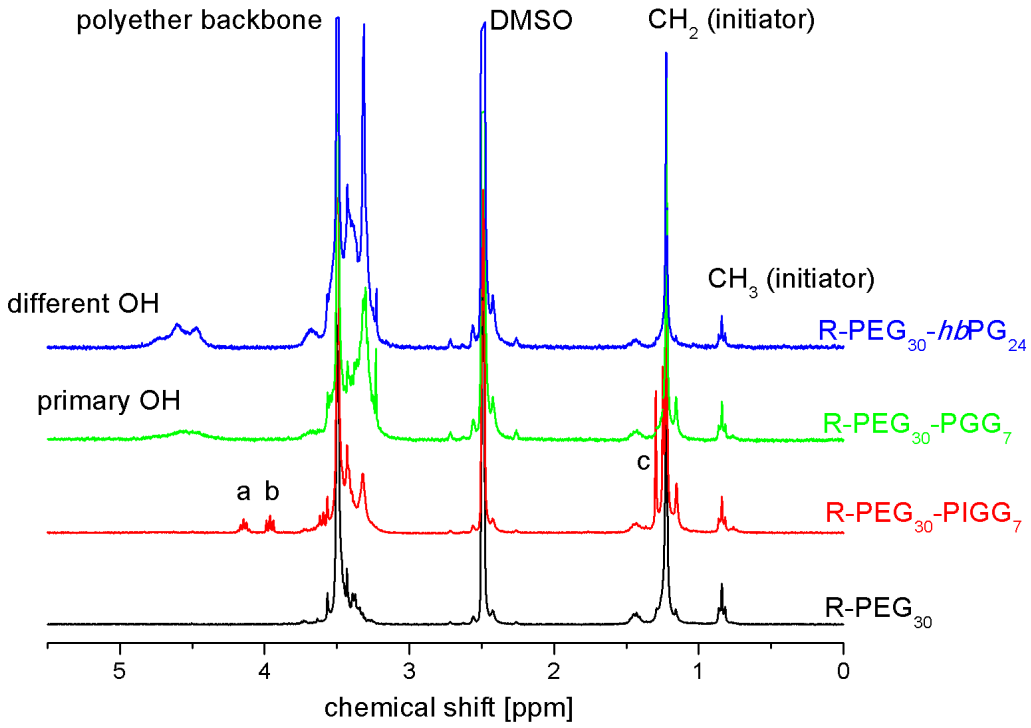

Figure 6. ^{1}H NMR spectra (300 MHz, DMSO-d_6) of different steps in the synthesis of a linear-hyperbranched PEG-*hb*PG block copolymer (cf. no. 5, Table 1) with 1,2-bis-*n*-tetradecyl glyceryl ether as initiator. Signals **a** (m, CHO acetal), **b** (m, CH_2O acetal), and **c** (br, CH_3 acetal) are characteristic.

Liposome characterization. Exploratory transmission electron microscopy (TEM) characterization and small angle neutron scattering (SANS) has been performed to demonstrate that the novel linear-branched block copolymer lipids can be incorporated into liposomes. TEM was used to visualize the shape of the lipid-polymer vesicles. Liposomes were prepared as described above using the thin film hydration method. Aqueous solutions with a lanthanide chelate as contrast agent (4 g/L, Tris2Lu-DTPA buffer (250 mM, pH 7.2)) were drop-cast onto hydrophilized copper grids and dried at room temperature before measurement.[36] TEM images in Figure 7a,b show that the lipid-polymer mixtures at a molar ratio of 98:2 form unilamellar liposomes.

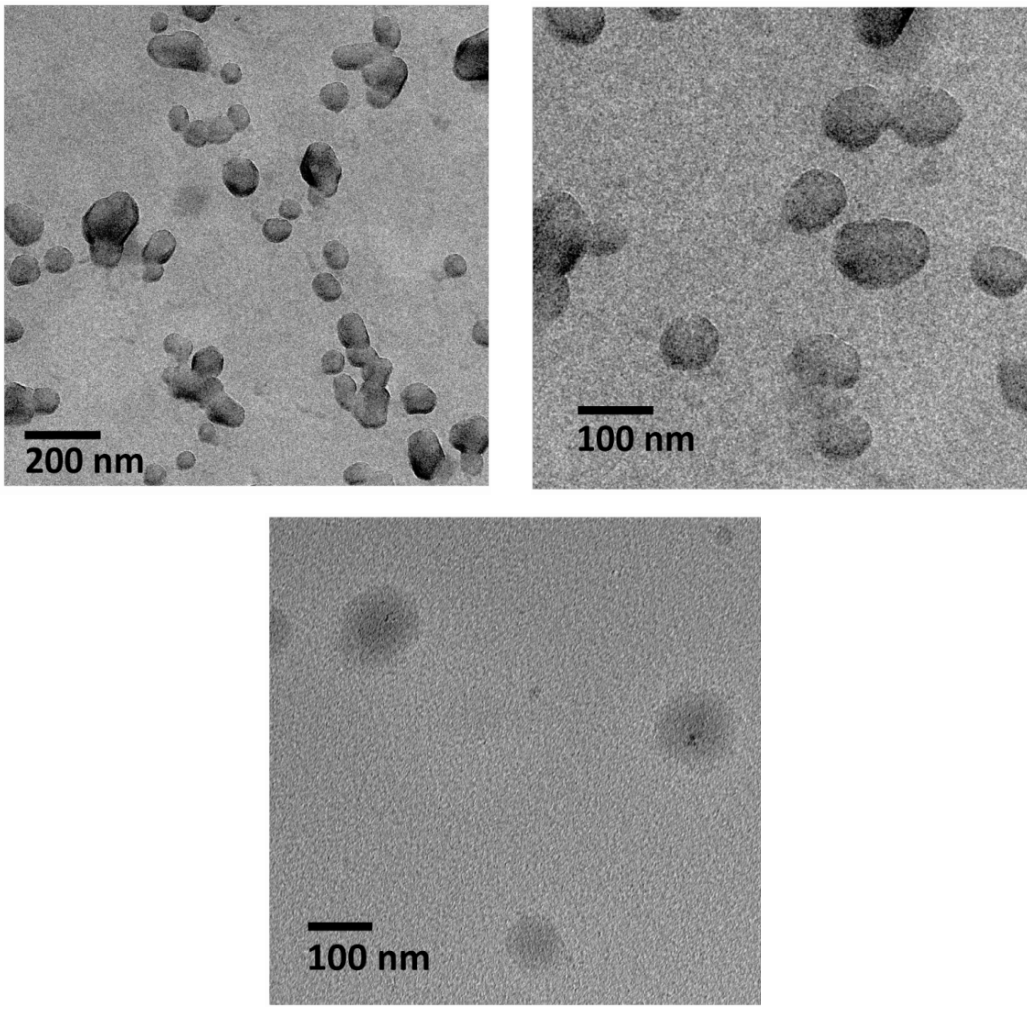

Figure 7. TEM images of liposomes consisting of DOPC (bottom) and of liposomes consisting of DOPC mixed with the amphiphilic PEG-*hb*PG block copolymers (top; cf. no. 3, Table 1). Liposomes were prepared with Tris2Lu-DTPA buffer (250 mM, pH 7.2).

The accurate size of the liposomes cannot be determined with TEM, because the aqueous suspensions were dried, leading to partial coalescence of the liposomes. In contrast to liposomes consisting of mere DOPC, liposomes based on a mixture of DOPC and the PEG-*hb*PG block copolymer lipids show dark and sharp edges in the TEM images. One may speculate that interactions of the surface hydroxyl groups with the citrate contained in the buffer solution permits improved complexation with Lu-DTPA at the surface. To determine the vesicle size of the liposome formulations size measurements were performed both with SANS and DLS. The small angle neutron scattering curve of the liposomes based on DOPC and cholesterol-PEG-*hb*PG (cf. no. 3, Table 1) at a molar ratio of 98:2 (40 g/L) is shown in Figure 8 a. The scattering profile of the liposomes shows a shoulder at $q_1 \approx 0.17$ Å^{-1}, which indicates the existence of loose aggregates of small liposomes with a membrane-membrane distance of $d = 2\pi/q_1 = 40$ Å. The radius of gyration R_g as well as the bilayer thickness d can be obtained by Guinier and Kratky-Porod plots.[37–40]

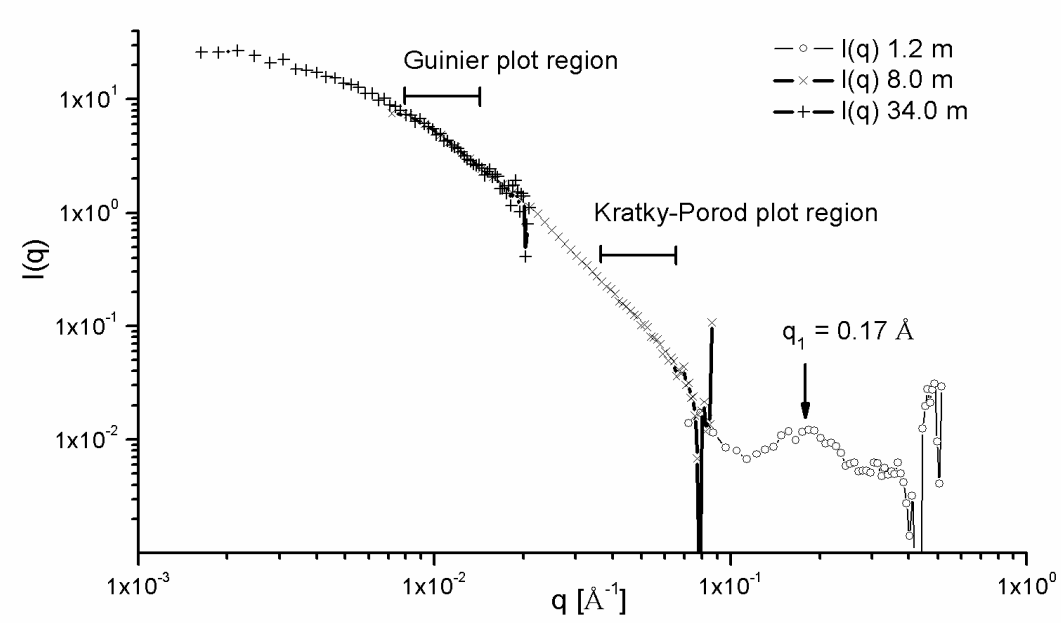

Figure 8. **a)** Experimentally determined scattering curve (SANS) of liposomes based on DOPC:PEG$_{30}$-*hb*PG$_{24}$ (cf. no. 3, Table 1) at a molar ratio of 98:2 (40 g/L) with different sample/detector distances of 1.2, 8.0 and 34.0 m and a neutron wavelength of 6 Å. Dependence of the scattered intensity I(q) on the scattering vector modulus q. Experimental errors of I(q) are indicated by vertical bars and the scatter of experimental points increases with the increase of q.

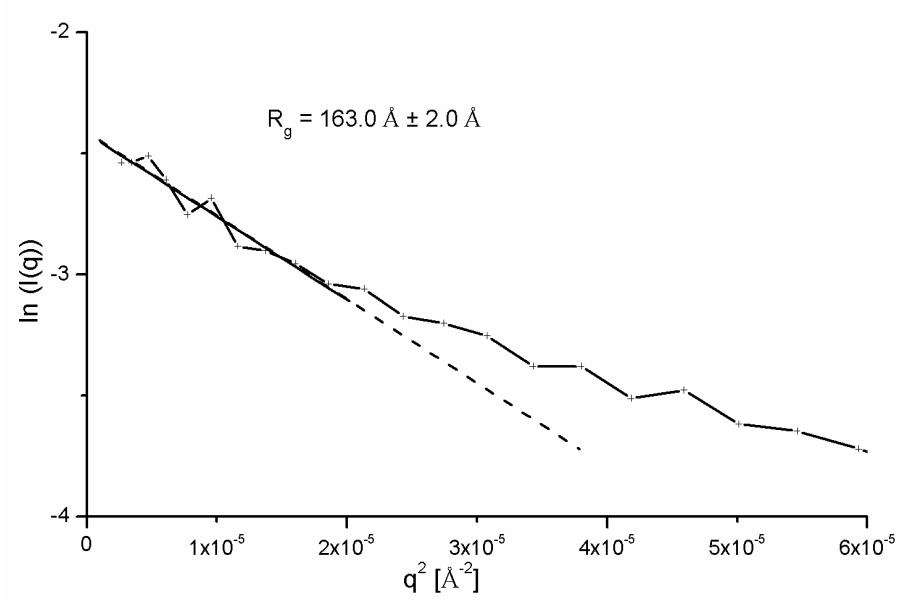

Figure 8. b) Guinier plot with a sample/detector distance of 34.0 m.

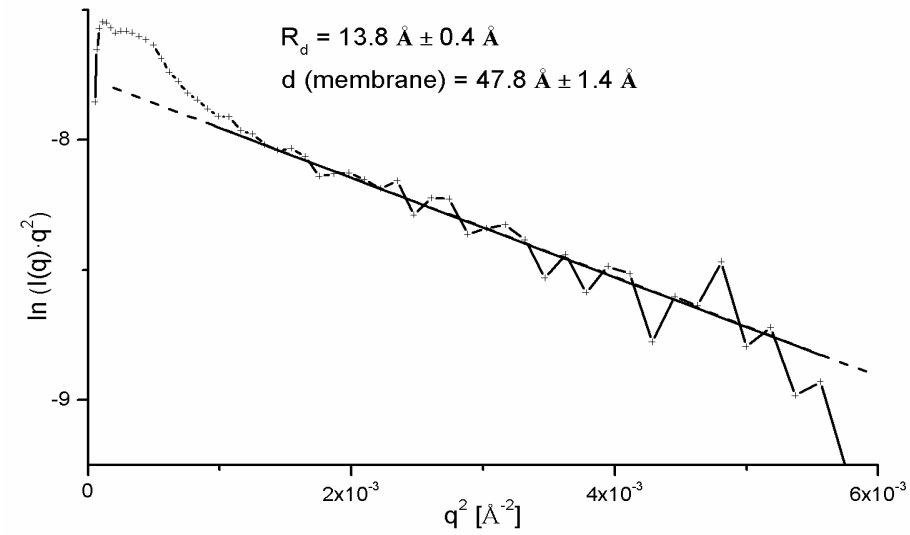

Figure 8. c) Kratky-Porod plot with a sample/detector distances of 8.0 m.

The radius of gyration R_g is defined as the geometric averaged distance of the scatters from the center of the object. In case of special unilamellar liposomes, the radius of gyration R_g is equivalent to the membrane radius r_m. The Guinier plot as demonstrated in Figure 8b allows determination of the radius of gyration R_g of the liposomes by taking the slope $m = -R_g^{(2/3)}$ of the linear part of the curve.[41]

The Kratky-Porod plot (see Figure 8c) permits determination of the thickness radius R_d and is related to the membrane thickness $d = R_d \cdot \sqrt{12}$ of the liposomes by taking the slope $m = R_d^2$ of

the linear part of the curve.[40] The size *s* of the liposomes can be estimated by small angle scattering by the following equation: $s = 2Rg + d$.

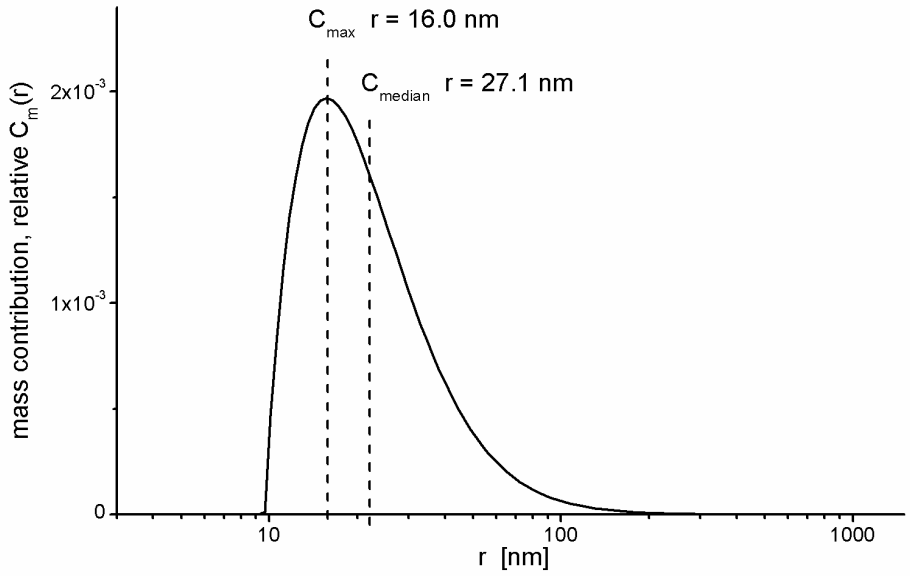

Figure 9. Experimentally determined scattering curve (DLS) of liposomes based on DOPC:PEG_{30}-*hb*PG_{24} (cf. no. 3, Table 1) at a molar ratio of 98:2 (40 g/L).

The calculated radii R_g and R_d, the bilayer thickness *d* and vesicle size *s* of a cholesterol-PEG-*hb*PG sample (cf. no. 3, Table 1) are summarized in Table 2 in comparison to the hydrodynamic radius R_h and vesicle size *s* obtained by DLS. The rough estimation of the size distribution of typical liposomes containing cholesterol-PEG-*hb*PG via DLS (see Figure 9) was carried out with a sterile original sample, containing lipid at a concentration of 40 g/L. The radii obtained by SANS and DLS are in good agreement and resemble the size distribution of phospholipid liposomes prepared by comparable methods. As expected, the values for R_h exceed R_g because R_h includes both solvent (hydro) and shape (dynamic) effects.

Table 2. The calculated radii R_g and R_d, the bilayer thickness *d* and vesicle size *s* determined via SANS in comparison to the hydrodynamic radius R_h and vesicle size s obtained by DLS.

R_g [nm]	R_d [nm]	d [nm]	s (SANS) [nm]	R_h (median) [nm]	s (DLS) [nm]
16.3	1.4	4.8	37.4	27.1	54.2

Conclusion

We have developed a straightforward two-step protocol for the synthesis of novel polyfunctional linear-hyperbranched polyether lipids for liposome preparation. The controlled polymerization conditions allowed us to prepare copolymer lipids with accurate degrees of polymerization, varying the lengths of both blocks while keeping polydispersity low. Adjusting the length of the PEG block permits tailoring the shielding properties of the polyether lipid further. The use of different initiators broadens the fields of application of these materials ranging from commercially available cholesterol to different aliphatic glyceryl ethers as the anchors for incorporation in the liposomes. MALDI-ToF mass spectrometry supported complete incorporation of the respective initiators. The reaction conditions had to be optimized for each of the systems presented (counterions, solvent etc.).

Clearly, the linear-hyperbranched polyethers are incorporated as the polyfunctional shell in liposome formulations with 1,2-dioleoyl-*sn*-glycero-3-phosphocholine (DOPC). Characterization via dynamic light scattering (DLS), small angle neutron scattering (SANS), and transmission electron microscopy (TEM) evidenced the formation of unilamellar liposomes.

Detailed studies regarding cytotoxicity of the novel block copolymers and also of the liposome formation, structure, and transport properties are in progress and will be reported in due course. It is obvious that the novel structures with their multiple functionality offer interesting options for the attachment of specific targeting sites, exploiting the multivalent nature for active drug targeting.

Acknowledgment

A.M.H. acknowledges the POLYMAT Graduate School of Excellence and the SAMT initiative for valuable financial support. T.N. thanks Ralf Schweins (Institut Laue-Langevin, Grenoble) for support with the SANS experiments. This work was supported by the Bundesministerium für Forschung und Technologie (BMBF, Grant No. 05KS7UMA).

References

(1) Immordino, M. L.; Dosio, F.; Cattel, L. *Int. J. Nanomed.* **2006**, *1*, 297-315.

(2) Woodle, M. C.; Lasic, D. D. *Biochim. Biophys. Acta, Biomembr.* **1992**, *1113*, 171-199.

(3) Allen, C.; Dos Santos, N.; Gallagher, R.; Chiu, G. N. C.; Shu, Y.; Li, W. M.; Johnstone, S. A.; Janoff, A. S.; Mayer, L. D.; Webb, M. S.; Bally, M. B. *Biosci. Rep.* **2002**, *22*, 225-250.

(4) Needham, D.; Kim, D. H. *Colloids Surf., B* **2000**, *18*, 183-195.

(5) Needham, D.; McIntosh, T. J.; Lasic, D. D. *Biochim. Biophys. Acta, Biomembr.* **1992**, *1108*, 40-48.

(6) Ahl, P. L.; Bhatia, S. K.; Meers, P.; Roberts, P.; Stevens, R.; Dause, R.; Perkins, W. R.; Janoff, A. S. *Biochim. Biophys. Acta, Biomembr.* **1997**, *1329*, 370-382.

(7) Blume, G.; Cevc, G. *Biochim. Biophys. Acta, Biomembr.* **1990**, *1029*, 91-97.

(8) Allen, T. M.; Hansen, C. *Biochim. Biophys. Acta, Biomembr.* **1991**, *1068*, 133-141.

(9) Lasic, D. D.; Papahadadjopoulos, D. *Science* **1995**, *267*, 1275-1276.

(10) Roberts, W. G.; Palade, G. E. *Cancer Res.* **1997**, *57*, 765-772.

(11) Dvorak, H.; Nagy, J.; Dvorak, J.; Dvorak, A. *Am. J. Pathol.* **1988**, *133*, 95-109.

(12) Thompson, M. S.; Vadala, T. P.; Vadala, M. L.; Lin, Y.; Riffle, J. S. *Polymer* **2008**, *49*, 345-373.

(13) (a) Wilms, D.; Wurm, F.; Nieberle, J.; Böhm, P.; Kemmer-Jonas, U.; Frey, H. *Macromolecules* **2009**, *42*, 3230–3236. (b) Wilms, D.; Stiriba, S. E.; Frey, H. *Acc. Chem. Res.* **2010**, *43*, 129-141.

(14) Kainthan, R. K.; Janzen, J.; Levin, E.; Devine, D. V.; Brooks, D. E. *Biomacromolecules* **2006**, *7*, 703-709.

(15) Kainthan, R. K.; Janzen, J.; Kizhakkedathu, J. N.; Devine, D. V.; Brooks, D. E. *Biomaterials* **2008**, *29*, 1693-1704.

(16) Calderón, M.; Quadir, M. A.; Sharma, S. K.; Haag, R. *Ad*V. *Mater.* **2010**, *22*, 190-218.

(17) Nguyen, P. M.; Hammond, P. T. *Langmuir* **2006**, *22*, 7825-7832.

(18) Gitsov, I.; Fréchet, J. M. J. *Macromolecules* **1993**, *26*, 6536.

(19) Gitsov, I.; Wooley, K. L.; Hawker, C. J.; Ivanova, P. T.; Fréchet, J. M. J. *Macromolecules* **1993**, *26*, 5621-5627.

(20) Istratov, V.; Kautz, H.; Kim, Y.-K.; Schubert, R.; Frey, H. *Tetrahedron* **2003**, *59*, 4017-4024.

(21) Demina, T.; Grozdova, I.; Krylova, O.; Zhirnov, A.; Istratov, V.; Frey, H.; Kautz, H.; Melik-Nubarov, N. *Biochemistry* **2005**, *44*, 4042-4054.

(22) Marcos, A. G.; Pusel, T. M.; Thomann, R.; Pakula, T.; Okrasa, L.; Geppert, S.; Gronski, W.; Frey, H. *Macromolecules* **2006**, *39*, 971-977.

(23) Khan, J. A.; Kainthan, R. K.; Ganguli, M.; Kizhakkedathu, J. N.; Singh, Y.; Maiti, S. *Biomacromolecules* **2006**, *7*, 1386-1388.

(24) Barriau, E.; Marcos, A. G.; Kautz, H.; Frey, H. *Macromol. Rapid Commun.* **2005**, *26*, 862-867.

(25) Wurm, F.; Nieberle, J.; Frey, H. *Macromolecules* **2008**, *41*, 1909-1911.

(26) Wurm, F.; Nieberle, J.; Frey, H. *Macromolecules* **2008**, *41*, 1184-1188.

(27) Wurm, F.; Klos, J.; Räder, H. J.; Frey, H. *J. Am. Chem. Soc.* **2009**, *131*, 7954-7955.

(28) Dworak, A.; Baran, G.; Trzebicka, B.; Walach, W. *React. Funct. Polym.* **1999**, *42*, 31-36.

(29) Dimitrov, P.; Utrata-Wesolek, A.; Rangelov, S.; Walach, W.; Trzebicka, B.; Dworak, A. *Polymer* **2006**, *47*, 4905-4915.

(30) Gutmayer, D.; Thomann, R.; Bakowsky, U.; Schubert, R. *Biomacromolecules* **2006**, *7*, 1422-1428.

(31) Stauch, O.; Uhlmann, T.; Fröhlich, M.; Thomann, R.; El-Badry, M.; Kim, Y.-K.; Schubert, R. *Biomacromolecules* **2002**, *3*, 324-332.

(32) Lainé, C.; Mornet, E.; Lemiègre, L.; Montier, T.; Cammas-Marion, S.; Neveu, C.; Carmoy, N.; Lehn, P.; Benvegnu, T. *Chem.sEur. J.* **2008**, *14*, 8330-8340.

(33) Zhao, X. B.; Muthusamy, N.; Byrd, J. C.; Lee, R. J. *J. Pharm. Sci.* **2007**, *96*, 2424-2435.

(34) Allen, T. M.; Hansen, C.; Martin, F.; Redemann, C.; Yau-Young, A. *Biochim. Biophys. Acta, Biomembr.* **1991**, *1066*, 29-36.

(35) Vertut-Doi, A.; Ishiwata, H.; Miyajima, K. *Biochim. Biophys. Acta, Biomembr.* **1996**, *1278*, 19-28.

(36) Mulder, W. J. M.; Strijkers, G. J.; van Tilborg, G. A. F.; Griffioen, W.; Nicolay, K. *NMR Biomed.* **2006**, *19*, 142-164.

(37) Guinier, A. *Ann. Phys. (Paris, Fr.)* **1939**, *12*, 161-236.

(38) Porod, G. *Acta Phys. Austria* **1948**, *2*, 255-292.

(39) Kratky, O. *Prog. Biophys.* **1963**, *13*, 105-173.

(40) Nawroth, T.; Conrad, H.; Dose, K. *Phys. B* **1989**, *156*, 477-480.

(41) Carrozzino, J. M.; Fuguet, E.; Helburn, R.; Khaledi, M. G. *J. Biochem. Biophys. Methods* **2004**, *60*, 97-115.

Supporting information

Hyperbranched polyglycerol-based lipids via oxyanionic polymerization: Toward multifunctional stealth liposomes

Anna Maria Hofmann,[1] Frederik Wurm,[1] Eva Hühn,[2] Thomas Nawroth,[2] Peter Langguth,[2] and Holger Frey*,[1]

1 Institute of Organic Chemistry, Johannes Gutenberg-Universität, Duesbergweg 10-14, Mainz, Germany,

2 Institute of Pharmacy and Biochemistry, Johannes Gutenberg-Universität, Staudingerweg 5, Mainz, Germany

Published in Biomacromolecules, 2010, 11 (3), 568-574.

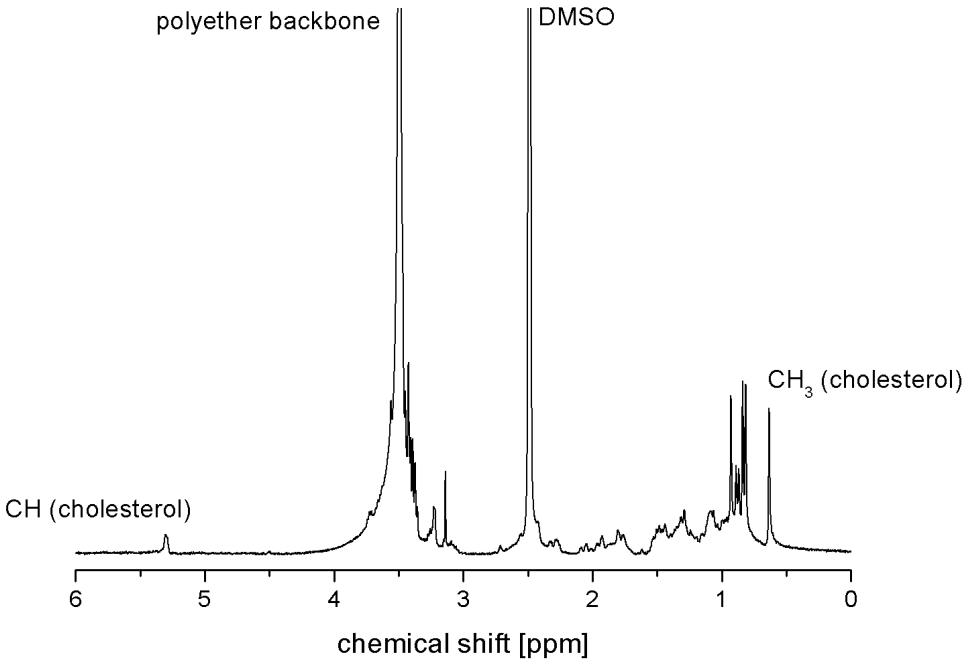

Figure S1. ^{1}H NMR spectrum (300 MHz, DMSO-d_6) of PEG initiated with cholesterol (cf. no. **3** in Table 1).

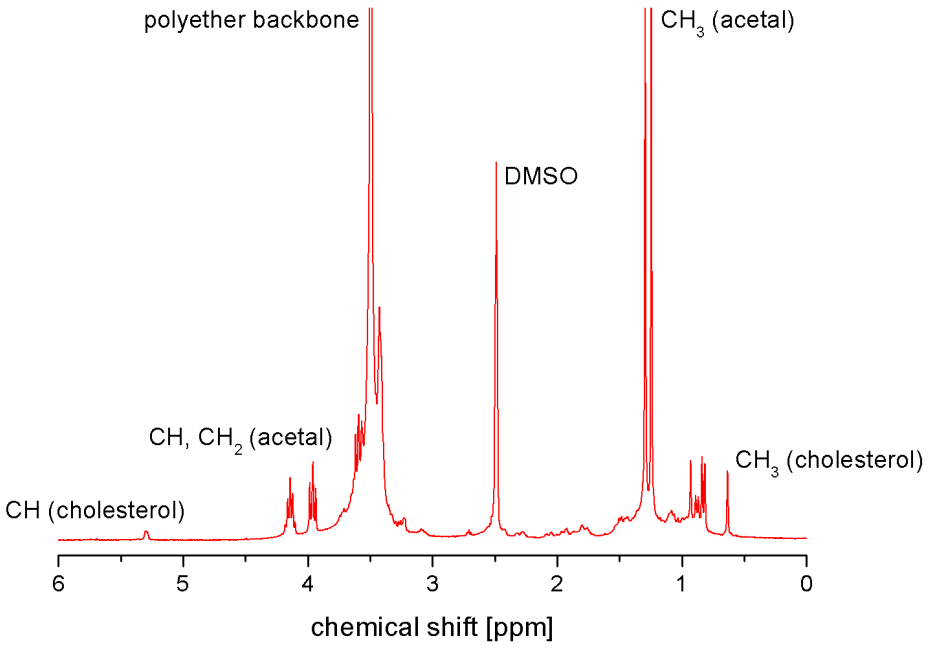

Figure S2. ^{1}H NMR spectrum (300 MHz, DMSO-d_6) of PEG-*b*-PIGG initiated with cholesterol (cf. no. **3** in Table 1).

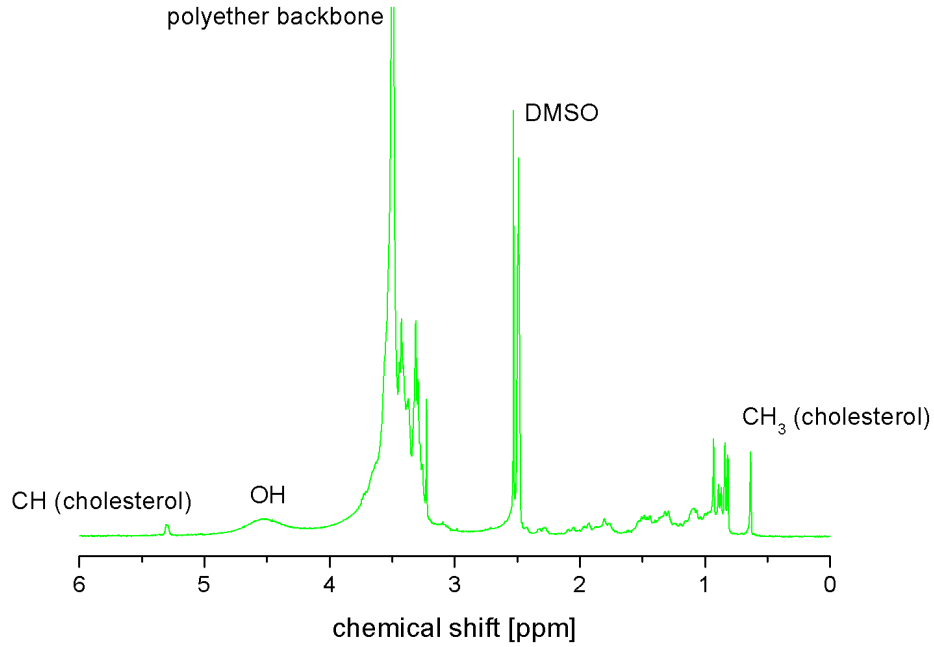

Figure S3. ^{1}H NMR spectrum (300 MHz, DMSO-d_6) of PEG-*b*-PGG initiated with cholesterol (cf. no. **3** in Table 1).

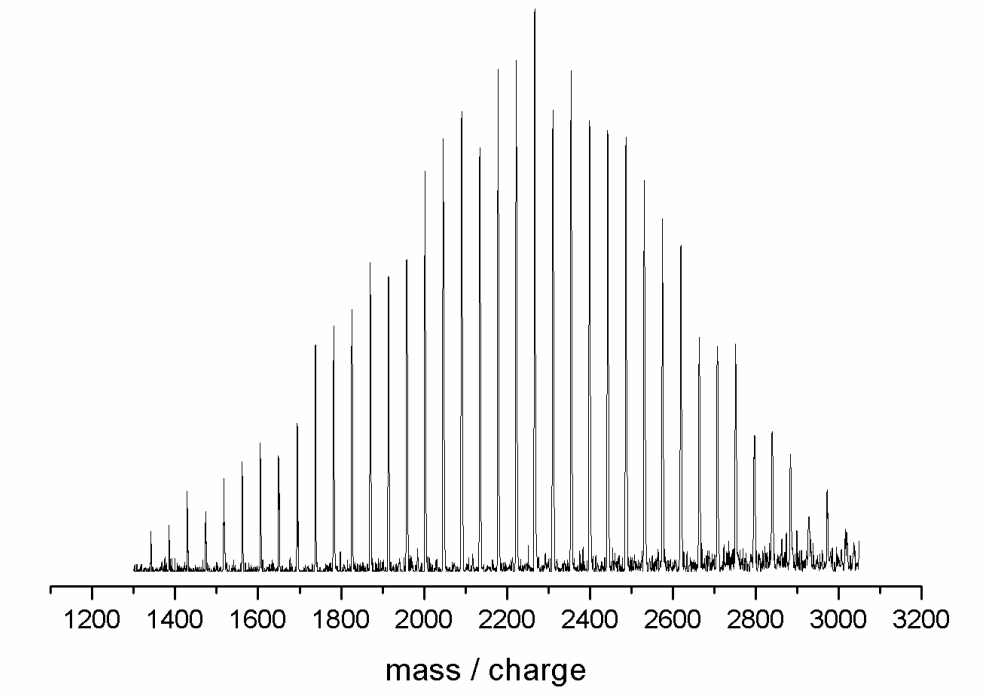

Figure S4. MALDI-ToF of PEG (cf. no. **9** in Table 1) initiated with 1,2-bis-*n*-octadecyl glyceryl ether using potassium trifluoroacetic acid as an additive.

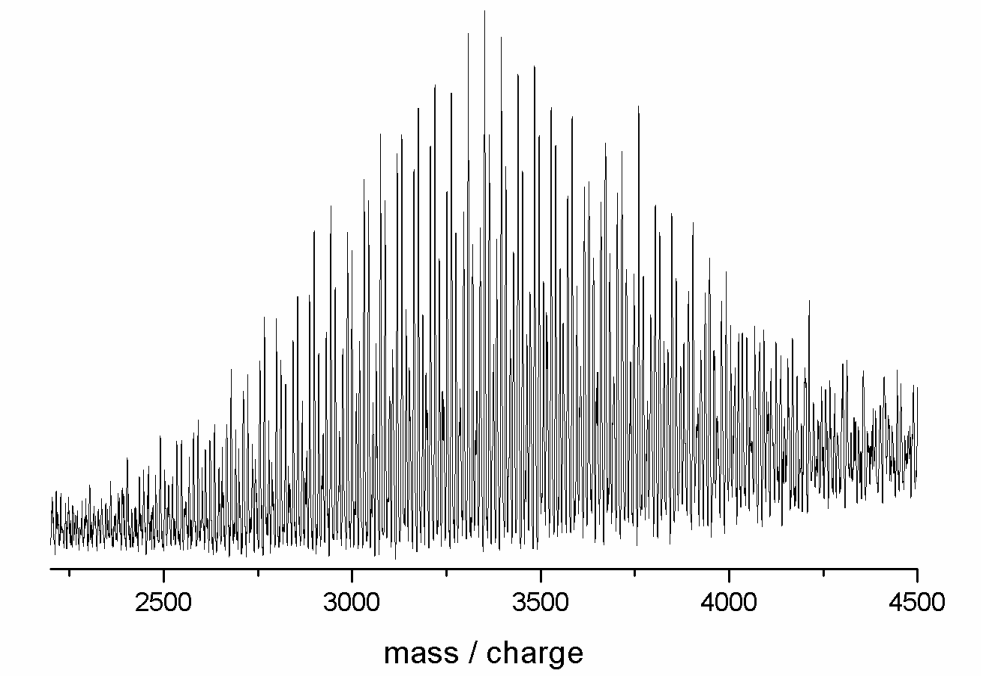

Figure S5. MALDI-ToF of PEG-PIGG (cf. no. **9** in Table 1) initiated with 1,2-bis-*n*-octadecyl glyceryl ether using potassium trifluoroacetic acid as an additive.

Chapter 2.2: Rapid access to polyfunctional lipids with complex architecture via oxyanionic ring-opening polymerization

Chapter 2.2:

Rapid access to polyfunctional lipids with complex architecture via oxyanionic ring-opening polymerization

Anna Maria Hofmann,[1] Frederik Wurm,[2] and Holger Frey[1,*]

1 Institut für Organische Chemie, Johannes Gutenberg-Universität, Duesbergweg 10-14, 55099 Mainz, Germany.

2 Ecole Polytechnique Fédérale de Lausanne (EPFL), Institut des Matériaux, Laboratoire des Polymères Batiment MXD, Station 12, 1015 Lausanne, Switzerland.

Published in Macromolecules 2011, 44 (12), 4648-4657.

Abstract

Polymer-coated liposomes, particularly poly(ethylene glycol) (PEG) substituted liposomes, have emerged as long-circulating carrier systems for drug delivery and diagnostic purposes. A rapid synthesis of three different types of multifunctional lipids with structurally diverse hydrophilic, polyether-based architectures via one- or two-pot approaches is described. Architectural variation is achieved by the combination of different oxyanionic polymerization strategies and various glycidyl ether building units. Branched polyglycerol lipids have been prepared via cholesterol- or 1,2-bis-*n*-alkyl glyceryl ether-initiated, oxyanionic ring-opening polymerization (ROP) of protected glycidyl ethers and glycidol, respectively. In addition to these polyglycerol-based lipids, we describe the synthesis of multifunctional PEGs as the hydrophilic part of the lipid, which can be compared to conventional stealth lipids, but bear an adjustable number of hydroxyl functions within the PEG backbone. These lipids can be readily obtained by random copolymerization of ethylene oxide and protected glycidyl ethers, such as ethoxyethyl glycidyl ether (EEGE) and isopropylidene glyceryl glycidyl ether (IGG). Polydispersities M_w/M_n of the amphiphilic polyether structures were in the range of 1.04 to 1.2 for the linear structures and 1.1 to 1.6 for the hyperbranched lipids. Critical micelle concentrations (CMC) have been

determined via the pyrene fluorescence method and were in the range of 1.4 to 40.7 mg/L, correlated to molecular weight and functionality of the polar polyether segment. Liposomes containing these hydroxy-functional lipids have been prepared via membrane extrusion method and have been visualized by transmission electron microscopy (TEM) and cryo TEM.

Keywords

polyethers, lipids, stealth lipids, liposomes, oxyanionic polymerization, polyglycerol

Introduction

Liposomes have emerged as versatile carrier systems for a variety of drugs, but intravenously administered they undergo fast opsonization and thus are rapidly cleared by macrophages of the mononuclear phagocyte system (MPS). Modification of liposomes with poly(ethylene glycol) (PEG) results in strongly reduced uptake by the liver and in prolonged blood circulation times of the drug carrier system due to the steric hindrance to the MPS.[1-8]

Sterically stabilized liposomes have been shown to lower harmful side effects, to protect the active ingredient and to transport high concentrations of a drug in specific tissues. Furthermore, PEG-coated liposomes show reduced vesicle aggregation and improved stability of the respective liposomal formulations. In addition to PEG, several other hydrophilic polymers have been reported as coatings for long-circulating liposomes, such as poly(oxazoline), poly(*N*-vinylpyrrolidone), poly(vinyl alcohol), poly(amino acid)s and linear polyglycerol.[9-14]

Besides the abilitiy of these sterically stabilized liposomes to target active compounds passively to the site of action due to the enhanced permeability and retention (EPR) effect of solid tumors, the specific delivery of drugs to target sites has been studied in a number of works in the last decades and represents an important topic in ongoing research.[15-17] The attachment of functional ligands, like monoclonal antibodies, peptides or folate to the surface of liposomes can lead to efficient recognition and selective binding to specific cells. However, the design of liposomes with prolonged circulation times offering the possibility of facile coupling of targeting or labeling species to the lipids still represents a challenge.

The use of commercially available linear PEG for the preparation of stealth type structures requires post polymerization derivatization to attach the polymer chain to lipids. Since coupling reactions often rely on tailored functionalities, research efforts have been focused on the synthesis of PEGs with different functional groups including carboxylic, amine, thiol, aldehyde, tosyl, epoxide, or succinimidyl succinate groups, either via modification of commercial PEG diol or PEG monomethyl ether (MPEG) or functional initiation or termination of the anionic ring-opening polymerization of ethylene oxide.[18-23] Further derivatization for labeling of the polymer or specific targeting of the liposomes can be necessary. In order to overcome the lack of multiple functionalities in the PEG chain, the number of end groups can be increased by dendronization of the chain ends. However, this approach often requires demanding multistep syntheses.[24-27]

Linear-hyperbranched block copolymers based on PEG and polyglycerol (PG) were synthesized via oxyanionic ROP of ethylene oxide and subsequent polymerization of protected glycidyl ethers, such as ethoxyethyl glycidyl ether (EEGE) or isopropylidene glyceryl glycidyl ether (IGG). After cleavage of the protecting groups, the linear precursor polymers can be used as macro-initiators for the ring-opening multibranching polymerization of glycidol.[28-30] While the above-mentioned synthetic strategies led to copolymers that bear functionalities in one block, random copolymerization of ethylene oxide with different protected glycidyl ethers provides heteromultifunctional PEGs with functional groups at the polymer backbone.[31-34]

Very recently, we gave a first account of the synthesis of complex lipids based on linear-hyperbranched PEG-*b*-PG block copolymers, which were successfully incorporated in liposomal formulations with 1,2-dioleoyl-*sn*-glycero-3-phosphocholine (DOPC) as a co-lipid.[35] In the current work, we describe a rapid access strategy to three different types of polyglycerol-derived lipids via cholesterol- or 1,2-bis-*n*-alkyl glyceryl ether-initiated oxyanionic polymerization (Scheme 1). Such lipid structures are promising for the preparation of liposomal formulations and can be conveniently coupled to labeling or targeting moieties.[14, 36-40]

The polymer lipids with polyfunctional polyether structure and systematically varied multifunctional architectures have been included in liposomal membranes with DOPC as co-lipid. The resulting liposomes have been visualized via transmission electron microscopy (TEM) and cryo TEM.

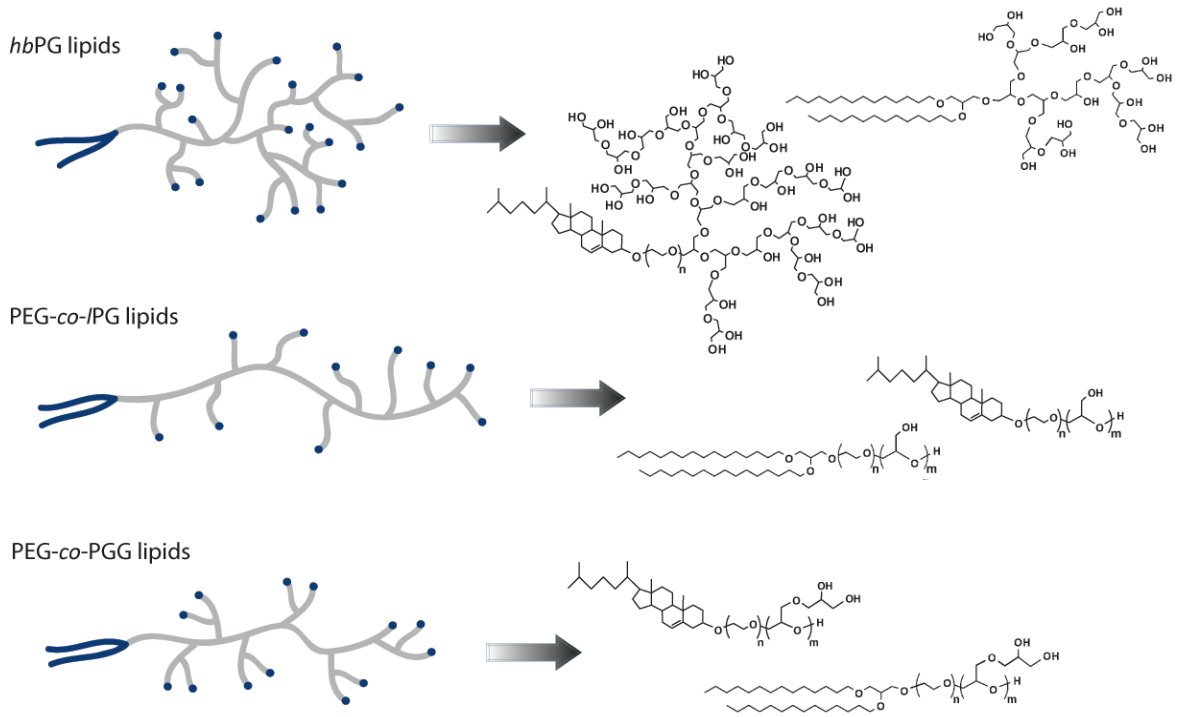

Scheme 1. Schematic architectures and chemical structures of the three different classes of multifunctional polyether lipids prepared via lipid-initiated oxyanionic ROP: (i) *hb*PG lipids; (ii) PEG-*co*-*l*PG lipids and (iii) PEG-*co*-PGG lipids.

Experimental section

Instrumentation. ^{1}H nuclear magnetic resonance (NMR) spectra were recorded using a Bruker AC 300 spectrometer operated at 300 MHz, employing $CDCl_3$ and DMSO-d_6 (dimethyl sulfoxide) as solvents. ^{13}C NMR spectra (referenced internally to solvent signals) were recorded at 100.15 MHz.

FT-IR spectra were recorded on a Nicolet SDXC FT-IR spectrometer equipped with an ATR unit.

SEC measurements were carried out in dimethylformamide (DMF) containing 0.25 g/L of lithium bromide. An Agilent 1100 Series GPC Setup (gel permeation chromatography) was used as an integrated instrument, including a PSS HEMA column ($10^6/10^5/10^4$ g/mol), a UV- (254 nm), and RI-detector. Calibration was achieved using poly(ethylene glycol) standards provided by Polymer Standards Service. The eluent was used at 50 °C and at a flow rate of 1 mL/min.

Matrix-assisted laser desorption and ionization time-of-flight (MALDI-ToF) measurements were performed on a Shimadzu Axima CFR MALDI-ToF mass spectrometer equipped with a nitrogen laser delivering 3 ns laser pulses at 337 nm. α-Cyano-3-hydroxy-cinnamic acid (CHCA) was used as a matrix. Samples were prepared by dissolving the polymer in methanol at a concentration of 10 g/L. A 10 µL aliquot of this solution was added to 10 µL of a 10 g/L solution of the matrix and 1 µL of a solution of potassium trifluoroacetic acid (KTFA) (0.1M in methanol as cationization agent). A 1 µL aliquot of the mixture was applied to a multistage target, methanol evaporated and a thin matrix/analyte film created.

Electron microscopy measurements were performed using a transmission electron microscope (FEI, XM12) with an acceleration voltage of 120 kV.

Reagents. All reagents and solvents were purchased from Acros and used as received, unless otherwise mentioned. Cholesterol was purchased from Fluka and stored at 4 °C. Dry solvents stored over molecular sieves were purchased from Fluka. Deuterated $CDCl_3$ and DMSO-d_6 were purchased from Deutero GmbH, dried and stored over molecular sieves.

Ethoxyethyl glycidyl ether (EEGE) was prepared as described in literature[41-43], using glycidol and dried over CaH_2 directly before use. ^{1}H NMR (300 MHz, $CDCl_3$): δ (ppm) = 4.76 ($OCH(CH_3)O$), 3.35-3.90 (OCH_2CH_3 and $OCH_2C_2H_3O$), 3.15 (CH epoxide), 2.61-2.91 (CH_2 epoxide), 1.33 ($OCH(CH_3)O$), 1.19 (OCH_3).

Isopropylidene glyceryl glycidyl ether (IGG) was prepared as described in literature,[29] dried over CaH_2 and freshly distilled before use. ^{1}H NMR (300 MHz, $CDCl_3$): δ (ppm) = 4.3 (m, 1H, CH acetal), 4.07 (m, 1H), 3.88-3.39 (m, 6H), 3.17 (m, 1H), 2.81 (t, 1H, CH_2 epoxide), 1.44 (s, 3H, CH_3), 1.38 (s, 3H, CH_3). Glycidol (99% Acros) was purified by distillation from CaH_2 directly prior to use.

Synthesis: Polymerizations. a) *Cholesterol-PGG precursor polymers:* Cholesterol was placed in a Schlenk flask, the appropriate amount of $CsOH{\cdot}H_2O$ (degree of deprotonation 90%) and benzene were added and the mixture was stirred for 30 min at 60 °C in argon atmosphere to generate the cesium alkoxide. The initiator was dried in vacuo at 90 °C, dissolved in dry diethylene glycol dimethyl ether under argon atmosphere (20 wt%) and IGG was added via syringe. The polymerization was carried out for 12 hours at 90 °C, a sample was removed for NMR- and SEC-characterization and then the isopropylidene protecting groups were cleaved by

addition of methanol, water and acidic ion-exchange resin, stirring for 12 h at room-temperature. Filtration and subsequent precipitation in cold diethyl ether resulted in the pure polymer that was dried in vacuo.

The 1,2-bis-*n*-alkyl glyceryl ether-initiated polymerizations could be accomplished in analogy to the previous procedures.

Cholesterol-poly(isopropylidene glyceryl glycidyl ether): ^{1}H NMR (300 MHz, DMSO-d_6): δ (ppm) = 5.30 (C=CH cholesterol), 4.14 (m, CHO acetal), 3.96 (m, CH_2O acetal), 3.76-3.22 (polyether backbone; CHO cholesterol), 2.28-0.82 (br, CH_2, CH cholesterol), 1.31-1.26 (br, CH_3 acetal), 0.63 (br, CH_3 cholesterol). The DP_n of PIGG was determined by comparison of the methyl signal (0.63 ppm) of cholesterol with the signals of PIGG at a chemical shift of 4.14 ppm.

Deprotection to cholesterol-poly(glyceryl glycidyl ether): ^{1}H NMR (300 MHz, DMSO-d_6): δ (ppm) = 5.30 (C=CH cholesterol), 4.27 (br, OH), 3.76-3.22 (polyether backbone; CHO cholesterol), 2.28-0.82 (br, CH_2, CH cholesterol), 0.63 (br, CH_3 cholesterol).

1,2-Bis-n-alkyl glyceryl ether-poly(isopropylidene glyceryl glycidyl ether): ^{1}H NMR (300 MHz, DMSO-d_6): δ (ppm) = 4.15 (m, CHO acetal), 3.97 (m, CH_2O acetal), 3.78-3.22 (polyether backbone; CH_2O, CHO initiator), 1.44 (br, CH_2CH_2O initiator), 1.31-1.26 (br, CH_3 acetal), 1.23 (br, CH_2 initiator), 0.85 (br, CH_3 initiator). The DP_n of PIGG was determined by comparison of methyl (0.85 ppm) and methylene (1.23 ppm) signals of the initiator with the signals for the PIGG block at a chemical shift of 4.15 ppm.

Deprotection to 1,2-bis-n-alkyl glyceryl ether-poly(glyceryl glycidyl ether): ^{1}H NMR (300 MHz, DMSO-d_6): δ (ppm) = 4.28 (br, OH), 3.78-3.22 (polyether backbone; CH_2O, CHO initiator), 1.44 (br, CH_2CH_2O initiator), 1.23 (br, CH_2 initiator), 0.85 (br, CH_3 initiator).

b) Hypergrafting of glycidol: The PGG precursor polymer was placed in a Schlenk flask, $CsOH{\cdot}H_2O$ (degree of deprotonation 20-30%) and benzene were added and the mixture was stirred at 60 °C for 30 min under argon atmosphere to generate the cesium alkoxide. After removal of the solvent in vacuo at 90 °C the macroinitiator was dissolved in dry diglyme (20 wt%), heated to 90 °C and a 20 wt% solution of glycidol in diglyme was added slowly with a syringe pump. The reaction was terminated by addition of an excess of methanol and acidic

cation exchange resin. The crude product was filtrated and precipitated into cold diethyl ether. The resulting material was assimilated in methanol and dried in vacuo.

Cholesterol-hyperbranched polyglycerol: ^{1}H NMR (300 MHz, DMSO-d_6): δ (ppm) = 5.30 (C=CH cholesterol), 4.77-4.43 (br, OH, different signals due to hyperbranched PG), 3.76-3.22 (polyether backbone; CHO cholesterol), 2.28-0.82 (br, CH_2, CH cholesterol), 0.63 (br, CH_3 cholesterol).

1,2-Bis-n-alkyl glyceryl ether-hyperbranched polyglycerol: ^{1}H NMR (300 MHz, DMSO-d_6): δ (ppm) = 4.77-4.43 (br, OH, different signals due to hyperbranched PG), 3.77-3.22 (polyether backbone; CH_2O, CHO initiator), 1.44 (br, CH_2CH_2O initiator), 1.23 (br, CH_2 initiator), 0.85 (br, CH_3 initiator).

c) *Cholesterol-PEG-co-lPG:* Cholesterol was placed in a Schlenk flask and the appropriate amounts of $CsOH{\cdot}H_20$ (degree of deprotonation 90%) and benzene were added and the mixture was stirred at 60 °C for 30 min in argon atmosphere to generate the cesium alkoxide. The initiator was dried in vacuo at 90 °C and dry tetrahydrofurane (THF) was cryo transferred to suspend the deprotonated cholesterol. Ethylene oxide was cryo transferred first to a graduated ampoule and then to the Schlenk flask containing the initiator suspension. Subsequently ethoxyethyl glycidyl ether (EEGE) was added to the reaction mixture via syringe. The polymerization was performed for 12 hours at 90 °C in vacuo. After removal of a sample for NMR- and SEC-characterization the acetal protecting groups were cleaved by addition of methanol, water and acidic cation exchange resin. The crude product was filtrated and precipitated into cold diethyl ether. The cholesterol-PEG-*co*-*l*PG was assimilated in methanol and dried in vacuo.

The 1,2-bis-*n*-alkyl glyceryl ether-initiated polymerizations could be accomplished analogously to the previous procedures.

Cholesterol-poly(ethylene glycol)-co-poly(ethoxyethyl glycidyl ether): ^{1}H NMR (300 MHz, DMSO-d_6): δ (ppm) = 5.30 (C=CH cholesterol), 4.63 (br, CHO acetal), 3.72-3.21 (polyether backbone; CHO cholesterol), 2.28-0.82 (br, CH_2, CH cholesterol), 1.18-1.06 (br, CH_3 acetal), 0.64 (br, CH_3 cholesterol). DP_n of PEO-*co*-PEEGE was determined by comparison of methyl signal (0.64 ppm) of cholesterol with the signals of the polyether backbone (3.72-3.21 ppm) and the acetal proton at a chemical shift of 4.63 ppm.

Cholesterol-poly(ethylene glycol)-co-linear polyglycerol: ^{1}H NMR (300 MHz, DMSO-d_6): δ (ppm) = 5.30 (C=CH cholesterol), 4.24 (br, OH), 3.72-3.21 (polyether backbone, CHO cholesterol), 2.28-0.82 (br, CH_2, CH cholesterol), 0.64 (br, CH_3 cholesterol).

1,2-Bis-n-alkyl glyceryl ether-poly(ethylene glycol)-co-poly(ethoxyethyl glyceryl ether): ^{1}H NMR (300 MHz, DMSO-d_6): δ (ppm) = 4.63 (br, CHO acetal), 3.74-3.22 (polyether backbone; CH_2O, CHO initiator), 1.42 (br, CH_2CH_2O initiator), 1.18-1.06 (br, CH_3 acetal; CH_2 initiator), 0.80 (br, CH_3 initiator). DP_n of PEO-*co*-PEEGE was determined by comparison of methyl signals (0.80 ppm) of the initiator with the signals for the polyether backbone (3.72-3.21 ppm) and the acetal proton at a chemical shift of 4.63 ppm.

1,2-Bis-n-alkyl glyceryl ether - poly(ethylene glycol)-co-linear polyglycerol: ^{1}H NMR (300 MHz, DMSO-d_6): δ (ppm) = 4.26 (br, OH), 3.74-3.22 (polyether backbone; CH_2O, CHO initiator), 1.42 (br, CH_2CH_2O initiator), 1.18-1.06 (br, CH_3 acetal; CH_2 initiator), 0.80 (br, CH_3 initiator).

d) ***Cholesterol-PEG-co-PGG****:* Cholesterol was placed in a Schlenk flask and the appropriate amount of $CsOH{\cdot}H_20$ (degree of deprotonation 90%) and benzene were added. Then the mixture was stirred for 30 min at 60 °C in argon atmosphere to generate the cesium alkoxide. The initiator was dried in vacuo at 90 °C and dry tetrahydrofurane (THF) was cryo transferred to suspend the deprotonated cholesterol. Ethylene oxide was cryo transferred first to a graduated ampoule and then to the Schlenk flask containing the initiator suspension. Subsequently IGG was added to the reaction mixture via syringe. The polymerization was performed for 12 hours at 90 °C in vacuo. After removal of a sample for NMR- and SEC-characterization the isopropylidene protecting groups were cleaved by addition of methanol, water and acidic cation exchange resin. The crude product was filtrated and precipitated into cold diethyl ether. The cholesterol-PEG-*co*-PGG was assimilated in methanol and dried in vacuo.

Cholesterol-poly(ethylene glycol)-co-poly(isopropylidene glyceryl glycidyl ether): ^{1}H NMR (300 MHz, DMSO-d_6): δ (ppm) = 5.31 (C=CH cholesterol), 4.15 (m, CHO acetal), 3.96 (m, CH_2O acetal), 3.70-3.21 (polyether backbone; CHO cholesterol), 2.28-0.82 (br, CH_2, CH cholesterol), 1.30-1.25 (br, CH_3 acetal), 0.64 (br, CH_3 cholesterol). DP_n of PEO-PIGG was determined by comparison of methyl signal (0.64 ppm) of cholesterol with the signals of the polyether backbone (3.70-3.21) and the PIGG at a chemical shift of 4.15 ppm.

Deprotection to cholesterol-poly(ethylene glycol)-co-poly(glyceryl glycidyl ether): ^{1}H NMR (300 MHz, DMSO-d_6): δ (ppm) = 5.31 (C=CH cholesterol), 4.50 (br, OH), 3.70-3.20 (polyether backbone; CH_2O, CHO cholesterol), 2.28-0.82 (br, CH_2, CH cholesterol), 0.63 (br, CH_3 cholesterol).

Derivatization reactions. a) *Etherification with propargylbromide:* The respective polymer was dissolved in dry toluene, sodium hydride was slowly added at 0 °C. The reaction mixture was stirred for 30 min and after slow addition of propargylbromide allowed to warm up to room temperature. The reaction was quenched with water after stirring at room temperature for 24 h. Removal of the solvent *in vacuo* and precipitation in cold diethyl ether resulted in the pure product.

Cholesterol-hbPG-OCH$_2$C≡CH: ^{1}H NMR (300 MHz, DMSO-d_6): δ (ppm) = 5.30 (C=CH cholesterol), 4.77-4.43 (br, OH, different signals due to hyperbranched PG), 4.31-4.17 ($OCH_2C{\equiv}CH$), 3.76-3.22 (polyether backbone; CHO cholesterol), 2.45 (C≡CH), 2.28-0.82 (br, CH_2, CH cholesterol), 0.63 (br, CH_3 cholesterol).

b) *Click reaction:* To a deoxygenized solution of cholesterol-*hb*PG-$OCH_2C{\equiv}CH$ in DMF $CuSO_4$ and sodium ascorbate were added in catalytic amounts. After addition of azido-rhodamine B dissolved in DMF the reaction mixture was stirred at 80 °C for 48 h. The crude product was purified via dialysis in methanol/water (1:1).

Fluorescence measurements/CMC determination. Stock solutions were prepared by dissolving the amphiphilic polymers, which were placed in a volumetric flask, in water (Milli-Q) to give a final concentration of 500 mg/L. These stock solutions were diluted in order to yield solutions varying in polymer concentration from 500 mg/L to 0.01 mg/L. Pyrene dissolved in THF was added to the sample solutions in sufficient amount to give a pyrene concentration of $6{\cdot}10^{-7}$ g/L. The samples were allowed to equilibrate for 24 h at room temperature prior to fluorescence measurements. Fluorescence measurements were carried out with an emission wavelength of 372 nm. The fluorescence intensities at excitation wavelengths of 339 and 335 nm have been determined.

Liposome preparation. Liposomes consisting of 1,2-dioleoyl-*sn*-glycero-3-phosphocholine (DOPC) and amphiphilic *hb*PG, PEG-*co*-*l*PG and PEG-*co*-PGG copolymers were prepared via the membrane extrusion method. Solutions of DOPC (100 g/L) and the respective polymer (10 g/L)

in chloroform were blended at a molar ratio of 98:2, and the organic solvents were removed under reduced pressure. The lipid film was hydrated with tris(hydroxymethyl)-aminomethane/citrate (tris3citrate) buffer (50 mM, pH 7.2) to a final lipid concentration of 40 g/L. The mixture was vortexed to yield multilamellar vesicles (MLV) and subsequent extrusion of the solution afforded the liposome formulations.

Results and discussion

Synthesis and characterization of polyglycerol based lipids. In a recent paper, we presented the first account of the synthesis of multifunctional lipids based on linear-hyperbranched PEG-*b*-PG block copolymers for liposomal application.[35] In the current work, several accelerated synthetic strategies have been developed that allow rapid access to complex, amphiphilic polyether architectures.

The synthesis of a series of hyperbranched polyglycerol (*hb*PG) derived lipids was carried out in a rapid two-pot approach using combined oxyanionic polymerization of different epoxide monomers (Scheme 2). In a first step the polymerization of isopropylidene glyceryl glycidyl ether (IGG), initiated directly with cholesterol or previously synthesized 1,2-bis-*n*-alkyl glyceryl ether, leads to a multifunctional amphiphilic macroinitiator after acidic cleavage of the acetal protecting groups.

This linear structure can be used for the ring-opening multibranching polymerization of glycidol following a slow monomer addition protocol. The preparation of the linear precursor polymer is necessary to obtain optimal conditions for the hypergrafting of glycidol and to ensure low polydispersity. Partial deprotonation of the large number of hydroxyl groups in combination with the slow monomer addition permits good control over the alkoxide concentration leading to growth of all chain ends, which narrows the molecular weight distribution and prevents undesired homopolymerization of the cyclic inimer glycidol. Since the concentration of alkoxides decreases in the course of the grafting reaction, a sufficient amount of deprotonated hydroxyl groups at the beginning of the polymerization, i.e., a multifunctional macroinitiator is mandatory.[44] This synthetic approach resulted in a number of well-defined amphiphilic *hb*PG structures (Table 1), which show monomodal molecular weight distributions at all stages of the synthesis (Figure 2) and low polydispersities in a range of 1.1 to 1.6.

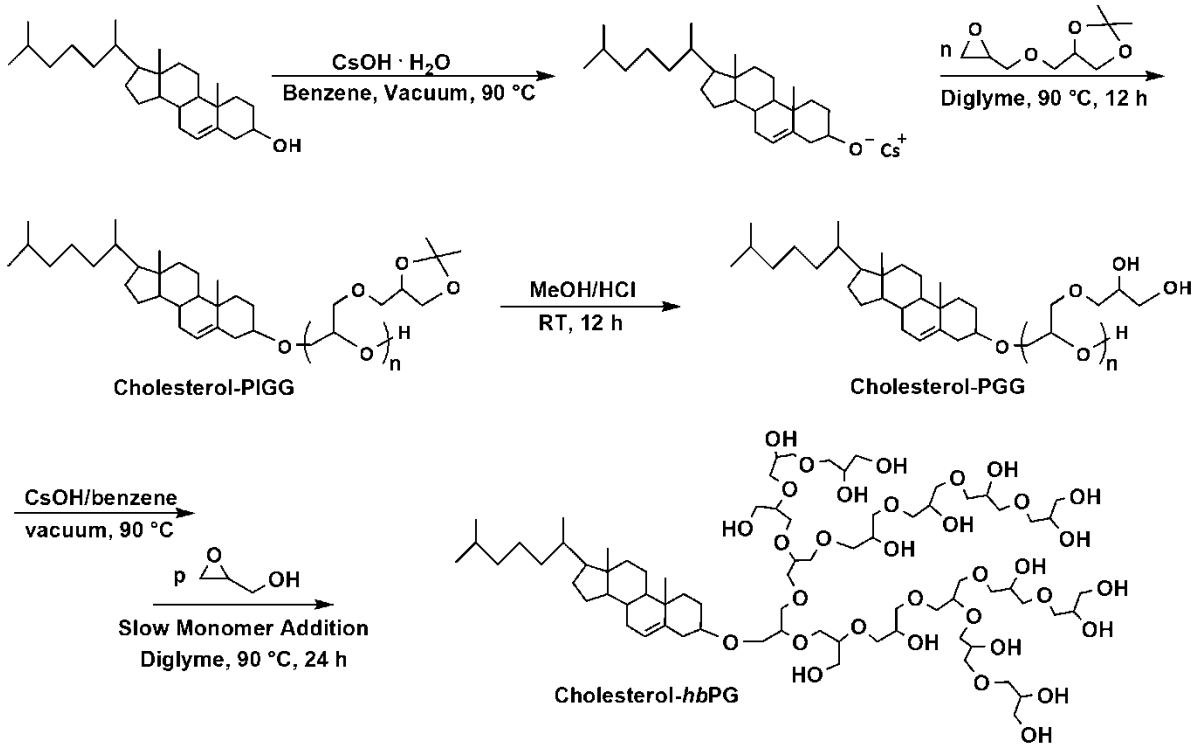

Scheme 2. Reaction sequence developed for the synthesis of the series of cholesterol-initiated hyperbranched polyglycerol *(hb*PG) lipids.

The degree of polymerization was determined via ^{1}H NMR spectroscopy, integrating the methyl groups of the initiator (cholesterol: 0.63 ppm, 1,2-bis-*n*-alkyl glyceryl ether: 0.85 ppm) and the acetal protecting groups for the precursor polymers or the polyether backbone for *hb*PGs. With respect to potential applications of the amphiphilic hyperbranched polymers in liposomal formulations the molecular weights of the polymers were adjusted in the range of 2000-3000 g/mol, representing a DP_n of glycidol of 28-40. It is known that liposomes containing linear PEG in this molecular weight range show increased blood circulation times due to an effective protection of the liposome by a steric barrier as well as sufficient anchoring of the PEG-lipid in the liposomal membrane.[7, 45-47]

Characterization data for all homopolymers are summarized in Table 1. Comparison of the molecular weights determined via SEC in DMF using PEG standards with the molecular weights obtained from ^{1}H NMR spectroscopy (Table 1), demonstrate a general underestimation by SEC. This is attributed to the strong influence of the hyperbranched, globular polyglycerol on the hydrodynamic radius of the polymers. Incorporation of the initiator moiety in every polymer

chain formed is crucial for the amphiphilic character of the resulting lipids. Full incorporation was evidenced via MALDI-ToF mass spectrometry for all structures prepared (Figure 1).

Table 1. Characterization data for hyperbranched polyglycerol lipids (*hb*PG lipids). [a] M_n determined via ^{1}H NMR spectroscopy. [b] M_n and M_w determined via SEC-RI in DMF with poly(ethylene glycol) standards. [c] CsOH used as initiator. tge = tetradecyl glyceryl ether, hge = hexadecyl glyceryl ether.

No.	polymer	initiator	M_n (th) g/mol	M_n[a] (NMR) g/mol	M_n[b] (SEC) g/mol	PDI[b]	CMC mg/L
1	*hb*PG_{25}	cholesterol[c]	1900	2200	1300	1.20	1.4
2	*hb*PG_{30}	cholesterol[c]	2400	2600	1400	1.63	4.5
3	*hb*PG_{35}	cholesterol[c]	2800	3000	1500	1.18	8.3
4	*hb*PG_{42}	bis(tge)[c]	3400	3600	1600	1.10	15.5
5	*hb*PG_{31}	bis(hge)[c]	2700	3100	1500	1.51	40.7

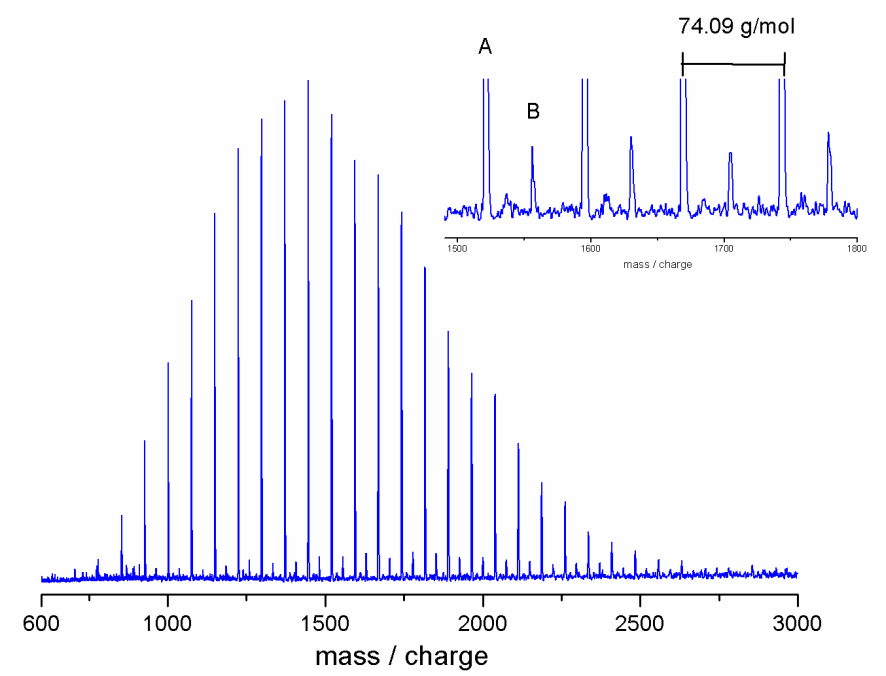

Figure 1. MALDI-ToF spectrum of amphiphilic hyperbranched polyglycerol (cf. compound **1**, Table 1) initiated with cholesterol. A: Main distribution with sodium as a counter ion. B: Sub-distribution with cesium as a counter ion.

The use of lipophilic initiators, such as the commercially available cholesterol or 1,2-bis-*n*-alkyl glyceryl ethers not only permits incorporation of the polymers in liposomal membranes, but also simplifies the synthetic approach, since no additional post polymerization derivatization with such units is required.

Synthesis and characterization of PEG-*co*-*l*PG lipids. Although the abovementioned strategy allows good control over molecular weights and afforded low polydispersities for the amphiphilic *hb*PGs, we aimed at shortening the synthetic approach to multifunctional linear polymer-lipids to one single polymerization step. The random copolymerization of ethylene oxide with ethoxyethyl glycidyl ether (EEGE), recently studied in detail by our group,[33] offers several advantages in comparison to other strategies. In the field of drug-delivery systems and especially of sterically stabilized liposomes, poly(ethylene glycol) is one of the best examined and most often used polymers. The introduction of additional hydroxyl functions via random copolymerization of ethylene oxide and the protected glycidyl ether and acidic hydrolysis allows further derivatization with targeting or labeling moieties in analogy to the above described amphiphilic hyperbranched polyglycerols. The synthesis of linear PEG-co-*l*PG lipids (Scheme 3) has been carried out using cholesterol or 1,2-bis-*n*-alkyl glyceryl ethers as initiator and potassium methanolate or cesium hydroxide monohydrate as deprotonating agent.

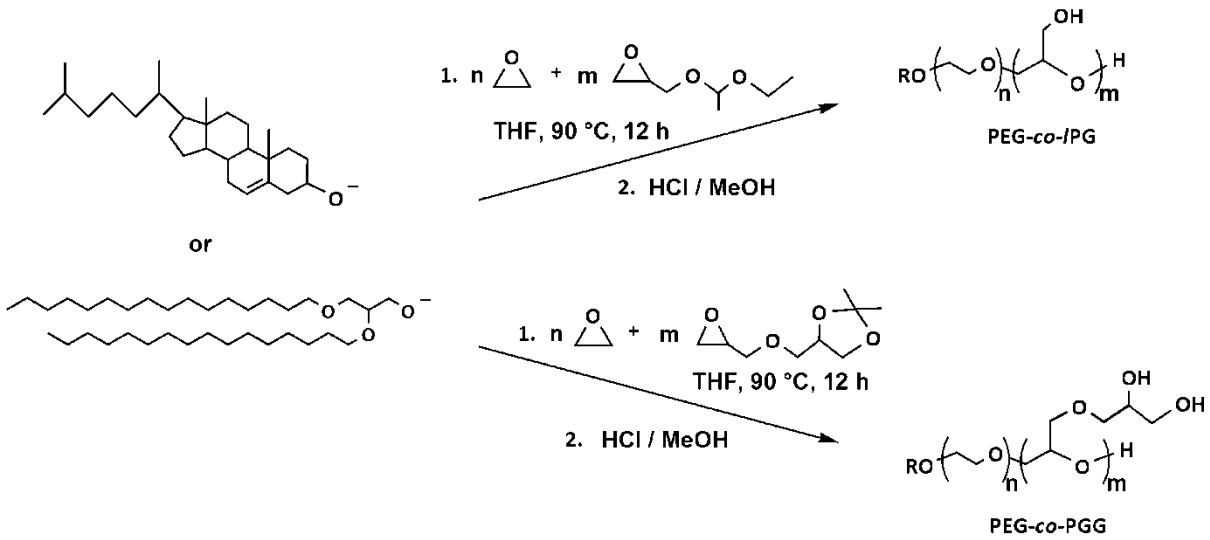

Scheme 3. Reaction sequence for the synthesis of PEG-*co*-*l*PG copolymer lipids and PEG-*co*-PGG copolymer lipids initiated with cholesterol or 1,2-bis-*n*-hexadecyl glyceryl ether.

The use of both initiating systems led to good control of molecular weights and the degree of functionalization. As expected for a linear copolymer, complex lipids based on PEG and linear PG with narrow molecular weight distributions were obtained. Polydispersities were generally lower (M_w / M_n < 1.2) than for the amphiphilic hyperbranched structures (Figure 2).

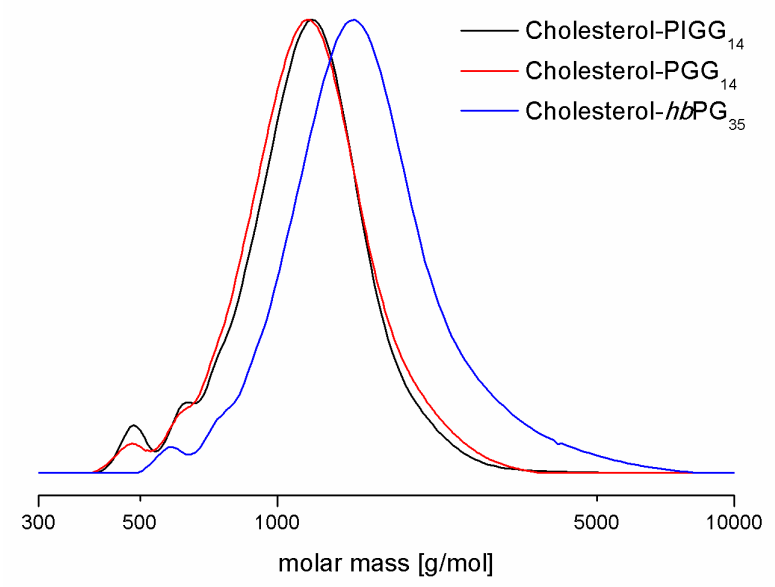

Figure 2. a) SEC-molecular weight distribution (RI-detection, PEG standards) of PIGG initiated with cholesterol before (black) and after removal of the isopropylidene protecting groups (red) and after hypergrafting of glycidol (blue, cf. compound **3**, Table 1).

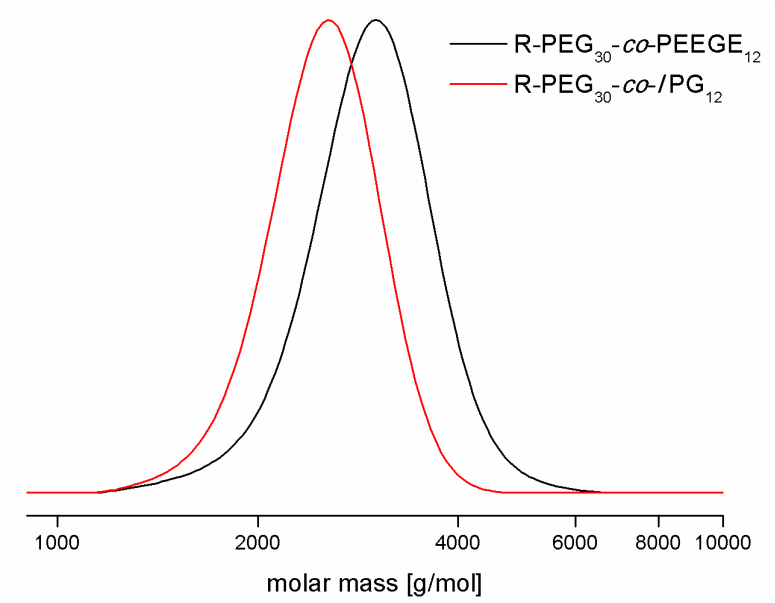

Figure 2. b) SEC-molecular weight distribution (RI-detection, PEG standards) of random PEG-*co*-/PG copolymers initiated with 1,2-bis-*n*-hexadecyl glyceryl ether (R) before (black) and after removal of the acetal protecting groups (red, cf. compound **6**, Table 2).

Characterization data of all PEG-*co*-*l*PG copolymer lipids are listed in Table 2. Again the molecular weights determined via SEC in DMF using PEG standards are underestimated in comparison to the values determined by ^{1}H NMR spectroscopy. This can be explained by the different chemical structure of the copolymer lipids in comparison with the calibration standard PEG (Table 2). The influence of the unusual architecture of the polymers on the hydrodynamic radii due to their amphiphilic character and high amounts of hydroxyl functions leads elution times varying with molecular weights as well as with molecular structure. This structural influence differs for PEG-*co*-*l*PG and PEG-*co*-PGG with varying molecular weights. However, the overall molecular weights of the copolymers lipids were adjusted to about 3000 g/mol in view of liposome formation.[7, 45-47]

In contrast to the series of amphiphilic hyperbranched polyglycerol lipids, the degree of functionalization for the lipids presented in Table 2 can be varied independently of the molecular weight of the polymer. The composition of the PEG-co-*l*PG copolymers has been varied in the range of 18 to 55% glycerol incorporation.

The degree of polymerization and functionalization was determined via ^{1}H NMR spectroscopy, integrating the methyl groups of the initiator (cholesterol: 0.63 ppm, 1,2-bis-*n*-alkyl glyceryl ether: 0.85 ppm), the acetal protecting groups of the comonomer and the polyether backbone (Figure 3).

Table 2. Characterization data of PEG-*co*-*l*PG lipids and PEG-*co*-PGG lipids. [a] M_n determined via ^{1}H NMR spectroscopy. [b] M_n and M_w determined via SEC-RI in DMF with poly(ethylene glycol) standards. [c] MeOK used as deprotonation agent. [d] CsOH used as a deprotonation agent. tge = tetradecyl glyceryl ether, hge = hexadecyl glyceryl ether.

No.	polymer	initiator	M_n (th) g/mol	M_n[a] (NMR) g/mol	M_n[b] (SEC) g/mol	PDI[b]	EEGEor IGG cont.	CMC mg/L
1	PEG_{20}-*co*-*l*PG_{25}	cholesterol[c]	2800	3100	1600	1.18	55%	8.8
2	PEG_{32}-*co*-*l*PG_{18}	cholesterol[c]	3000	3100	1800	1.15	36%	8.7
3	PEG_{36}-*co*-*l*PG_{35}	cholesterol[c]	3100	4600	2000	1.13	49%	13.9
4	PEG_{30}-*co*-*l*PG_{20}	bis(tge)[d]	3000	3300	2000	1.07	40%	15.6

5	PEG_{23}-*co*-/PG_{13}	bis(hge)[d]	2300	2500	2300	1.12	36%	5.8
6	PEG_{30}-*co*-/PG_{12}	bis(hge)[d]	2600	2800	3100	1.04	29%	12.1
7	PEG_{46}-*co*-/PG_{10}	bis(hge)[d]	3000	3000	3000	1.04	18%	10.5
8	PEG_{19}-*co*-PGG_{9}	cholesterol[c]	2700	2600	1000	1.21	32%	9.9
9	PEG_{30}-*co*-PGG_{8}	cholesterol[c]	2900	2900	1000	1.20	21%	13.4
10	PEG_{18}-*co*-PGG_{12}	cholesterol[c]	3000	3000	2000	1.17	40%	7.1
11	PEG_{29}-*co*-PGG_{11}	cholesterol[c]	2900	3300	1800	1.06	28%	10.7
12	PEG_{12}-*co*-PGG_{17}	cholesterol[c]	3000	3400	1900	1.15	59%	19.1
13	PEG_{12}-*co*-PGG_{18}	cholesterol[c]	3000	3600	1000	1.13	60%	15.3

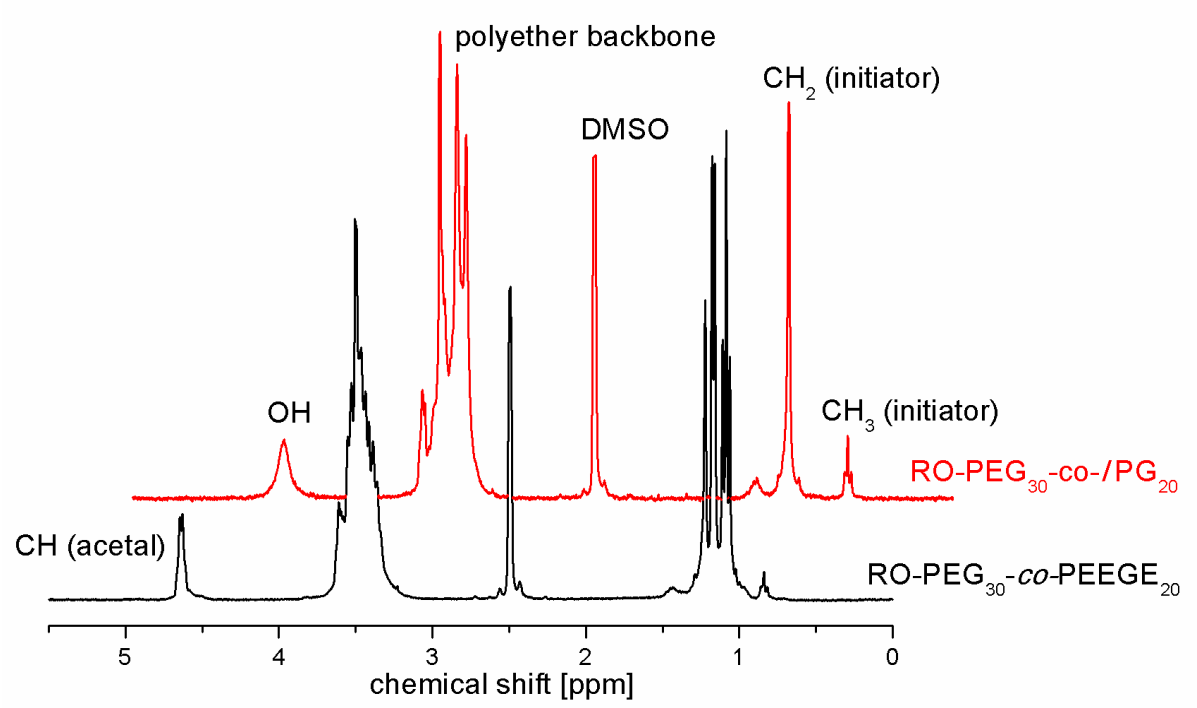

Figure 3. ^{1}H NMR spectra (300 MHz, DMSO-d_6) of PEG-*co*-/PG copolymer (cf. compound **4**, Table 2) with 1,2-bis-*n*-tetradecyl glyceryl ether as initiator before (bottom) and after (top) removal of acetal protective groups.

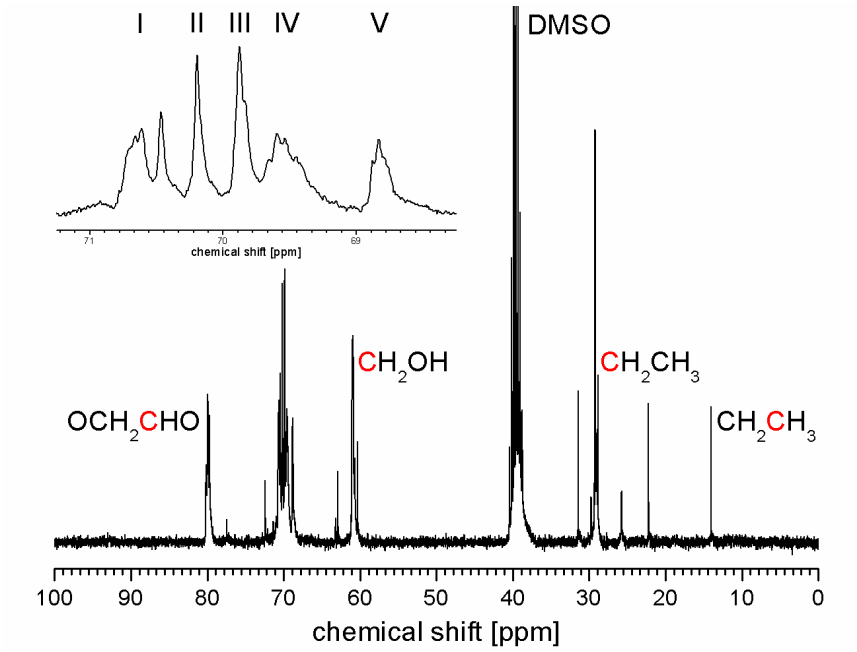

Figure 4. ^{13}C NMR spectra (75.5 MHz, DMSO-d_6) of PEG-*co*-*l*PG copolymer (cf. compound **4**, Table 2) with 1,2-bis-*n*-tetradecyl glyceryl ether as initiator. Inset for enlarged region: relevant EO centered triads, demonstrating random copolymerization.

The random distribution of the comonomer units within the PEG backbone was confirmed via ^{13}C NMR analysis, relying on the study of the triad sequence distribution, which evidences random incorporation of the monomers in the polymer chain.[33, 48] As an example, Figure 4 shows the ^{13}C NMR spectra of 1,2-bis-*n*-tetradecyl glyceryl ether-PEG$_{30}$-*co*-*l*PG$_{20}$ (cf. compound **4**, Table 2) measured in DMSO-d_6 including the enhanced regions related to the signals of the PEG (E) and PG (G) backbone. The signal of the E-E-E triad (I), which is due to both methylene groups of an EO unit adjacent to two other EO units, exhibits an intensity similar to the signals of the E-E-G, G-E-E and G-E-G triads, in which at least one glycerol unit is located adjacent to the central EO unit. This confirms the random incorporation of the functional comonomer within the polyether chain.

Synthesis of PEG-*co*-PGG lipids. While the copolymerization of ethylene oxide and the abovementioned ethoxyethyl glycidyl ether (EEGE) results in linear PEG structures with randomly distributed hydroxyl groups at the polymer backbone, the use of isopropylidene glyceryl glycidyl ether (IGG) leads to the incorporation of two adjacent hydroxyl groups in the resulting glycerol side chains for each comonomer in the polymer chain.[34] Thus, following an

analogue synthetic approach, copolymers with varied architectures can be obtained by use of the comonomer IGG, which in addition to etherification or esterification of single hydroxyl functions permits the further derivatization of the two vicinal hydroxyl groups via reaction of ketones or aldehydes to cyclic acetal or ketal structures.

Size exclusion chromatography was carried out for all samples, again demonstrating narrow molecular weight distributions with polydispersity indices within the range of 1.1-1.2 for this third class of polyether lipids (Table 2, compounds **8**-**13**). As expected, molecular weights obtained from SEC-measurements in DMF (PEG standards) deviate from the values determined via ^{1}H NMR measurements in DMSO-d_6. The underestimation of the values by SEC becomes more relevant with increasing amount of IGG. This can be attributed to a lower hydrodynamic radius despite incorporation of comonomers with a higher molecular weight.

The degree of polymerization and the degree of functionalization were determined via ^{1}H NMR spectroscopy by integrating the methyl groups of the initiator (cholesterol: 0.63 ppm), the acetal protecting groups of the comonomer and the polyether backbone. The molecular weights of the PEG-*co*-PGG copolymers were adjusted to 3000 g/mol, and the amount of comonomer was varied in the range of 21-60% IGG incorporation. Successful removal of the protecting groups was monitored by ^{1}H or ^{13}C NMR spectroscopy, since signals that are due to protons of the isopropylidene groups disappear after acidic hydrolysis. In analogy to the PEG-*co*-*l*PG lipids, the random distribution of the IGG units within the polymer was evidenced by investigation of the triad sequence distribution via ^{13}C NMR analysis.

Derivatization. Besides facile further modification the main advantage of the novel polymeric lipids is their large number of hydroxyl functionalities that clearly distinguishes them from “classical” stealth type PEG lipids. Although hydroxyl groups can be conveniently addressed by a variety of reactions, facile synthetic approaches under mild and neutral reaction conditions are often required. To this end, alkinyl-functionalized amphiphilic *hb*PGs, PEG-*co*-*l*PGs and PEG-*co*-PGG have been prepared by etherification with propargyl bromide. Facile attachment of targeting or labeling moieties, such as rhodamine B, can be accomplished using the respective azide in an azido-alkyne Huisgen cycloaddition, as it is shown in Figure 5. The amount of rhodamine B incorporated in the polyether lipids is determined by the number of alkyne functionalities, which is adjusted by the equivalent of propargyl bromide used in the etherification reaction and has been varied from an average of one to four functionalities.

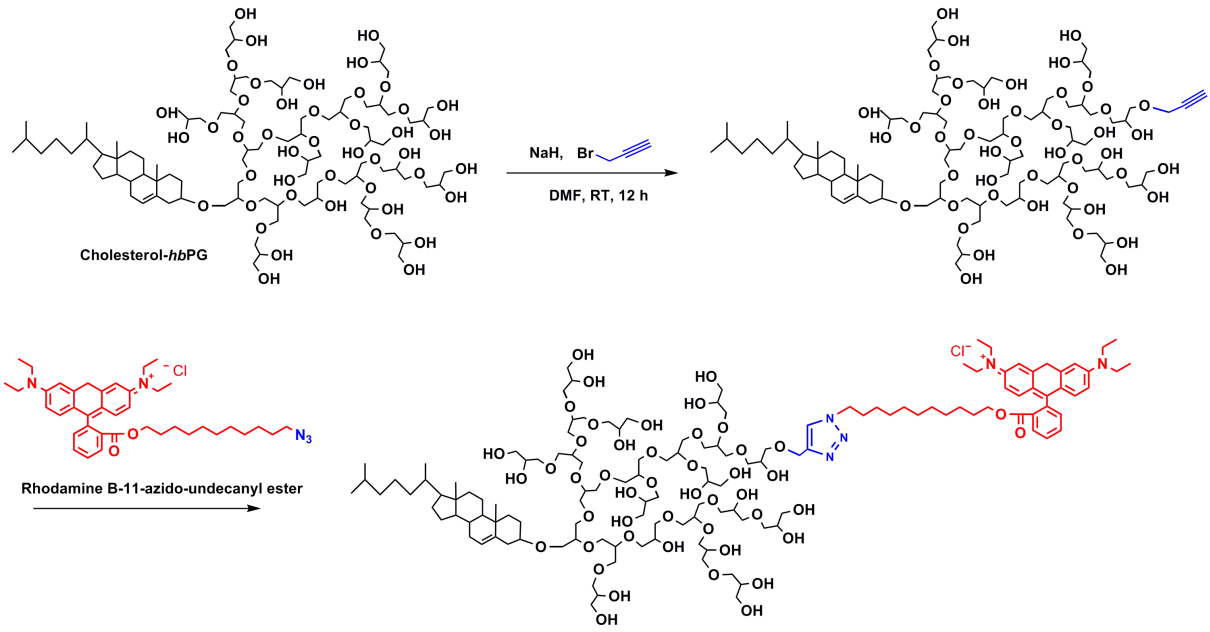

Figure 5. Reaction sequence for the synthesis of rhodamine B-labeled cholesterol-*hb*PG lipids via click-chemistry.

Following this example, functional derivatives can be incorporated in liposomal formulations based on these novel polyether-modified lipids. Facile attachment of fluorescent dyes onto liposomal surfaces via the reaction of alkinyl functionalized cholesterol-PEG-PGs and azido-derived fluorescent dyes has been carried out in order to evidence encapsulation of siRNA into polyether-modified liposomes. The preparation of siRNA complexes and a detailed investigation of their cellular uptake will be presented in a separate study devoted to cellular transport and targeting.

CMC-determination via pyrene fluorescence measurements. At first glimpse, the hydrophilic part of the amphiphilic polyether structures developed may appear to be large in comparison to the respective hydrophobic segment. However, the degree of polymerization of the hydrophilic polyether segment was chosen to be analogous to PEG-based “stealth” lipids.

In order to assess the amphiphilicity of the polyether structures developed in this work, the critical micelle concentrations (CMC) of all amphiphilic polymers and copolymers have been determined using an established fluorescence technique based on pyrene. This extremely hydrophobic dye is preferentially incorporated in the interior of micelles. The onset of micelle formation can be observed in a shift of the fluorescence excitation spectra of the samples at an

emission wavelength of 372 nm.[49, 50] In the concentration range of aqueous micellar solutions, a shift of the excitation band in the 335 nm region towards higher wavelengths confirms the incorporation of pyrene in the hydrophobic interior of micelles (Figure 6). The ratio of the fluorescence intensities at 339 and 335 nm was used to quantify the shift of the broad excitation band.

The critical micelle concentrations determined from the crossover point in the low concentration range (Figure 6) are summarized in Table 1 (*hb*PG lipids) and Table 2 (PEG-*co*-*l*PG and PEG-*co*-PGG lipids). Generally, the measured CMCs of the random copolymer lipids are in the range of 5 to 20 mg/L. Since the EO units show similar hydrophilic properties as the glyceryl units and the ratios between the lipophilic and the hydrophilic fractions of all copolymers were adjusted in a similar range, only a slight increase of the CMC with increasing molecular weight can be noticed. This trend is most pronounced in the series of amphiphilic *hb*PG homopolymers. The CMC for the cholesterol-initiated hyperbranched polyglycerol lipids increases from 1.4 mg/L for *hb*PG_{25} with a molar mass of 2200 g/mol to 4.5 mg/L for *hb*PG_{30} (2600 g/mol) and to 8.3 mg/L for *hb*PG_{35} (3000 g/mol). The growing steric demand of the hyperbranched polyglycerol segment with increasing degree of polymerization leads to formation of micelles at higher concentrations. We tentatively ascribe this to improved solubility of the amphiphilic molecules due to a lower ratio of lipophilic and hydrophilic moieties.

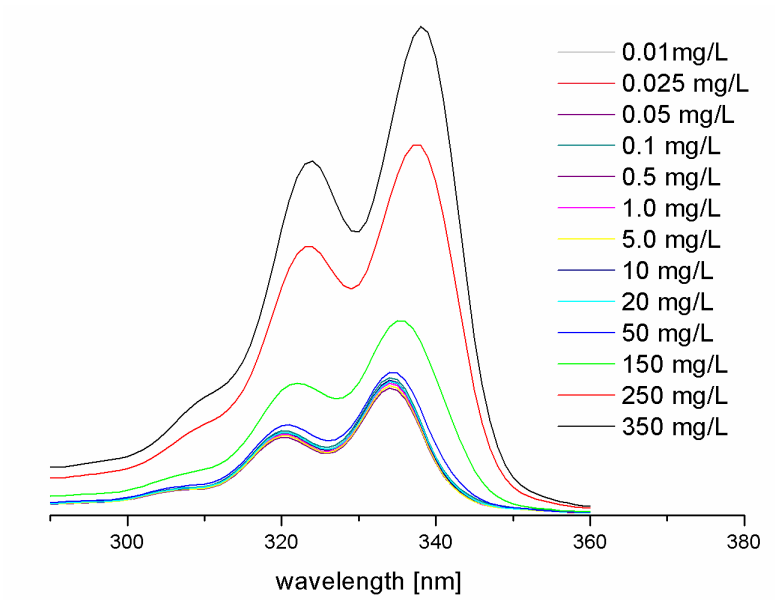

Figure 6. a) Excitation spectra of pyrene in water containing cholesterol-PEG_{12}-*co*-*l*PG_{18} (cf. compound 13, Table 2) at a concentration of 0.01 mg/L.

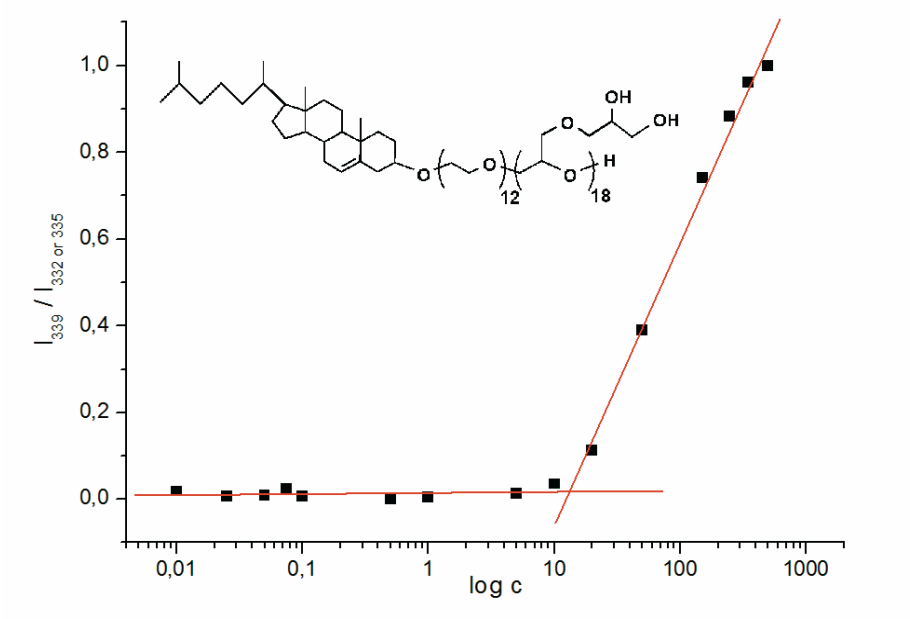

Figure 6. b) CMC determination using pyrene fluorescence excitation spectra at an emission wavelength of 372 nm.

Liposome preparation and characterization. Liposome formulations containing the amphiphilic polyglycerols or respectively the PEG-*co*-*l*PG and PEG-*co*-PGG copolymer lipids have been prepared via the membrane extrusion method. Solutions of DOPC (100 g/L) and the respective polymer (10 g/L) in chloroform were blended at a molar ratio of 98:2 and the organic solvents were removed under reduced pressure. The lipid film was hydrated with tris(hydroxymethyl)-aminomethane/citrate (tris3citrate) buffer (50 mM, pH 7.2) to a final lipid concentration of 40 g/L. The mixture was vortexed to yield multilamellar vesicles (MLV), and subsequent extrusion and further dilution of the solution afforded the liposome formulations.

The aqueous solutions were drop-cast onto hydrophilized copper grids and dried at room temperature before measurement. Cryo TEM images (Figure 7) show that unilamellar liposomes could be formed with particle sizes varying in a range of 70 to 100 nm.

In this manner all novel polyether lipids developed in this study, i.e., *hb*PG, PEG-*co*-*l*PG and PEG-*co*-PGG based lipids were incorporated into liposomal membranes. Both cholesterol and the 1,2-bis-*n*-alkyl glyceryl ethers are able to stabilize the attachment of the polyether lipids with molecular weights varying from 2200 to 4600 g/mol into lipid bilayers based on DOPC.

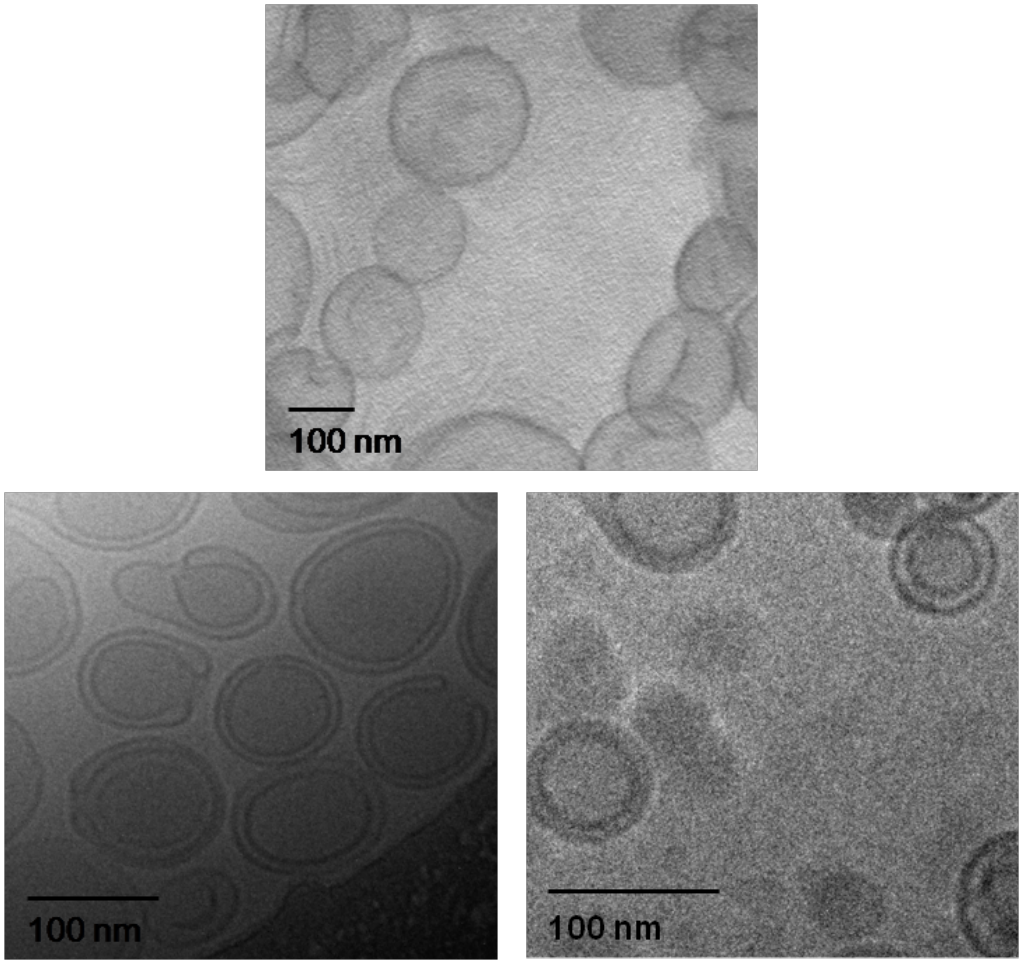

Figure 7. Top: TEM image of liposomes containing DOPC and cholesterol-PEG_{20}-*co*-/PG_{25} (compound **1**, Table 2) in a molar ratio of 98:2 (stained with uranyl acetate). Bottom left and right: cryo TEM image of liposomes containing DOPC and cholesterol-PEG_{32}-*co*-/PG_{18} (compound **2**, Table 2) in a molar ratio of 98:2 (stained with uranyl acetate).

Conclusion

We have developed rapid 2-3 step syntheses for three different types of amphiphilic polyether-based complex lipids with architectural variation of the hydrophilic segment. The syntheses rely on the anionic ring-opening polymerization of EO, glycidol and protected glycidyl ethers (EEGE or IGG) and can be performed in two-step protocols to obtain (i) amphiphilic *hb*PG lipids or in a single reaction step, generating (ii) amphiphilic linear multifunctional PEGs with either isolated or (iii) vicinal hydroxyl moieties at the backbone. Two vicinal hydroxyl groups have been incorporated in the PEG structure via random copolymerization of ethylene oxide with isopropylidene glyceryl glycidyl ether (IGG) and subsequent acidic hydrolysis, which opens

options for derivatization via formation of cyclic acetals or ketals with the respective ketones or aldehydes. All strategies developed are based on the direct use of the lipophilic segment as initiator for the oxyanionic polymerization and generate multifunctional amphiphilic structures. Potentially toxic moieties like amines or aromatic linkages are avoided. As an example for further functionalization the hydroxyl groups have been derivatized with rhodamine B via a two step protocol, based on etherification with propargyl bromide and subsequent click reaction with rhodamine B-azide.

We have also investigated the critical micelle concentrations (CMCs) of the complex lipids and were able to show that all lipids can be incorporated into liposomes, which were visualized via TEM and also by cryo TEM. In a recent paper the properties of the complex polyether lipids described here have been studied with respect to Langmuir and Langmuir-Blodgett films, however, without description of the synthesis.[51]

Due to the analogy of the polymer architectures of these PEG-co-*l*PG lipids and conventional stealth lipids based on PEG, liposome formulations are expected to show similar stealth effects with respect to protein binding and blood circulation times, but furthermore can be easily modified, e.g., by etherification or esterification. Currently, we are studying the application of these lipids for targeted drug transport, emphasizing receptor-mediated delivery strategies.

Acknowledgement

The authors thank Daniel Loeper and Eric Hoffmann for their valuable technical assistance, Eva Hühn for liposome preparation and Robert Branscheid for cryo TEM measurements. A. M. H. acknowledges the graduate school of excellence MAINZ (Material Sciences in Mainz) for a fellowship and valuable financial support. F.W. is grateful to the Alexander von Humboldt Foundation for a Feodor Lynen fellowship at the EPFL.

References

(1) Immordino, M. L.; Dosio, F.; Cattel, L. *Int. J. Nanomed.* **2006,** 1, 297-315.

(2) Allen, C.; Dos Santos, N.; Gallagher, R.; Chiu, G. N. C.; Shu, Y.; Li, W. M. Johnstone, S. A.; Janoff, A. S.; Mayer, L. D.; Webb, M. S.; Bally, M. B. *Biosci. Rep.* **2002,** 22, 225-250.

(3) Allen, T. M.; Cullis, P. R. *Science* **2004,** 303, 1818-1822.

(4) Lasic, D. D.; Martin, F. J.; Gabizon, A.; Huang, S. K.; Papahadjopoulos, D. *Biochimica et Biophysica Acta (BBA) - Biomembranes* **1991,** 1070, 187-192.

(5) Lasic, D. D.; Papahadadjopoulos, D. *Science* **1995,** 267, 1275-1276.

(6) Klibanov, A. L.; Maruyama, K.; Torchilin, V. P.; Huang, L. *FEBS Lett.* **1990,** 268, 235-237.

(7) Blume, G.; Cevc, G. *Biochim. Biophys. Acta, Biomembr.* **1990,** 1029, 91-97.

(8) Lasic, D. D.; Needham, D. *Chem. Rev.* **1995,** 95, 2601-2628.

(9) Woodle, M. C.; Engbers, C. M.; Zalipsky, S. *Bioconjug. Chem.* **1994,** 5, 493-496.

(10) Torchilin, V. P.; Shtilman, M. I.; Trubetskoy, V. S.; Whiteman, K.; Milstein, A. M. *Biochim. Biophys. Acta.* **1994,** 1195, 181-184.

(11) Torchilin, V. P.; Levchenk, T. S.; Whiteman, K. R.; Yaroslavov, A. A.; Tsatsakis, A. M.; Rizos, A. K.; Michailova, E. V.; Shtilman, M. I. *Biomaterials* **2001,** 22, 3035-3044.

(12) Takeuchi, H.; Kojima, H.; Yamamoto, H.; Kawashima, Y. *J. Control. Release* **2001,** 75, 83-91.

(13) Romberg, B.; Oussoren, C.; Snel, C. J.; Hennink, W. E.; Storm, G. *Pharm. Res.* **2007,** 24, 2394-2401.

(14) Maruyama, K.; Okuizumi, S.; Ishida, O.; Yamauchi, H.; Kikuchi, H.; Iwatsuru, M. *Int. J. Pharm.* **1994,** 111, 103-107.

(15) Roberts, W. G.; Palade, G. E. *Cancer Res.* **1997,** 57, 765-772.

(16) Allen, T. M.; Sapra, P.; Moase, E.; Moreira, J. O.; Iden, D. *J. Liposome Res.* **2002,** 12, 5-12.

(17) Dvorak, H.; Nagy, J.; Dvorak, J.; Dvorak, A. *Am. J. Pathol.* **1988,** 133, 95-109.

(18) Pasut, G.; Veronese, F. M. *Prog. Polym. Sci.* **2007,** 32, 933-961.

(19) Zalipsky, S. *Bioconjugate Chem.* **1995,** 6, 150-165.

(20) Thompson, M. S.; Vadala, T. P.; Vadala, M. L.; Lin, Y.; Riffle, J. S. *Polymer* **2008,** 49, 345-373.

(21) Herman, S.; Hooftman, G.; Schacht, E. J. *Bioact. Compat. Polym.* **1995,** 10, 145-187.

(22) Vadala, M. L.; Thompson, M. S.; Ashworth, M. A.; Lin, Y.; Vadala, T. P.; Ragheb, R.; Riffle, J. S. *Biomacromolecules* **2008,** 9, 1035-1043.

(23) Zeng, F.; Allen, C. *Macromolecules* **2006,** 39, 6391-6398.

(24) Pasut, G.; Scaramuzza, S.; Schiavon, O.; Mendichi, R.; Veronese, F. M. *J. Bioact. Compat. Polym.* **2005,** 20, 213-230.

(25) Choe, Y. H.; Conover, C. D.; Wu, D.; Royzen, M.; Gervacio, Y.; Borowski, V.; Mehlig, M.; Greenwald, R. B. *J. Controlled Release* **2002,** 79, 55-70.

(26) Hawker, C. J.; Chu, F.; Pomery, P. J.; Hill, D. J. T. *Macromolecules* **1996,** 29, 3831-3838.

(27) Taton, D.; Saule, M.; Logan, J.; Duran, R.; Hou, S.; Chaikof, E. L.; Gnanou, Y. *J. Polym. Sci., Part A: Polym. Chem.* **2003,** 41, 1669-1676.

(28) Wurm, F.; Nieberle, J.; Frey, H. *Macromolecules* **2008,** 41, 1184-1188.

(29) Wurm, F.; Nieberle, J.; Frey, H. *Macromolecules* **2008,** 41, 1909-1911.

(30) Wurm, F.; Klos, J.; Räder, H. J.; Frey, H. *J. Am. Chem. Soc.* **2009,** 131, 7954-7955.

(31) Koyama, Y.; Umehara, M.; Mizuno, A.; Itaba, M.; Yasukouchi, T.; Natsume, K.; Suginaka, A.; Watanabe, K. *Bioconjugate Chem.* **1996,** 7, 298-301.

(32) Mangold, C.; Wurm, F.; Obermeier, B.; Frey, H. *Macromol. Rapid Commun.* **2010,** (31, 258-264.

(33) Mangold, C.; Wurm, F.; Obermeier, B.; Frey, H. *Macromolecules* **2010,** 43, 8511-8518.

(34) Obermeier, B.; Wurm, F.; Frey, H. *Macromolecules* **2010,** 43, 2244-2251.

(35) Hofmann, A. M.; Wurm, F.; Hühn, E.; Nawroth, T.; Langguth, P.; Frey, H. *Biomacromolecules* **2010**, *11*, 568-574.

(36) Kainthan, R. K.; Janzen, J.; Levin, E.; Devine, D. V.; Brooks, D. E. *Biomacromolecules* **2006,** 7, 703-709.

(37) Kainthan, R. K.; Janzen, J.; Kizhakkedathu, J. N.; Devine, D. V.; Brooks, D. E. *Biomaterials* **2008,** 29, 1693-1704.

(38) Wilms, D.; Stiriba, S.-E.; Frey, H. *Acc. Chem. Res.* **2010,** 43, 129-141.

(39) Calderón, M.; Quadir, M. A.; Sharma, S. K.; Haag, R. *Adv. Mater.* **2009,** 22, 190-218.

(40) Jones, A. T.; Gumbleton, M.; Duncan, R. *Adv. Drug Delivery Rev.* **2003,** 55, 1353-1357.

(41) Fitton, A. O.; Hill, J.; Jane, D. E.; Millar, R. *Synthesis* **1987**, 1140-1142.

(42) Tokar, R.; Kubisa, P.; Penczek, S.; Dworak, A. *Macromolecules* **1994,** 27, 320-322.

(43) Dworak, A.; Walach, W.; Trzebicka, B. *Macromol. Chem. Phys.* **1995,** 196, 1963-1970.

(44) Sunder, A.; Hanselmann, R.; Frey, H.; Mülhaupt, R. *Macromolecules* **1999,** 32, 4240-4246.

(45) Ahl, P. L.; Bhatia, S. K.; Meers, P.; Roberts, P.; Stevens, R.; Dause, R.; Perkins, W. R.; Janoff, A. S. *Biochim. Biophys. Acta, Biomembr.* **1997,** 1329, 370-382.

(46) Allen, T. M.; Hansen, C. *Biochim. Biophys. Acta, Biomembr.* **1991,** 1068, (2), 133-141.

(47) Bedu-Addo, F. K.; Huang, L. *Adv. Drug Delivery Rev.* **1995,** 16, 235-247.

(48) Hamaide, T.; Goux, A.; Llauro, M. F.; Spitz, R.; Guyot, A. *Angew. Makromol. Chem.* **1996,** 237, 55-77.

(49) Wilhelm, M.; Zhao, C. L.; Wang, Y.; Xu, R.; Winnik, M. A.; Jean Luc Mura, G. R.; Croucher, M. D. *Macromolecules* **1991,** 24, 1033-1040.

(50) Wolf, F. K.; Hofmann, A. M.; Frey, H. *Macromolecules* **2010,** 43, 3314-3324.

(51) Reuter, S.; Hofmann, A. M.; Busse, K.; Frey, H.; Kressler, J. *Langmuir*, **2011**, 27, 1978-1989.

Chapter 2.3: Preparation of PEG-PG liposomes via dual asymmetric centrifugation for efficient encapsulation and targeted delivery of siRNA

Chapter 2.3

Preparation of PEG-PG liposomes via dual asymmetric centrifugation for efficient encapsulation and targeted delivery of siRNA

Markus Hirsch,[1] Anna Maria Hofmann,[2] Thomas Fritz,[1] Holger Frey,[2,*] and Mark Helm[1,*]

1 Institut für Pharmazie und Biochemie, Johannes Gutenberg-Universität, Staudinger Weg 5, 55128 Mainz, Germany.

2 Institut für Organische Chemie, Johannes Gutenberg-Universität, Duesbergweg 10-14, 55099 Mainz, Germany.

Abstract

Liposomal formulations of small interfering ribonucleic acid (siRNA) with amphiphilic polyether-modified lipids based on poly(ethylene glycol)-polyglycerol block copolymers (PEG-*b*-PG) have been prepared using the dual asymmetric centrifugation (DAC). This new technique combines rapid and sterile liposome preparation with very high entrapping efficiencies. Successful incorporation of cholesteryl-PEG-*b*-PG block copolymers with different molecular weights and structural architectures into the liposomes has been employed for the preparation of formulations with polyethers bearing clickable alkyne functions. Cycloaddition reactions with azide-functionalized fluorescent dyes on the surface of the preformed liposomes and subsequent fluorescent analysis showed full incorporation of the PEG-*b*-PG lipids into the liposomal membranes. The efficient and fast DAC preparation technique in combination with sensitive fluorescent analysis allows the preparation of liposomes coated with clickable, multifunctional PEG-*b*-PG block copolymers in very small batch sizes of about 60 mg. Compared to conventional liposomes, investigation of liposome sizes via dynamic light scattering (DLS) and fluorescence measurements revealed improved stabilization of the formulations during storage over months. Furthermore, the encapsulation and entrapment efficiencies of siRNA molecules into the PEG-*b*-PG coated liposomes have been determined employing fluorescently labeled siRNA. Using click chemistry, further functionalization of the liposomes via covalent attachment of other molecules such as azide-functionalized folate as targeting groups has been

carried out. In this manner the liposomal delivery of entrapped siRNA molecules might be improved by specific targeting, resulting in enhanced receptor-mediated endocytosis of the liposomal carrier. In the recent study, the calcein uptake in epithelial carcinoma cells (KB cells) has been investigated by flow cytometry.

Keywords

siRNA, dual asymmetric centrifugation, liposomes, poly(ethylene glycol), polyglycerol, block copolymer

Introduction

Since the observation of Fire and Mello roughly a decade ago that ribonucleic acid interference (RNAi) can induce the degradation of multiple copies of messenger RNA (mRNA) and therefore suppress specific protein expression significantly, this interaction has developed to a well known and widely used technique in life sciences.[1] Especially, the mechanisms of gene silencing by small interfering RNA (siRNA) has been investigated intensively and resulted in its application as a standard method in laboratories and its use in clinical trials.[2] While double-stranded RNA (dsRNA) molecules with more than 30 base pairs (bp) can provoke the interferone pathway, resulting in global reduction of protein synthesis, chemically synthesized siRNA with typical lengths of 21-22 nucleotides (nt) with 3' overhangs are able to evade the interferone response.[3-6] The breakthrough developments in the area of gene silencing during the past decade are based on the simple application of siRNA in *in vitro* experiments and its ability to selectively reduce gene expression by inhibiting protein translation. Besides the study of the detailed mechanisms involved in the unique effect of siRNA on protein expression, the screening of specific siRNA for biomedical investigations and clinical trials is one main task in the field of current RNAi research.

Nevertheless, the potential application of systemically administered siRNA in medical drug therapies depends on its effective delivery to the site of action. Selective release of any active agent in sufficient concentrations at the target site and reduced distribution to healthy tissue minimizes side reactions and strongly improves pharmacokinetic properties. Since negatively charged nucleic acids demand directed passage through the cell membrane, the development

of effective carrier systems has been of increasing interest.[7,8] In first approaches, the transfection of siRNA in cell cultures has been achieved via the simple addition of cationic lipids resulting in the formation of lipoplexes. However, *in vivo* studies demonstrated the transient effect on gene silencing and the lipid-mediated inflammatory properties of these lipoplexes. Alternative approaches have been based on the use of liposomes, consisting of self-assembled bilayers of lipids creating an aqueous compartment for the effective transport of siRNA into cells. Liposomal delivery of siRNA offers several advantages such as constant release of the pharmaceutical agent and improved pharmacokinetics.[9-13]

Additional coating of the liposomes with biocompatible polymers such as poly(ethylene glycol) (PEG) results in sterically stabilized, so-called stealth liposomes, with increased *in vivo* half-lifes of 40 hours to 5 days due to significantly reduced blood clearance.[14-24] In the case of siRNA, encapsulation in long-circulating liposomes inhibits early degradation by nucleases in blood plasma. Furthermore, tissue distribution characteristics change as a consequence of liposomal encapsulation, i.e., the main part of the administered dose allocates in the blood, while only a low percentage is deposited in the liver.

Thus, the incorporation of siRNA in liposomes offers two major benefits: (i) protection of the drug and (ii) prolonged circulation times as well as accumulation at the target site due to the enhanced permeability and retention effect (EPR-effect) of tumor tissue.[25-28] One main drawback of these formulations is the lack of additional functionalities that can be used for the covalent attachment of targeting and labeling moieties. In order to specifically address target tissue and increase selective, receptor-mediated endocytosis of liposomes, the respective ligands have been incorporated into liposomal formulations. Promising examples of targeting moieties are proteins such as the transferrin receptor or small molecules such as folic acid.[28-35] The combination of the encapsulation of hydrophilic siRNA in the inner aqueous compartment of a sterically stabilized liposome with the efficiency of receptor-mediated targeting offers the possibility of an extremely potent medical therapy with sufficiently minimized side effects. Furthermore, the formulations of liposomal siRNA should show improved stability due to the unfeasible passive diffusion of the water-soluble and negatively charged RNA molecule across the lipid bilayer.

In this study, we present the preparation and characterization of siRNA liposomes coated with multifunctional hydrophilic copolymer lipids based on poly(ethylene glycol) (PEG) and

polyglycerol (PG) synthesized via cholesterol-initiated ring-opening polymerization (ROP) of different epoxide monomers.[36,37] Chemical structures of all polyether-modified lipids used in this study are presented in Figure 1.

Liposome synthesis via the dual asymmetric centrifugation (DAC) allows the preparation of small batch sizes in the mg range, which is desirable for the investigation of siRNA liposomes due to the high cost of synthetic siRNA molecules. Nevertheless, high entrapment efficiencies of 50-80% as well as sterility during the synthesis have been achieved and are comparable to classical liposome fabrication techniques, i.e., extrusion, high pressure homogenization, ultrasound treatment and detergent dialysis.[38,39]

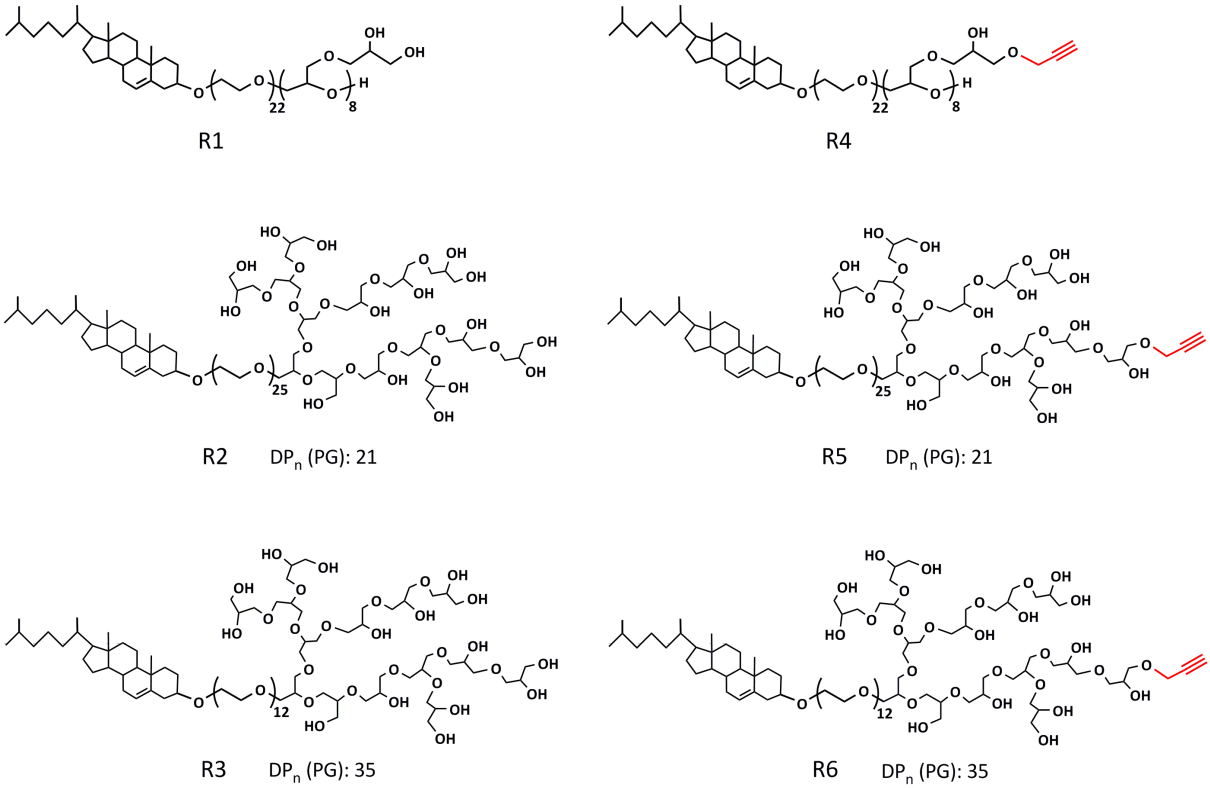

Figure 1. Chemical structures of cholesterol-initiated PEG-PG copolymers used for the coating of siRNA or calcein containing liposomes with different molecular architectures: R1 and R4: linear PEG-PGG block copolymers and R2, R3, R5 and R6: linear-hyperbranched PEG-*hb*PG block copolymers with and without clickable alkyne-functionality, respectively. The degree of polymerization of the hyperbranched PG block in compound R2, R3, R5 and R6 is not depicted by the chemical structures shown.

The successful incorporation of both the pharmacological active siRNA as well as the protective layer of PEG-PG block copolymer lipids have been confirmed via fluorescence measurements of covalently attached dyes, such as fluorescein, atto488, alexa488, tetramethyl rhodamine (TMR), atto590 and azide-functionalized alexa594-azide. The covalent attachment of fluorescent labels as well as targeting moieties, e.g., folate to the PEG-PG copolymers has been achieved via copper(I)-catalyzed Huisgen-cycloaddition of alkyne-modified polymers with different azide-compounds on the surface of the preformed siRNA liposomes. An improved cellular uptake of the folate-functionalized liposomes has been determined using flow cytometry.

Experimental section

siRNA. Dye-siRNA constructs labeled with fluorescein (FL), tetramethyl rhodamine (TMR), atto488, atto590 and alexa488 were purchased from IBA GmbH (Göttingen, Germany). The siRNA sequence is directed against the EGFP protein (GenBank Accession) (sense: 5′-GCAAGCUGACCCUGAAGUUCAdC-donor-3′ and antisense 5′-acceptor-GCCGUUCGACUGGGACUUCAAG-3′). FL, atto488 and alexa488 serve as donor dye, while TMR and atto590 function as acceptor dye. For the formation of siRNA duplexes, sense and antisense strand solutions were mixed in a ratio of 1:1.1 as stated in earlier studies. The final solution contained 1x PBS at pH 7.4 and 43°µM of the sense and 47°µM of the antisense strand to achieve physiological conditions. . The siRNA mixture was annealed for 1 h at 37 °C after 5 min separation at 90 °C. siRNA duplex solutions were stored at −20 °C.

Cholesterol-PEG-*b*-PG block copolymers. The amphiphilic copolymers for this study have been synthesized via cholesterol-initiated oxyanionic polymerization of different epoxide monomers as reported previously.[36,37] Further derivatization of the hydroxyl-functionalized polyether lipids with propargyl bromide under basic conditions resulted in cholesterol-PEG-*b*-PG block copolymers containing clickable alkyne-functionalities. Modification reactions have been carried out as described in literature.[36] Chemical structures of all polymers investigated in this study are presented in Figure 1. Characterization data including molecular weights determined via integration of ^{1}H NMR spectra in dimethylsulfoxide (DMSO) and polydispersities (PDI) determined by size exclusion chromatography (SEC) in dimethylformamide (DMF) are summarized in Table 1.

Table 1. Characterization data of the cholesterol-initiated PEG-*b*-PG block copolymers used for stealth liposome preparation.

#	polymer	M_n (NMR) [g/mol]	PDI
R1	cholesterol-PEG_{22}-*b*-PGG_8	2540	1.10
R2	cholesterol-PEG_{25}-*b*-*hb*PG_{21}	3040	1.19
R3	cholesterol-PEG_{12}-*b*-*hb*PG_{35}	3500	1.08
R4	cholesterol-PEG_{22}-*b*-PGG_8-$(OCH_2CCH)_4$	2780	1.08
R5	cholesterol-PEG_{25}-*b*-*hb*PG_{21}-(OCH_2CCH)	3100	1.11
R6	cholesterol-PEG_{12}-*b*-*hb*PG_{35}-(OCH_2CCH)	3560	1.15

Liposome preparation by DAC. Conventional and polyether-modified liposomes have been prepared as described in previous studies.[39] To this end, the lipids, i.e., cholesterol, hydrogenated egg phosphatidylcholin (EPC3) (Lipoid GmbH; Ludwigshafen, Germany) and the respective stealth PEG-PG lipids were dissolved in absolute ethanol in a molar ratio of 40:55:5. Aliquots containing 21 mg of the lipids were dried in 2.0 mL reaction tubes using a vacuum centrifuge (Concentrator plus, Eppendorf, Hamburg, Germany) for about 4-6 h. Batch sizes of 60 mg vesicular phospholipid gels (VPG) have been prepared. As containers, standard 2.0 mL reaction tubes (Eppendorf AG, Hamburg, Germany) were used. Each batch consisted of 3 parts: the lipid mixture, the aqueous solution and glass beads of 1 mm diameter (Sartorius GmbH, Göttingen, Germany). As aqueous solutions, PBS (for empty liposomes), 50 mM calcein solution (pH 8, in PBS) or siRNA solution (containing 43 µM of the sense and 47 µM of the antisense strands; described above) were used. For the preparation of conventional liposomes (CL), a batch consisted of 35% lipid mixture and 65% aqueous solution plus the same mass of the glass beads (100%) were used (compositions are always expressed as wt.%). After mixing all components and sealing of reaction tubes, the batches were incubated for 10 min at room temperature to allow hydration of the lipids. The reaction tube was placed in the respective tube holder in a horizontal orientation and processed in a dual asymmetric centrifuge (DAC 150 FVZ; Hauschild GmbH & Co KG, Hamm, Germany) at 3540 rpm for 30 min in six steps of 5 min to prepare the VPG. The resulting VPGs were redispersed by adding 200% (related to the VPG) of

PBS and subsequent dual asymmetric centrifugation for 2 x 30 sec to obtain a liposomal dispersion. Samples were stored at 4 °C.

Removal of non-entrapped siRNA. The 1:3 diluted VPG containing siRNA were purified from non entrapped molecules by the use of Centrisart I inverted spin filters (100 000 MWCO; Sartorius AG). A portion of the diluted VPG (60 mg batch: 130 µl) was placed in the outer sample tube of the filter device and volume was adjusted to 2 mL with PBS. After placing the inner filter tube in the outer tube, the filter device was incubated for 5 min at room temperature to wet the membrane. The spin filters were centrifuged 3 to 4 times at 2000×*g* and 23 °C for 30 min. Between the runs, the filtrate was carefully removed to facilitate the further filtering process until a rest volume of about 200 µl remained in the sample tube.

Removal of non-entrapped calcein. The purification of liposomes containing calcein or liposomes modified by click reaction was achieved by size exclusion chromatography (Illustra NAP 5).

Fluorescence spectroscopy. Fluorescence of the dyes attached to the siRNA or clicked to the liposome was detected using a fluorescence spectrometer (FP-6500 Fluorimeter, Jasco, Tokyo, Japan)). Measurement is performed at an excitation wavelength of 488 nm for fluorescein, atto488 and alexa488 and emission profile is recorded between 500 nm and 750°nm. For atto590 ore alexa594 analysis samples were excited at 590nm and the emission was recorded from 600 nm to 750 nm. All measurements were conducted in in 15µl Hellma black quartz glass cuvettes (1.5mm path length).

Quantification by fluorescence spectroscopy. Calcein containing liposomes were diluted to a final concentration of around 150 nM with 1x PBS containing 1% Triton X-100 to disintegrate the liposomes. Finally EDTA was added to reach a concentration of 5mM to prevent a quenching of calcein. The calcein content of the samples was quantified using a fluorescence spectrometer (FP-6500 Fluorimeter, Jasco, Tokyo, Japan). The measurements were performed at an excitation wavelength of 490 nm and an emission wavelength of 520 nm in 15µl Hellma black quartz glass cuvettes (1.5mm pathlength). For calibration calcein dilutions ranging from 5-200 nM were used.

Click reactions. Cycloaddition reactions have been performed with the vesicular lipid gels in phosphate buffer solution (PB 100 mM) using tris(hydroxylpropyltriazolylmethyl)amine (TPTA) 2.5 mM, sodium ascorbate 5 mM, $CuSO_4$ 0.5 mM, folate-azide 0.1 mM, cholesterol-PEG-*b*-PG

copolymers 2 mM. Negative controls have been prepared by absence of the folate-azide (L4-) or using the non-functionalized cholesterol-PEG-*b*-PG (L1). All click reactions were carried out at 25 °C for 2 hours. The purification of the reaction mixtures was achieved by size exclusion chromatography as described above.

Calcein uptake. *In vitro* cell experiments were performed with KB cells, an epithelial carcinoma cell line that is adherent and grows in monolayers. The cells were treated and cultivated at standard sterile conditions under a flow bench and an incubator at 37 °C and 5% CO_2. The cells were grown until 80-90% confluence in sterile culture flasks (75 cm^2, Sarstedt, Germany) and detached with 3 mL trypsin-EDTA (Gibco, Invitrogen), incubating at 37 °C for 5 minutes. After adding 7 mL growth media, the cell suspension was centrifuged at 200×g for 5 minutes, the obtained pellet was resuspended in 10 mL media. Aliquots of 10% and 20% of the cell suspension were transferred to new sterile flasks and growth media was added to a total volume of 25 mL. Cells were incubated for at least one day prior to the next splitting, in order to guarantee the attachment of all cells to the surface. The concentration of the cell suspension described above was evaluated using a Beckmann particle counter, and stock suspensions of 160 000 cells/mL were obtained by dilution with growth media. In sterile 24-well culture plates (Sarstedt, Germany), 0.5 mL of these suspensions were added resulting in 80 000 cells/well and incubated for at least 12 hours before adding the liposomal formulation. The media was substituted with the liposomal formulation in growth media, containing 5 mM EDTA and specific concentrations (250 nM, 1000 nM, 2000 nM and 4000 nM) of total calcein. The total calcein concentration was determined by spectral fluorometry as described above. After incubation, the liposomal formulations were removed, rinsed once with 0.6 mL sterile PBS, resuspended in 0.6 mL sterile PBS and transferred to flow cytometry round bottom tubes (Becton, Dickinson and Company, Franklin Lakes, USA) and stored on ice to prevent cell degradation. Flow cytometry experiments were performed on a BD FACSCalibur flow cytometer (Becton, Dickinson and Company, Franklin Lakes, USA), equipped with an 488 nm (15 mW) argon ion laser. A total of 15 000 to 20 000 events were registered while measuring forward and sideward scatter for identification and the fluorescence intensity with a 530 nm bandpass filter. The flow rate was adjusted to be below 500 events per second at all times. For the calibration with negative cells, the photomultiplier current was regulated to obtain a signal within the first decade of the logarithmic scale of fluorescence intensity.

Results and discussion

Liposome preparation. Liposomal formulations with amphiphilic poly(ethylene glycol)-*b*-polyglycerol-modified lipids have been prepared using the dual asymmetric centrifugation (DAC). In order to demonstrate successful incorporation of the block copolymers into the liposomes fluorescent analysis of polymer-conjugated dyes was carried out. Furthermore, liposomes coated with PEG-*b*-PG of different molecular weights and structural architectures were characterized by DLS regarding the effect of the polymer structure on the lipid vesicles.

Liposomes and polymer-coated liposomes entrapping siRNAs or calcein were prepared using DAC in a batch size of 60 mg. Coating and potential sterical stabilization of the liposomes have been achieved by the incorporation of amphiphilic poly(ethylene glycol)-polyglycerol block copolymers into the liposomal formulation of cholesterol and hydrogenated egg phosphatidylcholin (EPC3) in a molar ratio of 5:40:55.

Liposome sizes and size distributions were determined via dynamic light scattering (DLS) (Figure 2). Interestingly, the size of the resulting liposomes depended only slightly on the molecular weight of the polymer lipid mixtures employed. Thus, liposomes consisting merely of cholesterol and EPC3 showed similar and to some extent larger sizes than liposomes with diameters of about 150 nm containing also polymer lipids. On the other hand, the introduction of propargyl groups in the periphery of the polyethers (R4-R6) resulted in a general increase of the final liposome sizes up to 250 nm.

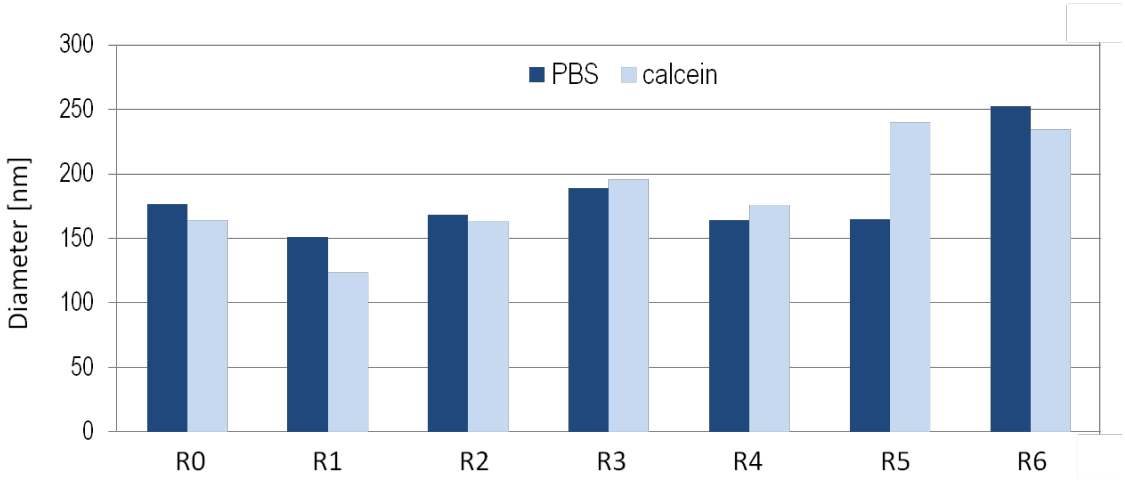

Figure 2. Sizes of polymer-coated liposomes determined via DLS of the samples directly after preparation by DAC. Liposomes R1 to R6 refers to the incorporation of polymer R1 to R6 in the

lipid mixture of cholesterol and EPC3 in a molar ratio of 5:40:55. In R0 cholesterol and EPC3 were mixed in a molar ratio of 45:55 and no stealth lipid was added.

Furthermore, the sizes of the PEG-*b*-PG coated liposomes determined via dynamic light scattering (DLS) were found to be stable during storage over a long period of time (up to 7 months). While previous studies revealed an increase of the liposome size during storage for conventional liposomes without polymer coating, the recent liposomal formulations showed similar sizes even after storage over months. The enhanced stability of the formulations might be due to the shielding effect of the polymer chains. Thus, we conclude that the interaction of lipids and especially ionic lipid head groups of the liposomal surfaces with each other or not fully entrapped guest molecules, such as calcein are avoided due to the steric stabilization of the PEG-*b*-PG block copolymers.

Fluorescence labeling via click reaction. Incorporation of the stealth PEG-*b*-PG lipids in the liposomes formed has been evidenced by the covalent attachment of fluorescent dyes at the preformed liposomal surface. In order to simplify the synthetic approach, cholesterol-initiated PEG-*b*-PG copolymers bearing multiple hydroxyl groups have been functionalized using propargyl bromide, as described elsewhere.[36] Thus, the conjugation of azide-functionalized dyes, i.e., alexa594 (Figure 3) has been achieved via copper-catalyzed 1,3-dipolar cycloaddition reactions (Huisgen reaction) of alkyne-modified cholesterol-PEG-*b*-PGs in buffer solution. Purification of the reaction mixtures was achieved by preparative size exclusion chromatography. Fluorescence intensities of the liposomal formulations with and without clickable alkyne functionalities confirm the incorporation of the amphiphilic PEG-*b*-PG copolymers in the lipid membrane as well as the effective modification with fluorescent labels via cycloaddition (Figure 4). Thus, strong fluorescence of alexa594 has been observed in liposomal formulations containing alkyne-modified polymers (LipoR4-LipoR6). In order to remove unattached dye or other compounds of the reaction mixture from the liposome solutions, all mixtures have been purified via SEC. Clearly, the lack of alkyne groups in the respective non-functionalized PEG-*b*-PG block copolymers (LipoR1-LipoR3) resulted in the absence of fluorescence after purification as well as the preparation of liposomes based on cholesterol and EPC3 without additional stealth lipids (LipoR0).

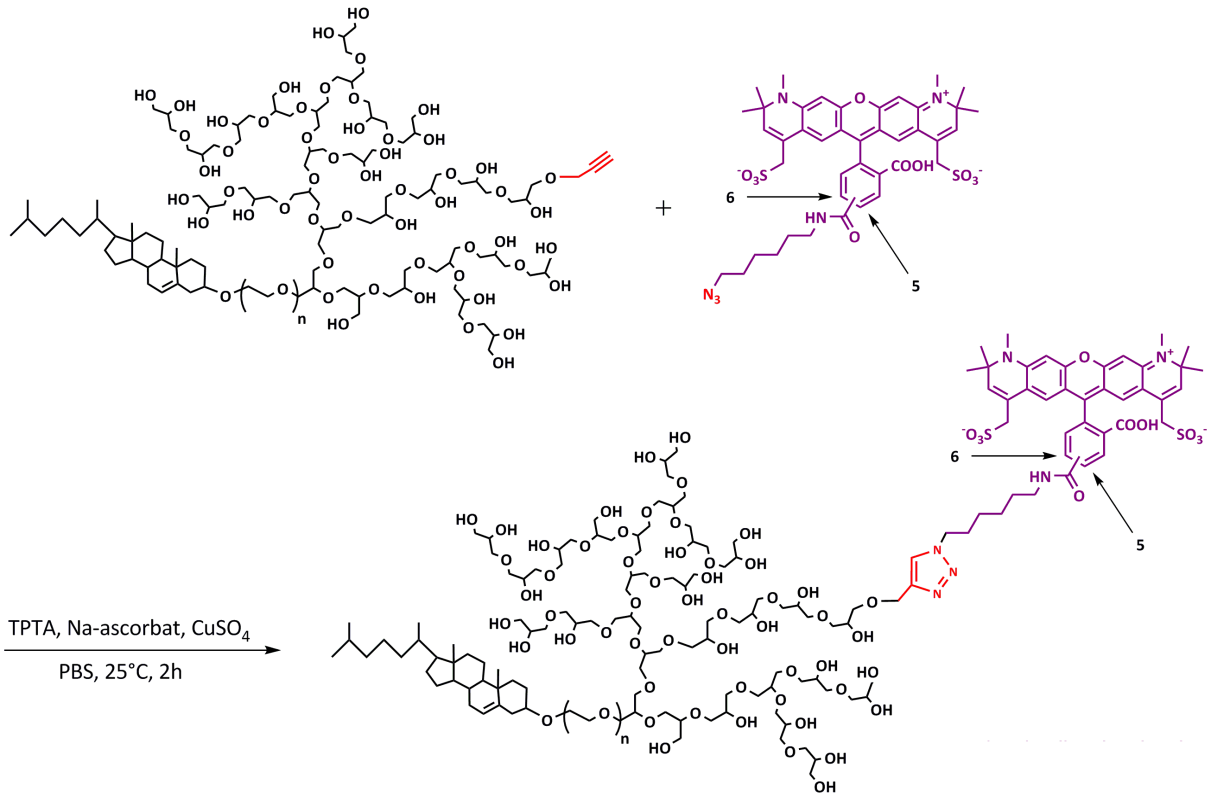

Figure 3. Reaction sequence of the copper-mediated cycloaddition between an alkyne-modified cholesterol-PEG-*b*-*hb*PG copolymer lipid and alexa594-azide at the preformed liposomes in aqueous solution.

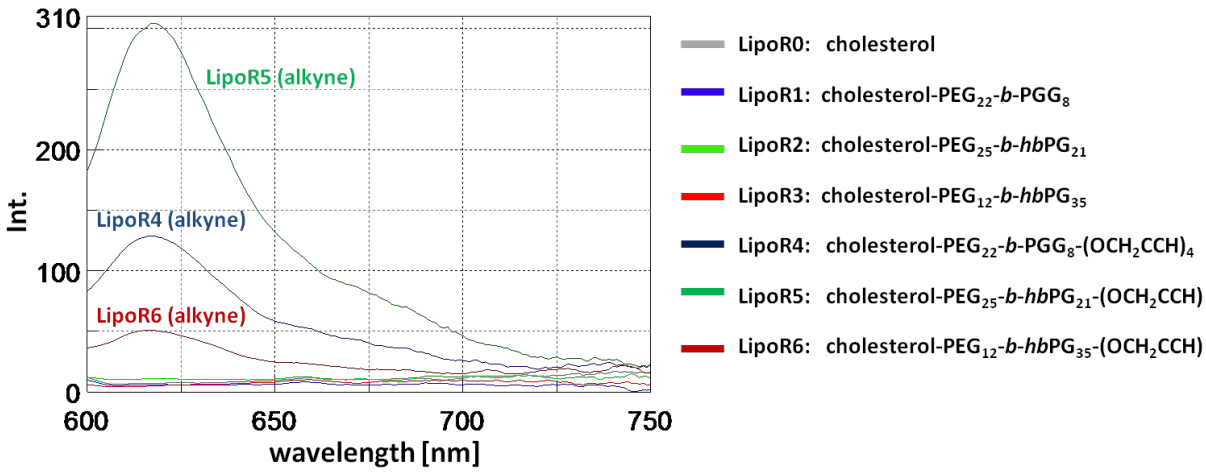

Figure 4. Fluorescence spectra obtained for the purified liposomes containing different cholesterol-PEG-*b*-PGs. The number LipoR# refers to the polymeric compound added to the liposomal formulation (compare Figure 1 and Table 1). The observation of fluorescence for

liposomes R4-R6 confirms incorporation of the PEG-*b*-PG lipids in the liposomal membrane as well as the successful attachment of the fluorescent label via click reaction.
The successful covalent attachment of a fluorescent dye gives on one hand strong evidence for the incorporation of the polyether-modified lipids into the liposomal formulation. On the other hand, the cycloaddition allows the facile and quantitative incorporation of other functional molecules such as targeting moieties using mild reaction conditions.

As presented above, liposomes coated with the novel PEG-*b*-PG lipids have been successfully prepared, furthermore modified with dyes via click reaction and characterized by fluorescence measurements. In a next step, the entrapment of small interfering RNA (siRNA) in the polyether-stabilized liposomes has been investigated. With this objective in mind, siRNA molecules with covalently attached fluorescent dyes have been encapsulated into liposomal formulations containing PEG-*b*-PG block copolymer lipids. After preparation and purification of the liposomes, the incorporation has been examined by detailed fluorescence measurements.

Figure 5 shows the fluorescence spectra of liposomal formulations containing different fluorescently labeled siRNA molecules after removal of excess, i.e., not entrapped siRNA. A spectrum of free, non-encapsulated siRNA has been measured and a calculated spectrum of the empty liposomes was subtracted from the siRNA containing one. Fluorescence measurements permit to confirm encapsulation of the respective labeled intact siRNA (for FL/TMR and atto488/atto590) into the liposomes as well as to quantify the entrapping efficiency by comparison of the fluorescence intensities. In this manner the fluorescence of empty liposomes (cf. Figure 5, empty liposomes) has been subtracted from the fluorescence of the labeled siRNA molecules entrapped into liposomes (cf. Figure 5, lip), resulting in the corrected intensities for the encapsulated dyes (cf. Figure 5, lip corr). Experiments with different fluorescent labels, e.g., FL/TMR (Figure 5a), atto488/atto590 (Figure 5b) and alexa488 (Figure 5c), clearly evidence incorporation of siRNA into the liposomal formulations.

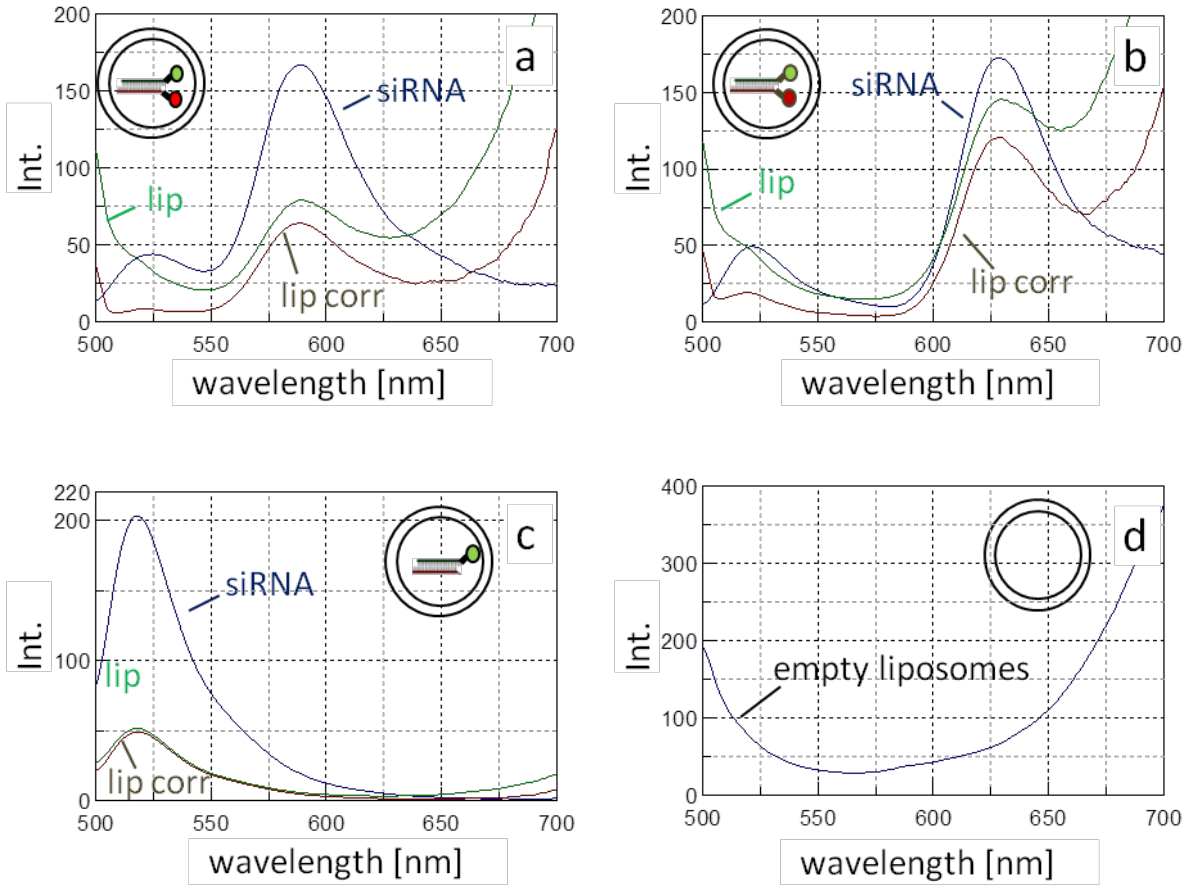

Figure 5. Fluorescence spectra obtained for the purified liposomes containing siRNA molecules with different fluorescent labels and "empty" liposomal formulations, respectively (Figure 5d). Fluorescence intensities of free labeled siRNA (blue, siRNA), of labeled siRNA entrapped into liposomes (green, lip) and the corrected fluorescence intensities of labeled siRNA entrapped into liposomes (lip - siRNA = lip corr). The experiments were carried out with different fluorescent labels, e.g., FL/TMR (Figure 5a), atto488/atto590 (Figure 5b) and alexa488 (Figure 5c).

Calcein uptake. The calcein uptake in KB cells has been investigated by flow cytometry as described above. The comparison of the fluorescence intensities between liposome-incubated cells and the cells that were treated with mere calcein solution (negative control) showed significant deviations using concentrations below 2000 nM. Thus further experiments were performed with 250 nM and 1000 nM total calcein concentrations. In addition, the studies were focused on the investigation of incubation times of 4 and 24 h, since prolonged incubation times of 36 h revealed similar results as the experiments with 24 h.

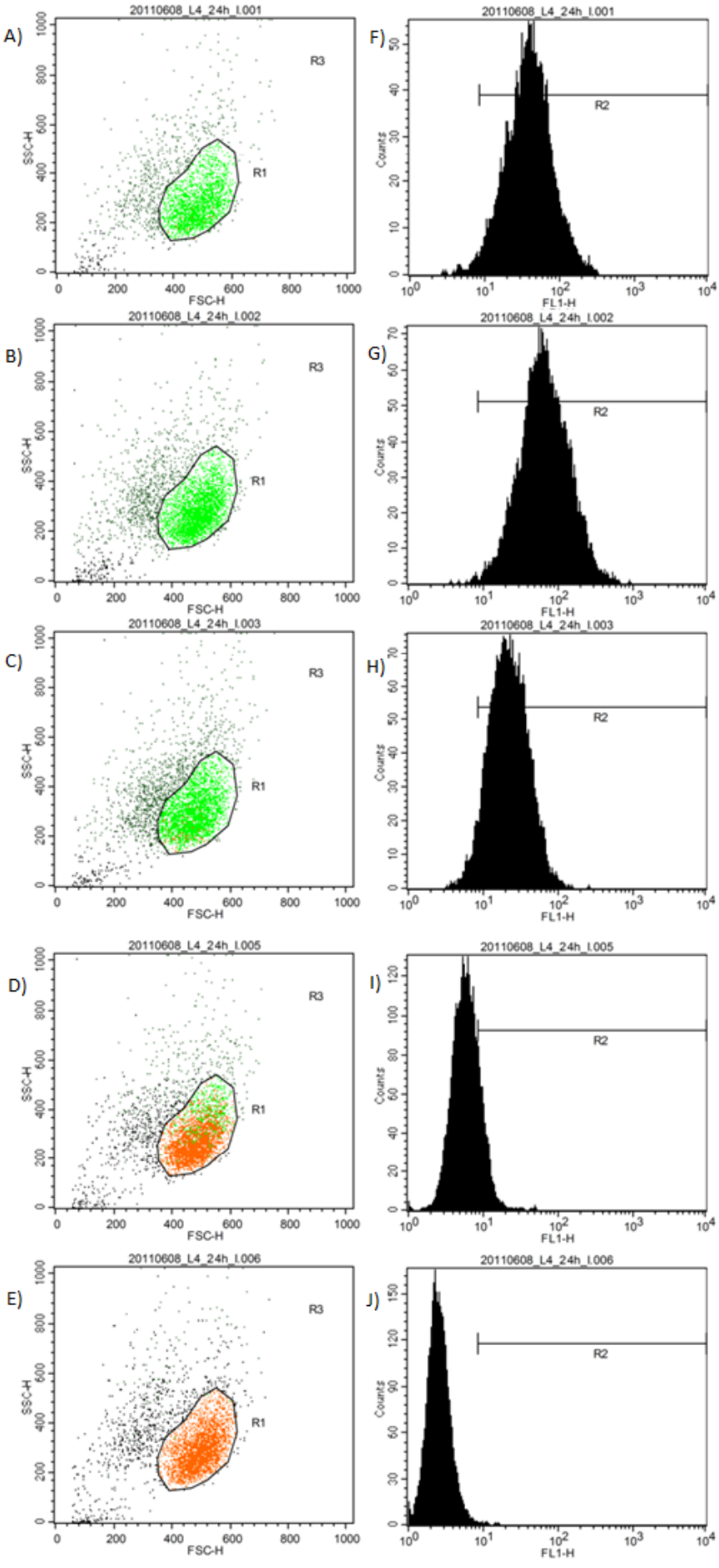
A)
20110608_L4_24h_I.001
R3
R1
SSC-H
FSC-H
F)
20110608_L4_24h_I.001
R2
Counts
FL1-H
B)
20110608_L4_24h_I.002
R3
R1
SSC-H
FSC-H
G)
20110608_L4_24h_I.002
R2
Counts
FL1-H
C)
20110608_L4_24h_I.003
R3
R1
SSC-H
FSC-H
H)
20110608_L4_24h_I.003
R2
Counts
FL1-H
D)
20110608_L4_24h_I.005
R3
R1
SSC-H
FSC-H
I)
20110608_L4_24h_I.005
R2
Counts
FL1-H
E)
20110608_L4_24h_I.006
R3
R1
SSC-H
FSC-H
J)
20110608_L4_24h_I.006
R2
Counts
FL1-H

Figure 6. Dot plots (A-E) and fluorescence intensity histograms (F-J) of different liposomal formulations, LipoX refers to the different functionalized liposomes LipoR1, LipoR2 and LipoR4 as described above. Figure 6A and 6F: 1000 nM calcein-equivalent LipoR4-folate; Figure 6B and 6G: 1000 nM calcein-equivalent LipoR4 (not functionalized); Figure 6C and 6H: 1000 nM calcein-equivalent LipoR1 (click reaction conditions); Figure 6D and 6I: 1000 nM calcein in media; Figure 6E and 6J: negative control (plain cells). The populations of viable cells have been identified in the area R1, the histograms show the number of events plotted against the fluorescence intensity of these. Events that are located in area R2 are colored green (positive), all others in R1 orange (negative). A shift to the positive interval can be observed.

The data of the calcein uptake experiments generated by flow cytometry is plotted using two different methods: In Figure 6A-6E dot plots are presented, while Figure 6F-J gives single dimension plots. In these histograms the number of events is plotted against the intensity of the fluorescence at the events. In general, higher fluorescence intensities of the cells incubated with liposomal formulations were observed. Furthermore, intensities vary between liposomal formulations using different PEG-PG block copolymers with and without folate-functionalization. Compared to not-incubated cells and cells that were incubated with an equivalent concentration of calcein in media, the fluorescence intensity is higher for the liposomal samples.

Quantification of the mean fluorescence intensities of the different liposomal formulations, with varying concentrations and incubation times are shown in Figure 7. As expected, the calcein uptake is significantly increased in the folate-modified liposomes compared to the negative control. Higher fluorescence intensities in the folate-treated cells might indicate the presence of receptor-mediated endocytosis of the calcein-loaded PEG-PG-folate liposomes into the epithelial carcinoma cells, resulting in enhanced intracellular calcein concentrations. Thus, the intensified calcein uptake of liposomes containing PEG-PG-folates demonstrates the potential of these novel types of liposomes for the efficient encapsulation and targeted transport of other guest molecules, i.e., siRNA.

Interestingly, very high mean fluorescence has been observed in KB cells treated with calcein-loaded, alkyne-functionalized liposomes (LipoR4). In this specific liposomal formulation no folate-ligands are covalently attached onto the membrane surface. Comparison with the

fluorescence intensity of the analogous folate-conjugated liposomes (Lipo4-folate) revealed increased calcein uptake of the alkyne-functionalized liposomes. Since no receptor-mediated calcein uptake can be present in the formulation LipoR4, the exceptionally high fluorescence intensity / calcein concentration might be referred to unspecific interactions of the alkyne functionalities on the liposomal surface with the KB cells. Further studies regarding the calcein uptake and continuing studies concerning the cellular uptake of liposome-encapsulated siRNA will be reported in due course.

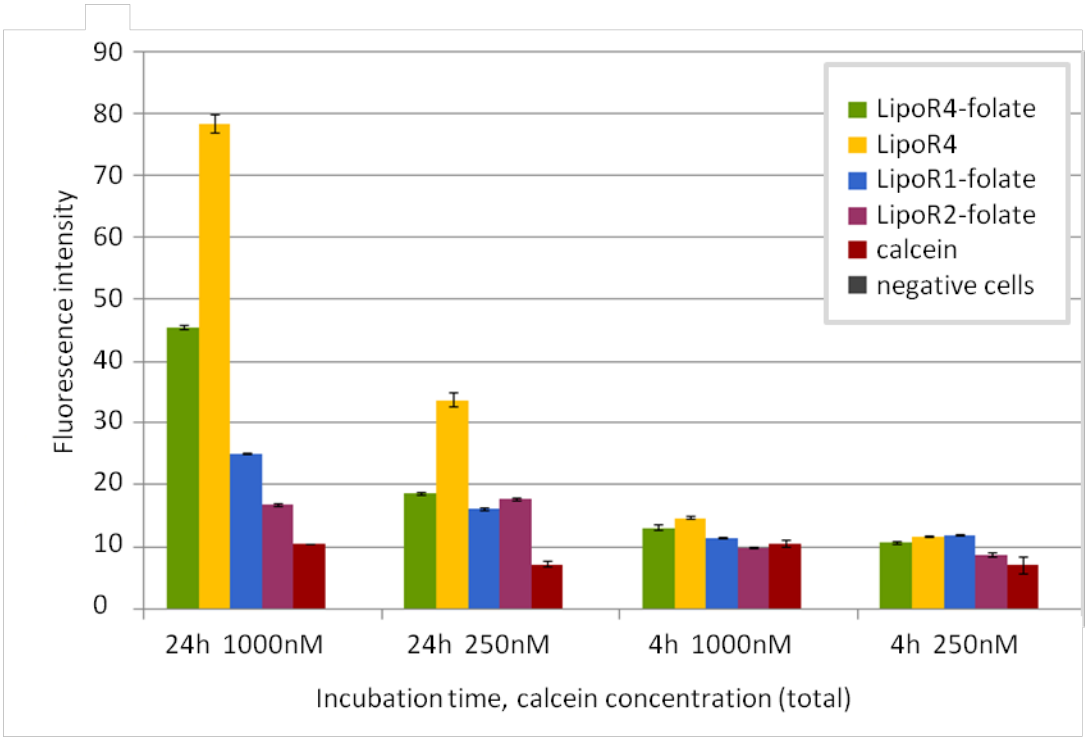

Figure 7. Mean fluorescence intensities of 15000 cells for different liposomal formulations, calcein equivalent concentrations and different incubation times. LipoRX refers to the different functionalized liposomes LipoR1, LipoR2 and LipoR4 as described above, calcein is the negative control with the same total calcein concentration in the media and the negative cells are plain cells.

Conclusion

In the recent study, we presented the preparation of novel types of multifunctional poly(ethylene glycol)-polyglycerol (PEG-PG) coated siRNA liposomes using dual asymmetric centrifugation (DAC). Combining the use of an efficient and fast preparation technique with incorporated complex stealth lipids based on multifunctional block copolymers allows for the

preparation of siRNA liposomes with high entrapping efficiencies. Encapsulation of hydrophilic siRNA molecules in the liposomal core has been demonstrated, relying on florescence analysis of labeled siRNA. Furthermore, due to the multiple functionalities in the molecular structure of the PEG-*b*-PG lipids covalent attachment of alkyne groups has been achieved. A broad range of azide-functionalized ligand can be attached onto the liposomal surface under very mild reaction conditions with this procedure. For instance, the incorporation of the polyether lipids into the liposomal membranes has been evidenced using fluorescence labels covalently attached via cycloaddition chemistry.

Using a similar synthetic approach, folate units as targeting moieties have been added to the liposomal formulations, inducing receptor-mediated endocytosis and therefore increased uptake of the liposomes into the cells. The investigated endothelial carcinoma cells demonstrated enhanced uptake of calcein-loaded liposomes containing the polyether-modified lipids. Detailed studies regarding the calcein uptake and the cellular uptake of encapsulated siRNA will be reported in due course. Nevertheless, the preparation of siRNA liposomes with the efficient and fast dual asymmetric centrifugation (DAC) in combination with the use of multifunctional and clickable PEG-PG lipids offers interesting options for further investigation of protected liposomal siRNA transport *in vivo* as well as active drug targeting. Further studies on mediated transport and uptake of the siRNA loaded liposomes will be required to obtain a clear idea on the effect of the novel lipids presented here.

References

(1) Fire, A.; Xu, S.; Montgomery, M. K.; Kostas, S. A.; Driver, S. E.; Mello, C. C. *Nature* **1998**, *391*, 806-811.

(2) Kurreck, J. *Eur. J. Biochem.* **2003**, *270*, 1628-1644.

(3) Mittal, V. *Nat. Rev. Genet.* **2004**, *5*, 355-365.

(4) McManus, M. T.; Sharp, P. A. *Nat. Rev. Genet.* **2002**, *3*, 737-747.

(5) Elbashir, S. M.; Lendeckel, W.; Tuschl, T. *Genes Dev.* **2001**, *15*, 188-200.

(6) Caplen, N. J.; Parrish, S.; Imani, F.; Fire, A.; Morgan, R. A. *Proc. Natl. Acad. Sci. USA* **2001**, *98*, 9742-9747.

(7) Kawakami, S.; Hashida, M. *Drug Metab. Pharmacokinet.* **2007**, *22*, 142-151.

(8) Bumcrot, D.; Manoharan, M.; Koteliansky, V.; Sah, D. W. *Nat. Chem. Biol.* **2006**, *2*, 711-719.

(9) Lasic, D. D.; Papahadadjopoulos, D. *Science* **1995**, *267*, 1275-1276.

(10) Allen, T. M.; Cullis, P. R. *Science* **2004**, *303*, 1818-1822.

(11) Immordino, M. L.; Dosio, F.; Cattel, L. *Int. J. Nanomed.* **2006**, *1*, 297-315.

(12) Torchilin, V. P. *Nat. Rev. Drug Discovery* **2005**, *4*, 145-160.

(13) Petros, R. A.; DeSimone, J. M. *Nat. Rev. Drug Discov.*, *9*, 615-627.

(14) Klibanov, A. L.; Maruyama, K.; Torchilin, V. P.; Huang, L. *FEBS Lett.* **1990**, *268*, 235-238.

(15) Lasic, D. D.; Martin, F. J.; Gabizon, A.; Huang, S. K.; Papahadjopoulos, D. *Biochim. Biophys. Act.* **1991**, *1070*, 187-192.

(16) Lasic, D. D.; Needham, D. *Chem. Rev.* **1995**, *95*, 2601-2628.

(17) Needham, D.; Hristova, K.; McIntosh, T. J.; Dewhirst, M.; Wu, N.; Lasic, D. D. *J. Liposome Res.* **1992**, *2*, 411-430.

(18) Woodle, M. C.; Lasic, D. D. *Biochim. Biophys. Acta, Biomembr.* **1992**, *1113*, 171-199.

(19) Blume, G.; Cevc, G. *Biochim. Biophys. Acta, Biomembr.* **1990**, *1029*, 91-97.

(20) Allen, T. M.; Hansen, C.; Martin, F.; Redemann, C.; Yau-Young, A. *Biochim. Biophys. Acta, Biomembr.* **1991**, *1066*, 29-36.

(21) Papahadjopoulos, D.; Allen, T. M.; Gabizon, A.; Mayhew, E.; Matthay, K.; Huang, S. K.; Lee, K. D.; Woodle, M. C.; Lasic, D. D.; Redemann, C. *Proc. Natl. Acad. Sci. USA* **1991**, *88*, 11460-11464.

(22) Gabizon, A. A.; Barenholz, Y.; Bialer, M. *Pharm. Res.* **1993**, *10*, 703-708.

(23) Maruyama, K.; Yuda, T.; Okamoto, A.; Kojima, S.; Suginaka, A.; Iwatsuru, M. *Biochim. Biophys. Acta* **1992**, *1128*, 44-49.

(24) Stathopoulos, G. P.; Boulikas, T.; Vougiouka, M.; Deliconstantinos, G.; Rigatos, S.; Darli, E.; Viliotous, V.; Stathopoulos, J. G. *Oncol. Rep.* **2005**, *13*, 589-595.

(25) Waalkes, M. v. B.; Galen, M. v.; Morselt, H.; Sternberg, B.; Scherphof, G. L. *Biochim. Biophys. Acta* **1993**, *1148*, 161-172.

(26) Gabizon, A.; Papahadjopoulos, D. *Biochim. Biophys. Acta* **1992**, *1103*, 94-100.

(27) Roberts, W. G.; Palade, G. E. *Cancer Res.* **1997**, *57*, 765-772.

(28) Wang, M.; Thanou, M. *Pharm. Res.* **2010**, *62*, 90-99.

(29) Jones, A. T.; Gumbleton, M.; Duncan, R. *Adv. Drug Deliv. Rev.* **2003**, *55*, 1353-1357.

(30) Widera, A.; Norouziyan, F.; Shen, W.-C. *Adv. Drug Deliv. Rev.* **2003**, *55*, 1439-1466.

(31) Lee, R. J.; Low, P. S. *J. Biol. Chem.* **1994**, *269*, 3198-3204.

(32) Wang, X.; Li, J.; Wang, Y.; Cho, K. J.; Kim, G.; Gjyrezi, A.; Koenig, L.; Giannakakou, P.; Shin, H. J. C.; Tighiouart, M.; Nie, S.; Chen, Z.; Shin, D. M. *ACS Nano* **2009**, *3*, 3165-3174.

(33) Goren, D.; Horowitz, A. T.; Tzemach, D.; Tarshish, M.; Zalipsky, S.; Gabizon, A. *Clin. Cancer Res.* **2000**, 1949-1957.

(34) Pan, X.; Lee, R. J. *Expert Opin. Drug Deliv.* **2004**, 7-17.

(35) Lu, Y.; Low, P. S. *Adv. Drug Deliv. Rev.* **2002**, *54*, 675-693.

(36) Hofmann, A. M.; Wurm, F.; Frey, H. *Macromolecules* **2011**.

(37) Hofmann, A. M.; Wurm, F.; Hühn, E.; Nawroth, T.; Langguth, P.; Frey, H. *Biomacromolecules* **2010**, 568-574.

(38) Massing, U.; Cicko, S.; Ziroli, V. *J. Control. Rel.* **2008**, *125*, 16-24.

(39) Hirsch, M.; Ziroli, V.; Helm, M.; Massing, U. *J. Control. Rel.* **2009**, *135*, 80-88.

Chapter 3.1: Langmuir and Langmuir-Blodgett films of multifunctional, amphiphilic polyethers with cholesterol moieties

Chapter 3.1:

Langmuir and Langmuir-Blodgett films of multifunctional, amphiphilic polyethers with cholesterol moieties

Sascha Reuter,[1] Anna Maria Hofmann,[2] Karsten Busse,[1] Holger Frey,[2] and Jörg Kressler*,[1]

1 Department of Chemistry, Martin Luther University Halle-Wittenberg, Halle (Saale), Germany.

2 Institute of Organic Chemistry, Duesbergweg 10-14, Johannes Gutenberg-University, Mainz, Germany.

Published in Langmuir 2011, 27 (5), 1978-1989.

Abstract

Langmuir films of multifunctional, hydrophilic polyethers containing a hydrophobic cholesterol group (Ch) were studied by surface pressure-mean molecular area (π-mmA) measurements and Brewster angle microscopy (BAM). The polyethers were either homopolymers or diblock copolymers of linear polyglycerol (*l*PG), linear poly(glyceryl glycidyl ether) (*l*PGG), linear poly(ethylene glycol) (*l*PEG), or hyperbranched polyglycerol (*hb*PG). Surface pressure measurements revealed that the homopolymers *l*PG and *hb*PG did not stay at the water surface after spreading and solvent evaporation, in contrast to *l*PEG. Because of the incorporation of the Ch group in the polymer structure, stable Langmuir films were formed by Ch-*l*PG$_n$, Ch-*l*PGG$_n$, and Ch-*hb*PG$_n$. The Ch-*hb*PG$_n$, Ch-*l*PEG$_n$, Ch-*l*PEG$_n$-*b*-*l*PG$_m$, Ch-*l*PEG$_n$-*b*-*l*PGG$_m$, and Ch-*l*PEG$_n$-*b*-*hb*PG$_m$ systems showed an extended plateau region assigned to a phase transition involving the Ch groups. Typical hierarchically ordered morphologies of the LB films on hydrophilic substrates were observed for all Ch-initiated polymers. All LB films showed that Ch of the Ch-initiated homopolymers is able to crystallize. This strong tendency of self-aggregation then triggers further dewetting effects of the respective polyether entities. Fingerlike

morphologies are observed for Ch-/PEG$_{69}$, since the /PEG$_{69}$ entity is able to undergo crystallization after transfer onto the silicon substrate.

Keywords

cholesterol, polyglycerol, poly(glyceryl glycidyl ether), poly(ethylene glycol), diblock copolymer, Langmuir isotherm, Langmuir-Blodgett film, atomic force microscopy, Brewster angle microscopy.

Introduction

The behavior of Langmuir films, i.e., insoluble monolayers of amphiphilic molecules spread at the air-water interface, can be studied by Langmuir trough measurements in order to obtain Langmuir isotherms recording the surface pressureπ as a function of the mean molecular area (mmA).[1] By Brewster angle microscopy (BAM), it is possible to detect domains in Langmuir films in the micrometer range.[2,3] Structural information in the nanometer range can be obtained by atomic force microscopy (AFM) after transfer of Langmuir films to solid supports using the Langmuir-Blodgett (LB) technique.[4-9] Langmuir and LB films are used as simplified models for biological membranes.[10] Cholesterol (Ch), a naturally occurring sterol, is essential for stabilization and fluidization of the lipid bilayer of cell membranes.[10-15] It is strongly involved in the biosynthesis of bile salts and hormones in the human biliary system.[12,15-17] Because of the hydrophilic hydroxyl group and the hydrophobic residual parts consisting of the rigid skeleton and an isooctyl chain, Ch represents an amphiphilic molecule. Several reports deal with Langmuir and LB films of Ch, either as a pure compound[11,13,15,16,18,19] or as a mixed monolayer in interaction with fatty acids,[10,20,21] lipids,[17,22-25] or polystyrene.[26] As demonstrated by BAM, Ch already exists in a mixed gaseous (G) and liquid condensed (LC) state at π values of around 0 mNm^{-1}.[16,20,22] The first significant increase of the surface pressure appears at mmA of ~39 A$^{\circ 2}$, followed by a steep increase resulting from the formation of the LC phase.[16,19,22,24] With further compression, the Langmuir isotherm of Ch has a sharp "spike" at mmA of ~36A$^{\circ 2}$ and a π value of ~45 mN m^{-1}, followed by a plateau region of slightly increasing π values. The "spike" is interpreted as the collapse point of the Ch monolayer.[11,13,18,19,21,26] During compression in the plateau region, Ch transforms into a trilayer composed of a highly crystalline bilayer and a

disordered Ch top layer.[15,17] Large crystals with a platelike morphology are identified by corresponding AFM investigations of the LB films.[16,17] In contrast, reports about hydrophilically modified Ch derivatives demonstrate that these molecules are tilted with respect to the normal of the water surface or even lying parallel to the air-water interface prior to compression.[27-29] Furthermore, Langmuir and LB films of Ch esters forming stable monolayers, bilayer films, and 3D crystallites at the air-water interface have been studied.[30-32] Some reports describe the phase behavior of poly(ethylene glycol) Ch ethers in water[33,34] as well as their morphology in the bulk state.[35,36] This is to the best of our knowledge the first investigation of Langmuir and LB films of Ch-initiated polyethers at the air-water interface. The hydroxyl group of Ch is directly deprotonated and employed to initiate the polymerization of a series of different polyethers with systematically varied structure. The Ch-initiated homopolymers and diblock copolymers are amphiphilic, since they are composed of the hydrophobic Ch group and a hydrophilic polyether entity. Linear polyglycerol (*l*PG), linear poly(glyceryl glycidyl ether) (*l*PGG), hyperbranched polyglycerol (*hb*PG), and linear poly(ethylene glycol) (*l*PEG) are attached to the Ch group. Overall, four different types of Ch-initiated homopolymers (Ch-*l*PG_n, Ch-*l*PGG_n, Ch-*hb*PG_n, Ch-*l*PEG_n) and three different types of Ch-initiated diblock copolymers (Ch-*l*PEG_n-*b*-*l*PG_m, Ch-*l*PEG_n-*b*-*l*PGG_m, Ch-*l*PEG_n-*b*-*hb*PG_m have been used for Langmuir trough and BAM experiments. After transfer of the Langmuir films onto silicon substrates, the surface morphologies of the resulting LB films are observed by AFM.

Experimental section

Materials. Ch-initiated polyethers were synthesized via anionic ring-opening polymerization and characterized as reported elsewhere.[37-41] All polyethers were composed of a single hydrophobic Ch group and either a hydrophilic polyether or a hydrophilic diblock polyether chain. Linear polyglycerol (*l*PG), linear poly(glyceryl glycidyl ether) (*l*PGG), hyperbranched polyglycerol (*hb*PG), and linear poly(ethylene glycol) (*l*PEG) were used as hydrophilic entities. General chemical structures of the different Ch-initiated polyethers are shown in Charts 1 and 2. Molar mass data of the two homopolymers *l*PG_{54} and *hb*PG_{29} as well as of the Ch-initiated homopolymers are listed in Table 1. Table 2 provides the data for the Ch-initiated diblock copolymers. Pure Ch was purchased from Avanti Polar Lipids (Alabaster,AL) and used as received.

Chart 1. Chemical structures of Ch-initiated homopolymers [a] n represents the degree of polymerization of *l*PG, *l*PGG, and *l*PEG. For the *hb*PG entity, n accounts for the number of glycerol units (the structure shows a typical example).

a) Ch-*l*PG$_n$

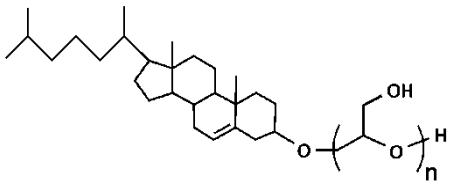

b) Ch-*l*PGGn

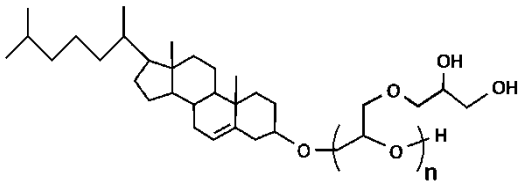

c) Ch-*hb*PG$_n$

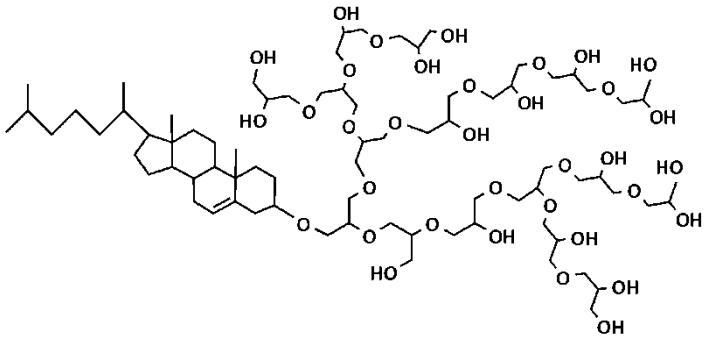

d) Ch-*l*PEG$_n$

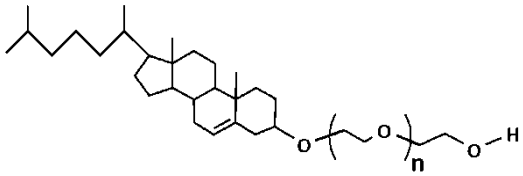

Chart 2. Chemical structures of Ch-initiated diblock copolymers. *n* is the degree of polymerization of *l*PEG, and *m* represents the block lengths of *l*PG and *l*PGG. For the *hb*PG block, *m* accounts for the number of glycerol units (the structure shows a typical example).

a) Ch-*l*PEG$_n$-*b*-*l*PG$_m$

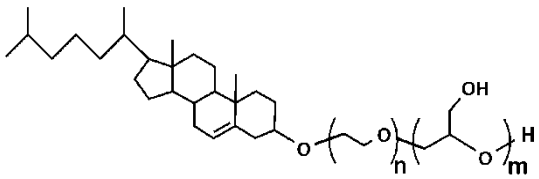

b) Ch-*l*PEG$_n$-b-*l*PGG$_m$

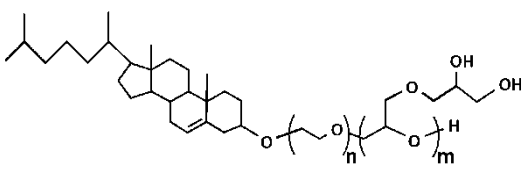

c) Ch-*l*PEG$_n$-b-*hb*PG$_m$

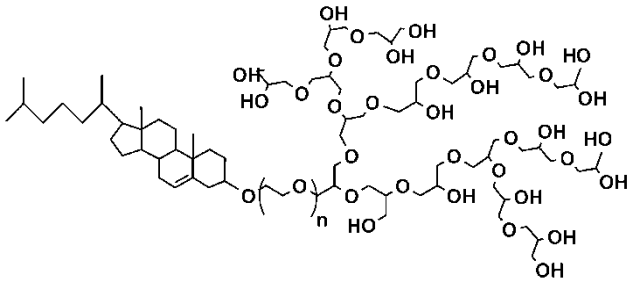

Molar mass data of the two homopolymers *l*PG$_{54}$ and *hb*PG$_{29}$ as well as of the Ch-initiated homopolymers are listed in Table 1. Table 2 provides the data for the Ch-initiated diblock copolymers. Pure Ch was purchased from Avanti Polar Lipids (Alabaster, USA) and used as received.

Table 1. Molar masses and polydispersities of homopolymers and of Ch-initiated homopolymers.

Homopolymers	M_n[a] (g·mol^{-1})	PDI[b]
*l*PG$_{54}$	4000	1.20
*hb*PG$_{29}$	2300	1.55
Ch-initiated homopolymers	**M_n[a] (g·mol^{-1})**	**PDI[b]**
Ch-*l*PG$_{15}$	1500	1.18
Ch-*l*PGG$_7$	1420	1.24
Ch-*hb*PG$_{25}$	2240	1.20
Ch-*hb*PG$_{35}$	2980	1.18
Ch-*l*PEG$_{35}$	1930	1.20
Ch-*l*PEG$_{41}$	2200	1.09
Ch-*l*PEG$_{50}$	2600	1.12
Ch-*l*PEG$_{69}$	3250	1.10

[a] The number average molar mass (M_n) was determined by ^{1}H NMR spectroscopy. [b] For the calculation of the polydispersity indices (PDI), M_n and M_w were determined via SEC-RI in DMF with poly(ethylene glycol) standards.

Table 2. Molar masses and polydispersities of Ch-initiated diblock copolymers.

Ch-initiated diblock copolymers	M_n[a] (g·mol^{-1})	PDI[b]
Ch-*l*PEG$_{25}$-*b*-*l*PG$_{15}$	2820	1.05
Ch-*l*PEG$_{22}$-*b*-*l*PGG$_8$	2540	1.07
Ch-*l*PEG$_{30}$-*b*-*l*PGG$_7$	2750	1.07
Ch-*l*PEG$_{35}$-*b*-*l*PGG$_7$	2970	1.08
Ch-*l*PEG$_{18}$-*b*-*hb*PG$_{24}$	2960	1.18
Ch-*l*PEG$_{30}$-*b*-*hb*PG$_{24}$	3470	1.08
Ch-*l*PEG$_{35}$-*b*-*hb*PG$_{19}$	3340	1.09

[a] The number average molar mass (M_n) was determined by ^{1}H NMR spectroscopy. [b] For the calculation of the polydispersity indices (PDI), M_n and M_w were determined via SEC-RI in DMF with poly(ethylene glycol) standards.

Surface pressure measurements. The Langmuir isotherms of pure Ch and of Ch-initiated polyethers at the air-water interface were obtained at 20 °C, using a Langmuir trough system working with two symmetrically moving barriers for compression (KSV Instruments Ltd., Finland) placed in a sealed box. A microroughened platinum Wilhelmy plate was applied for measuring the surface pressure π as a function of the mean molecular area *mmA*. The maximum available surface of the Langmuir trough was 768 cm^2. Double distilled water was purified by a GenPure system (TKA GmbH, Germany) equipped with an organic removal cartridge (conductance < 0.07 µS·cm^{-1}). Before each measurement, the purity of the bare water surface was checked by a maximum compression (π < 0.15 mN·m^{-1}).

Spreading solutions of pure Ch and of Ch-initiated polyethers were prepared in concentrations ranging from 1 to 7 g·L^{-1}. HPLC-grade chloroform or a 2:1 (v:v) mixture of HPLC-grade chloroform and HPLC-grade methanol were used as solvents. The solutions were spread in

various amounts (1-65 µl) evenly and dropwise at the air-water interface using a digital Hamilton microsyringe. After 20 min to ensure the total evaporation of the solvent and the uniform dispersion of the molecules at the air-water interface, the measurements were performed using a compression rate of 15 $cm^2 \cdot min^{-1}$. To obtain complete Langmuir isotherms, the solutions of the Ch-initiated polyethers were spread at different initial surface pressures. Thus, different parts of the isotherms were recorded. After combining these data into one plot, the different parts fit together within the experimental error. Reversibility experiments using Ch-*l*PGG_7 and Ch-*l*PEG_{35}-b-*hb*PG_{19} indicated reversible behavior of the Ch-initiated homopolymers and diblock copolymers without the dissolution of polymers into the water subphase (see Supporting information).

Brewster angle microscopy (BAM) on the Langmuir trough. BAM was performed for direct observation of the Langmuir films of pure Ch and of Ch-initiated polyethers at the air-water interface by using a MiniBAM instrument (Nanofilm Technologie GmbH, Germany).

Deposition of LB films. LB films of pure Ch and of Ch-initiated polyethers were generated at different π values. The deposition was performed onto silicon substrates cut into approximately 25 x 15 mm substrates and cleaned with double distilled water to gain a hydrophilic SiO_2 surface. The cleaned substrates were submersed into the subphase before starting the compression. The compression was performed with a compression rate of 15 $cm^2 \cdot min^{-1}$ until the desired transfer surface pressure was achieved. Then, the films were allowed to equilibrate for 20 min. Afterwards, the film transfer onto the silicon substrates was carried out at constant surface pressure by vertical uptake through the film with a constant transfer rate of $2 mm \cdot min^{-1}$. Finally, the LB films were stored for drying in an exsiccator at room temperature for 24 h.

Atomic force microscopy (AFM) of LB films. The surface morphology of the LB films was analyzed using an atomic force microscope NanoWizard (JPK Instruments AG, Germany) working in tapping-mode. Silicon cantilevers of type Arrow (NanoWorld AG, Switzerland) with a resonance frequency of about 285 kHz and a force constant of about 42 $N \cdot m^{-1}$ were used.

Results and discussion

Langmuir isotherms. Figure 1 represents the Langmuir isotherm for pure Ch (solid line). It is obvious that Ch forms an insoluble Langmuir film upon compression at the air-water interface.

In contrast, the homopolymers *l*PG$_{54}$ (dashed line) and *hb*PG$_{29}$ (dotted line) with linear and hyperbranched polyglycerol structures exhibit almost no surface activity and dissolve immediately in the water subphase with decreasing *mmA* (increasing π), indicative of the higher hydrophilicity of polyglycerol in comparison to *l*PEG.

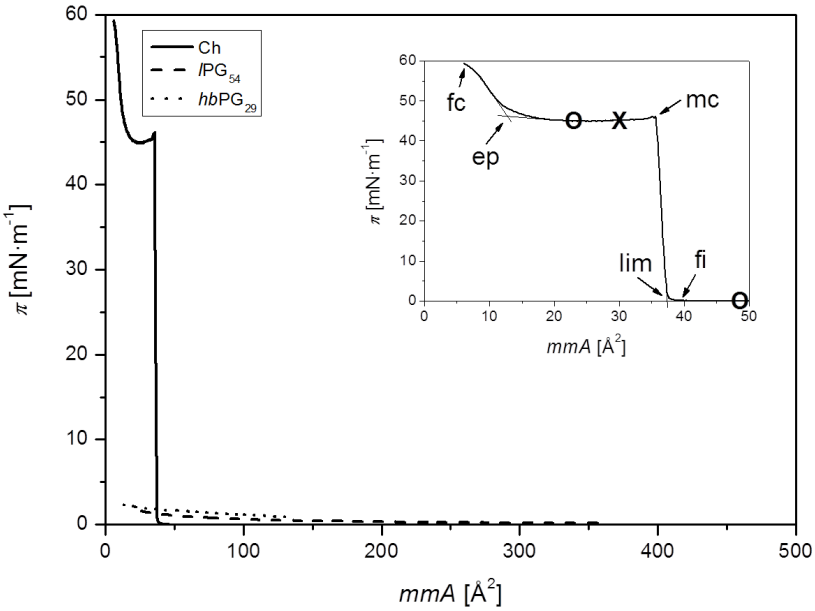

Figure 1. Langmuir isotherms of pure Ch measured at 20 °C. Compression measurements for the homopolymers *l*PG$_{54}$ and *hb*PG$_{29}$ are added. The abbreviations and the lines in the inset showing the Langmuir isotherm of Ch in more detail exemplify the determination of characteristic *mmA* and π values (see text). BAM images of Ch are recorded at *mmA* values indicated by **O**, and the LB film of Ch is transferred at the surface pressure marked by **X**.

At *mmA* values larger than 39 Å^2 and π values of 0 mN·m^{-1}, the presence of the G phase would be expected with singular Ch molecules arranged perpendicular to the water surface anchored by their hydroxyl group.[11,15,19,21,23,42] However, the G phase and the LC phase already coexist in different domains indicating the strong tendency of Ch for self-aggregation.[16,19,20,22] This is confirmed by the BAM image of Ch which is recorded at *mmA* of 49 Å^2 and a π value close to 0 mN·m^{-1} (see Supporting information). The first significant increase of π in the Langmuir isotherm of Ch in Figure 1 occurs at *mmA* of around 39 Å^2 (mmA_{fi}, first significant deviation of π from zero). This increase becomes very steep at a limiting *mmA* value of 37 Å^2 (mmA_{lim}, limiting value for one Ch molecule in the monolayer).[11,13,18,21,25,31,32,42,43] The Ch molecules are thus arranged in a monolayer with complete coverage of the water surface and with the ordering of

the LC phase.[16,19,22,24] Hence, the Langmuir film does not show any domain formation by BAM. Upon further compression, the Ch monolayer of low crystallinity collapses at *mmA* of 36 Å^2 (*mmA*$_{mc}$, value at monolayer collapse) and a π value of 46 mN·m^{-1} (π_{mc}, value at monolayer collapse),[11,13,18,19,21,26,32,43] and transforms after collapse into a film composed of a trilayer with a rough upper surface, a smooth, highly crystalline bilayer and a more disordered monolayer contributing to a relative surface coverage with the ratio of 7:2:1.[15,17] The film continues transformation into a crystalline trilayer phase including a layer of ordered water between the top and the middle layer upon further compression. This corresponds to the 3D monohydrate crystal structure of Ch.[15,17] The formation of the trilayer phase is in agreement with our measurements, since the *mmA* value of 13 Å^2 at the end of the plateau (*mmA*$_{ep}$, value at the end of the plateau region) in the Langmuir isotherm corresponds approximately to one-third of the *mmA*$_{lim}$ value of 37 Å^2. During compression in the plateau region, Ch domains appear as bright regions in the BAM image which is recorded at *mmA* of 23 Å^2 (see Supporting information). These domains are assigned to Ch crystals.[16,19,20,22] The sharp 'spike' at *mmA*$_{mc}$ in the Langmuir isotherms has been discussed as an indication of the formation of 3D crystals of fatty acids[44] and hydrophobically substituted dicarboxylates.[45] Due to further compression, the second steep increase of π ends in the final collapse of Ch at a nominal *mmA* of 6 Å^2 (*mmA*$_{fc}$, value at final collapse) and a π value of 59 mN·m^{-1} (π_{fc}, value at final collapse).

It should be mentioned that the *mmA* values are nominal values, automatically recorded and not taking into account the formation of multilayers or the submersion of parts of the Ch-initiated polymers into the water subphase. The almost absent surface activity of *l*PG$_{54}$ and *hb*PG$_{29}$ shown in Figure 1 clearly differs from the behavior of *l*PEG. *l*PEG is known to be surface active, despite its good solubility in water. It forms stable monolayers at the air-water interface[46-50] at a molar mass as small as 2000 g·mol^{-1},[51] when spread on the water surface. Thus, it is obvious that *l*PG and *hb*PG homopolymers are more hydrophilic compared to *l*PEG, caused by the large number of hydroxyl groups in *l*PG and *hb*PG. This result is important in order to understand the results of the more complex Ch-based polyether structures discussed below.

In Figure 2, the Langmuir isotherms for all Ch-initiated amphiphilic homopolymers are shown. It is demonstrated that Ch-*l*PG$_{15}$ and Ch-*l*PGG$_7$ are surface active and form stable films upon compression at the air-water interface until collapse (Figure 2 (a)).

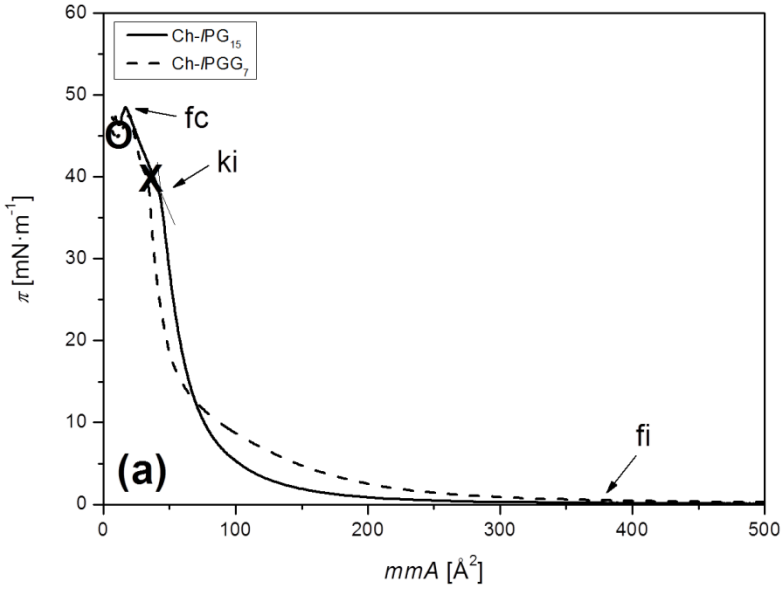

Figure 2. (a) Langmuir isotherms measured at 20 °C for the Ch-initiated homopolymers of (a) Ch-/PG$_{15}$. The insets show the complete Langmuir isotherms within the full *mmA* range under investigation. BAM images of Ch-/PGG$_7$ are recorded at *mmA* values indicated by **O** (see Supporting information), and LB films of the Ch-initiated homopolymers are transferred at surface pressures marked by **X**.

Remarkably, a single Ch unit is able to anchor the /PG$_{15}$ entity of Ch-/PG$_{15}$ at the air-water interface effectively (in contrast to the /PG54 homopolymer), and prevents its dissolution in the water bulk phase up to a surface pressure of 49 mN·m^{-1}. The first significant increase of the surface pressure in the Langmuir isotherm of Ch-/PG$_{15}$ is observed at mmA_{fi} of around 380 Å^2. This value is much larger than the mmA_{fi} value for pure Ch (39 Å^2), i.e., /PG$_{15}$ is also located at the air-water interface and contributes to the mmA_{fi} value. With further compression, the surface pressure increases, until it reaches a kink at *mmA* of 43 Å^2 (mmA_{ki}, value at the kink) and a π value of 38 mN·m^{-1} (π_{ki}, value at the kink). During this increase, the /PG$_{15}$ part of Ch-/PG$_{15}$ is assumed to submerge into the water subphase. The kink at mmA_{ki} and π_{ki} occurs at similar values as the mmA_{mc} and π_{mc} of pure Ch, indicating a similar arrangement of the Ch group in Ch-/PG$_{15}$ compared to pure Ch. The surface pressure further increases upon compression, until the final collapse of Ch-/PG$_{15}$ is observed at mmA_{fc} of 17 Å^2 and a π_{fc} value of 49 mN·m^{-1}.

A summary of all relevant *mmA* and π values for all Ch-initiated homopolymers is given in Table 3. Ch-/PGG$_7$ with linear structure, but higher hydroxyl group density, shows a similar Langmuir isotherm as Ch-/PG$_{15}$, suggesting a similar behavior at the air-water interface (Figure 2 (a)). The only difference of Ch-/PGG$_7$ compared to Ch-/PG$_{15}$ is the first significant increase of the surface pressure observed at a higher mmA_{fi} value of around 590 Å^2 compared to 380 Å^2. This indicates a larger *mmA* requirement of the sterically more demanding /PGG monomer unit compared to the /PG monomer unit in the Ch-initiated homopolymers.

Figure 2 (b) displays the Langmuir isotherms of the hyperbranched structures Ch-*hb*PG$_{25}$ and Ch-*hb*PG$_{35}$, showing the existence of stable films during the compression at the air-water interface. This once more confirms the anchoring capability of the Ch group, since the corresponding homopolymer *hb*PG$_{29}$ does not show any surface activity (see Figure 1). In comparison to the Langmuir isotherms of Ch-/PG$_{15}$ and Ch-/PGG$_7$ shown in Figure 2 (a), the first significant increase of the surface pressure in the Langmuir isotherms of Ch-*hb*PG$_{25}$ and Ch-*hb*PG$_{35}$ is observed at larger mmA_{fi} values (see Table 3) as assumed from their higher molar masses. For the same reason, the mmA_{fi} value of Ch-*hb*PG$_{35}$ is larger than the mmA_{fi} value of Ch-*hb*PG$_{25}$. Due to further compression, the Langmuir isotherms of the Ch-*hb*PG$_n$ homopolymers show a gradual increase of the surface pressure, indicating interactions of the *hb*PG$_n$ parts already submerged into the water subphase. The kink might be related to re-arrangement processes of the Ch group of the Ch-initiated homopolymers.[27-29] As result of the large space requirement of *hb*PG$_n$, the mmA_{ki} is not exclusively determined by the hydrophobic Ch anchor. The size and shape of the hyperbranched polymer tail prevents crystallization of the Ch group in all Ch-*hb*PG$_n$ samples. This is also supported by the fact that BAM does not provide any image of domains in the Langmuir film. After the plateau-like region, a second steep increase of the surface pressure follows and results in the final collapse of the Ch-*hb*PG$_n$ homopolymers. In comparison to the Langmuir isotherms of Ch-/PG$_{15}$ and Ch-/PGG$_7$, it is obvious that the surface pressure at the characteristic mmA_{fc} values in the Langmuir isotherms of Ch-*hb*PG$_{25}$ and Ch-*hb*PG$_{35}$ is shifted to lower π values caused by the higher hydrophilicity of the Ch-initiated hyperbranched polymers. The same argument can be used for the higher π_{fc} value of Ch-*hb*PG$_{25}$ compared to Ch-*hb*PG$_{35}$.

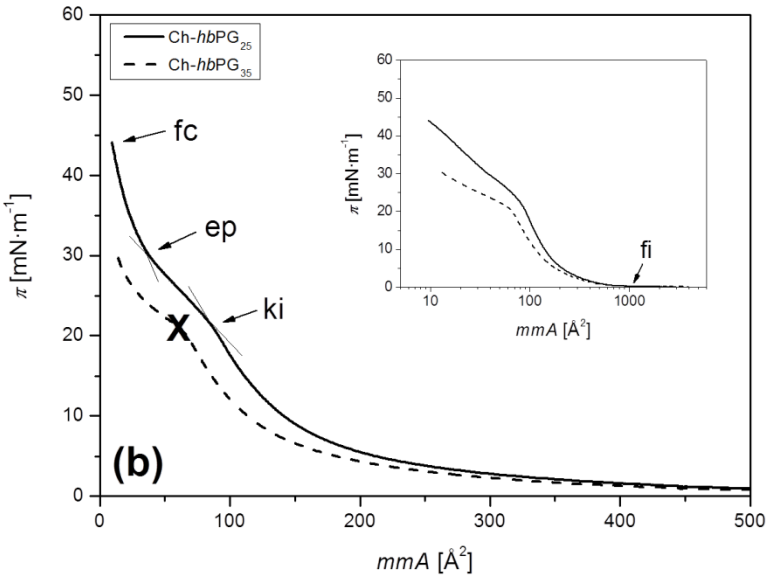

Figure 2. (b) Langmuir isotherms measured at 20 °C for the Ch-initiated homopolymers of (b) Ch-*hb*PG$_n$. The insets show the complete Langmuir isotherms within the full *mmA* range under investigation. LB films of the Ch-initiated homopolymers are transferred at surface pressures marked by **X**.

In Figure 2 (c), the Langmuir isotherms for the Ch-initiated homopolymers of the type Ch-*l*PEG$_n$ are shown. They form insoluble Langmuir films at the air-water interface. The mmA_{fi} values at the first significant increase of the surface pressure in the Langmuir isotherms shift with increasing molar mass of the *l*PEG$_n$ entity towards larger *mmA* values (see Table 3). During compression, a small shoulder appears in the Langmuir isotherms at π values of approximately 5 to 10 mN·m^{-1} (marked by an ellipse in the inset), indicating the typical pancake-to-brush transition region of the *l*PEG.[52-60] An extended plateau occurs for all four Ch-*l*PEG$_n$ homopolymers which can be assigned to the phase transition region of the G phase to the LC phase of the Ch group.[27-29] Obviously, the presence of the attached polymer chains prevents initially after spreading the LC domain formation which has been discussed for pure Ch above, i.e., only the G phase is present at the air-water interface prior to compression. Thus, the transition of the G phase to the LC phase of the Ch groups can be observed as a defined region in the Langmuir isotherms of Ch-*l*PEG$_n$. With decreasing molar mass, the behavior of the Ch-*l*PEG$_n$ becomes more and more similar to that of the neat Ch.

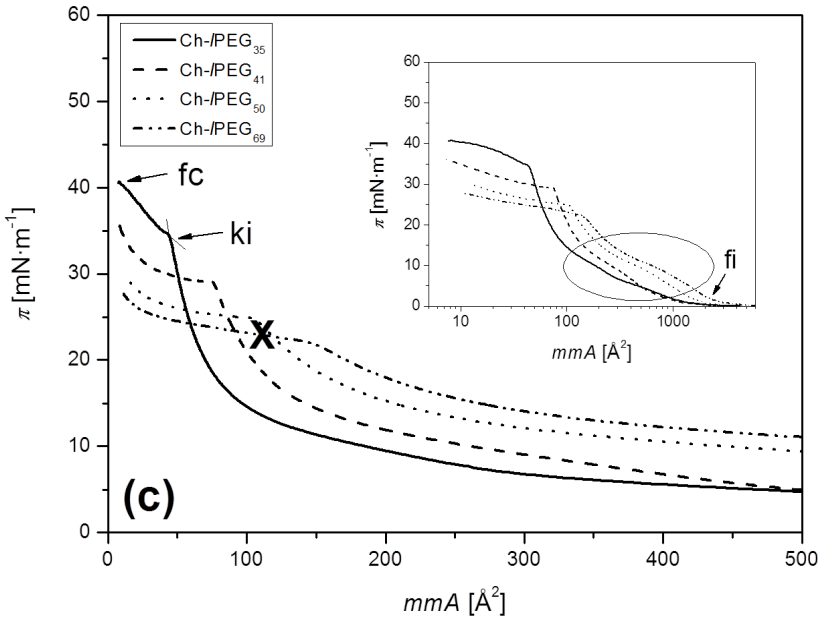

Figure 2. (c) Langmuir isotherms measured at 20 °C for the Ch-initiated homopolymers (c) Ch-/PEG$_n$. The insets show the complete Langmuir isotherms within the full *mmA* range under investigation. The ellipse in the inset of (c) indicates the pancake-to-brush transition region of the /PEG entity of Ch-/PEG$_n$. LB films of the Ch-initiated homopolymers are transferred at surface pressures marked by **X**.

Table 3. Characteristic data for the Langmuir isotherms of the Ch-initiated homopolymers. The meaning of the subscripts of the *mmA* and π values is given in the text.

Ch-initiated homopolymers	mmA_{fi} [Å^2]	mmA_{ki} / π_{ki} [Å^2] / [mN·m^{-1}]	mmA_{ep} / π_{ep} [Å^2] / [mN·m^{-1}]	mmA_{fc} / π_{fc} [Å^2] / [mN·m^{-1}]
Ch-/PG$_{15}$	380	43 / 38	-	17 / 49
Ch-/PGG$_7$	590	35 / 39	-	20 / 47
Ch-*hb*PG$_{25}$	1050	85 / 22	37 / 30	9 / 44
Ch-*hb*PG$_{35}$	1200	66 / 21	31 / 25	12 /31
Ch-/PEG$_{35}$	2270	45 / 34	-	8 / 41
Ch-/PEG$_{41}$	2490	76 / 29	22 / 31	8 / 36
Ch-/PEG$_{50}$	3370	105 / 25	27 / 27	13 / 30
Ch-/PEG$_{69}$	7670	148 / 22	25 / 25	11 / 28

Figure 3 shows the Langmuir isotherms for the Ch-initiated diblock copolymers forming stable films at the air-water interface where they are anchored via their Ch group. In Figure 3 (a), the Langmuir isotherm for Ch-/PEG$_{25}$-b-/PG$_{15}$ is displayed. Due to the additional /PEG$_{25}$ block in comparison to the corresponding Ch-/PG$_{15}$ homopolymer, the first significant increase of the surface pressure is observed at *mmA*$_{fi}$ of around 2250 Å^2, which is much larger than the *mmA*$_{fi}$ value of 380 Å^2 for Ch-/PG$_{15}$ (see Figure 2 (a)). Hence, it is obvious that the /PEG$_{25}$ block is located at the air-water interface at the beginning of the compression, in addition to the Ch group and /PG$_{15}$. With further compression, the Langmuir isotherm of Ch-/PEG$_{25}$-b-/PG$_{15}$ shows a small shoulder and a plateau region similar to the Langmuir isotherms of the Ch-/PEG$_n$ homopolymers (see Figure 2 (c)), thus leading to similar conclusions. Characteristic *mmA* and π values of for all Ch-initiated diblock copolymers are summarized in Table 4.

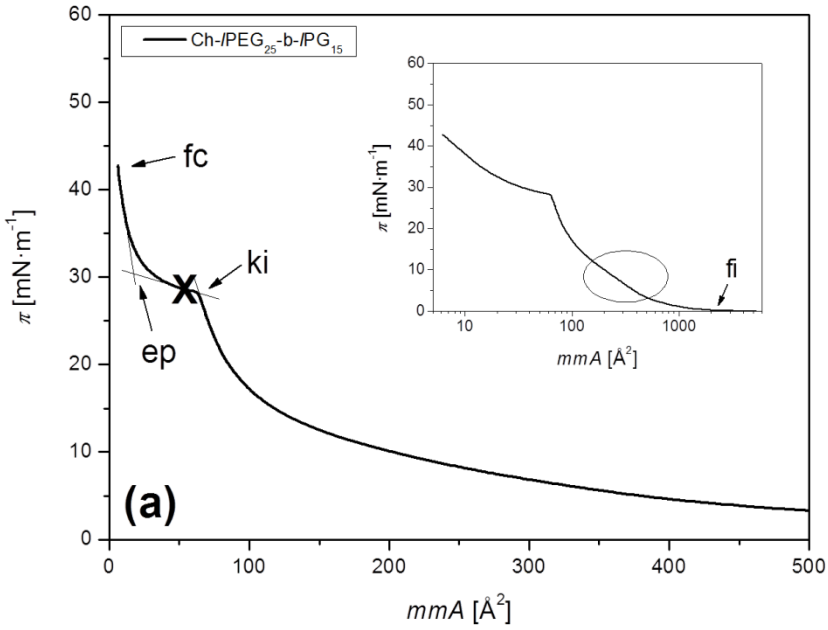

Figure 3.(a) Langmuir isotherms measured at 20 °C for the Ch-initiated diblock copolymers of (a) Ch-/PEG$_n$-b-/PG$_m$. The insets show the complete Langmuir isotherms within the full *mmA* range under investigation. The ellipses in the insets indicate the pancake-to-brush transition region of the /PEG block of the Ch-initiated diblock copolymers. The LB film of Ch-/PEG$_{25}$-b-/PG$_{15}$ is transferred at a surface pressure marked by **X**.

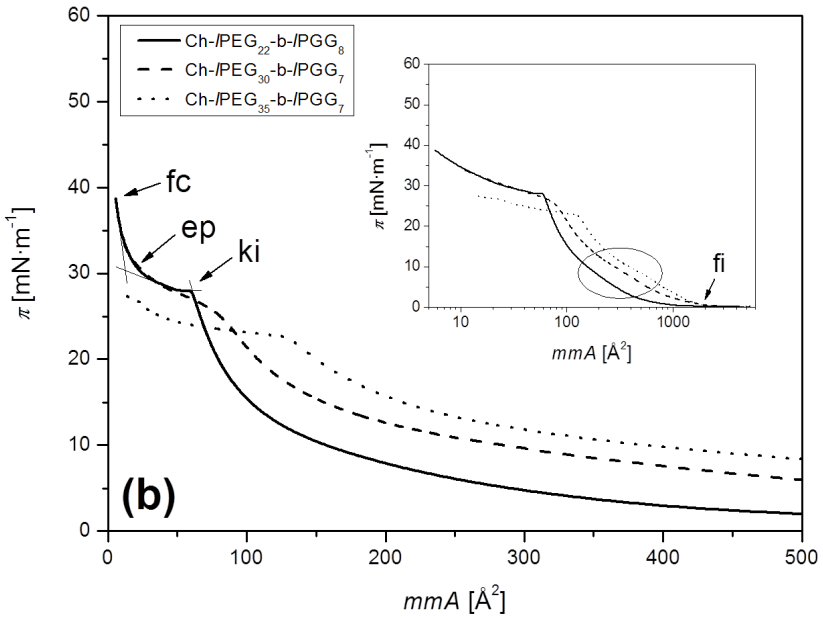

Figure 3 (b) Langmuir isotherms measured at 20 °C for the Ch-initiated diblock copolymers (b) Ch-/PEG$_n$-b-/PGG$_m$. The insets show the complete Langmuir isotherms within the full *mmA* range under investigation. The ellipses in the insets indicate the pancake-to-brush transition region of the /PEG block of the Ch-initiated diblock copolymers.

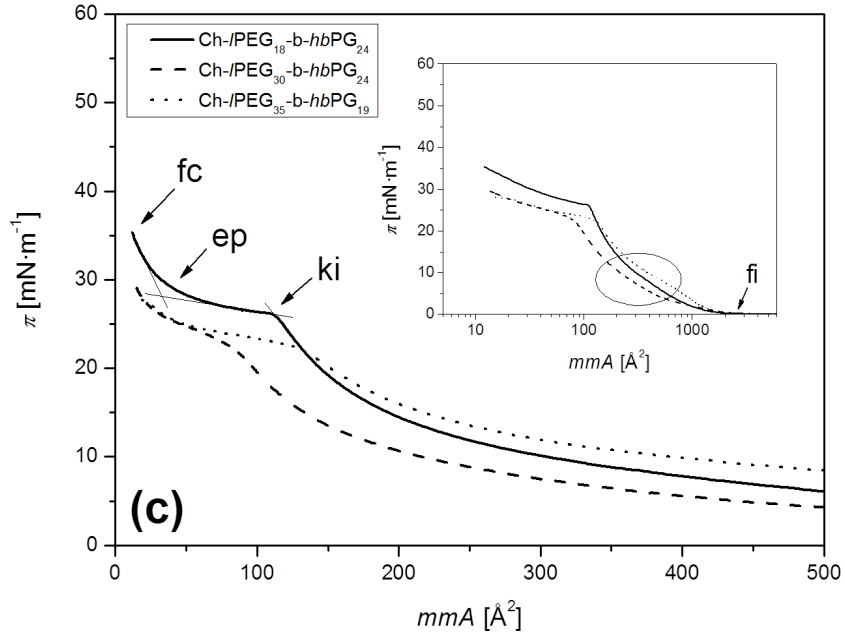

Figure 3. (c) Langmuir isotherms measured at 20 °C for the Ch-initiated diblock copolymers of (a) Ch-/PEG$_n$-b-/PG$_m$, (b) Ch-/PEG$_n$-b-/PGG$_m$, and (c) Ch-/PEG$_n$-b-*hb*PG$_m$. The insets show the complete Langmuir isotherms within the full *mmA* range under investigation. The ellipses in the

insets indicate the pancake-to-brush transition region of the *l*PEG block of the Ch-initiated diblock copolymers. The LB film of Ch-*l*PEG$_{25}$-b-*l*PG$_{15}$ is transferred at a surface pressure marked by **X**.

The Langmuir isotherms of the Ch-*l*PEG$_n$-b-*l*PGG$_m$ copolymers in Figure 3 (b) confirm a shift of the first significant increase of the surface pressure to larger *mmA*$_{fi}$ values with increasing *l*PEG$_n$ block length (i.e. increasing area requirement of the copolymers). During compression, the Langmuir isotherms show similar characteristic features (small shoulder, plateau region) as already observed for the other Ch-initiated homopolymers and diblock copolymers containing a *l*PEG$_n$ entity. The same conclusions are also drawn for the Ch-*l*PEG$_n$-b-*hb*PG$_m$ copolymers, since the corresponding Langmuir isotherms represented in Figure 3 (c) provide again a small shoulder and a plateau region.

Table 4. Characteristic data for the Langmuir isotherms of the Ch-initiated diblock copolymers. The meaning of the subscripts of the *mmA* and π values is given in the text.

Ch-initiated diblock copolymer	*mmA*$_{fi}$ [Å^2]	*mmA*$_{ki}$ / π_{ki} [Å^2] / [mN·m^{-1}]	*mmA*$_{ep}$ / π_{ep} [Å^2] / [mN·m^{-1}]	*mmA*$_{fc}$ / π_{fc} [Å^2] / [mN·m^{-1}]
Ch-*l*PEG$_{25}$-b-*l*PG$_{15}$	2250	64 / 28	17 / 30	6 / 43
Ch-*l*PEG$_{22}$-b-*l*PGG$_8$	1980	60 / 28	13 / 30	6 / 39
Ch-*l*PEG$_{30}$-b-*l*PGG$_7$	3090	78 / 26	25 / 29	11 / 34
Ch-*l*PEG$_{35}$-b-*l*PGG$_7$	3310	129 / 23	36 / 25	14 / 28
Ch-*l*PEG$_{18}$-b-*hb*PG$_{24}$	2550	112 / 26	33 / 28	12 / 35
Ch-*l*PEG$_{30}$-b-*hb*PG$_{24}$	3100	80 / 23	24 / 26	13 / 30
Ch-*l*PEG$_{35}$-b-*hb*PG$_{19}$	2830	130 / 23	40 / 25	14 / 28

Morphology of LB films. AFM is used to study the morphology of the LB films of Ch as well as of the Ch-initiated homopolymers transferred onto silicon substrates. For the LB films of the pure homopolymers *l*PG$_n$, *l*PGG$_n$, and *hb*PG$_n$, it is expected that they form homogeneous films on the SiO_2 surface of the substrate due to the hydrophilicity of both species. Since *l*PEG$_n$ is able to

crystallize in thin layers when the molar mass is sufficiently large, finger-like crystal structures are expected.[68-70] Thus, the morphologies of the Ch-initiated homopolymers are expected to be governed by the strong tendency of Ch to self-aggregate (crystallize), the film formation behavior of the polyethers and by additional crystal structures of *l*PEG$_n$.

Figure 4 (a) and (b) show the height image and a corresponding height profile of an LB film of pure Ch transferred at a π value of 45 mN·m^{-1} and *mmA* of 30 Å^2 (indicated by **X** in Figure 1). Large layered crystals of plate-like morphology resembling the Ch monohydrate crystals are observed.[15-17] Height differences of distinct steps of up to 10 nm obviously indicate that these crystals represent multilayer aggregates, occasionally larger than trilayers. This explanation is reasonable, since the height of the upright arranged Ch molecule is reported with values of around 1.6 nm.[10,12,15-17,25] Steps that fit to Ch trilayers are indicated by arrows in the height profile (Figure 4 (b)). Grazing incidence X-ray diffraction (GIXD) and ellipsometry measurements demonstrate that the formation of the large multilayer aggregates is not the result of the compression of Ch at the air-water interface, but is caused by the transfer of the LB films.[17] This is deduced from the fact that only mono-, bi- and trilayer phases of Ch appear within the plateau region of the Langmuir isotherm in agreement with our discussion (cf. Figure 1).

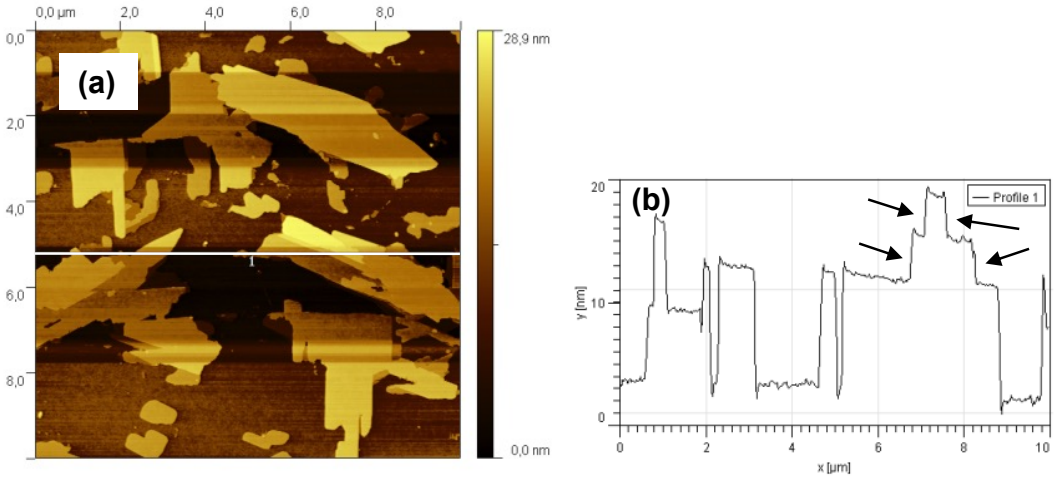

Figure 4. (a) AFM height image of the LB film of Ch transferred at a π value of 45 mN·m^{-1} (indicated by **X** in Figure 1). (b) Height profile along the line in (a). The arrows indicate Ch trilayers.

Figure 5 represents the AFM results for the LB film of Ch-*l*PG$_{15}$ transferred at a π value of 40 mN·m^{-1} and *mmA* of 38 Å^2 (indicated by **X** in Figure 2 (a)). This transfer is carried out after

the characteristic kink had been reached in the Langmuir isotherm. The morphology observed on the silicon substrate can be described as regular, worm-like structures dispersed in a continuous phase with a roughly uniform height varying from 4.2 to 4.8 nm (Figure 5 (b)). Comparing height image and phase contrast image leads to the result that the worm-like structures are formed by a polymer rich phase. This polymer rich phase is soft and appears darker in the phase contrast image compared to the surroundings (indicated by arrows in Figure 5 (c)). The brighter phase in the phase contrast image appears heterogeneous, and the bright dots are formed by Ch crystals of Ch-/PG_{15}. Obviously, the phase segregation or rather the crystallization of the hydrophobic Ch units triggers also dewetting effects of the hydrophilic /PG_{15} part of Ch-/PG_{15}.[61-67] Otherwise, a homogeneous polymer film with dispersed Ch crystals would be expected.

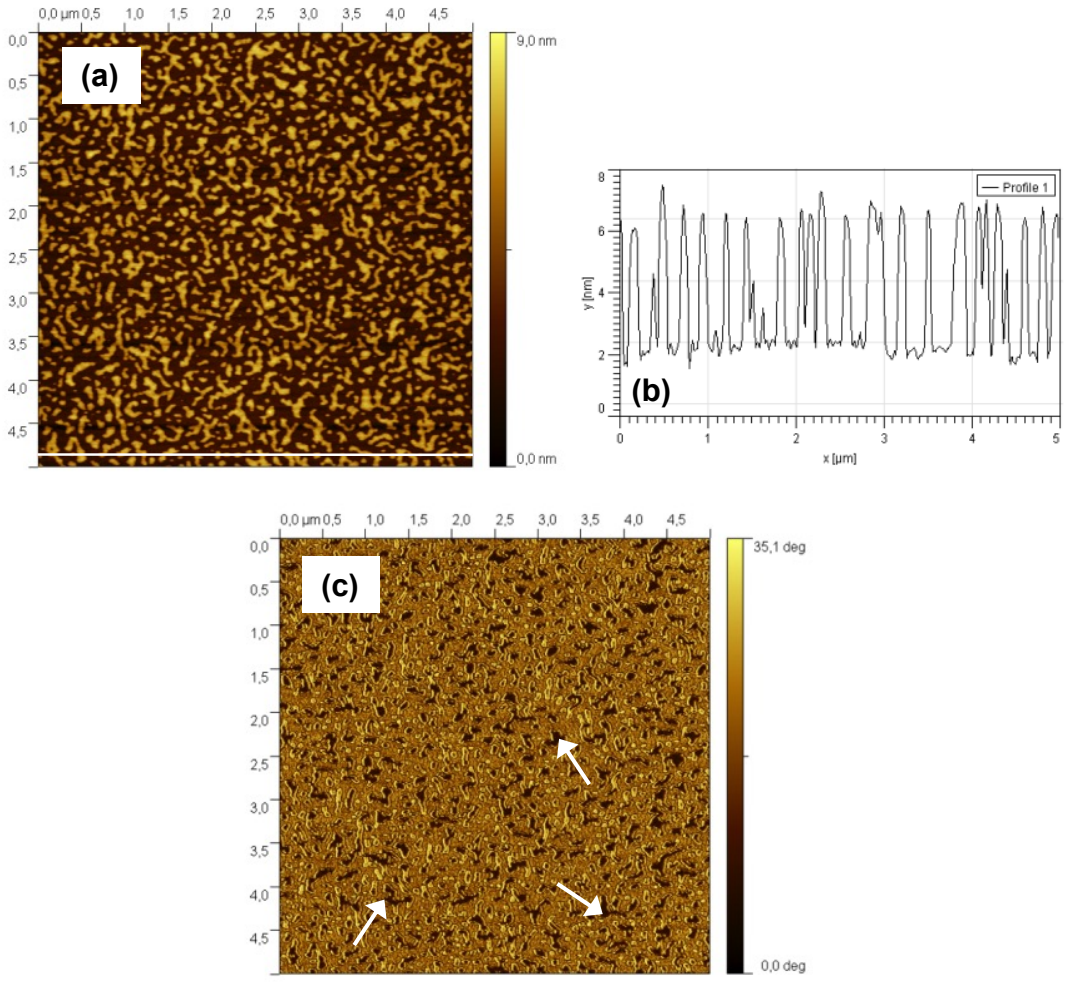

Figure 5. (a) AFM height image of the LB film of Ch-/PG_{15} transferred at a π value of 40 $mN \cdot m^{-1}$ (indicated by **X** in Figure 2 (a)). (b) Height profile along the line in (a). (c) Phase contrast image of (a). The arrows indicate the /PG_{15} rich phase of Ch-/PG_{15}.

In Figure 6, the AFM measurements for the LB film of Ch-*l*PGG$_7$ transferred at a π value of 40 mN·m^{-1} and *mmA* of 31 Å^2 (indicated by **X** in Figure 2 (a)) are shown. Ch-*l*PGG$_7$ forms circular structures that are reminiscent of 'sunnyside up' structures. Despite the facts, that this LB film was deposited at similar π and *mmA* values as the LB film of Ch-*l*PG$_{15}$ (see Figure 5), and that the Langmuir isotherms of these two Ch-initiated homopolymers are similar (see Figure 2 (a)), the morphologies of the LB films are completely different.

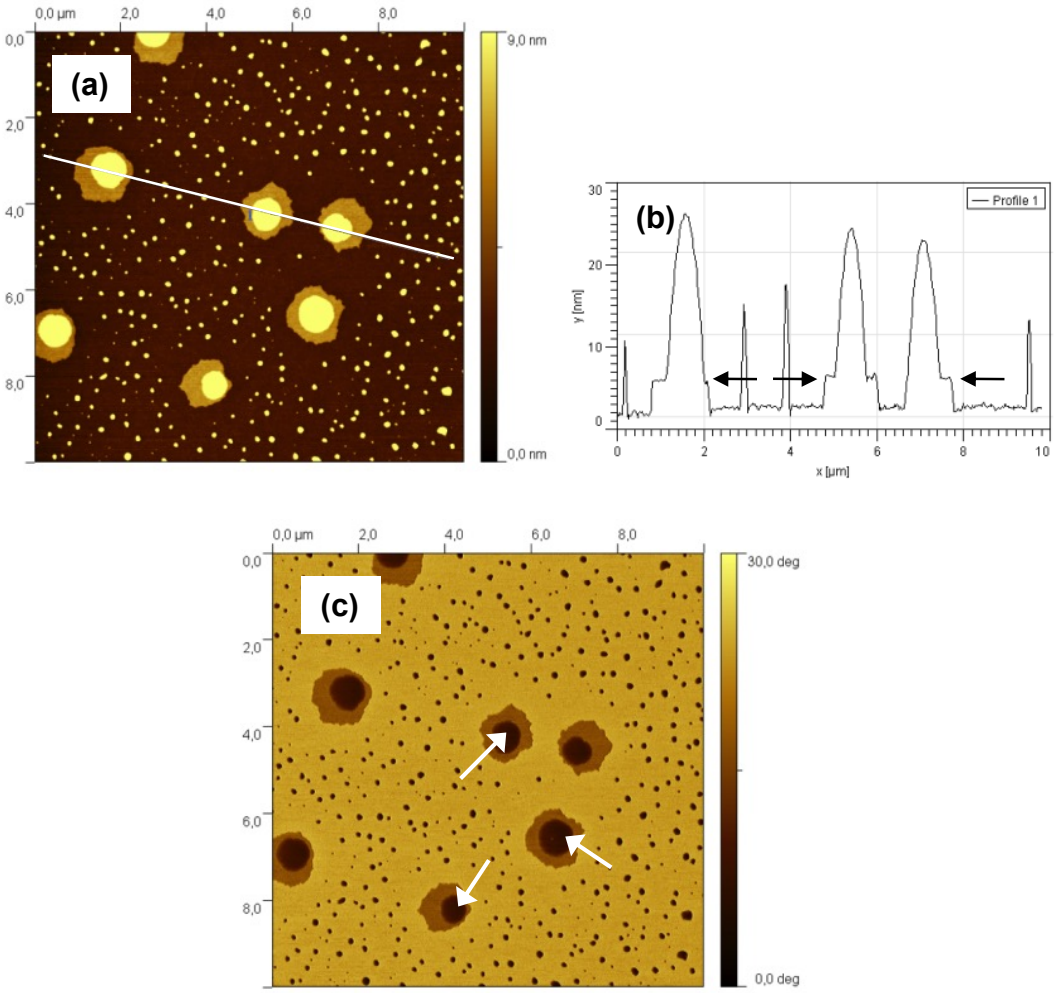

Figure 6. (a) AFM height image of the LB film of Ch-*l*PGG$_7$ transferred at a π value of 40 mN·m^{-1} (indicated by **X** in Figure 2 (a)). (b) Height profile along the line in (a). The arrows indicate trilayers of Ch units. (c) Phase contrast image of (a). The arrows indicate the *l*PGG$_7$ rich phase of Ch-*l*PGG$_7$.

Based on the phase contrast image in Figure 6 (c), it is concluded that the first step of the 'sunnyside up' structures representing the 'albumen' is formed by the Ch units of Ch-*l*PGG$_7$. Due to the height of the 'albumen' of around 5 nm (indicated by arrows in Figure 6 (b)), it can

be considered as trilayers of upright standing Ch units in the crystalline state (3 x 1.6 nm).[10,12,15-17,25] Since the anchoring of the hydrophobic Ch units on the hydrophilic silicon substrate is unlikely, Ch-*l*PGG$_7$ is assumed to be anchored via the hydrophilic *l*PGG$_7$ entity of the first Ch-*l*PGG$_7$ layer of the trilayer on the substrate. The residual *l*PGG$_7$ chains of the Ch-*l*PGG$_7$ trilayer form the soft 'yolk' domains of the 'sunnyside up' structures (indicated by arrows in Figure 6 (c)) with a significant larger height than the 'albumen' (maximum between 15 to 22 nm) on top of the Ch units of Ch-*l*PGG$_7$ due to the connectivity of these both entities.

The AFM results for the LB film of Ch-*hb*PG$_{35}$ transferred at a π value of 21 mN·m^{-1} and *mmA* of 60 Å^2 in the plateau-like region of the Langmuir isotherm (indicated by **X** in Figure 2 (b)) are presented in Figure 7.

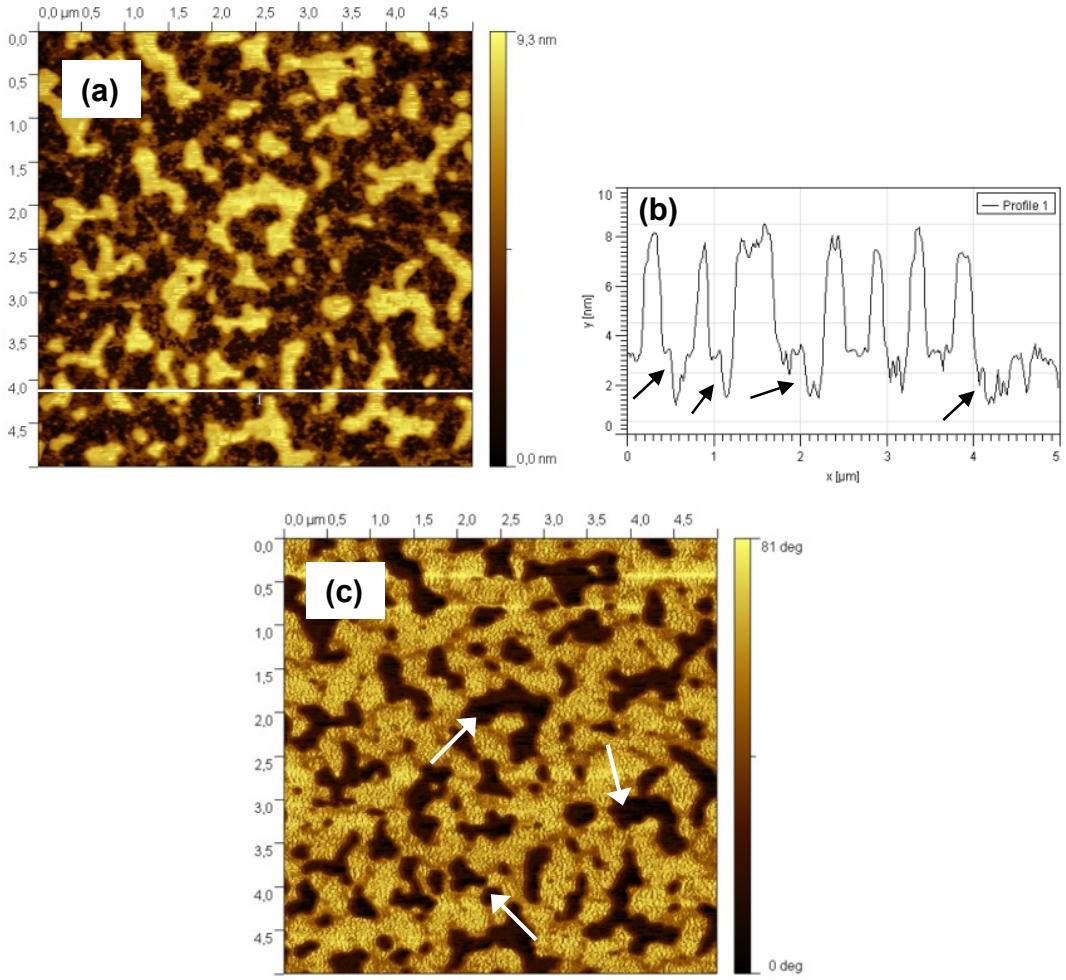

Figure 7. (a) AFM height image of the LB film of Ch-*hb*PG$_{35}$ transferred at a π value of 21 mN·m^{-1} (indicated by **X** in Figure 2 (b)). (b) Height profile along the line in (a). The arrows indicate a layer of upright arranged Ch units. (c) Phase contrast image of (a). The arrows indicate the *hb*PG$_{35}$ rich phase of Ch-*hb*PG$_{35}$

In comparison to the previously discussed Ch-initiated homopolymer Ch-*l*PG$_{15}$, Ch-*hb*PG$_{35}$ shows larger aggregated structures, which might be related to the more bulky structure of the hyperbranched segment. The brighter regions in the height image of Figure 7 (a) are formed by the *hb*PG$_{35}$ rich phase (dark in the phase image, indicated by arrows in Figure 7 (c)). The height profile of Figure 7 (b) indicates that a Ch rich single layer is formed with a step height of 1.6 nm (indicated by arrows in Figure 7 (b)), which is in good agreement with the height of one upright arranged Ch molecule.[10,12,15-17,25] Obviously, the hyperbranched polymer prevents the formation of Ch trilayers due to their bulky structure. The observations prove the phase segregation in the LB film of Ch-*hb*PG$_{35}$ into a hydrophobic Ch rich phase and a hydrophilic *hb*PG$_{35}$ rich phase.

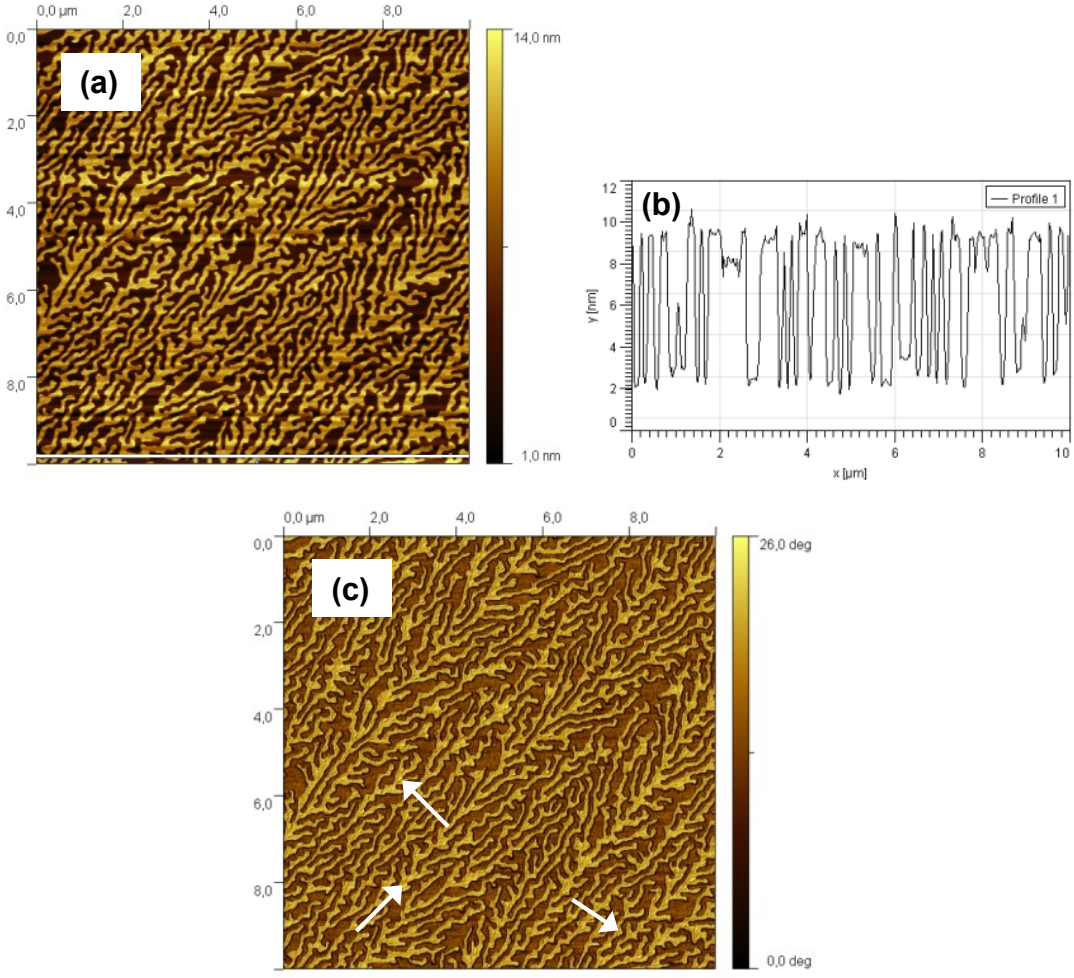

Figure 8. (a) AFM height image of the LB film of Ch-*l*PEG$_{69}$ transferred at a π value of 23 mN·m^{-1} (indicated by **X** in Figure 2 (c)). (b) Height profile along the line in (a). (c) Phase contrast image of (a). The arrows indicate aggregated Ch units.

Figure 8 shows the AFM results for the LB film of Ch-/PEG$_{69}$ transferred at a π value of 23 mN·m^{-1} and *mmA* of 110 Å^2 in the plateau region of the Langmuir isotherm (indicated by **X** in Figure 2 (c)). The dominant morphology is a finger-like branched structure typical for crystallized /PEG monolayers.[54,68-73] Thus, the finger-like crystals represent the crystallized /PEG$_{69}$ units of Ch-/PEG$_{69}$ together with homogeneously dispersed Ch units (indicated by arrows in Figure 8 (c)). The Ch units appear as bright spots, since they are harder than the /PEG$_{69}$ crystals. The uniform height of the /PEG$_{69}$ crystals is about 7.5 nm as shown in Figure 8 (b). From the phase contrast image, it can be concluded that the surroundings of the finger-like crystals is formed by a homogeneous Ch-/PEG$_{69}$ layer, since the surface of the silicon substrate would require a brighter phase contrast. This means, the influence of the Ch units on the morphology of the LB films is definitely smaller compared to the LB films of the Ch-initiated homopolymers discussed before. Obviously, the crystallization of the long /PEG$_{69}$ entity of Ch-/PEG$_{69}$ dominates the morphology development.

First studies on the LB film morphology of the Ch-initiated diblock copolymers with Ch-/PEG$_n$-b-/PG$_m$ structure have also been carried out by AFM. As expected, the morphology becomes even more complicated in these cases. An example for Ch-/PEG$_{25}$-b-/PG$_{15}$ is discussed in the Supporting information.

Conclusions.

The surface activity of a series of Ch-initiated polyethers with systematically varied linear and branched structures has been investigated by Langmuir trough measurements. The Ch-initiated homopolymers and diblock copolymers were composed of a hydrophobic Ch group and either one or two hydrophilic blocks of the type /PG, /PGG, *hb*PG, or /PEG. Langmuir films of these polymers revealed that already marginal variations in the molecular structures had pronounced consequences for their behavior at the air-water interface. For the first time, also the behavior of well defined polymers with hyperbranched blocks has been investigated at the air-water interface. Surface pressure measurements of the /PG$_{54}$ and *hb*PG$_{29}$ homopolymers showed the absence of surface activity at the air-water interface due to a strong tendency to dissolve in the water subphase after spreading from a chloroform solution (in clear contrast to /PEG). Surprisingly, this behavior changed drastically, when only one Ch group was covalently linked to /PG and *hb*PG. For the other Ch-initiated homopolymers, the Langmuir isotherms proved also

the existence of stable Langmuir films at the air-water interface. All Ch-initiated polymers showed a reduction of the collapse surface pressure of the monolayer compared to the corresponding value of the monolayer of pure Ch. Typical hierarchically ordered morphologies of the LB films on hydrophilic substrates were observed for all Ch-initiated polymers. Most prominent in all LB films was the Ch crystallization. The strong tendency of Ch self-aggregation is then connected with dewetting effects of the respective polyether entities. Additionally, crystallization of the /PEG_{69} chain in Ch-/PEG_{69} is observed resulting in a finger-like morphology of the LB films.

The polymers under investigation should have a high potential for biomedical applications, since they contain many binding motives to phospholipid bilayers of cell membranes.[74] It can be expected that Ch is incorporated in the hydrophobic bilayer of a membrane, and additionally the hydrophilic parts may contribute to a closure of holes in membranes, or to the formation of holes depending on the hydrophobic-hydrophilic balance, and on the molar masses of the respective blocks.[75,76] With this respect, especially the hyperbranched polymers deserve further attention.

Acknowledgements.

S.R. thanks Agrochemisches Institut Piesteritz e.V. for financial support and J.K. thanks Deutsche Forschungsgemeinschaft (FOR 1145). A.M.H. acknowledges MAINZ (Material science in Mainz) for valuable financial support.

Supporting information available.

BAM images of pure Ch and Ch-/PGG_7, reversibility studies of Ch-/PGG_7 and Ch-/PEG_{35}-b-*hb*PG_{19}, and AFM results of Ch-/PEG_{25}-/PG_{15}. This material is available free of charge via the Internet at http://pubs.acs.org.

References

(1) Dynarowicz-Latka, P.; Dhanabalan, A.; Oliveira Jr., O.N. *Adv. Colloid Interface Sci.* **2001**, *91*, 221.

(2) Hénon, S.; Meunier, J. *Rev. Sci. Instrum.* **1991**, *62*, 936.

(3) Hönig, D.; Möbius, D. *J. Phys. Chem.* **1991**, *95*, 4590.

(4) Roberts, G. *Langmuir-Blodgett Films*; Springer: Berlin, 1990.

(5) Petty, M.C. *Langmuir-Blodgett films*; Cambridge University Press: Cambridge, 1996.

(6) Birdi, K.S. *Self-Assembly Monolayer Structures of Lipids and Macromolecular Interfaces*; Springer: Berlin, 1999.

(7) Hubbard, A.T. *Encyclopedia of Surface and Colloid Science*, Dekker: New York, 2002.

(8) Krafft, M.-P.; Ries, J.G. *Chem. Rev.* **2009**, *109*, 1714.

(9) Schwartz, D.K.; Garnaes, J.; Viswanathan, R.; Chirovolu, S.; Zasadzinski, J.A.N. *Phys. Rev. E* **1992**, *47*, 452.

(10) Sparr, E.; Ekelund, K.; Engblom, J.; Engström, S.; Wennerström, H. *Langmuir* **1999**, *15*, 6950.

(11) Baumeister, W. *Fette, Seifen, Anstrichmittel* **1975**, *77*, 109.

(12) Abendan, R.S.; Swift, J.A. *Langmuir* **2002**, *18*, 4847.

(13) Takano, E.; Ishida, Y.; Iwahashi, M.; Araki, T.; Iriyama, K. *Langmuir* **1997**, *13*, 5782.

(14) Vist, M.R.; Davis, J.H. *Biochemistry* **1990**, *29*, 451.

(15) Rapaport, H.; Kuzmenko, I.; Lafont, S.; Kjaer, K.; Howes, P.B.; Als-Nielsen, J.; Lahav, M.; Leiserowitz, L. *Biophys. J.* **2001**, *81*, 2729.

(16) Cadena-Nava, R.D.; Martin-Mirones, J.M.; Vázquez-Martínez, E.A.; Roca, J.A.; Ruiz-García, J. *Rev. Mex. Fis. S* **2006**, *52*, 32.

(17) Lafont, S.; Rapaport, H.; Sömjen, G.J.; Renault, A.; Howes, P.B.; Kjaer, K.; Als-Nielsen, J.; Leiserowitz, L.; Lahav, M. *J. Phys. Chem. B* **1998**, *102*, 761.

(18) Müller-Landau, F.; Cadenhead, D.A. *Chem. Phys. Lipids* **1979**, *25*, 299.

(19) Gupta, R.K.; Suresh, K.A. *Eur. Phys. J. E* **2004**, *14*, 35.

(20) Seoane, R.; Miñones, J.; Conde, O.; Miñones Jr., J.; Casas, M.; Iribarnegaray, E. *J. Phys. Chem. B* **2000**, *104*, 7735.

(21) Seoane, R.; Miñones, J.; Conde, O.; Iribarnegaray, E.; Casas, M. *Langmuir* **1999**, *15*, 5567.

(22) Flach, C.R.; Mendelsohn, R.; Rerek, M.E.; Moore, D.J. *J. Phys. Chem. B* **2000**, *104*, 2159.

(23) Gálvez Ruiz, M.J.; Cabrerizo Vilchez, M.A. *Colloid Polym. Sci.* **1991**, *269*, 77.

(24) Eeman, M.; Francius, G.; Dufrêne, Y.F.; Nott, K.; Paquot, M.; Deleu, M. *Langmuir* **2009**, *25*, 3029.

(25) Sparr, E.; Eriksson, L.; Bouwstra, J.A.; Ekelund, K. *Langmuir* **2001**, *17*, 164.

(26) Mudgil, P.; Dennis, G.R.; Millar, T.J. *Langmuir* **2005**, *21*, 1338.

(27) Kauffmann, J.M.; Westerman, P.W.; Carey, M.C. *J. Lipid Res.* **2000**, *41*, 991.

(28) Gallay, J.; de Kruijff, B.; Demel, R.A. *Biochim. Biophys. Acta* **1984**, *769*, 96.

(29) Theunissen, J.J.H.; Jackson, R.L.; Kempen, H.J.M.; Demel, R.A. *Biochim. Biophys. Acta* **1986**, *860*, 66.

(30) Kwong, C.N.; Heikkila, R.E.; Cornwell, D.G. *J. Lipid Res.* **1971**, *12*, 31.

(31) Alonso, C.; Kuzmenko, I.; Jensen, T.R.; Kjaer, K.; Lahav, M.; Leiserowitz, L. *J. Phys. Chem. B* **2001**, *105*, 8563.

(32) Viswanath, P.; Suresh, K.A. *J. Phys. Chem. B* **2004**, *108*, 9198.

(33) Söderlund, H.; Sjöblom, J.; Wärnheim, T. *J. Dispersion Sci. Technol.* **1989**, *10*, 131.

(34) Sato, T.; Hossain, M.K.; Acharya, D.P.; Glatter, O.; Chiba, A.; Kunieda, H. *J. Phys. Chem. B* **2004**, *108*, 12927.

(35) López-Quintela, M.A.; Akahane, A.; Rodriguez, C.; Kunieda, H. *J. Colloid Interface Sci.* **2002**, *247*, 186.

(36) Xu, J.-T.; Xue, L.; Fan, Z.-Q. *Macromolecules* **2006**, *39*, 2981.

(37) Wurm, F.; Nieberle, J.; Frey, H. *Macromolecules* **2008**, *41*, 1184.

(38) Wurm, F.; Nieberle, J.; Frey, H. *Macromolecules* **2008**, *41*, 1909.

(39) Wilms, D.; Wurm, F.; Nieberle, J.; Böhm, P.; Kemmer-Jonas, U.; Frey, H. *Macromolecules* **2009**, *42*, 3230.

(40) Wilms, D.; Stiriba, S.-E.; Frey, H. *Acc. Chem. Res.* **2010**, *43*, 129.

(41) Hofmann, A.M.; Wurm, F.; Nawroth, T.; Langguth, P.; Frey, H. *Biomacromolecules* **2010**, *11*, 568.

(42) Vandenheuvel, F.A. *J. Am. Oil Chem. Soc.* **1963**, *40*, 455.

(43) Ries Jr., H.E.; Swift, H. *Colloid Surf.* **1989**, *40*, 145.

(44) Kundu, S.; Datta, A.; Hazra, S. *Langmuir* **2005**, *21*, 5894.

(45) Diep-Quang, H.; Ueberreiter, K. *Colloid Polym. Sci.* **1980**, *258*, 1055.

(46) Shuler, R.L.; Zisman, W.A. *J. Phys. Chem.* **1970**, *74*, 1523.

(47) Kawaguchi, M.; Komatsu, S.; Matsuzumi, M.; Takahashi, A. *J. Colloid Interface Sci.* **1984**, *102*, 356.

(48) Sauer, B.B.; Kawaguchi, M.; Yu, H. *Macromolecules* **1987**, *20*, 2732.

(49) Kuzmenka, D.J.; Granick, S. *Macromolecules* **1988**, *21*, 779.

(50) Sauer, B.B.; Yu, H. *Macromolecules* **1989**, *22*, 786.

(51) Joncheray, T.J.; Denoncourt, K.M.; Mathieu, C.; Meier, M.A.R.; Schubert, U.S.; Duran, R.S. *Langmuir* **2006**, *22*, 9264.

(52) Gonçalves da Silva, A.M.; Filipe, E.J.M.; d´Oliveira, J.M.R.; Martinho, J.M.G. *Langmuir* **1996**, *12*, 6547.

(53) Baker, S.M.; Leach, K.A.; Devereaux, C.E.; Gragson, D.E. *Macromolecules* **2000**, *33*, 5432.

(54) Li, H.; Sachsenhofer, R.; Binder, W.H.; Henze, T.; Thurn-Albrecht, T.; Busse, K.; Kressler, J. *Langmuir* **2009**, *25*, 8320.

(55) Gragson, D.E.; Jensen, J.M.; Baker, S.M. *Langmuir* **1999**, *15*, 6127.

(56) Peetla, C.; Graf, K.; Kressler, J. *Colloid Polym. Sci.* **2006**, *285*, 27.

(57) Busse, K.; Peetla, C.; Kressler, J. *Langmuir* **2007**, *23*, 6975.

(58) Fauré, M.C.; Bassereau, P.; Carignano, M.A.; Szleifer, I.; Gallot, Y.; Andelman, D. *Eur. Phys. J. B* **1998**, *3*, 365.

(59) Fauré, M.C.; Bassereau, P.; Lee, L.T.; Menelle, A.; Lheveder, C. *Macromolecules* **1999**, *32*, 8538.

(60) Barentin, C.; Muller, P.; Joanny, J.F. *Macromolecules* **1998**, *31*, 2198.

(61) Reiter, G. *Langmuir* **1993**, *9*, 1344.

(62) Deschênes, L.; Bousmina, M.; Ritcey, A.M. *Langmuir* **2008**, *24*, 3699.

(63) Liang, G.D.; Xu, J.-T.; Fan, Z.-Q.; Mai, S.-M.; Ryan, A.J. *J. Phys. Chem. B* **2006**, *110*, 24384.

(64) Cheyne, R.B.; Moffitt, G. *Langmuir* **2006**, *22*, 8387.

(65) Sehgal, A.; Ferreiro, V.; Douglas, J.F.; Amis, E.J.; Karim, A. *Langmuir* **2002**, *18*, 7041.

(66) Fredin, N.J.; Zhang, J.; Lynn, D.M. *Langmuir* **2007**, *23*, 2273.

(67) Wei, B.; Lam, P.G.; Braunfeld, M.B.; Agard, D.A.; Genzer, J.; Spontak, R.J. *Langmuir* **2006**, *22*, 8642.

(68) Reiter, G.; Sommer, J.-U. *J. Chem. Phys.* **2000**, *112*, 4376.

(69) Sommer, J.-U.; Reiter, G. *J. Chem. Phys.* **2000**, *112*, 4384.

(70) Reiter, G. *J. Polym. Sci., Part B: Polym. Phys.* **2003**, *41*, 1869.

(71) Zhai, X.-M.; Wang, W.; Ma, Z.-P.; Wen, X.-J.; Yuan, F.; Tang, X.-F.; He, B.-L. *Macromolecules* **2005**, *38*, 1717.

(72) Zhai, X.; Wang, W.; Zhang, G.; He, B. *Macromolecules* **2006**, *39*, 324.

(73) Chen, R.; Li, L.; Zhao, J. *Langmuir* **2010**, *26*, 5951.

(74) Seelig, A.; Gerebtzoff, G. *Expert Opin. Drug Metab. Toxicol.* **2006**, *2*, 733.

(75) Sommer, K.; Kaiser, S.; Krylova, O.O., Kressler, J.; Pohl, P.; Busse, K. *J. Med. Chem.* **2008**, *51*, 4253.

(76) Amado, E.; Blume, A.; Kressler, J. *Reactive & Functional Polymers* **2009**, *69*, 450.

Supporting information

Langmuir and Langmuir-Blodgett films of multifunctional, amphiphilic polyethers with cholesterol moieties

Sascha Reuter,[1] Anna Maria Hofmann,[2] Karsten Busse,[1] Holger Frey,[2] and Jörg Kressler*,[1]

1 Department of Chemistry, Martin Luther University Halle-Wittenberg, Halle (Saale), Germany.

2 Institute of Organic Chemistry, Duesbergweg 10-14, Johannes Gutenberg-University, Mainz, Germany.

Published in Langmuir 2011, 27 (5), 1978-1989.

BAM studies. Figure S.1 (a) shows the BAM image of Ch recorded in the coexistence region of the LC phase and the G phase at *mmA* of 49 Å^2 and a π value close to 0 mN·m^{-1}. The bright regions are large domains of the LC phase, and the dark regions represent the G phase. During compression of Ch in the plateau region, bright domains of Ch crystals are observed within the darker, homogeneous LC phase of Ch in the BAM image recorded at *mmA* of 23 Å^2 (see Figure S.1 (b)).

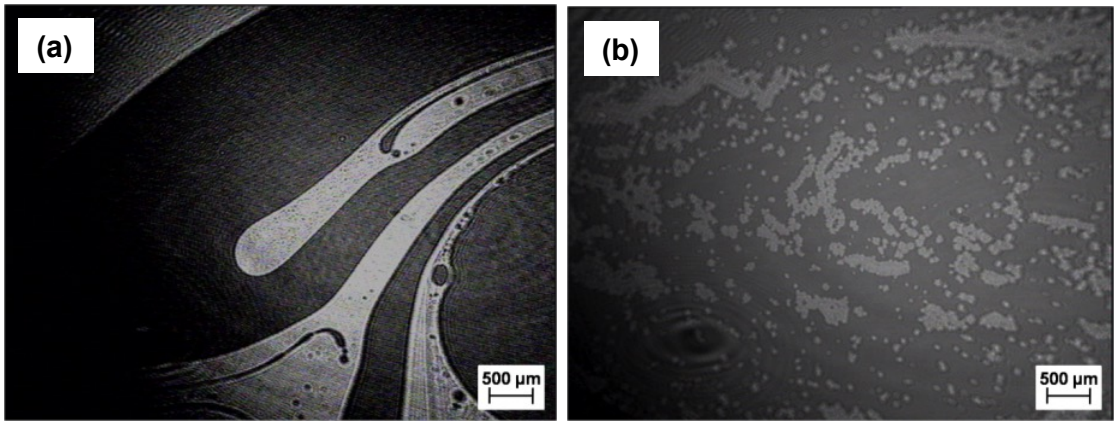

Figure S.1. BAM images of Ch recorded at (a) *mmA* = 49 Å^2, and (b) *mmA* = 23 Å^2. The corresponding Langmuir isotherm is given in Figure 1.

The BAM images of the Langmuir films of Ch-*l*PGG$_7$ in Figure S.2 recorded at the air-water interface during the compression at *mmA* values of 14 and 11 Å^2 show circular domains of different lateral size. The maximum diameter for these domains is identified with a value of around 200 µm. Since the BAM images were recorded after the final collapse of Ch-*l*PGG$_7$, the circular domains are supposed to represent collapsed structures of Ch-*l*PGG$_7$ (e.g. multilayer crystals).

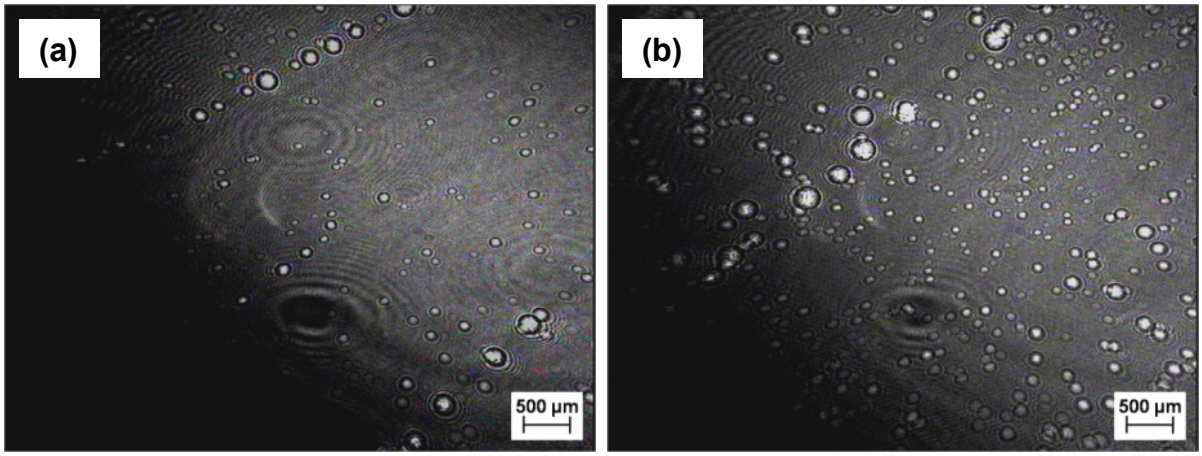

Figure S.2. BAM images of Ch-*l*PGG$_7$ recorded at (a) *mmA* = 14 Å^2, and (b) *mmA* = 11 Å^2. The corresponding Langmuir isotherm is given in Figure 2 (a).

BAM investigations are also carried out for the Langmuir films of the other Ch-initiated homopolymers and diblock copolymers, but only unstructured films are observed. This indicates the formation of quite homogeneous monolayers up to the end of the plateau regions of the Langmuir isotherms.

Reversibility studies. Reversibility experiments are carried out by measuring compression and expansion cycles of the Ch-initiated homopolymers and diblock copolymers. Figure S.3 using the examples of Ch-*l*PGG$_7$ and Ch-*l*PEG$_{35}$-b-*hb*PG$_{19}$ demonstrates a hysteresis observed between the compression and expansion cycles. The most important fact is the second compression run, which is identical with the first compression run at small *mmA* values. This indicates that the copolymers do not dissolve in the water subphase.

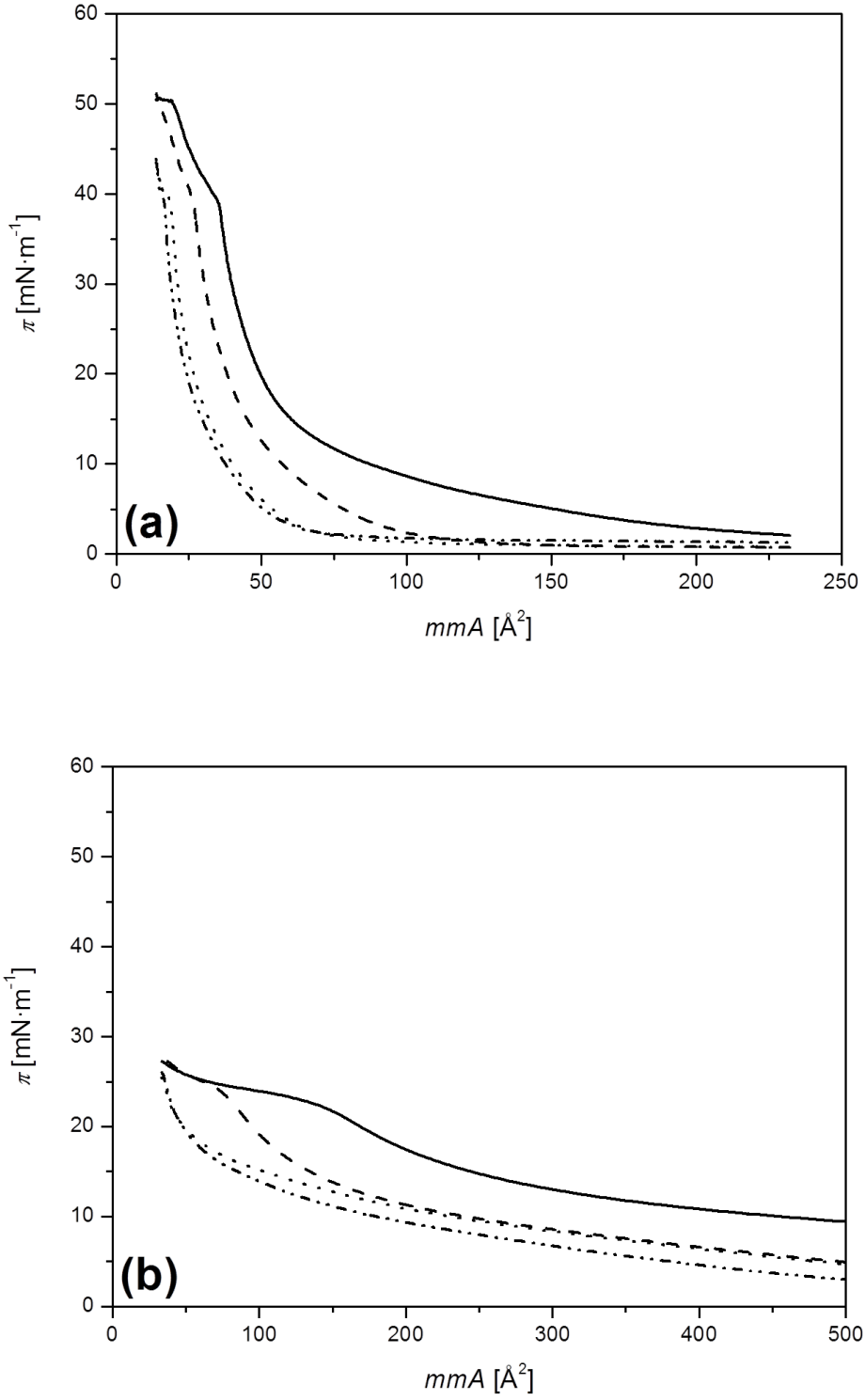

Figure S.3. Reversibility studies of the Langmuir isotherms of (a) Ch-*l*PGG$_7$ and (b) Ch-*l*PEG$_{35}$-b-*hb*PG$_{19}$ at 20 °C using a compression/expansion rate of 15 cm^2·min^{-1}. The different cycles show first compression (solid line), first expansion 2 min after reaching the collapse pressure (dotted line), second compression after 20 min (dashed line), second expansion 2 min after reaching the collapse pressure (chain double-dotted line).

AFM studies. Figure S.4 shows the AFM measurements for the LB film of Ch-/PEG_{25}-b-/PG_{15} transferred at a π value of 29 $mN \cdot m^{-1}$ and *mmA* of 54 $Å^2$ in the plateau region of the Langmuir isotherm (indicated by **X** in Figure 3 (a)). The observed morphology is completely different from the AFM results of the Ch-initiated homopolymers. It shows a very smooth, homogeneous film with large cavities of lateral dimensions in the micrometer range. These cavities contain also structured material, which is harder than the softer surrounding (arrows) as indicated by the phase contrast image (Figure S.4 (c)).

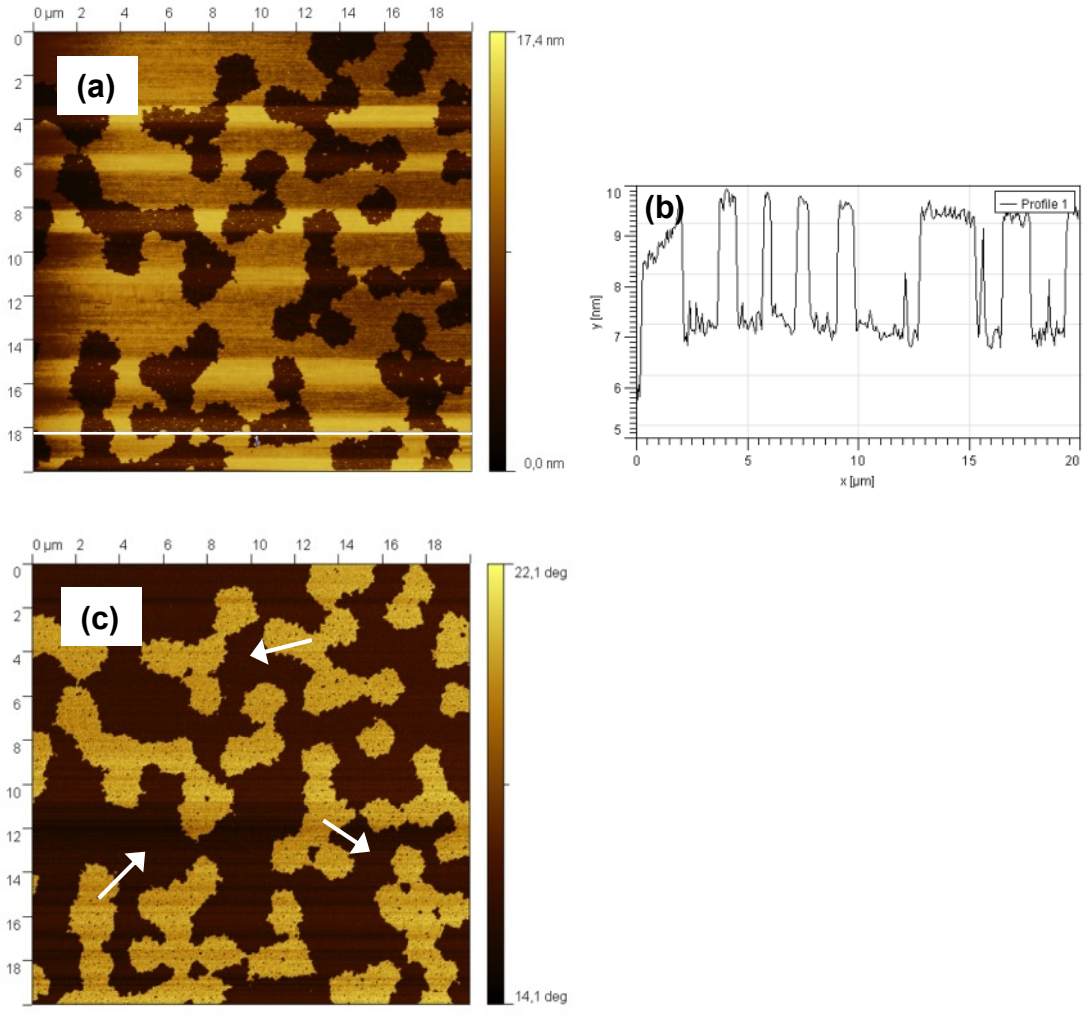

Figure S.4. (a) AFM height image of the LB film of Ch-/PEG_{25}-b-/PG_{15} transferred at a π value of 29 $mN \cdot m^{-1}$ (indicated by **X** in Figure 3 (a)). (b) Height profile along the line in (a). (c) Phase contrast image of (a). The arrows indicate the softer regions of the LB film.

Chapter 3.2: Strong interactions between DPPC and a cholesteryl moiety covalently bound to a linear-hyperbranched polyether diblock copolymer

Chapter 3.2:

Strong interactions between DPPC and a cholesteryl moiety covalently bound to a linear-hyperbranched polyether diblock copolymer

Xiaoju Peng,[1] Anna Maria Hofmann,[2] Sascha Reuter,[1] Holger Frey,[2] Jörg Kressler[1,*]

1 Institut für Chemie, Martin Luther Universität Halle-Wittenberg, Halle (Saale), Germany

2 Institut für organische Chemie, Johannes Gutenberg-Universität, Mainz, Germany

Submitted to Colloid. Polym. Sci.

Abstract

Interactions of the phospholipid 1,2-dipalmitoyl-*sn*-glycero-3-phosphocholine (DPPC) with the amphiphilic diblock copolymer Ch-*l*PEG$_{30}$-*b*-*hb*PG$_{24}$ (ChP) are studied at the air-water interface by surface pressure-mean molecular area (π-*mmA*) measurements of mixed Langmuir films and adsorption measurements of ChP to DPPC monolayers at different initial surface pressure values π_0. ChP is composed of a single hydrophobic cholesteryl (Ch) moiety covalently bound to a a diblock copolymer consisting of a hydrophilic linear poly(ethylene glycol) (*l*PEG) block and a hydrophilic hyperbranched polyglycerol (*hb*PG) block. Langmuir isotherms and compression moduli of the mixed Langmuir films of different molar ratios reveal distinct interactions between DPPC and ChP during compression. It is demonstrated that the behavior of the DPPC/ChP mixtures is dominated by DPPC up to a molar ratio of 10:1, whereas the behavior is predominantly governed by ChP in mixtures with lower DPPC content (molar ratios of 5:1, 2:1, 1:1). In adsorption measurements, a strong affinity of ChP to DPPC is observed after injection into the water subphase. The surface pressure value π_{in} up to which ChP is able to penetrate into DPPC monolayers is determined to the remarkably high value of 50.3 mN/m which can only be caused by strong favorable interactions between DPPC and the Ch moiety of ChP. Atomic force microscopy (AFM) on LB films of DPPC/ChP mixtures of different molar ratios transferred onto hydrophilic silicon substrates confirm attractive interactions between these

compounds, since large domains characteristic for macroscopic phase separation do not occur unless the *l*PEG block of ChP crystallizes.

Keywords

cholesteryl moiety, diblock copolymer, poly(ethylene glycol), hyperbranched polyglycerol, DPPC, adsorption

Introduction

Membranes acting as cell walls of biological cells are basically composed of lipid bilayers and proteins embedded within the lipid matrix.[1,2] Biological membranes are of particular relevance in the field of drug delivery and targeting, where it is attempted to deliver active species into cells by penetrating these membranes.[3-5] In order to study the capability of penetration of synthetic molecules into cell membranes, simplified models are often employed. Typical examples in this context are Langmuir monolayers of phospholipids at the airwater interface, which represent a half leaflet analogue of biological membranes.[6-9] Due to the simple preparation and characterization of Langmuir films, they are used to study the interactions between membrane components,[10] protein interactions with the lipid matrix,[11] and the penetrability for synthetic molecules.[12-14] Investigations of Langmuir films are performed on a Langmuir trough at the air-water interface by surface pressure-mean molecular area (π-*mmA*) measurements in order to obtain Langmuir isotherms.[15] Further methods applied to visualize domains in the micrometer range in these films are Brewster angle microscopy (BAM)[16,17] and fluorescence microscopy (FM).[18] Detailed information about molecular structures and orientations in Langmuir films can be achieved by infrared reflection absorption spectroscopy (IRRAS)[13,14] and X-ray or neutron reflectivity measurements (XR or NR).[8,15,19]

After transfer of the Langmuir films onto solid supports by using the Langmuir-Blodgett (LB) technique, morphology information of the resulting LB films can be studied in the nanometer range by atomic force microscopy (AFM).[6,20-23] Another essential component in biological membranes is cholesterol, which is responsible for stabilization and fluidization of the membranes.[7,24-28] In literature, numerous publications investigate the interaction of cholesterol and phospholipids in mixed Langmuir and LB films.[29-41] The most important result is the

incorporation of cholesterol molecules into phospholipid monolayers, leading to an increase of the structural order of the hydrocarbon acyl chains of the phospholipids (i.e. denser packing) and to a reduction of the *mmA* values for the cholesterol/phospholipid monolayer mixtures at constant π. This interaction is known as "condensing effect" and demonstrates the stabilizing impact of cholesterol on membranes. Studying the penetration of amphiphilic polymers into phospholipid monolayers is of high scientific interest, since they may contain various binding motives to phospholipid bilayers of cell membranes.[13,14,42-45]

Amphiphilic block copolymers have been known to be able to close or to form holes in the membranes depending on the hydrophobic-hydrophilic balance and on the molar masses of the involved blocks.[46-48] Due to the design and architecture of polymers, tailor-made solutions for special biomedical and pharmaceutical applications can be generated. Multifunctional, amphiphilic polyether-based polymers with cholesteryl (Ch) moieties represent a new class of biocompatible and bioactive polymers.[49,50] The polymers are homopolymers or diblock copolymers composed of either one or two hydrophilic blocks of the type linear polyglycerol (*l*PG), linear poly(glyceryl glycidyl ether) (PGG), linear poly(ethylene glycol) (PEG) or hyperbranched polyglycerol (*hb*PG), and one single hydrophobic Ch moiety covalently bound to one of the blocks. It has been demonstrated that some of these polymers can be incorporated into liposomal formulations with the phospholipid 1,2-dioleoyl-*sn*-glycero-3-phosphocholine (DOPC). Furthermore, a series of the polyether-based polymers with Ch moieties and systematically varied molecular architectures has been studied in a recent report on Langmuir and LB films.[51] For all polymers, stable Langmuir films were obtained due to the anchoring effect of the Ch moiety at the air-water interface whereas the LB films show hierarchically ordered morphologies.

In the current work, the interaction of the phospholipid 1,2-dipalmitoyl-*sn*-glycero-3-phosphocholine (DPPC) with Ch-*l*PEG$_{30}$-*b*-*hb*PG$_{24}$ (ChP) are investigated by Langmuir trough measurements with Langmuir films of the pure compounds and the DPPC/ChP mixtures of different molar ratios. Additionally, adsorption measurements are performed to verify the penetration ability of ChP into DPPC monolayers at different initial surface pressure values. After transfer of mixed Langmuir films onto hydrophilic silicon substrates, surface morphologies of the resulting mixed LB films are studied by AFM.

Experimental

Materials. The polyether-based diblock copolymer Ch-*l*PEG$_{30}$-*b*-*hb*PG$_{24}$ (ChP) was synthesized via anionic ring-opening polymerization and characterized by a combination of methods as reported elsewhere.[48,49] The chemical structure is shown in Figure 1a. The number-average molar mass M_n of 3470 g/mol was determined by ^{1}H NMR spectroscopy, and the polydispersity index (PDI) was found to be 1.08 (SEC in DMF employing PEG standards). Due to the Ch moiety as hydrophobic component and the *l*PEG and *hb*PG blocks as hydrophilic entities, ChP possesses an amphiphilic nature.

(a)

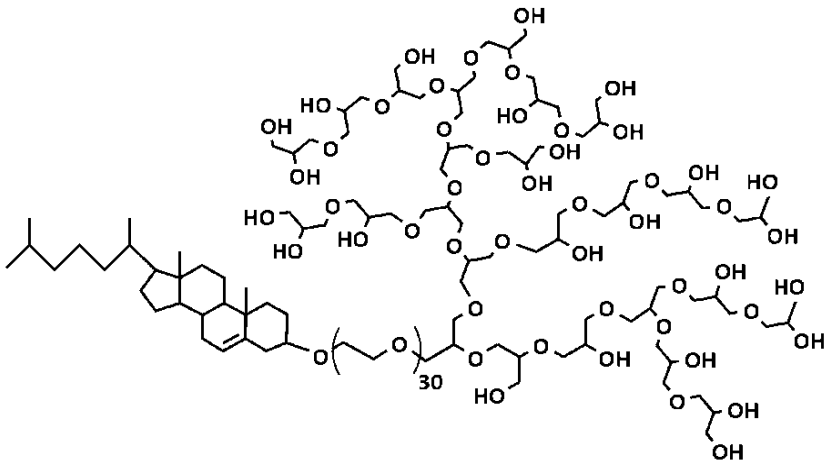

(b)

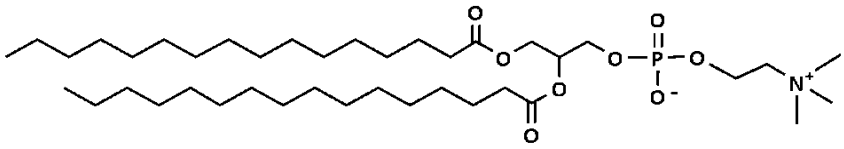

Figure 1. Chemical structures of (a) Ch-*l*PEG$_{30}$-*b*-*hb*PG$_{24}$ (ChP) and (b) DPPC. For the *hb*PG$_{24}$ block of ChP, the structure and the number of glycerol units represent a typical example.

DPPC of TLC grade ≥ 99% (chemical structure shown in Figure 1b, molar mass *M* of 734 g/mol) and ammonium hydroxide (NH4OH) were purchased from Sigma-Aldrich (Germany). Chloroform ($CHCl_3$) of HPLC grade > 99% was obtained from TCI (Japan). Hydrogen peroxide (H_2O_2) of 30% was purchased from Merck (Germany), and hydrochloric acid (HCl) of 0.1 mol/L was obtained from Carl Roth (Germany). All chemicals were used as received.

Surface pressure-mean molecular area (*π-mmA*) measurements. Langmuir isotherms at the air-water interface were obtained at 20 °C using a rectangular Langmuir trough with the dimensions 78.3 cm × 6.84 cm yielding a maximum available surface of 535.57 cm^2 (Riegler & Kirstein, Germany). The surface pressure π (calculated from $\gamma_0 - \gamma$ with γ_0 as surface tension of the pure air-water interface and γ as reduced surface tension of the air-water interface caused by the presence of surface-active molecules) was recorded as a function of the mean molecular area *mmA*. For measuring the surface tensions, a filter paper was applied as Wilhelmy plate. Water of Millipore quality (conductivity < 0.055 µS/cm, TOC grade < 5 ppm) was used as subphase. Spreading solutions of the pure compounds (DPPC and ChP) and the DPPC/ChP mixtures of different molar ratios (1000:1, 100:1, 10:1, 5:1, 2:1, 1:1) were prepared in final concentrations of 2 mM using $CHCl_3$ as solvent. After spreading the solutions with a glass microsyringe onto the subphase, a waiting time of 20 min was allowed for complete solvent evaporation and uniform dispersion of the molecules at the air-water interface. Afterwards, the measurements were started with a compression rate of 5 $Å^2$/molecule/min.

For better characterization of the properties of the Langmuir films at the air-water interface, the compression modulus *K* was derived from the Langmuir isotherms. *K* is the reciprocal value of the compressibility *κ* of the Langmuir film and is defined as

(1) $$\boldsymbol{K = \frac{1}{\kappa} = -A\left(\frac{\partial \pi}{\partial A}\right)_r}$$

where *A* is the *mmA* value.[51]

Adsorption measurements. Adsorption experiments at the air-water interface were carried out at 20 °C at different initial surface pressure values of DPPC monolayers on a circular Langmuir trough with a diameter of 3 cm, a depth of 1.39 cm, and a subphase volume of 10.25 ml (Riegler & Kirstein, Germany). For preparation of the DPPC monolayers, a defined amount of fresh DPPC solution in $CHCl_3$ was spread with a digital Hamilton microsyringe onto the water subphase of Millipore quality. After waiting for 20 min for complete solvent evaporation and uniform dispersion of the DPPC molecules at the air-water interface, an aqueous solution of ChP in a concentration of 2 µM was injected into the subphase below the DPPC monolayers through a channel located at the bottom of the Langmuir trough. In order to ensure a homogeneous bulk concentration of ChP in the subphase and in order to avoid large

perturbations at the air-water interface, the subphase was stirred with a small rolling sphere. The changes of π at the air-water interface caused by the injected aqueous solution of ChP were monitored as a function of time t by measuring γ_0 and γ using a filter paper as Wilhelmy plate ($\pi = \gamma_0 - \gamma$).

Deposition of Langmuir-Blodgett (LB) films. Mixed Langmuir films of DPPC and ChP were transferred at different π values using a Langmuir trough system equipped with a dipping mechanism (KSV Instruments, Finland). The transfer was performed onto silicon substrates cut into pieces of around 2 × 1 cm. In order to gain a clean hydrophilic SiO_2 surface, the substrates were initially chemically cleaned by a modified Shiraki technique.[52] The substrates were stored at first in a 5:1:1 (v:v:v) solution of H_20:H_2O_2:NH_4OH at 80 °C for 5 min, after cooling rinsed with deionized water, then stored in a 5:1:1 (v:v:v) solution H_20:H_2O_2:HCl at 80 °C for 5 min, and after cooling finally rinsed again with deionized water. Afterwards, the substrates were stored in double distilled water until use. Before the experiment, they were cleaned again with a CO_2 dry snow jet and immersed into the subphase. Then, the DPPC/ChP mixtures were spread onto the water subphase of Millipore quality. After a waiting time of 20 min to ensure complete solvent evaporation and uniform dispersion of the molecules at the air-water interface, the compression was started with a compression rate of 15 cm^2/min. When the desired surface pressure was achieved, it was kept constant for 1 min to allow equilibration and stabilization of the Langmuir films. Subsequently, the LB film transfer was performed at constant surface pressure by vertical withdrawing of the substrates through the mixed Langmuir films with a constant transfer rate of 1 mm/min. The transferred LB films were stored for drying for maximum 24 h.

Atomic force microscopy (AFM). Surface morphologies of LB films were studied using an atomic force microscope NanoWizard (JPK Instruments, Germany) working in tapping mode with silicon cantilevers. Cantilevers were of type Arrow (NanoWorld, Switzerland) and had a resonance frequency of about 285 kHz and a force constant of about 42 N/m.

Results and discussion

Langmuir isotherms. Langmuir isotherms and corresponding compression moduli of DPPC, ChP and of DPPC/ChP mixtures of different mixing ratios are shown in Figure 2. For reasons of

clarity, only the parts of the *mmA* range are shown that are relevant for comparison of the interactions between DPPC and ChP in their mixtures. The first significant increase of π in the Langmuir isotherm of DPPC (black curves in Figure 2a and Figure 2b) occurs at *mmA* = 90 Å^2 and indicates the formation of the liquid-expanded (LE) state. A distinct plateau region starts at *mmA* = 78 Å^2 in which π increases only slightly upon further compression (from 3.8 to 5 mN/m). This can be considered as the phase transition region between the LE state to the liquid-condensed (LC) state of DPPC.[53-56] After the LE/LC plateau region, a steep increase of π characteristic for the condensed state follows and results in the collapse of the DPPC monolayer at π = 54 mN/m and *mmA* = 41 Å^2. The different states of DPPC can be clearly identified using the compression modulus *K* as a function of *mmA* shown as black curves in Figure 2c and Figure 2d. Low *K* values obtained at *mmA* values larger than 90 Å^2 and between 78 and 57 Å^2 indicate the coexistence regions of gaseous (G)/LE states and LE/LC states, respectively, where the Langmuir film is highly compressible. In the *mmA* range from 90 to 78 Å^2, the *K* value is slightly increased up to 27 mN/m. This is due to the less compressible Langmuir film within the LE state. The rapid increase of *K* from *mmA* = 57 Å^2 resulting in a high maximum value of 295 mN/m upon further compression is caused by the very small compressibility in the condensed state. After this maximum, *K* decreases due to the collapse of the monolayer. The *K* values are in agreement with literature data.[54]

Compared to DPPC, the first significant increase of π in the Langmuir isotherm of ChP is observed at a larger *mmA* value of 2500 Å^2 as assumed from its higher molar mass leading to a higher *mmA* requirement of the molecule. In our previous studies on polyether-based polymers with Ch moieties and systematically varied molecular architectures, it has been found that at this point the *l*PEG and *hb*PG blocks of ChP are located at the air-water interface (in addition to the Ch moiety) and contribute to the *mmA* value.[50] Thus, the Ch moiety is forced to be only in the G state and the LC domain formation typical for pure Ch in this region is prevented.[57-60] The Langmuir isotherms of the neat diblock copolymer in the relevant region are shown as grey curves in Figure 2a and Figure 2b. Upon further compression, the surface pressure gradually increases while the *l*PEG and *hb*PG blocks submerge into the subphase until a kink is reached at π = 21.4 mN/m and *mmA* = 95 Å^2. The subsequent extended plateau region is assigned to the phase transition of the Ch moiety from the G state to the LC state and ends in the collapse of the monolayer at π = 26.3 mN/m and *mm* = 22 Å^2. As can be seen from the *K*-*mmA* curves during compression (grey curves in Figure 2c and Figure 2d), ChP is less compressible at *mmA*

values larger than 95 Å^2 compared to the region of lower *mmA* values, since the corresponding *K* values are slightly larger. This is caused by the *l*PEG and *hb*PG blocks of ChP still located at the air-water interface until this *mmA* value is reached. After submersion of these blocks into the subphase, ChP is easier to compress, as indicated by lower *K* values. This low compression modulus is kept constant upon further compression up to the collapse of the monolayer.

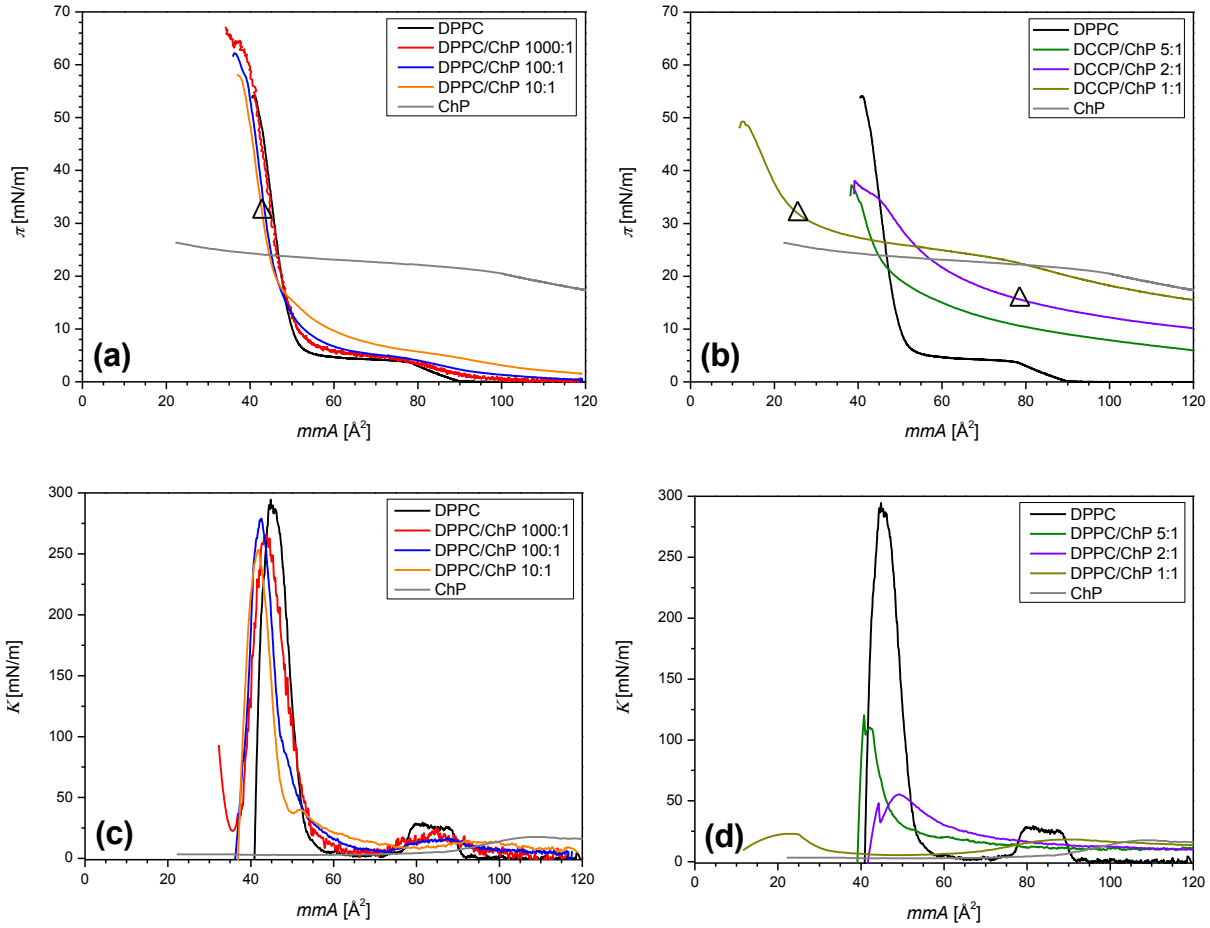

Figure 2. Langmuir isotherms for DPPC/ChP mixtures of (a) high DPPC content and (b) low DPPC content measured at 20 °C. For comparison, Langmuir isotherms of the pure compounds DPPC and ChP are shown as black and grey curves, respectively. LB films were transferred at surface pressures indicated by (Δ). (c) and (d) show compression moduli corresponding to the Langmuir isotherms in (a) and (b)

Figure 2a and Figure 2b demonstrate that the Langmuir isotherms of the DPPC/ChP mixtures are located between the Langmuir isotherms of the pure compounds whereas the first significant increase of π occurs with increasing ChP content at larger *mmA* values (not shown for all mixtures). This is as expected, since ChP is the compound of higher molar mass

compared to DPPC which leads to a higher *mmA* requirement of the mixtures. The Langmuir isotherms can be classified into two groups, one group of high DPPC content (DPPC/ChP mixtures 1000:1, 100:1, 10:1) showing Langmuir isotherms similar to pure DPPC (Figure 2a) and another group of low DPPC content (DPPC/ChP mixtures 5:1, 2:1, 1:1) showing Langmuir isotherms similar to pure ChP (Figure 2b). As can be seen, the LE/LC plateau region for DPPC is only observed in the Langmuir isotherms of the DPPC/ChP mixtures of high DPPC content (Figure 2a). Compared to pure DPPC, this plateau is less pronounced and is shifted with increasing ChP content in the mixtures to higher π values and larger *mmA* values. Obviously, ChP affects the rearrangement of the DPPC molecules and disturbs their packing into the LC state at the air-water interface. The collapse of the DPPC/ChP mixtures of high DPPC content occurs at comparable *mmA* values as observed for pure DPPC. Figure 2c shows the *K-mmA* curves for these mixtures with a shape similar to pure DPPC, but the characteristic regions of increased *K* values for DPPC (LE state and condensed state) tend to result in less pronounced regions with increasing ChP content in the mixtures. This indicates an easier compressibility for the mixed monolayers compared to the monolayer of pure DPPC which is probably caused by the *l*PEG and *hb*PG blocks of ChP already submerged into the water subphase in these *mmA* regions. Thus, it can be concluded that DPPC and ChP interact with each other.

For the DPPC/ChP mixtures of low DPPC content, the LE/LC plateau region for DPPC could not be observed. Instead, the G/LC plateau region for the Ch moiety of ChP is apparent as shown in Figure 2b. In the Langmuir isotherm of the DPPC/ChP mixture 5:1 (green curve), this plateau is slightly indicated at lower *mmA* values and higher π values compared to pure ChP. The plateau region becomes more distinct and more similar to the original plateau of pure ChP at comparable *mmA* and π values with increasing ChP content in the mixtures. Furthermore, the surface pressure values of the mixed monolayers at collapse are higher compared to pure ChP indicating that these monolayers are more stable anchored at the air-water interface than the pure ChP monolayer. The *K-mmA* curves for the DPPC/ChP mixtures of low DPPC content in Figure 2d confirm the tendency of the disappearance for the characteristic regions of increased *K* values for DPPC (LE state and condensed state, see Figure 2c) with increasing ChP content in the mixtures. This indicates a higher compressibility for the mixtures compared to pure DPPC in these regions. The shape of the *K-mmA* curves for the mixed monolayers approach more and more to the shape of pure ChP as shown for the DPPC/ChP mixture 1:1 (beige curve) where the

characteristic regions of increased *K* values observed for neat DPPC have completely disappeared.

Adsorption experiments. Figure 3a shows the changes of π as a function of time *t* during adsorption of ChP to the pure air-water interface and to DPPC monolayers at different initial surface pressure values π_0 reflecting the different lateral packing densities of DPPC. The π_0 values are determined at zero time (indicated by the dashed line at *t* = 0 min) which is corresponding to the injection time of ChP into the subphase. Time sections prior to zero time are related to the equilibration period of the DPPC monolayers.

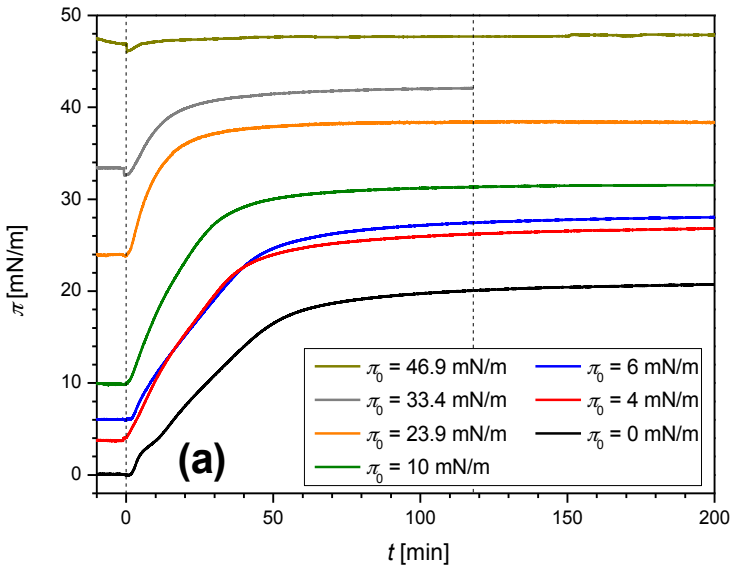

Figure 3. (a) Time-dependent increases of π induced by the adsorption of ChP injected at t = 0 min with a concentration of 2 µM to the pure air-water interface and to DPPC monolayers at different initial surface pressure values π_0 measured at 20 °C.

From the adsorption measurements it is obvious that immediately after the injection of ChP the surface pressure drops slightly to smaller π values for a short moment (probably caused by the experimental procedure), before it starts to increase continuously with increasing time until the equilibrium value π_{eq} (indicated by the dashed line at *t* = 118 min) is achieved. This is in contrast to a literature report dealing with the adsorption of amphiphilic triblock copolymers, where π shows no variation immediately after the injection of the copolymers.[13] The increase of the surface pressure indicates that ChP adsorbs from the bottom of the Langmuir trough to the DPPC monolayers at the air-water interface and disturbs these monolayers. This is possible due

to the strong affinity of the Ch moiety of ChP to DPPC. It becomes apparent that the adsorption of ChP to the DPPC monolayers is less pronounced with increasing π_0 values. At π_0 = 46.9 mN/m, almost no adsorption is observed. This is caused by the more and more perfect lateral packing of the DPPC monolayers in the condensed state. Thus, the increased density of DPPC impedes the adsorption of ChP.

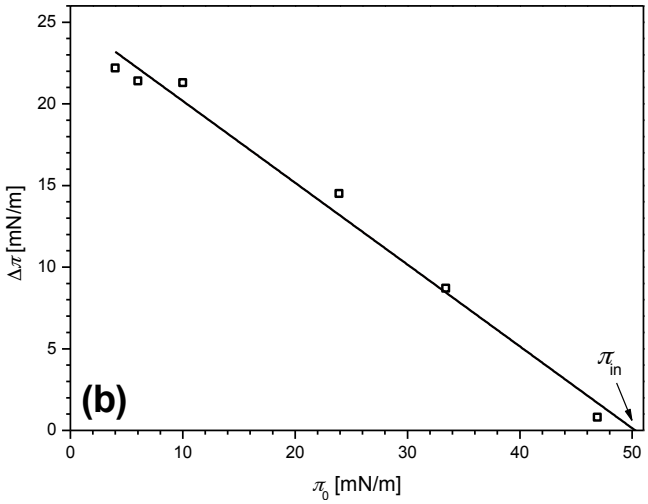

Figure 3. (b) Surface pressure value $\Delta\pi$ indicating the differences between the surface pressure value at equilibrium πeq and the surface pressure value at the beginning of adsorption π_0 ($\Delta\pi = \pi_{eq} - \pi_0$) as a function of π_0. π_0 and π_{eq} are taken from (a) at 0 min and after 118 min as indicated by dashed lines. The meaning of π_{in} is discussed in the text.

Figure 3b demonstrates the dependence of $\Delta\pi$ ($\Delta\pi = \pi_{eq} - \pi_0$) on π_0. The line represents the linear fit to the experimental data and the extrapolation to $\Delta\pi$ = 0 mN/m.[13,61] The data of the adsorption of ChP to the pure air-water interface (i.e. at π_0 = 0 mN/m) are not used. It appears to be a different mechanism when compared to the adsorption of ChP to DPPC monolayers. The characteristic surface pressure value πin is determined as intersection of the extrapolated linear fit at $\Delta\pi$ = 0 mN/m to the remarkably high value of 50.3 mN/m. This value represents the surface pressure of DPPC above which the adsorption of ChP to the DPPC monolayers becomes impossible. Due to the ability of ChP to penetrate into DPPC monolayers up to this πin value which is clearly higher than the limiting surface pressure values πM for penetration into biologically relevant bilayer membranes (*e.g.* πM ~35 mN/m in blood-brain barrier membranes or πM ~31 to 35 mN/m in erythrocyte membranes),[2,42] it can be concluded that ChP should also be able to penetrate into such biological bilayer membranes. Thus, ChP offers a high potential for biomedical and pharmaceutical applications.

In Figure 4, the adsorption of the Ch moiety of ChP to the air-water interface covered with DPPC monolayers is shown schematically.

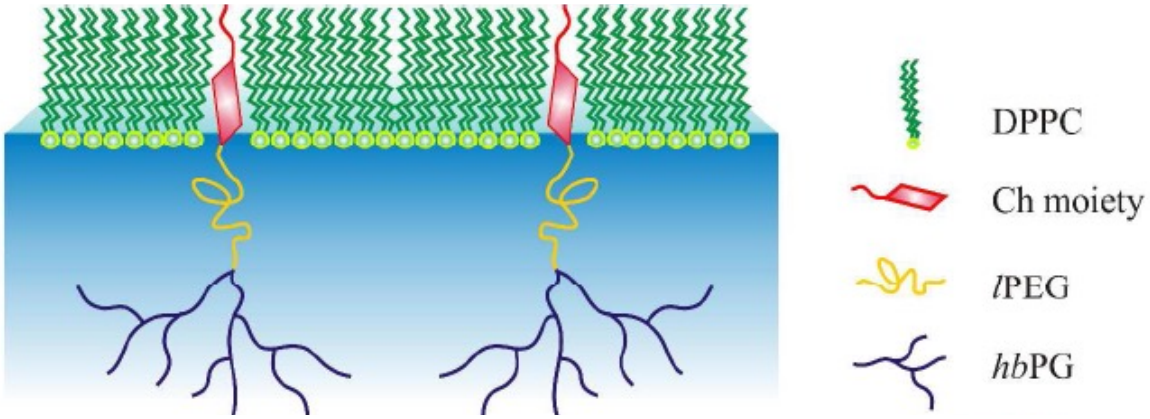

Figure 4. Schematic representation for the adsorption of the Ch moiety of ChP to the air-water interface already covered with a DPPC monolayer.

Morphology of mixed LB films. Figure 5 shows the AFM results for the LB film of a DPPC/ChP mixture 10:1 transferred at π = 32 mN/m and *mmA* = 43 Å^2 (indicated by Δ in Figure 2a). Two distinct phases are observed on the silicon substrates, one continuous phase and another phase represented by small dots of significant height inside the continuous phase (Figure 5a).

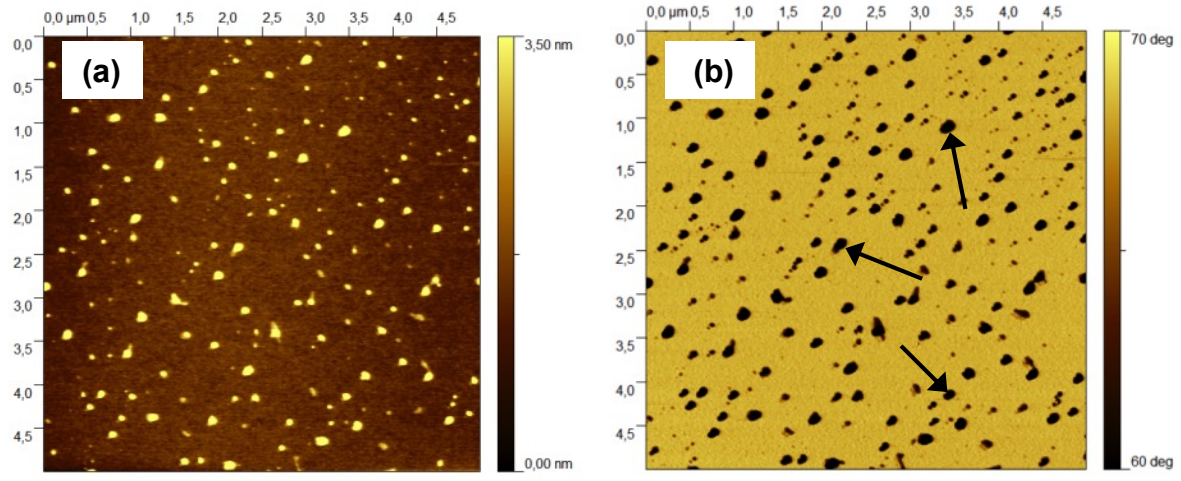

Figure 5. (a) AFM height image for the LB film of the DPPC/ChP mixture 10:1 transferred at π = 32 mN/m and *mmA* = 43 Å^2 (indicated by Δ in Figure 2a). (b) Phase contrast image of (a). The black arrows indicate the phase rich in *hb*PG blocks of ChP in the LB film.

From the phase contrast image (Figure 5b) it is concluded that the small dots represent the phase rich in *hb*PG blocks of ChP (indicated by black arrows), since they appear darker (softer) than the brighter (harder) continuous phase. Thus, the continuous phase is formed by the DPPC-rich phase containing also *l*PEG blocks and Ch moieties of ChP. The good distribution of the small dots in the continuous phase demonstrates a uniform incorporation of ChP in DPPC indicating attractive interactions of the compounds with each other. This seems to be reasonable, since large domains would be expected in the LB film in case of macroscopic phase separations between DPPC and ChP.

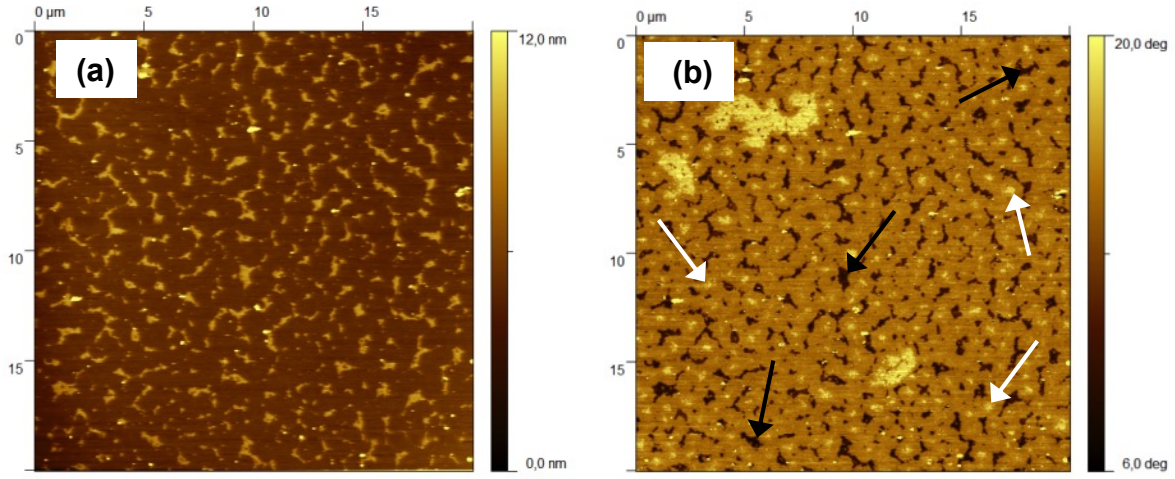

Figure 6. (a) AFM height image for the LB film of the DPPC/ChP mixture 2:1 transferred at π = 15.7 mN/m and *mmA* = 79 Å^2 (indicated by Δ in Figure 2b). (b) Phase contrast image of (a). The black and white arrows indicate the phase rich in *hb*PG blocks of ChP and the self-aggregated Ch moieties of ChP in the LB film, respectively.

LB films of DCCP/ChP mixtures gain more complex structures when the ChP content in the mixtures is increased which leads to an increased influence of the different components of ChP on the morphology of the LB films. This can be seen in the AFM results for the LB film of the DPPC/ChP mixture 2:1 transferred at π = 15.7 mN/m and *mmA* = 79 Å^2 (indicated by Δ in Figure 2b) in Figure 6 showing wormlike structures embedded homogenously in a continuous phase. The uniform distribution of the two different phases indicates again attractive interactions between DPPC and ChP. The wormlike structures are similar to morphologies recently reported for pure polyether-based polymers with Ch moieties.[50] In the AFM height image (Figure 6a), significant height differences between the two phases can be observed. Due to the fact that the

wormlike structures appear darker (softer) than their surrounding continuous phase in the phase contrast image (Figure 6b), they are supposed to be the phase rich in *hb*PG blocks of ChP (indicated by black arrows). In contrast, the brighter (harder) appearing continuous phase is rich in DPPC and *l*PEG blocks of ChP. Additionally, regions even brighter than the continuous phase, but located in a similar height level, are observed in the phase contrast image. It is assumed that these rigid regions represent densely packed Ch moieties of ChP (indicated by white arrows) ordered due to their tendency of self-aggregation (crystallization).[7,24,25,29,50, 57,62]

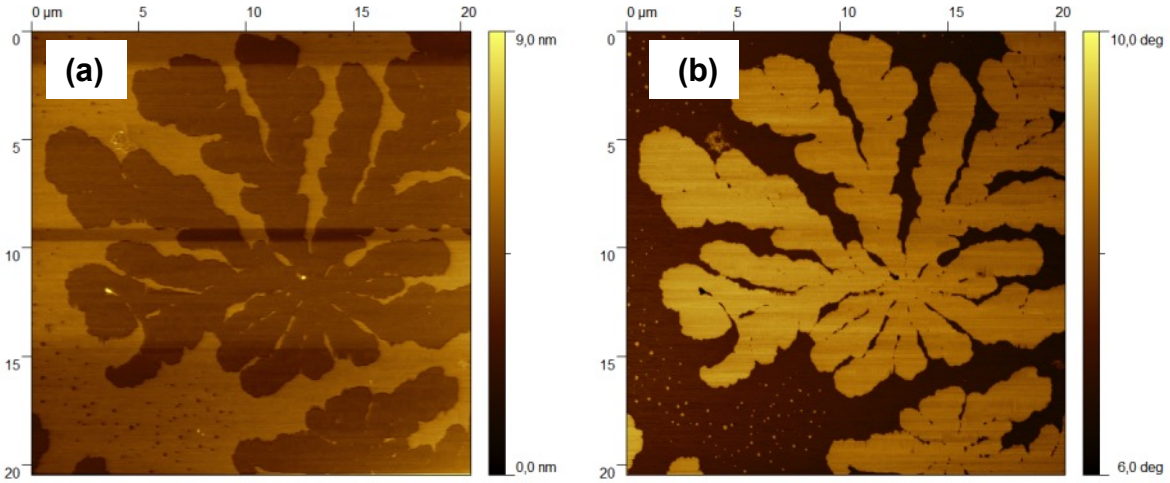

Figure 7. (a) AFM height image for the LB film of the DPPC/ChP mixture 1:1 transferred at π = 32 mN/m and *mmA* = 26 Å^2 (indicated by Δ in Figure 2b). (b) Phase contrast image of (a).

The dominant morphology in Figure 7 for the LB film of the DPPC/ChP mixture 1:1 transferred at π = 32 mN/m and *mmA* = 26 Å^2 (indicated by Δ in Figure 2b) is a fingerlike branched structure that is typically observed for crystallized *l*PEG monolayers.[50,63-70] Hence, the fingerlike pattern is mainly formed by crystallized *l*PEG blocks of ChP and is probably also rich in DPPC and Ch moieties of ChP.[50] The finger crystals are located lower than their surroundings as shown in the AFM height image (Figure 7a). Since the surroundings appear darker (softer) than the finger crystals in the phase contrast image (Figure 7b), it can be concluded that these areas are the phase rich in *hb*PG blocks of ChP.

Conclusions

In this report, mixed Langmuir and LB films of the phospholipid DPPC and the novel polyether-based diblock copolymer Ch-*l*PEG$_{30}$-*b*-*hb*PG$_{24}$ (ChP) were studied in different molar ratios in

order to investigate their interactions with each other. Additionally, adsorption experiments of ChP to DPPC monolayers at different initial surface pressure values were carried out for analysis of the penetration ability of ChP to DPPC. From Langmuir isotherms and compression moduli of the different mixtures, two different types of behavior were found for the mixed Langmuir films.

For the first group represented by DPPC/ChP mixtures of high DPPC content (molar ratios of 1000:1, 100:1, 10:1) a behavior similar to pure DPPC with a shift of the LE/LC plateau region for DPPC to higher π values and larger *mmA* values was observed with increasing ChP content in the mixtures. This indicated the hindrance of the reorientation of the *n*-alkyl chains of DPPC to a higher order (LC packing of DPPC) due to the incorporation of the Ch moieties of ChP into DPPC. The compression moduli for these mixed Langmuir films during compression supported this behavior, since the *K* values became lower meaning a higher compressibility with increasing ChP content in the mixtures compared to the pure DPPC monolayer.

This tendency was confirmed for the second group of the DPPC/ChP mixtures with low DPPC content (molar ratios of 5:1, 2:1, 1:1) showing a similar behavior as pure ChP. For the mixed Langmuir films, the increasing influence of ChP was apparent, since the G/LC plateau region for the Ch moiety of ChP became more pronounced with increasing ChP content in the mixtures.

Adsorption experiments demonstrated a strong penetration ability of ChP to DPPC monolayers after injection into the water subphase. The most important result was the determination of the surface pressure value πin for DPPC (surface pressure value above which the penetration of ChP to DPPC monolayers is impossible) to the remarkably high value of 50.3 mN/m. This π_{in} value suggests the ability of ChP to be incorporated in biologically relevant bilayer membranes whereas the hydrophilic *l*PEG and *hb*PG blocks of ChP may contribute to the formation or closure of pores in these membranes.[46,47] Thus, a wide range of applications in biomedicine, pharmacy and material science appears tob e possible for ChP.

Investigations of the LB films of DCCP/ChP mixtures by AFM revealed an increasing influence of the different components of ChP with increasing ChP content in the mixtures resulting in more complex structures. All morphologies were characterized by a uniform distribution of the two compounds in the LB films indicating attractive interactions between DCCP and ChP unless the *l*PEG block crystallizes. Crystallization phenomena were observed for the Ch moieties and *l*PEG blocks of ChP (*e.g.* a fingerlike morphology for *l*PEG blocks).

Acknowledgments

J.K. thanks the Deutsche Forschungsgemeinschaft for funding (FOR 1145). A.M.H. is a recipient of a fellowship of the Graduate School of Excellence MAINZ (Materials Science in Mainz) through funding of the Excellence Initiative (DFG/GSC 266).

References

(1) Horton HR, Moran L, Scrimgeour KG, Peryy MD, Rawn JD (2005) Principles of Biochemistry. Prentice Hall

(2) Marsh D (1996) Biochim Biophys Acta 1286:183

(3) Fahr A, van Hoogevest P, May S, Bergstrand N, Leigh MLS (2005) Eur J Pharm Sci 26:251

(4) Immordino ML, Dosio F, Cattel L (2006) Int J Nanomed 1:297

(5) Discher DE, Ahmed F (2006) Annu Rev Biomed Eng 8:323

(6) Petty MC (1996) Langmuir-Blodgett Films. Cambridge University Press, Cambridge

(7) Sparr E, Ekelund K, Engblom J, Engström S, Wennerström H (1999) Langmuir 15:6950

(8) Kaganer VM, Möhwald H, Dutta P (1999) Rev Mod Phys 71:779

(9) Blume A (1979) Biochim Biophys Acta 557:32

(10) Mattjus P, Slotte JP (1996) Chem Phys Lipids 81:69

(11) Subirade M, Salesse C, Marion D, Pezolet M (1995) Biophys J 69:974

(12) Maget-Dana R (1999) Biochim Biophys Acta 1462:109

(13) Amado E, Kerth A, Blume A, Kressler J (2008) Langmuir 24:10041

(14) Hussain H, Kerth A, Blume A, Kressler J (2004) J Phys Chem B 108:9962

(15) Dynarowicz-Latka P, Dhanabalan A, Oliveira Jr ON (2001) Adv Colloid Interface Sci 91:221

(16) Hénon S, Meunier J (1991) Rev Sci Instrum 62:936

(17) Hönig D, Möbius D (1991) J Phys Chem 95:4590

(18) Weis RM (1991) Chem Phys Lipids 57:227

(19) Ivankin A, Kuzmenko I, Gidalevitz D (2010) Phys Rev Lett 104:108101

(20) Roberts G (1990) Langmuir-Blodgett Films. Springer, Berlin

(21) Krafft M-P, Ries JG (2009) Chem Rev 109:1714

(22) Birdi KS (1999) Self-Assembly Monolayer Structures of Lipids and Macromolecular Interfaces. Springer, Berlin

(23) Hubbard AT (2002) Encyclopedia of Surface and Colloid Science. Dekker, New York

(24) Abendan RS, Swift JA (2002) Langmuir 18:4847

(25) Rapaport H, Kuzmenko I, Lafont S, Kjaer K, Howes PB, Als-Nielsen J, Lahav M, Leiserowitz L. (2001) Biophys J 81:2729

(26) Takano E, Ishida Y, Iwahashi M, Araki T, Iriyima K (1997) Langmuir 13:5782

(27) Vist MR, Davis JH (1990) Biochemistry 29:451

(28) Demel RA, de Kruyff (1976) Biochim Biophys Acta 457:109

(29) Lafont S, Rapaport H, Sömjen GJ, Renault A, Howes PB, Kjaer K, Als-Nielsen J, Leiserowitz L, Lahav M (1998) J Phys Chem B 102:761

(30) Ohvo-Rekilä H, Ramstedt B, Leppimäki P, Slotte JP (2002) Prog Lipid Res 41:66

(31) Bonn M, Roke S, Berg O, Juurlink LBF, Stamouli A, Müller M (2004) J Phys Chem B 108:19083

(32) Hac-Wydro K, Dynarowicz-Latka P (2008) J Phys Chem B 112:11324

(33) Berring EE, Borrenpohl K, Fliesler SJ, Serfis AB (2005) Chem Phys Lipids 136:1

(34) Kim K, Kim C, Byun Y (2001) Langmuir 17:5066

(35) Ohe C, Sasaki T, Noi M, Goto Y, Itoh K (2007) Anal Bioanal Chem 388:73

(36) Stottrup BL, Keller SL (2006) Biophys J 90:3176

(37) Mattjus P, Bittmann R, Slotte JP (1996) Langmuir 12:1284

(38) Mattjus P, Hedström G, Slotte JP (1994) Chem Phys Lipids 74:195

(39) Slotte JP (1995) Biochim Biophys Acta 1237:127

(40) Slotte JP (1995) Biochim Biophys Acta 1235:419

(41) Sabatini K, Mattila JP, Kinnunen PKJ (2008) Biophys J 95:2340

(42) Seelig A, Gerebtzoff G (2006) Expert Opin Drug Metab Toxicol 2:733

(43) Chang LC, Chang YY, Gau CS (2008) J Colloid Interface Sci 322:263

(44) Maskarinec SA, Lee KYC (2003) Langmuir 19:1809

(45) Wu G, Majewski J, Ege C, Kjaer K, Weygand MJ, Lee KYC (2005) Biophys J 89:3159

(46) Sommer K, Kaiser S, Krylova OO, Kressler J, Pohl P, Busse K (2008) J Med Chem 51:4253

(47) Amado E, Blume A, Kressler J (2009) React Funct Polym 69:450

(48) Hofmann AM, Wurm F, Hühn E, Nawroth T, Langguth P, Frey H (2010) Biomacromolecules 11:568

(49) Hofmann AM, Wurm F, Frey H (2011) Macromolecules 44:4648

(50) Reuter S, Hofmann AM, Busse K, Frey H, Kressler J (2011) Langmuir 27:1978

(51) Vollhardt D, Fainerman VB (2006) Adv Colloid Interface Sci 127:83

(52) Peetla C, Graf K, Kressler J (2006) Colloid Polym Sci 285:27

(53) Yuan C, Johnston LJ (2002) Journal of Microscopy 205:136

(54) McConlogue CW, Vanderlick TK (1997) Langmuir 13:7158

(55) Montanha EA, Caseli L, Kaczmarek O, Liebscher J, Huster D, Oliveira ON Jr (2011) Biophys Chem 153:154

(56) Charron JR, Tilton RD (1997) Langmuir 13:5524

(57) Cadena-Nava RD, Martin-Mirones JM, Vázquez-Martínez EA, Roca JA, Ruiz-García J (2006) Rev Mex Fis S 52:32

(58) Gupta RK, Suresh KA (2004) Eur Phys J E 14:35

(59) Seoane R, Miñones J, Conde O, Miñones Jr J, Casas M, Iribarnegaray E (2000) J Phys Chem B 104:7735

(60) Flach CR, Mendelsohn R, Rerek ME, Moore DJ (2000) J Phys Chem B 104:2159

(61) Bhakoo M, Birkbeck TH, Freer JH (1982) Biochemistry 21:6879

(62) Sparr E, Eriksson L, Bouwstra JA, Ekelund K (2001) Langmuir 17:164

(63) Li H, Sachsenhofer R, Binder WH, Henze T, Thurn-Albrecht T, Busse K, Kressler J (2009) Langmuir 25:8320

(64) Reiter G, Sommer JU (2000) J Chem Phys 112:4376

(65) Sommer JU, Reiter (2000) J Chem Phys 112:4384

(66) Reiter G (2003) J Polym Sci, Part B: Polym Phys 41:1869

(67) Zhai XM, Wang W, Ma ZP, Wen XJ, Yuan F, Tang XF, He BL (2005) Macromolecules 38:1717

(68) Zhai X, Wang W, Zhang G, He B (2006) Macromolecules 39, 324

(69) Chen R, Li L, Zhao J (2010) Langmuir 26:5951

(70) Huang Y, Liu XB, Zhang HL, Zhu DS, Sun YJ, Yan SK, Wang J, Chen XF, Wan XH, Chen EQ, Zhou QF (2006) Polymer 47:1217

Chapter 4.1: Mesogen-initiated linear polyglycerol isomers: The ordering effect of a single cholesterol unit on “sticky” isotropic chains

Chapter 4.1:

Mesogen-initiated linear polyglycerol isomers: The ordering effect of a single cholesterol unit on “sticky” isotropic chains

Anna Maria Hofmann,[1] Robert Wipf,[2] Bernd Stühn,[2,*] Holger Frey[1,*]

1 Institut für Organische Chemie, Johannes Gutenberg-Universität, Duesbergweg 10-14, 55099 Mainz, Germany.

2 Institut für Festkörperphysik, Technische Universität Darmstadt, Hochschulstraße 8, 64289 Darmstadt, Germany.

Published in Macromolecules 2011, 44 (17), 6767-6775.

Abstract

Synthesis, thermal properties and liquid crystalline (LC) order of polymers consisting of a single mesogenic cholesterol unit and flexible, linear polyglycerol (PG) or poly(glyceryl glycerol) (PGG) chains have been investigated. Incorporation of the single mesogen has been achieved by using cholesterol directly as an initiator for the oxyanionic ring-opening polymerization of ethoxyethyl glycidyl ether (EEGE) or isopropylidene glyceryl glycidyl ether (IGG). The controlled polymerization allowed the synthesis of a series of peculiar rod-coil type polyethers with molecular weights of 600-2300 g/mol, representing a degree of polymerization (DP_n) of 4-30 for both PG and PGG with polydispersity M_w/M_n in the range of 1.07-1.25. The resulting linear polyglycerols exhibit extremely stable thermotropic liquid crystalline (LC) order in a broad temperature range up to 260 °C, forming mainly layered smectic A phases with varying layer thicknesses, depending on the degree of polymerization of the respective polymer structure. LC phases were observed up to a chain length of 26 glycerol units, while poly(glyceryl glycerol ether)s showed no liquid crystalline order. This is explained both by the steric hindrance of the branched monomer units and the higher hydrophilicity of the polymer backbone. Permethylation of the cholesterol-PG samples resulted in strongly reduced LC order or in the

entire loss of the self-assembly in LC phases, which is a consequence of the disappearance of hydrogen-bonding between the functional coil segments. Detailed characterization of the phase behavior of the polymers has been achieved by differential scanning calorimetry (DSC), polarized optical microscopy (POM) and small angle X-ray scattering (SAXS), confirming the smectic layer structure of the materials.

Keywords

liquid crystalline polymers, polyethers, polyglycerol, cholesterol, rod-coil block copolymers

Introduction

Self-assembly in thermotropic liquid crystalline phases has been long known for cholesterol-derived compounds. In fact, the first observation of liquid crystalline phases ever was made for cholesteryl benzoates and cholesteryl acetates.[1] The functionalization of dendrimers and polymers with cholesterol or other mesogenic moieties is a common strategy for the preparation of unusual types of liquid crystalline (LC) materials.[2-4] Both main-chain and side-chain type LC dendrimers, in which the mesogenic moieties are grafted onto functional groups in the periphery of the preformed precursor, have been reported.[5-11] A large variety of side-chain LC polymers based on various polymer scaffolds, such as linear poly(ethylene glycol) (PEG), poly(DL-lactide) (P-DL-LA), polyacrylates, hyperbranched polyglycerol (*hb*PG) or poly(*p*-chloromethylstyrene) and others has been prepared by polymer modification with cholesterol groups.[12-18] LC polymers with cholesterol moieties have also been prepared by the polymerization of monomers containing mesogenic moieties such as cholesterol-based epoxides or cholesteryl methacrylates.[19, 20]

In pronounced contrast to polymers bearing multiple mesogens, in only few cases the terminal functionalization of polymer chains with a single mesogen has been achieved by using these directly for the initiation of polymerizations, namely for several polyester structures, such as poly(L-lactid acid), poly(trimethylene carbonate) (PTMC), poly(ε-caprolactone) (PCL) and poly(lactide-*co*-glycolide) (PLG).[21-24] In all cases LC phases are formed by self-assembly of the mesogen-initiated oligomers in neat state, such as smectic phases at elevated temperatures for the cholesteryl end-capped oligo(l-lactic acid).

To the best of our knowledge, the incorporation of mesogens in polymers using the respective mesogenic molecule directly as an initiator for the anionic or oxyanionic polymerization has not been reported to date. In the present study polyglycerols with varied molecular architectures have been synthesized via oxyanionic ring-opening polymerization (ROP) of different glycidyl ether monomers, i.e., ethoxyethyl glycidyl ether (EEGE)[25-28] and isopropylidene glyceryl glycidyl ether (IGG) (Figure 1).[25, 26, 29-36] Direct initiation of the polymerizations with deprotonated cholesterol has been employed to introduce the mesogenic cholesterol unit as an end group of the polymer structure. The central issue of this work is, to which extent one single cholesterol unit can direct the structure of an otherwise isotropic, hydrophilic polymer structure. The phase behavior of the amphiphilic LC oligomers consisting both of polar, linear polyglycerols and poly(glyceryl glycerol ether)s, respectively and their methylated derivatives has been investigated via differential scanning calorimetry (DSC), polarized optical microscopy (POM) and small angle X-ray scattering (SAXS).

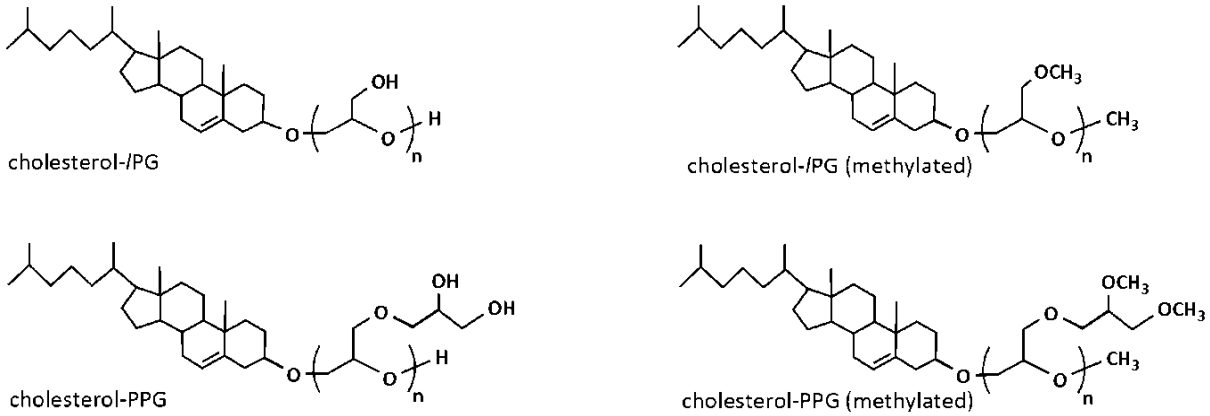

Figure 1: Chemical structures of the cholesterol-initiated polyethers before and after methylation; the respective values of the degree of polymerization n are given in Table 1.

The chemical structures of the different polyether architectures investigated in this work are shown in Figure 1. We were particularly interested in a comparison of our results to the studies of Kunieda et al.[12] and Xu et al.,[13] respectively, on structurally related rod-coil polymers consisting of cholesterol and polar (but crystallizable) poly(ethylene glycol) chains. Another related system based on rod-coil polymers of poly(ethylene glycol) and poly(propylene glycol) as flexible coils, respectively and ethyl 4'-(4'-oxy-4-biphenylcarbonyloxy)-4-biphenylcarboxylate as rod-like segment has been described in a series of important works by Lee et al.[37] In these

works, the influence of the length of an apolar poly(propylene oxide) coil was studied in a systematic manner, keeping the rod segment constant.[37c,d]

In contrast to these previous studies, the linear polyglycerols employed as coil segment in this paper are both non-crystalline and exhibit one or two functional hydroxyl groups in each monomer unit of the flexible polymer chain, which are capable of interaction via multiple hydrogen bonding. The structures may thus be considered as peculiar rod-coil topologies with a "sticky" coil architecture. We have also studied the consequences of "switching off" these hydrogen-bond interactions by full methylation of the hydroxyl groups.

Experimental section

Instrumentation. ^{1}H nuclear magnetic resonance (NMR) spectra were recorded using a Bruker AC 300 spectrometer operated at 300 MHz, employing $CDCl_3$ and DMSO-d_6 (dimethylsulfoxide) as solvents. ^{13}C NMR spectra (referenced internally to solvent signals) were recorded at 100.15 MHz. FT-IR spectra were recorded on a Nicolet iS 10 spectrometer equipped with a diamond ATR unit. SEC measurements were carried out in dimethylformamide (DMF) containing 0.25 g/L of lithium bromide. An Agilent 1100 Series GPC Setup (gel permeation chromatography) was used as an integrated instrument, including a PSS HEMA column ($10^6/10^5/10^4$ g/mol), a UV- (254 nm) and RI-detector. Calibration was achieved using poly(ethylene glycol) standards provided by Polymer Standards Service. The eluent was used at 50 °C and at a flow rate of 1 mL/min. For SEC measurements in chloroform, a setup consisting of a Waters 717 plus autosampler, a TSP Spectra Series P 100 pump, three PSS-SDV-5 µl-columns with 100, 1000, and 10000 Å pore diameter, respectively, a UV (275 nm) and an RI detector was used. Calibration was carried out using poly(styrene) standards provided by Polymer Standards Service (PSS). Matrix-assisted laser desorption and ionization time-of-flight (MALDI-ToF) measurements were performed on a Shimadzu Axima CFR MALDI-ToF mass spectrometer equipped with a nitrogen laser delivering 3 ns laser pulses at 337 nm. α-Cyano-3-hydroxy-cinnamic acid (CHCA) was used as matrix. Samples were prepared by dissolving the polymer in methanol at a concentration of 10 g/L. A 10 µL aliquot of this solution was added to 10 µL of a 10 g/L solution of the matrix and 1 µL of a solution of potassium trifluoroacetic acid (KTFA) (0.1M in methanol as cationization agent). A 1 µL aliquot of the mixture was applied to a multistage target, methanol evaporated and a thin matrix/analyte film created.

DSC measurements were carried out using a Perkin-Elmer DSC 7 with a Perkin-Elmer thermal analysis controller TAC7/DX in the temperature range of -100 to 100 °C using heating rates of 20 and 10 K/min. The melting points of indium (T_m = 156.6 °C) and Millipore water (T_m = 0 °C) were used for calibration.

Polarized optical microscopy (POM) experiments were carried out at different temperatures on an Olympus BX-51 polarized optical microscope equipped with a digital camera. A small amount of the respective sample was placed on an object plate and covered with a thin glass slide.

Small-angle X-ray scattering (SAXS) measurements were obtained with a system based on a conventional X-ray source for CuK_α radiation with a wavelength λ= 0.1542 nm, an X-ray mirror, three pinholes to focus the beam and a two dimensional multi wire detector (Molecular metrology). This provides an accessible range of scattering vectors $q = 4\pi/(\lambda\sin(\theta))$ from $q = 0.013$ Å^{-1} to $q = 0.5$ Å^{-1}. Beam path and sample chamber were evacuated. Sample detector distance was 75 mm. The samples were put into a sandwich of three metal discs with central holes and kapton foil to keep the sample in place. In order to exclude any effects of sample preparation onto the formation of the LC structures, the samples were heated over transition temperature in the sample holder, slowly cooled down to room temperature and the SAXS experiments were measured at 20 °C.

Reagents. All reagents and solvents were purchased from Acros and used as received, unless otherwise mentioned. Cholesterol was purchased from Fluka and stored at 4 °C. Dry solvents stored over molecular sieves were purchased from Fluka. Deuterated $CDCl_3$ and DMSO-d_6 were purchased from Deutero GmbH, dried and stored over molecular sieves. Ethoxyethyl glycidyl ether (EEGE) was prepared as described in literature using glycidol and dried over CaH_2 directly before use.[25, 26, 28, 38] ^{1}H NMR (300 MHz, $CDCl_3$): δ (ppm) = 4.76 ($OCH(CH_3)O$), 3.35-3.90 (OCH_2CH_3 and $OCH_2C_2H_3O$), 3.15 (CH epoxide), 2.61-2.91 (CH_2 epoxide), 1.33 ($OCH(CH_3)O$), 1.19 (OCH_3). Isopropylidene glyceryl glycidyl ether (IGG) was prepared as described in literature, dried over CaH_2 and freshly distilled before use.[29] ^{1}H NMR (300 MHz, $CDCl_3$): δ (ppm) = 4.3 (CH acetal), 4.07 (CH acetal), 3.88-3.39 (OCH_2), 3.17 (CH epoxide), 2.81 (CH_2 epoxide), 1.44 (CH_3), 1.38 (CH_3).

Synthesis: Polymerization reactions. The cholesterol-initiated rod-coil polymers were prepared in analogy to a method introduced recently.[30, 31]

Cholesterol-poly(ethoxyethyl glycidyl ether): ^{1}H NMR (300 MHz, DMSO-d_6): δ (ppm) = 5.30 (C=CH cholesterol), 4.63 (m, CHO acetal), 3.76-3.22 (polyether backbone; CHO cholesterol), 2.28-0.82 (br, CH_2, CH cholesterol), 1.17-1.06 (br, CH_3 acetal), 0.63 (br, CH_3 cholesterol). DP_n of PEEGE was determined by comparison of methyl signal (0.63 ppm) of cholesterol with the signals of the acetal proton at a chemical shift of 4.63 ppm.

Deprotection to cholesterol-linear polyglycerol: ^{1}H NMR (300 MHz, DMSO-d_6): δ (ppm) = 5.30 (C=CH cholesterol), 4.27 (br, OH), 3.76-3.22 (polyether backbone; CHO cholesterol), 2.28-0.82 (br, CH_2, CH cholesterol), 0.63 (br, CH_3 cholesterol).

Cholesterol-poly(isopropylidene glyceryl glycidyl ether): ^{1}H NMR (300 MHz, DMSO-d_6): δ (ppm) = 5.30 (C=CH cholesterol), 4.14 (m, CHO acetal), 3.96 (m, CH_2O acetal), 3.76-3.22 (polyether backbone; CHO cholesterol), 2.28-0.82 (br, CH_2, CH cholesterol), 1.31-1.26 (br, CH_3 acetal), 0.63 (br, CH_3 cholesterol). DP_n of PIGG was determined by comparison of methyl signal (0.63 ppm) of cholesterol with the signals of the PIGG at a chemical shift of 4.14 ppm.

Deprotection to cholesterol-poly(glyceryl glycerol ether): ^{1}H NMR (300 MHz, DMSO-d_6): δ (ppm) = 5.30 (C=CH cholesterol), 4.27 (br, OH), 3.76-3.22 (polyether backbone; CHO cholesterol), 2.28-0.82 (br, CH_2, CH cholesterol), 0.63 (br, CH_3 cholesterol).

Permethylation of the polyether-polyols was carried out by dissolving 500 mg of the respective polymer in water (2 mL), adding sodium hydroxide to yield a 1 n solution and benzene (2 mL). Methyl iodide (10 eq. of hydroxyl groups) was added slowly via syringe under vigorous stirring at room temperature. After additional 12 hours of stirring the reaction mixture was extracted with toluene, the organic phases dried over $MgSO_4$ and the solvents were removed to obtain the methylated product in yields of about 90%.

Cholesterol-polyglycerol (methylated): ^{1}H NMR (300 MHz, DMSO-d_6): δ (ppm) = 5.30 (C=CH cholesterol), 3.76-3.22 (polyether backbone; CHO cholesterol), 3.23 (OCH_3), 2.28-0.82 (br, CH_2, CH cholesterol), 0.63 (br, CH_3 cholesterol).

Results and discussion

A. Synthesis and characterization of cholesterol-polyethers. The synthesis of the cholesterol-initiated linear polyglycerols (*l*PG) and poly(glyceryl glycerol ether)s (PGG) has been carried out combining recently disclosed synthetic strategies.[26, 29, 31] Cholesterol has been directly used as an initiator and cesium hydroxide monohydrate as a deprotonating agent for the

polymerization of different acetal-protected glycidyl derivatives. The oxyanionic ring-opening polymerization (ROP) of ethoxyethyl glycidyl ether (EEGE) initiated with commercially available cholesterol and subsequent removal of the acetal protecting groups of the PEEGE precursors under acidic conditions leads to amphiphilic linear polyglycerols with one hydroxyl function per monomer unit in the flexible coil segment.[25, 26, 31-35, 39] In contrast the polymerization of isopropylidene glyceryl glycidyl ether (IGG) followed by acidic hydrolysis, i.e., deprotection of the hydroxyl groups at the PIGG backbone, results in aliphatic polyethers bearing two additional adjacent hydroxyl groups in every PGG unit.[29, 31, 36] The use of cholesterol and cesium hydroxide monohydrate as an initiating system permitted good control over the molecular weights and over the degree of functionalization for the preparation of both polymers (Table 1). Nevertheless, full conversion of the initiator was not achieved during the synthesis of polymers with very low molecular weights (degree of polymerization $DP_n < 6$). This necessitated purification by precipitation of the crude products in cold diethyl ether. In this manner a series of polyether-polyols bearing one cholesterol moiety with systematically varied chain lengths as well as different polymer architectures has been prepared. By systematic alteration of both chain length and structure and thus the ratio between the lipophilic and mesogenic cholesterol and the hydrophilic, flexible polyether the parameters governing liquid crystalline behavior have been studied. In addition, the effect of the additional branching unit of poly(glyceryl glycerol ether) in comparison with the strictly linear polyglycerols has been investigated with respect to the formation of LC phases.

Incorporation of cholesterol in every polymer chain of the molecular weight distribution is crucial for the potential liquid crystalline behavior of the resulting polyethers and is also expected for the living oxyanionic polymerization. Complete incorporation has been confirmed via matrix-assisted laser desorption and ionization time-of-flight (MALDI-ToF) measurements of the materials prepared (Figure 2).

The controlled oxyanionic polymerization conditions lead to narrow molecular weight distributions with low polydispersity indices ($M_w / M_n < 1.2$), which have been determined via size exclusion chromatography (SEC) in DMF using poly(ethylene glycol) (PEG) standards (Figure 3). Due to the strong impact of the hydroxyl groups and the lipophilic initiator on the hydrodynamic radii of the polymers, molecular weights determined via SEC are generally underestimated, as it is obvious from the comparison with values determined from NMR.

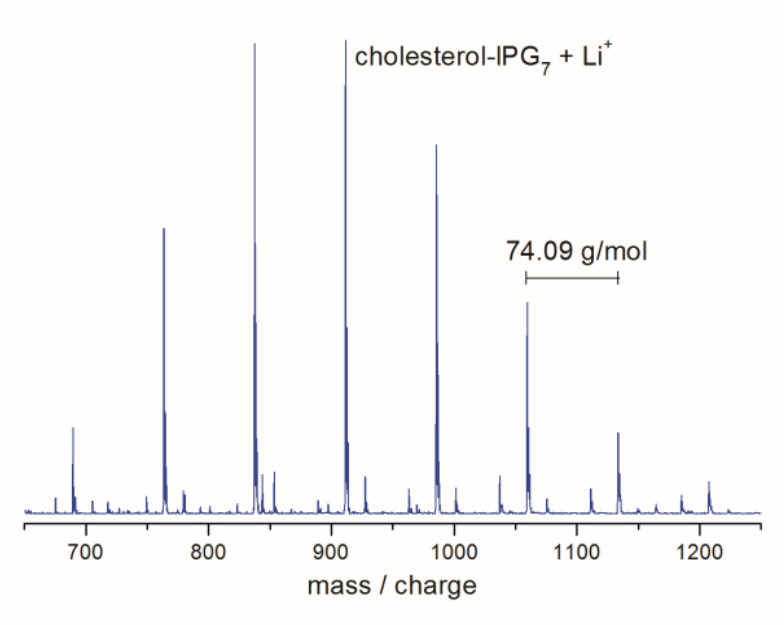

Figure 2. Typical MALDI-ToF of linear polyglycerol (cf. compound 4, Table 1), initiated with cholesterol. The main distribution is obtained with lithium as a counter ion; the subdistribution is due to sodium as a counter ion. Attachment of cholesterol to all polyether chains is confirmed.

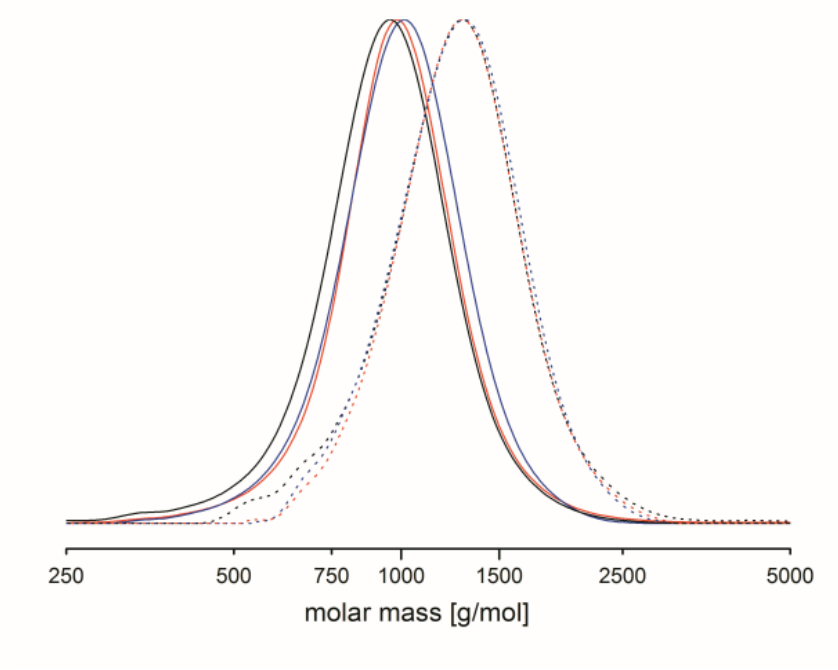

Figure 3. SEC measurements (DMF) of linear polyglycerols with different molecular weights before (solid lines) and after removal of the acetal protecting groups (dotted lines). Black: cholesterol-PEEGE$_{10}$, cholesterol-/PG$_{10}$ (cf. compound 4, Table 1). Red: cholesterol-PEEGE$_{12}$, cholesterol-/PG$_{12}$ (cf. compound 5, Table 1). Blue: cholesterol-PEEGE$_{16}$, cholesterol-/PG$_{16}$ (cf. compound 6, Table 1).

Therefore the degree of polymerization (DP_n) was determined via ^{1}H NMR spectroscopy from the integration of the methyl group of the initiator at a chemical shift of 0.63 ppm and the acetal protecting groups at 4.63 ppm for PEEGE or rather 4.14 ppm and 3.96 ppm for PIGG. NMR spectroscopy also confirmed full conversion of the respective monomer by disappearance of the epoxide signals at a chemical shift of 3.15 ppm and 2.61-2.91 for EEGE and at 3.17 ppm and 2.81 ppm for IGG (Figure 4). Characterization data of all polymers prepared in this study are summarized in Table 1.With respect to their potential liquid crystalline order, molecular weights of the amphiphilic polyethers were systematically varied in the range of 600-2300 g/mol, representing a DP_n of PG of 4-30. Cholesterol-initiated polyethers with chain lengths exceeding a DP_n of 26 showed no liquid crystalline phases (Table 1, compound 8).

Based on the expectation that not only the variation of the ratio between the lipophilic, rigid cholesterol moiety and the hydrophilic, flexible polyether chain would influence the formation of LC phases, but also the introduction of further branching units in the polymer backbone, also PGG chains based on isopropylidene glyceryl glycidyl ether as the respective polyether monomer have been prepared.

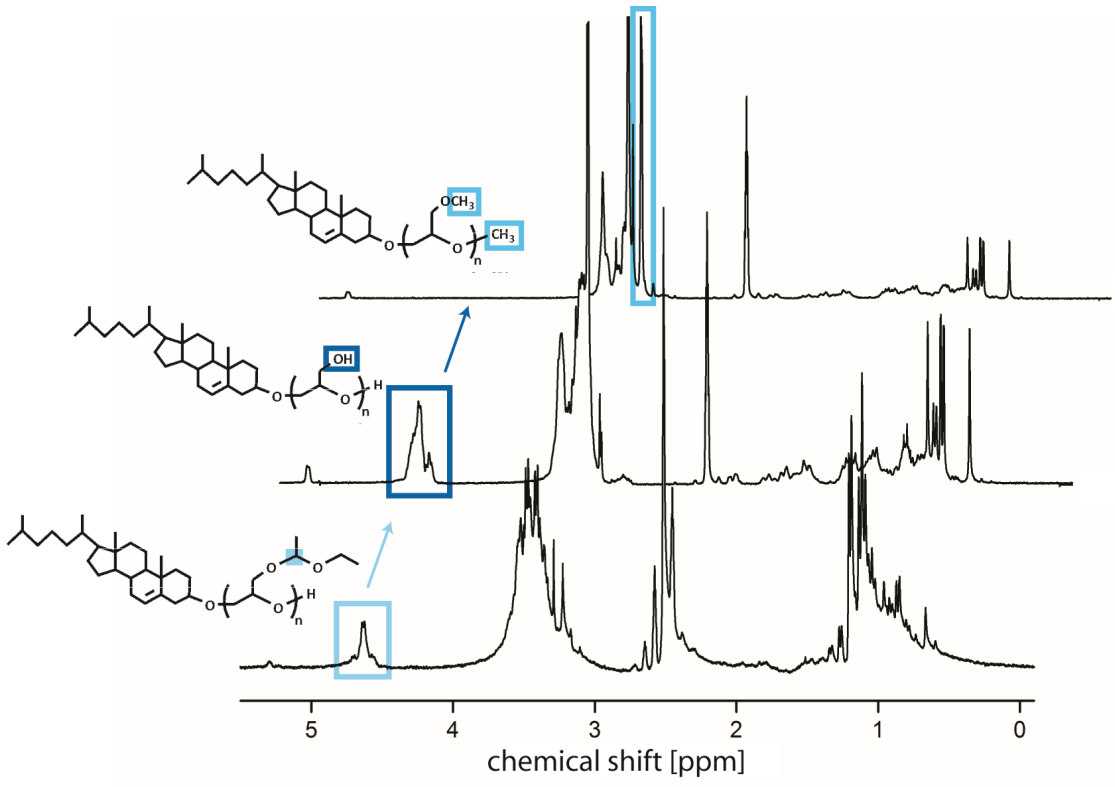

Figure 4. ^{1}H NMR spectra of linear cholesterol-PEEGE, cholesterol-*l*PG (bottom, cf. compound 4, Table 1) and methylated *l*PG-OMe (top spectrum, compound 14, Table 1) measured in DMSO-d_6.

In addition, we were interested in the effect of amphiphilicity on mesophase formation. The impact of this parameter on LC behavior has been studied by "switching off" the polarity of the polyether chains via permethylation of the hydroxyl groups at the polymer backbone. Full methylation was achieved by use of methyl iodide in benzene/sodium hydroxide solution, as evidenced via ^{1}H NMR and infrared (IR) spectroscopy by the complete disappearance of the signals at a chemical shift of 4.27 ppm or respectively at a wave number of 3200-3550 cm^{-1} (Figure 4 and Figure 5). In contrast to the amphiphilic cholesterol PGs, the permethylated samples exhibit good solubility in apolar solvents and $CHCl_3$, as expected.

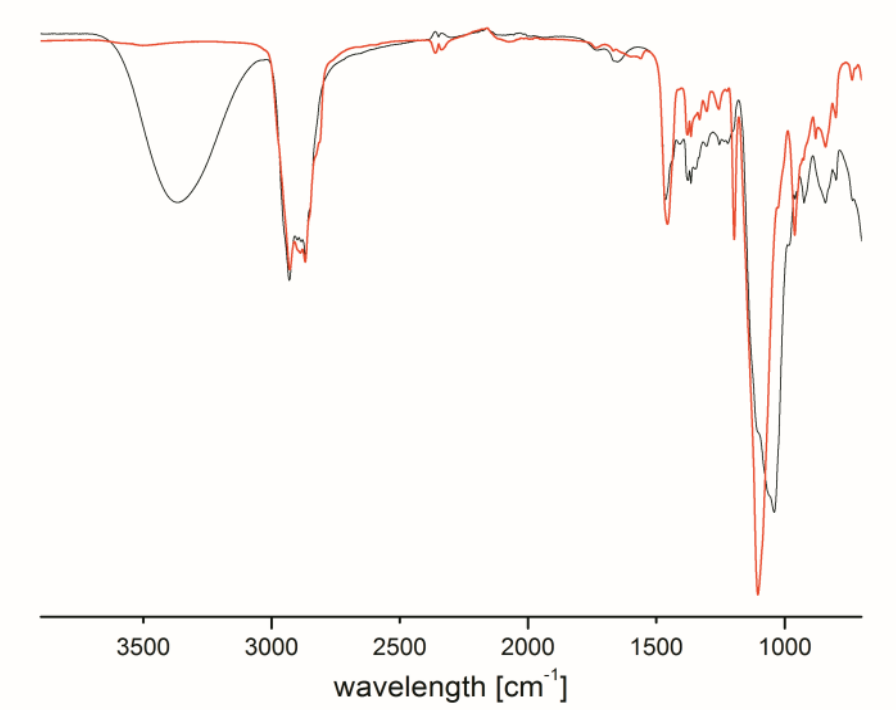

Figure 5. IR spectrum of linear polyglycerol (black, cf. compound 2, Table 1) and methylated *l*PG (red, cf. compound 12, Table 1). The disappearance of the band at 3500 cm^{-1} confirms full methylation.

Table 1. Characterization data of cholesterol-initiated polyglycerol and poly(glyceryl glycerol ether). [a] M_n determined via ^{1}H NMR spectroscopy. [b] M_n and M_w determined via SEC-RI in DMF with PEG standards. [c] M_n and M_w determined via SEC-RI in $CHCl_3$ with poly(styrene) standards. [d] Isotropic/liquid crystal transition temperature determined via POM.

No.	polymer	M_n (th) g/mol	M_n [a] (NMR) g/mol	M_n (SEC) g/mol	PDI [b] (SEC)	T_g (DSC) °C	I/LC transition [d] °C
1	cholesterol-/PG_4	640	680	620 [b]	1.23 [b]	-38.8	160
2	cholesterol-/PG_5	760	760	630 [b]	1.12 [b]	-37.1	210
3	cholesterol-/PG_9	760	1050	690 [b]	1.10 [b]	-28.8	250
4	cholesterol-/PG_{10}	1050	1130	770 [b]	1.09 [b]	-25.8	260
5	cholesterol-/PG_{12}	1200	1280	940 [b]	1.07 [b]	-25.0	170
6	cholesterol-/PG_{16}	1420	1570	1090 [b]	1.10 [b]	-17.2	190
7	cholesterol-/PG_{26}	2240	2310	1360 [b]	1.25 [b]	-14.1	120
8	cholesterol-/PG_{30}	2460	2610	1480 [b]	1.27 [b]	-10.2	-
9	cholesterol-PGG_4	830	980	840 [b]	1.15 [b]	-49.8	-
10	cholesterol-PGG_7	1220	1420	980 [b]	1.21 [b]	-49.5	-
11	cholesterol-PGG_9	1470	1720	1080 [b]	1.08 [b]	-33.9	-
12	cholesterol-PGG_{13}	2290	2320	1240 [b]	1.17 [b]	-41.3	-
13	cholesterol-/PG_4 (methylated)	750	750	640 [b] 930 [c]	1.27 [b] 1.75 [c]	-81.6	-
14	cholesterol-/PG_5 (methylated)	840	840	650 [b] 980 [c]	1.18 [b] 1.17 [c]	-65.5	5
15	cholesterol-/PG_9 (methylated)	1190	1190	590 [b] 720 [c]	1.09 [b] 1.23 [c]	-66.3	25
16	cholesterol-/PG_{10} (methylated)	1280	1280	750 [b] 1000 [c]	1.08 [b] 1.23 [c]	-74.0	35
17	cholesterol-/PG_{12} (methylated)	1460	1460	910 [b] 1270 [c]	1.17 [b] 1.17 [c]	-66.3	-
18	cholesterol-/PG_{16} (methylated)	1810	1810	940 [b] 1650 [c]	1.06 [b] 1.23 [c]	-67.7	-
19	cholesterol-PGG_4 (methylated)	1110	1110	900 [b] 1400 [c]	1.07 [b] 1.16 [c]	-77.1	-
20	cholesterol-PGG_7 (methylated)	1630	1630	920 [b] 1550 [c]	1.21 [b] 1.44 [c]	-75.9	-
21	cholesterol-PGG_9 (methylated)	1990	1990	990 [b] 1820 [c]	1.20 [b] 1.23 [c]	-73.8	-
22	cholesterol-PGG_{13} (methylated)	2700	2700	1200 [b] 2170 [c]	1.10 [b] 1.25 [c]	-71.9	-

As it is clearly confirmed by the above mentioned characterization methods (SEC, NMR, MALDI-ToF) two series of cholesterol-initiated oligo- and polyglycerols with different molecular architectures have been obtained via the oxyanionic ROP of ethoxyethyl glycidyl ether and isopropylidene glyceryl glycidyl ether and subsequent acidic removal of the acetal protecting groups. In order to study fully hydrophobic materials that exhibit no amphiphilic character, permethylation of the polyethers has been carried out, using methyl iodide. The successful transformation has been confirmed via NMR and IR spectroscopy.

B. Thermal and optical characterization of the cholesterol-polyethers. Central issues in the context of the current study are: (i) up to which chain length can an isotropic, hydrophilic polymer structure still be ordered in an LC structure by a single cholesterol mesogen at the chain end and (ii) what is the influence of the structure and polarity of the flexible chain on LC order? The materials studied may either be considered as rod-coil polymers with a small, rigid unit and a “sticky” coil segment or as single-mesogen terminated isotropic and flexible polymer liquids at room temperature. In comparison to previous works on rod-coil structures with poly(ethylene oxide) (PEO) or poly(propylene oxide) (PPO) chains, the materials discussed in this paper are of a different nature, since they cannot crystallize like PEO and possess a highly polar, isotropic structure in contrast to PPO.[37c,d]

Since formation of liquid crystalline phases of amphiphilic polymers is often induced by segregation of the incompatible chain ends, the thermotropic behavior of the cholesterol-initiated polyethers will most probably depend on their amphiphilicity and the phase separation of hydrophilic polymer chain and the hydrophobic cholesterol.[6, 12, 13, 37, 40-48] To this end, the structure of the polyglycerols has been transformed via permethylation of the hydroxyl groups at the polymer backbone, resulting in an apolar coil structure.

The thermotropic LC behavior of the amphiphilic polyglycerols with different polymer architectures and chain lengths (Table 1) has been investigated via polarizing optical microscopy (POM) and differential scanning calorimetry (DSC). The glass transition temperatures (T_g) of the cholesterol-initiated polyethers determined by DSC measurements range from -20 to -50 °C, depending on their structure and their chain lengths (Table 1). Especially in the series of linear polyglycerols, a clear correlation of T_g with the degree of polymerization has been observed, i.e., the glass transition temperatures systematically vary

from -39 °C for cholesterol-/PG_4, -37 °C for cholesterol-/PG_5, -29 °C for cholesterol-/PG_9, -26 °C for cholesterol-/PG_{10}, -25 °C for cholesterol-/PG_{12} to -17 °C for cholesterol-/PG_{16}. This tendency reflects the higher chain mobility of lower molar mass chains and the increasing influence of hydrogen bonds of the hydroxyl functional polymers. In contrast, poly(glyceryl glycerol ether)s with different molecular weights showed transition temperatures in the range of -50 °C to -33 °C without clear dependence on molecular weights. Full methylation of the polyether-polyols generally leads to strongly lowered T_gs varying from -82 °C to -66 °C due to the absence of polar hydroxyl groups that restrict mobility of the polyether chains by formation of hydrogen bonds.

Investigation of the amphiphilic polymers with polarizing optical microscopy revealed liquid crystalline phases for all linear polyglycerols presented in this study up to a DP_n of 25 within a broad temperature range (Figure 6). Since the glass transition temperatures of the cholesterol-/PGs vary from -20 °C to -40 °C, the birefringence observed via POM between crossed polarizers at higher temperatures resulted from anisotropic fluids, evidencing the presence of LC phases. At temperatures below the T_gs of the cholesterol-initiated polyglycerols the birefringence was caused by vitrification of the LC-phase to an anisotropic glass. Although no further phase transitions were observed via DSC, different liquid crystalline phases have been observed with POM before isotropization. With increasing chain length the temperatures for the LC/isotropic transitions of the amphiphilic polyglycerols rise from 160 °C for cholesterol-/PG_4, 210 °C for cholesterol-/PG_5 and 250 °C for cholesterol-/PG_9 to 260 °C for cholesterol-/PG_{10}. This is explained by the increasing number of interacting hydroxyl groups.

Polymers with higher molecular weights showed lower transition temperatures, i.e., 170 °C for cholesterol-/PG_{12}, 190 °C for cholesterol-/PG_{16} and 120 °C for cholesterol-/PG_{26}. POM revealed well-developed optical textures, including smectic A (SmA) bâtonnets on cooling from the isotropic melt of all cholesterol-/PGs presented in this study, suggesting the formation of smectic A phases due to microphase separation of the hydrophobic cholesterol and the hydrophilic polyether chain (Figure 6). For polyglycerols with a degree of polymerization exceeding 26 glycerol units no birefringence has been observed with POM. At lower temperatures, i.e., 150 °C for cholesterol-/PG_{16} (cf. compound 6, Table 1), the formation of fan-like textures similar to twist grain boundary A (TGBA) phases has been observed. This is in good agreement with theoretical considerations as well as results from small angle X-ray scattering (SAXS) experiments discussed in the following. The driving forces for liquid crystalline order in

this type of polymers may on one hand be the amphiphilicity of the cholesterol-polyglycerols, leading to nanosegregation in layered structures, such as SmA phases. On the other hand cholesterol tends to form chiral nematic or cholesteric phases.[49] The incompatibility of the twist observed in the cholesteric phase with the layered structure of the smectic A phase presumably results in a frustrated structure similar to TGBA phases. The formation of oily streaks on cooling from the isotropic melt has been observed only in one compound, namely cholesterol-/$PG_{10,}$ at 180 °C, while further cooling lead to formation of smA phases in analogy to the phase behavior of the related compounds.

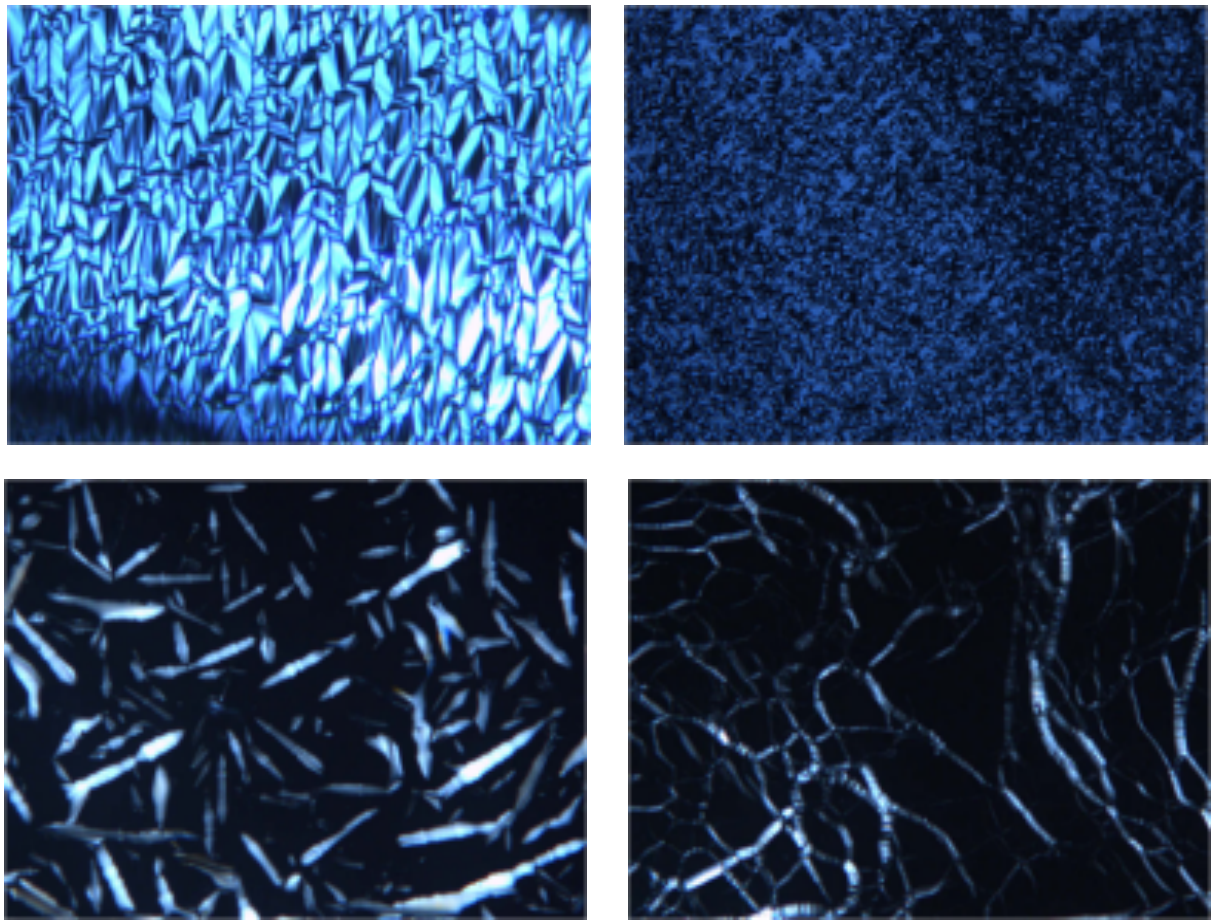

Figure 6. Optical textures of cholesterol-/PG observed with the polarizing microscope at different temperatures (crossed polarizers): POM micrographs of cholesterol-/PG_{16} (cf. compound 6, Table 1) at 160 °C (top, left) and 100 °C (top, right) and of cholesterol-/PG_{10} (cf. compound 12, Table 1) at 255 °C (bottom, left) and 180 °C (bottom, right).

Comparing our results to the studies of Lee et al. on the three-dimensional supramolecular organization of molecular rods depending on the coil cross section,[37] the formation of lamellar

phases of the cholesterol-initiated polyglycerols is in good agreement with the results for the LC behavior of poly(ethylene glycol) (PEG) and poly(propylene oxide) (PPO) rod-coil oligomers with ABA structures.[50,51] However, the investigated polymers as well as the employed mesogens, i.e., biphenyl compounds, presented by Lee et al. only permit a limited comparison with the cholesterol-/PGs with different cross-sections and hydroxyl functionality. Compared to our results, cholesteryl end-capped poly(ethylene glycol)s reported by Xu, Fan et al. in 2006 self-assemble in layered liquid crystalline phases up to a degree of polymerization of n = 25-30, where the mesogenic cholesterol moiety loses its influence on the superstructure of the polymer due to the dominating crystallization of the PEG chain.[13] In contrast to these cholesterol-PEGs, where thermotropic behavior of the materials strongly depends not only on their amphiphilic character but also on the formation of spherulites, linear cholesterol-initiated polyglycerols are unable to crystallize due to their atactic structure. However, the influence of the additional hydroxyl functions at the polyether backbone distinguishes the herein presented complex polymers from previously studied systems.

Since amphiphilicity of the polyglycerols appears to be an important driving force for the formation of LC phases, methylation of the hydroxyl functionalities was expected to give insight into the significance of the interplay of flexibility and rigidity for mesophase formation by "switching off" the amphiphilic nature. It is obvious from the data compiled in Table 1 (samples 13-22) that permethylation of the polymer backbone leads to strongly reduced stability of the liquid crystalline order. Only the methylated polyglycerol samples 14-16 with a degree of polymerization between 5 and 10 glycerol units showed LC order in this case. For all samples permethylation generally resulted in strongly reduced viscosity and glass transitions between -65 and -82°C, i.e., 40 K lower than for the hydroxyl-functional samples. In the case of the LC samples 14-16 isotropization occurred already at fairly low temperatures between 5 and 35°C. Thus, the temperature regime for the existence of LC order was considerably narrower than in the original samples, confirming the important role of an amphiphilic structure and hydrogen bonding of the polar segment for the stabilization of the LC phases. For samples with shorter or longer methylated oligoglycerol segments the mesophases vanished completely upon methylation. We conclude that strong immiscibility leading to phase segregation represents the major driving force for LC order in these systems.

C. SAXS measurements of cholesterol-polyethers. The presence of domain ordering was investigated by small-angle X-ray scattering (SAXS) measurements at 20 °C. In Figure 7 we present two typical examples of the scattering patterns. The two dimensional pattern clearly shows a partial orientation of the domains. Taking the azimuthal average we arrive at the intensity in dependence on $s = (2/\lambda)\sin\theta$ with 2θ being the scattering angle shown in the left part of the figure. For n=12 two series of reflections can be discriminated. Their lowest order reflection is labeled I and II in Figure 7. They are related to differently oriented domains as can be seen in the two dimensional intensity distribution. The higher order reflections of series I are apparently of low intensity and covered by the strong reflections of series II: Sample 4 (/PG_{10}) displays only one series of reflections with three narrow peaks indicative of a well-formed lamellar structure. Also the intensity distribution only displays one dominant domain orientation.

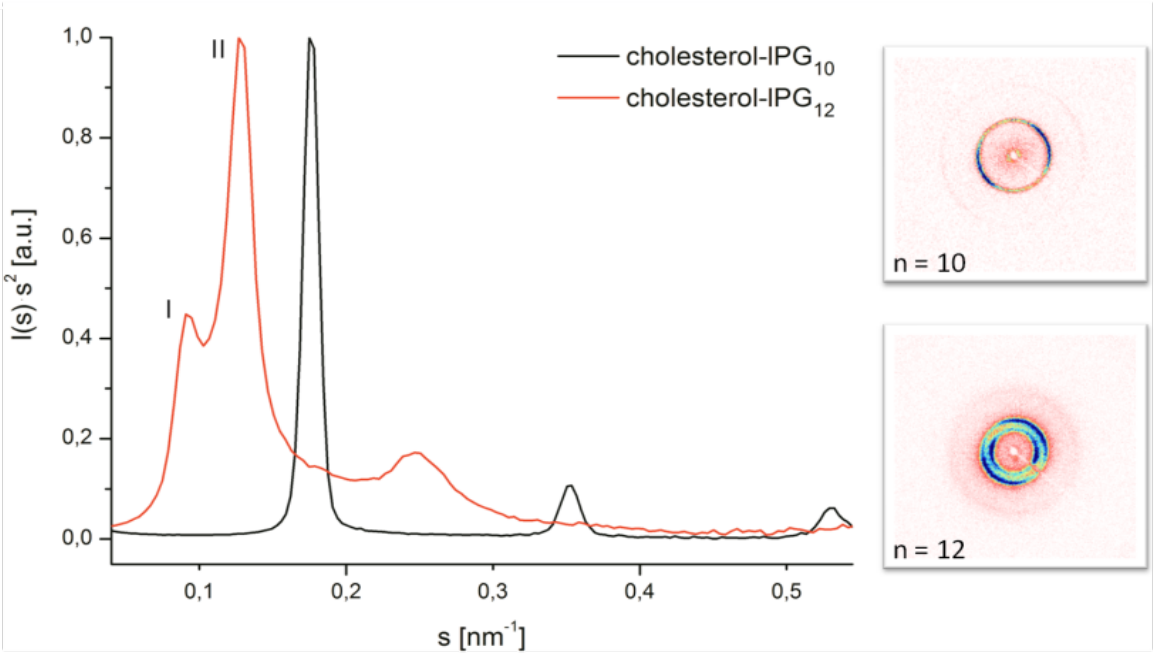

Figure 7. Left: SAXS profiles of cholesterol-/PG_{10} (black) and cholesterol-/PG_{12} (red) measured at 20 °C. Right: 2D SAXS images of cholesterol-/PG_{10} (top) and cholesterol-/PG_{12} (bottom).

In the following we discuss the variation of the lamellar structure with molecular weight. For samples /PG_{10} and /PG_{12} this refers to the reflection series II in Figure 7. The s value of the first order reflection is directly related to the period of the structure d=1/s. In order to characterize the lamellar structure in more detail, we calculated the linear correlation function. This allows

to determine not only the period of the lamellar structure but also the thickness of the cholesterol and PG domains separately.[52] In parallel we use the position of the peaks shown in Figure 7 to calculate the period of the lamellar structure d. Linear cholesterol-initiated polyglycerols showed several characteristic diffraction peaks, suggesting the presence of lamellar phases (Figure 7). Thus, a minimum of two clear peaks at s_1=1/d and s_2=2/d are observed for cholesterol-/PGs with degrees of polymerization of n = 5, 9, 10, 12 and 16, indicating the formation of layered structures in all amphiphilic linear polyglycerols presented in this study.

Additionally, SAXS measurements revealed an increase of the layer thicknesses with increasing chain lengths of the cholesterol-modified polyethers, whereas similar values in a range of d_c = 2.3-2.5 nm are obtained for the rigid cholesterol moiety. Its length is constant in all scattering experiments (Figure 8). Thus, the layer spacing varies from d_{ac} = 6.3 nm for cholesterol-/PG_5 to d_{ac} = 7.0 nm for cholesterol-/PG_{10} and d_{ac} = 8.1 nm for cholesterol-/PG_{12} (Figure 8). Small variations in this trend might be related to the closer packing of polymers in layered structures with increasing DP_n due to higher overlap of alternating polymer chains. Nevertheless, the values of the layer thickness are in good accordance with theoretical considerations, i.e., comparing these structures to analogous PEG-containing LCs presented by Xu et al. Therefore, a single layered structure of the polyether chains is most likely formed, while the rigid cholesterol end groups are packed in double layered conformations (Figure 8).

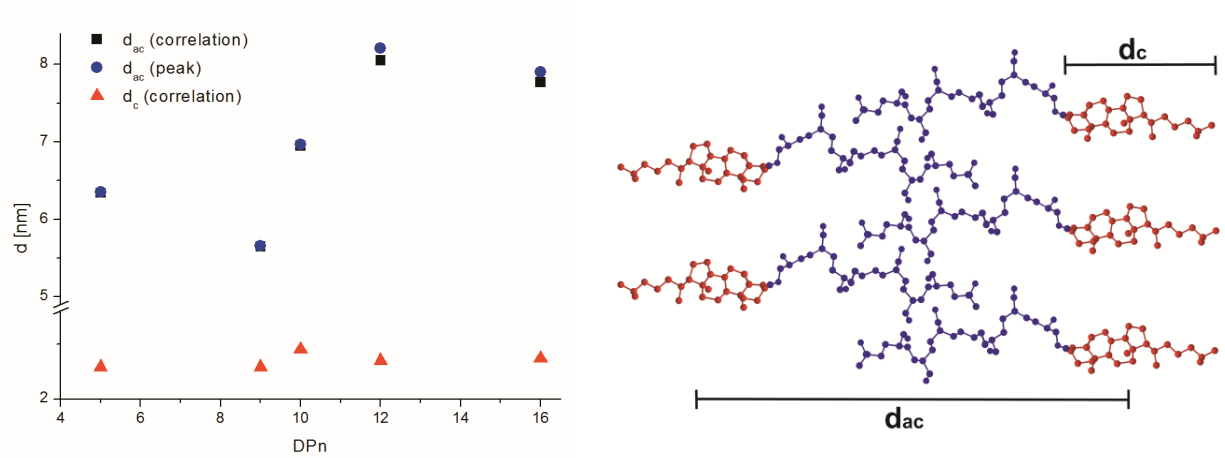

Figure 8. Left: Layer thickness obtained via SAXS measurements (peaks and correlation function) vs. chain length of cholesterol-initiated polyglycerols. Right: Packing model for the amphiphilic polyglycerols with rigid cholesterol end-groups and flexible polyether chains.

As mentioned above, in cholesterol-polyglycerols with higher molecular weights two types of structure with varying layer spacing were identified by SAXS measurements (Figure 7). Assuming the reflection labeled I in Figure 7 to be the first order of a lamellar series layer thicknesses of $d_{ac}' = 10.9$ nm were obtained for cholesterol-/PG_{12} and $d_{ac}' = 13.7$ nm for cholesterol-/PG_{16}. The presence of different lamellar phases might result from varying overlap of the polyether chains due to diverse chain lengths, which is more pronounced in polymers with higher DP_n. The observed thickness indeed fits well with the assumption of overlapping polyether chains. The different structures may also derive from the incompatibility of the chiral nematic ordering of cholesterol with the lamellar ordering of amphiphiles, leading to frustrated layered phases which are tilted to each other.

Analogous measurements with cholesteryl end-capped PEGs revealed layer thicknesses of 5.1 nm for n = 5 to 9.3 nm for n = 20 and similar packing models.[13] However, in contrast to these previous studies on the self-assembly of cholesterol-PEGs, where the layer spacing also depends on the crystallization of the PEG chain, leading to the coexistence of different lamellar structures due to nearly amorphous LC or crystalline phases, the linear cholesterol-initiated PGs are unable to crystallize. The amorphous, flexible polyether chains of cholesterol-PGs allow good overlap in spite of their spatially demanding hydroxyl groups at the polymer backbone. Contrary, the presence of hydrogen bonds between the closely packed polymer chains and the highly amphiphilic character of the materials actually results in very stable LC order in a very broad temperature range up to 260 °C, while analogous cholesterol-PEGs exhibit LC ordering only up to 100 °C.[12] Since the enhanced stability of the LC order by higher amphiphilicity is limited by sterical constraints, poly(glyceryl glycerol ether)s with comparable molecular weights exhibit no LC behavior (Table 1).

Conclusion

We have studied the synthesis and thermal properties of linear polyglycerol (PG) and poly(glyceryl glycerol ether), functionalized with one single mesogenic cholesterol unit. This was achieved by using cholesterol directly as an initiator for the oxyanionic ring-opening polymerization of the respective epoxide monomers, i.e., ethoxyethyl glycidyl ether (EEGE) and isopropylidene glyceryl glycidyl ether (IGG). The resulting linear polyglycerols showed liquid crystalline order in an extremely broad temperature range up to 260 °C. POM and SAXS

experiments revealed self-assembly of the linear, cholesterol-initiated polyglycerols in layered phases with varying layer thicknesses in the range of 5.7 to 8.1 nm, depending on the chain lengths of the respective polymer up to a degree of polymerization (DP_n) of 26. This demonstrates the strong structure-directing effect of the single cholesterol unit, forcing an isotropic liquid, highly polar polymer structure into an ordered mesophase state.

The formation of LC phases in cholesterol-initiated polyglycerols is controlled by three main parameters: (i) by the ratio between the hydrophobic mesogen at the chain end and the hydrophilic polyether moiety; (ii) by the molecular architecture of the respective monomer, i.e., linear glycerol moieties or branched glyceryl glycerol units, (iii) by the hydroxyl functionalities at the polymer chain, contributing to the hydrophilicity and the generation of strong intermolecular interactions. The thermotropic behavior of cholesteryl-modified poly(ethylene glycol) (PEG) depends on the crystallization of the PEG chains, which becomes more relevant with increasing chain length.[13] Since linear polyglycerols and poly(glyceryl glycerol ether)s show no crystallization and the amphiphilic character is more distinct in these polymers due to the multiple hydroxyl groups at the polyether backbone, highly stable LC order is observed in comparison to the structurally related cholesterol-PEGs and previously studied rod-coil structures consisting of extended rods with biphenyl structures and PEO or PPO coils.[37c,d] Hydrogen bonds between the polymer chains in the layered structures, stabilize LC order in a very broad temperature range up to 260 °C, while the analogous cholesterol-PEGs exhibit LC ordering only up to 100 °C.[12] From this study it is obvious that the formation of LC phases depends on one hand on the amphiphilicity of the polymers, but on the other hand is limited by steric constraints, poly(glyceryl glycerol ether)s with comparable molecular weights as showed no liquid crystalline order.

Given their convenient availability in a single step and their biocompatibility, the liquid crystalline cholesterol-initiated polyglycerols are promising for structured hydrogels, lyotropic LC hydrogels or novel types of hybrid materials by combination with inorganic components. In this context, we are presently investigating to which extent the highly stable mesophases are affected by partial functional transformation of the hydroxyl groups of PG.

Acknowledgement

We thank Prof. Rudolf Zentel for valuable discussions. We are grateful to Dr. Florian Wolf for MALDI-ToF measurements. Furthermore, the authors thank Daniel Loeper and Eric Hoffmann

for their valuable technical assistance. A. M. H. is a recipient of a fellowship of the Graduate School of Excellence MAINZ (Materials Science in Mainz) through funding of the Excellence Initiative (DFG/GSC 266).

References

(1) Reinitzer, F. *Monatsh. Chem.* **1888**, 9, 421-441.

(2) Marcos, M.; Martin-Rapun, R.; Omenat, A.; Serrano, J. L. *Chem. Soc. Rev.* **2007**, 36, 1889-1901.

(3) Imrie, C. T.; Henderson, P. A. *Chem. Soc. Rev.* 2007, 36, 2096-2124.

(4) Zhou, Y.; Briand, V. A.; Sharma, N.; Ahn, S.-k.; Kasi, R. M. *Materials* 2009, 2, 636-660.

(5) Donnio, B.; Guillon, D. *Adv. Polym. Sci.* 2006, 201, 45-155.

(6) Tschierske, C. *J. Mater. Chem.* 1998, 8, 1485-1508.

(7) Schlüter, A. D.; Rabe, J. P. *Angew. Chem., Int. Ed.* 2000, 39, 864-883.

(8) Meier, H.; Lehmann, M. *Angew. Chem., Int. Ed.* 1998, 37, 643-645.

(9) Cameron, J. H.; Facher, A.; Lattermann, G.; Diele, S. *Adv. Mater.* 1997, 9, 398-403.

(10) Barberá, J.; Donnio, B.; Gehringer, L.; Guillon, D.; Marcos, M.; Omenat, A.; Serrano, J. L. *J. Mater. Chem.* 2005, 15, 4093-4105.

(11) Bosman, A. W.; Janssen, H.; Meijer, E. W. *Chem. Rev.* 1999, 99, 1665-1688.

(12) Lopez-Quintela, M. A.; Akahane, A.; Rodriguez, C.; Kunieda, H. *J. Colloid Interface Sci.* 2002, 247, 186-192.

(13) Xu, J.-T.; Xue, L.; Fan, Z.-Q.; Wu, Z.-H.; Kim, J. K. *Macromolecules* 2006, 39, 2981-2988.

(14) Sunder, A.; Quincy, M. F.; Mülhaupt, R.; Frey, H. *Angew. Chem., Int. Ed.* 1999, 38, 2928-2930.

(15) Zhang, X.; Chen, Y.; Gong, A.; Chen, C.; Xi, F. *Liq. Cryst.* 1998, 25, 767-769.

(16) Quincy, M. F.; Kautz, H.; Frey, H. *Polym. Mater. Sci. Eng.* 2001, 84, 647-648.

(17) Nagahama, K.; Ueda, Y.; Ouchi, T.; Ohya, Y. *Biomacromolecules* 2007, 3938-3943.

(18) Kaneko, T.; Nagasawa, H.; Gong, J. P.; Osada, Y. *Macromolecules* 2004, 37, 187-191.

(19) Hartwig, A.; Mahato, T. K.; Kaese, T.; Wöhrle, D. *Macromol. Chem. Phys.* 2005, 206, 1718-1730.

(20) Zhou, Y.; Kasi, R. M. *J. Polym. Sci., Part A: Polym. Chem.* 2008, 46, 6801-6809.

(21) Klok, H. A.; Hwang, J.; Iyer, S.; Stupp, S. *Macromolecules* 2002, 35, 746-759.

(22) Zhou, T.; Li, F.; Cheng, S. X.; Zhuo, R. X. *J. Biomater. Sci, Polym. Ed.* 2006, 17, 1093-1106.

(23) Zhang, L.; Wang, Q. R.; Jiang, X. S.; Zhuo, R. X. *J. Biomater. Sci, Polym. Ed.* 2005, 16, 1095-1108.

(24) Zou, T.; Cheng, S. X.; Zhuo, R. X. *Colloid Polym. Sci.* 2005, 283, 1091-1099.

(25) Lapienis, G.; Penczek, S. *Biomacromolecules* 2005, 6, 752-762.

(26) Wurm, F.; Nieberle, J.; Frey, H. *Macromolecules* 2008, 41, 1184-1188.

(27) Dworak, A.; Baran, G.; Trzebicka, B.; Walach, W. *React. Funct. Polym.* 1999, 42, (1), 31-36.

(28) Dimitrov, P.; Utrata-Wesolek, A.; Rangelov, S.; Walach, W.; Trzebicka, B.; Dworak, A. *Polymer* 2006, 47, 4905-4915.

(29) Wurm, F.; Nieberle, J.; Frey, H. *Macromolecules* 2008, 41, 1909-1911.

(30) Hofmann, A. M.; Wurm, F.; Hühn, E.; Nawroth, T.; Langguth, P.; Frey, H. *Biomacromolecules* 2010, 568-574.

(31) Hofmann, A. M.; Wurm, F.; Frey, H. *Macromolecules* 2011, *44*, 4648–4657.

(32) Mangold, C.; Wurm, F.; Obermeier, B.; Frey, H. *Macromol. Rapid Commun.* 2010, 31, 258-264.

(33) Eberich, M.; Keul, H.; Möller, M. *Macromolecules* 2007, 40, 3070-3079.

(34) Halacheva, S.; Rangelov, S.; Tsvetanov, C. B. *Macromolecules* 2006, 39, 6845-6852.

(35) Dimitrov, P.; Rangelov, S.; Dworak, A.; Haraguchi, N.; Hirao, A.; Tsvetanov, C. B. *Macromol. Symp.* 2004, 215, 127-139.

(36) Mangold, C.; Wurm, F.; Obermeier, B.; Frey, H. *Macromolecules* 2010, 43, 8511-8518.

(37) a) Lee, M.; Oh, N.-K. *J. Mater. Chem.* 1996, 6, 1079-1086; b) Lee, M.; Oh, N.-K.; Zin. W.-C. *Chem. Commun.* 1996, 1787-1788; c) Lee, M.; Cho. B.-K.; Kim, H.; Zin, W.-C. *Angew. Chem., Int. Ed.*1998, *37*, 638-640; d) Lee, M.; Cho, B.-K.; Kim, H.; Yoon, J.-Y.; Zin, W.-C. *J. Am. Chem. Soc.* 1998, *120*, 9168-9179.

(38) Dworak, A.; Baran, G.; Trzebicka, B.; Walach, W. *React. Funct. Polym.* 1999, 42, 31-36.

(39) Taton, D.; Borgne, A. L.; Sepulchre, M.; Spassky, N. *Macromol. Chem. Phys.* 1994, 195, 139.

(40) Förster, S.; Plantenberg, T. *Angew. Chem., Int. Ed.* 2002, 41, 689-694.

(41) Loo, Y. L.; Register, R. A.; Ryan, A. *Macromolecules* 2002, 35, 2365-2374.

(42) Fischer, H.; Poser, S.; Arnold, M. *Liq. Cryst.* 1995, 18, 503-508.

(43) Schneider, A.; Zanna, J. J.; Yamada, M.; Finkelmann, H.; Thomann, R. *Macromolecules* 2000, 33, 649-651.

(44) Abeysekera, R.; Bushby, R. J.; Caillet, C.; Hamley, I. W.; Lozman, O. R.; Lu, Z. B.; Robards, A. W. *Macromolecules* 2003, 36, 1526-1533.

(45) Ansari, I. A.; Castelletto, V.; Mykhaylyk, T.; Hamley, I. W.; Lu, Z. B.; Itoh, T.; Imrie, C. T. *Macromolecules* 2003, 36, 8898-8901.

(46) Yi, Y.; Fan, X. H.; Wan, X. H.; Li, L.; Zhao, N.; Chen, X. F.; Xu, J.; Zhou, Q. F. *Macromolecules* 2004, 37, 7610-7618.

(47) Li, C. Y.; Tenneti, K. K.; Zhang, D.; Zhang, H. L.; Wan, X. H.; Chen, E. Q.; Zhou, Q. F.; Carlos, A. O.; Igos, S.; Hsiao, B. S. *Macromolecules* 2004, 37, 2854-2860.

(48) Tschierske, C. *Curr. Opin. Colloid Interface Sci.* 2002, 7, 355-370.

(49) Goodbye, J. W. *Curr. Opin. Colloid Interface Sci.* 2002, 7, 326-332.

(50) Cho, B.-K.; Chung, Y.-W.; Lee, M. *Macromolecules* 2005, 38, 10261-10265.

(51) Lee, M.; Cho, B.-K.; Zin, W.-C. *Chem. Rev.* 2001, 101, 3869-3892.

(52) Ivanova, R.; Staneva, R.; Geppert, S.; Heck, B.; Walter, B.; Gronski, W.; Stühn, B. *Colloid Polym. Sci.* 2004, 282, 810-824.

Supporting information

Mesogen-initiated linear polyglycerol isomers: The ordering effect of a single cholesterol unit on “sticky” isotropic chains

Anna Maria Hofmann,[1] Robert Wipf,[2] Bernd Stühn,[2,*] Holger Frey[1,*]

1 Institut für Organische Chemie, Johannes Gutenberg-Universität, Duesbergweg 10-14, 55099 Mainz, Germany.

2 Institut für Festkörperphysik, Technische Universität Darmstadt, Hochschulstraße 8, 64289 Darmstadt, Germany.

Published in Macromolecules 2011, 44 (17), 6767-6775.

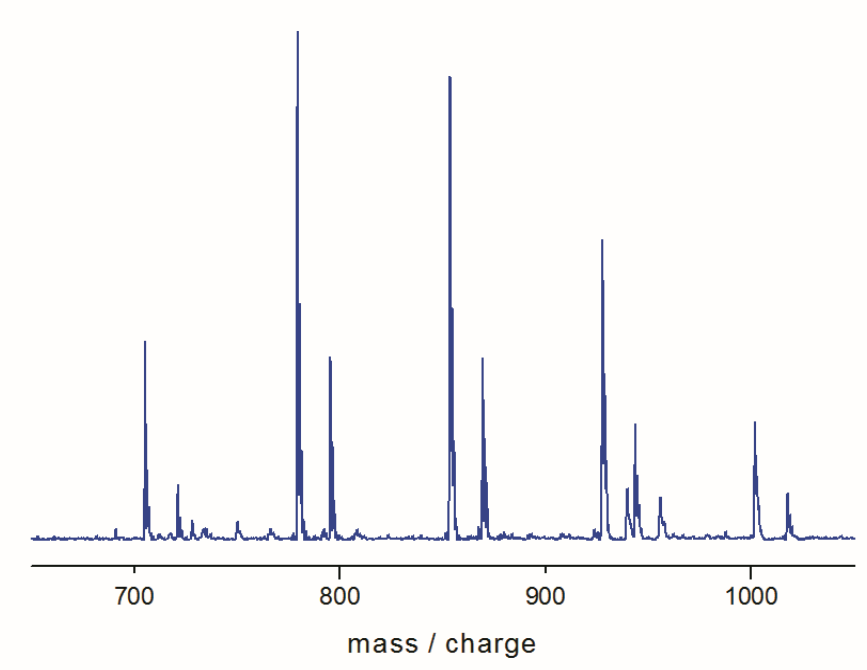

Figure S1. MALDI-ToF of linear polyglycerol (cf. compound 3, Table 1), initiated with cholesterol. The main distribution is obtained with sodium as a counter ion; sub distribution is due to potassium as a counter ion.

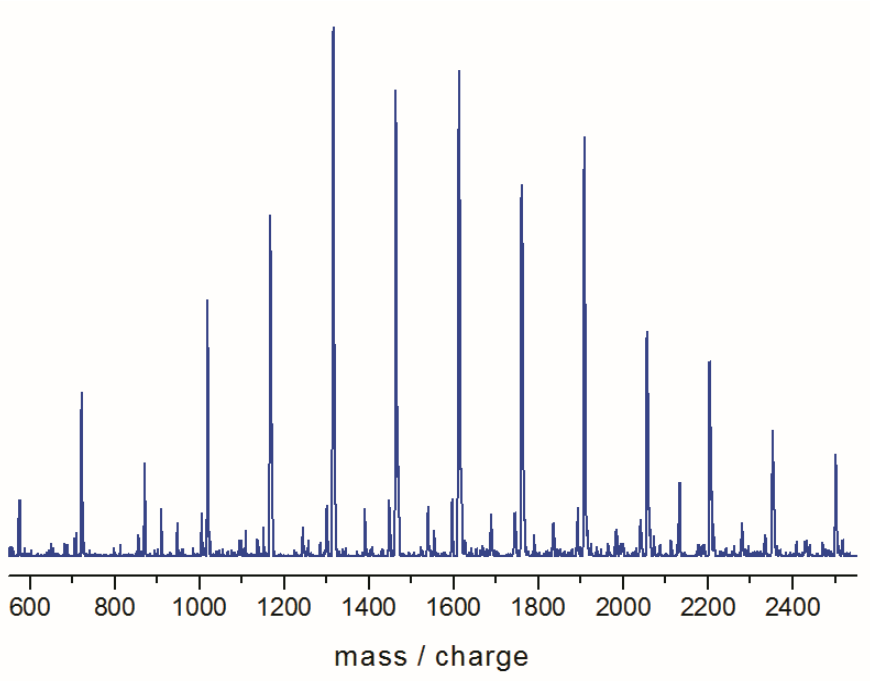

Figure S2. MALDI-ToF of linear poly(glyceryl glycidyl ether) (cf. compound 12, Table 1), initiated with cholesterol. The main distribution is obtained with potassium as a counter ion; sub distribution is due to sodium as a counter ion.

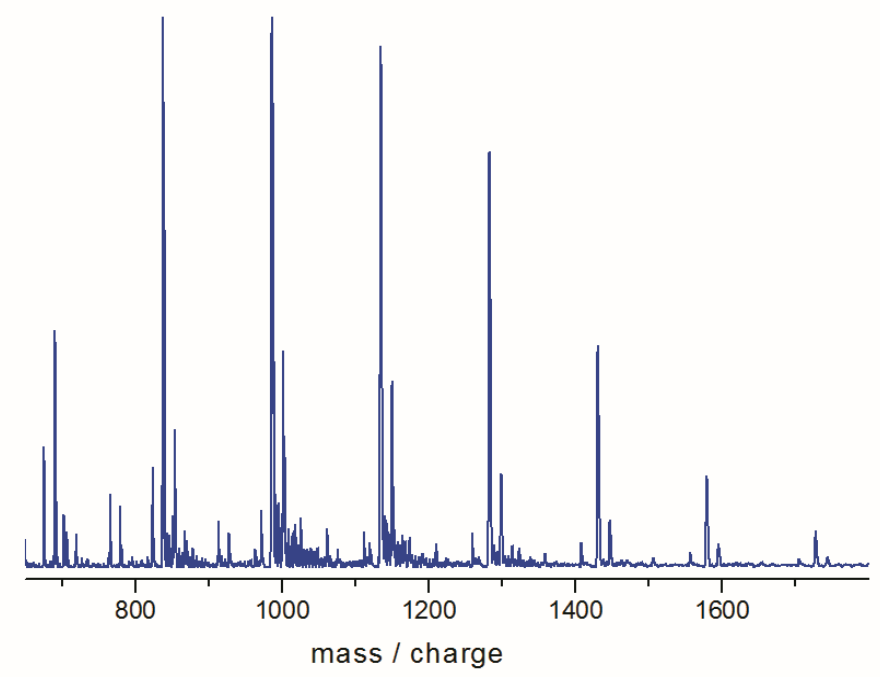

Figure S3. MALDI-ToF of linear poly(glyceryl glycidyl ether) (cf. compound 9, Table 1), initiated with cholesterol. The main distribution is obtained with lithium as a counter ion; sub distributions are due to sodium and cesium as counter ions.

Chapter 4.2: Introduction of a PEG-spacer block in amphiphilic polyether-polyol block copolymers permits formation of ordered structures

Chapter 4.2:

Introduction of a PEG-spacer block in amphiphilic polyether-polyol block copolymers permits formation of ordered structures

Anna Maria Hofmann,[1] Tinka Spehr,[2] Bernd Stühn,[2,*] Holger Frey[1,*]

1 Institut für Organische Chemie, Johannes Gutenberg-Universität, Duesbergweg 10-14, 55099 Mainz, Germany.

2 Institut für Festkörperphysik, Technische Universität Darmstadt, Hochschulstraße 8, 64289 Darmstadt, Germany.

To be submitted to Polymer

Abstract

The liquid crystalline (LC) behavior of a series of complex double-hydrophilic polyether block copolymers comprising both polar ethylene glycol and glyceryl units is described that bear one single apolar cholesterol moiety. The synthesis of the materials consisting of poly(ethylene glycol)-*block*-polyglycerols (PEG-*b*-*l*PG) and of poly(ethylene glycol)-*block*-poly(glyceryl glycidyl ether) (PEG-*b*-PGG) was carried out via cholesterol-initiated ring-opening oxyanionic polymerization (ROP) of ethylene oxide (EO) and ethoxyethyl glycidyl ether (EEGE) or isopropylidene glyceryl glycidyl ether (IGG). Complete incorporation of the mesogenic unit in the complex molecular structure of the polyether block copolymers was achieved by direct use of cholesterol as an initiator for the polymerization. Varying chain lengths, different molecular architectures and amphiphilic or predominantly lipophilic materials have been prepared in order to elucidate the formation of the resulting LC phases, relying on differential scanning calorimetry (DSC), polarized optical microscopy (POM) and small angle X-ray scattering (SAXS).

Keywords

LC polymers, polyethers, poly(ethylene glycol), polyglycerol, cholesterol

Introduction

The formation of liquid crystalline (LC) phases of cholesterol-containing compounds has been a subject of interest since their first observation in the 19th century.[1] Self-assembly of polymers or dendrimers functionalized with cholesterol moieties in thermotropic and lyotropic phases has been intensively studied over the last decades.[2-10] On the other hand cholesterol is a key molecule in biological liquid crystalline systems, more precisely in eukaryotic cell membranes, in which permeability, fluidity and formation of lipid microdomains is determined not only by the lipid composition but also by the cholesterol content (up to 40%).[11, 12] In these complex molecular assemblies cholesterol is able to increase lipid order while the diffusion rate in the fluid membrane is maintained.

In general the driving forces for self-assembly in such ordered structures are formation of hydrogen bonds and ionic as well as hydrophobic interactions that depend on the chemical structure of the respective mesogen and scaffold.[13-22] These driving forces determine the eventual microphase separation, liquid crystalline order and crystallization. The phase behavior of hydrophilic polyethers such as poly(ethylene glycol) (PEG) attached to cholesterol-moieties has been studied with regard to the influence of crystallization and the formation of LC structures.[3, 5] Furthermore, the strong ordering effect of one single cholesteryl unit on hydroxyl-functional, i.e. “sticky” linear, isotropic polyglycerol chains has been investigated in a recent study by our group.[23] In this report, cholesterol-initiated polyglycerol has been shown to possess lamellar liquid crystalline ordering in a broad temperature range up to 260 °C and up to a degree of polymerization of 26 glyceryl units. On the other hand for cholesterol-poly(glyceryl glycidyl ether), an analogous structure with one branching unit per monomer incorporated into the backbone, no LC behavior was observed.

To the best of our knowledge liquid crystalline phases of complex amphiphilic polyether architectures based on PEG and polyglyceryl chains, bearing one single cholesterol moiety, has not been reported. In contrast to our recent work, a linear PEG spacer was incorporated into the polyether structure and studied with respect to the formation of LC phases.

The synthesis of the amphiphilic polyethers consisting of poly(ethylene glycol)-*block*-polyglycerol (PEG-*b*-*l*PG) and poly(ethylene glycol)-*block*-poly(glyceryl glycidyl ether) (PEG-*b*-PGG) has been carried out via ring-opening oxyanionic polymerization (ROP) of ethylene oxide (EO) and ethoxyethyl glycidyl ether (EEGE)[24-27] or isopropylidene glyceryl glycidyl ether (IGG).[28-

[35] Incorporation of the mesogen in each polymer chain was achieved by the use of cholesterol as an initiator for the polymerization (Figure 1), which shortens the synthetic effort by avoiding additional derivatization and purification steps subsequent to the polymerization reaction and guarantees covalent attachment of one mesogenic unit to each polymer chain.

Following this straightforward synthetic approach, the formation of LC phases is driven by the ordering effect of one single cholesterol moiety. The impact of other structural parameters on the LC behavior has been investigated by variation of molecular weights, block lengths and molecular architectures as well as polarity. In the present study various structural parameters controlling the phase behavior, such as the influence of one mesogenic unit onto the self-assembly of an otherwise amorphous material, the effect of the second polyglycerol block on the crystallization of the PEG chains and the dependence of the formation of LC on microphase separation have been characterized. The synthesis of the respective cholesterol-based block copolymers is shown in Figure 1.

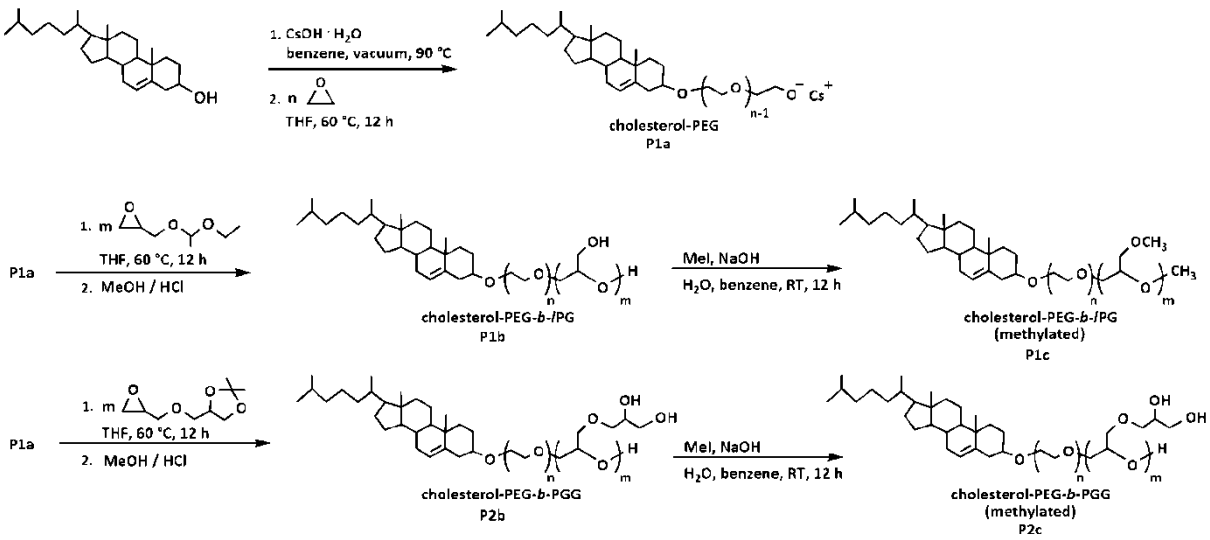

Figure 1: Reaction sequence for the synthesis of cholesterol-PEG-*b*-*l*PG block copolymers and cholesterol-PEG-*b*-PGG block copolymers and their respective methylated derivatives.

Experimental section

Instrumentation. Instrumentation. ^{1}H nuclear magnetic resonance (NMR) spectra were recorded using a Bruker AC 300 spectrometer operated at 300 MHz, employing $CDCl_3$ and

DMSO-d_6 as solvents. ^{13}C NMR spectra (referenced internally to solvent signals) were recorded at 100.15 MHz.

FT-IR spectra were recorded on a Nicolet iS 10 spectrometer equipped with a diamond ATR unit.

SEC measurements were carried out in dimethylformamide (DMF) containing 0.25 g/L of lithium bromide. An Agilent 1100 Series GPC (gel permeation chromatography) setup was used as an integrated instrument, including a PSS HEMA column ($10^6/10^5/10^4$ g/mol), a UV- (254 nm) and RI-detector. Calibration was achieved using poly(ethylene glycol) standards provided by Polymer Standards Service. The eluent was used at 50 °C and at a flow rate of 1 mL/min. For SEC measurements in chloroform, a setup consisting of a Waters 717 plus autosampler, a TSP Spectra Series P 100 pump, three PSS-SDV-5 µl-columns with 100, 1000, and 10000 Å pore diameter, respectively, a UV (275 nm) and an RI detector was used. Calibration was carried out using poly(styrene) standards provided by Polymer Standards Service (PSS).

Matrix-assisted laser desorption and ionization time-of-flight (MALDI-ToF) measurements were performed on a Shimadzu Axima CFR MALDI-ToF mass spectrometer equipped with a nitrogen laser delivering 3 ns laser pulses at 337 nm. α-Cyano-3-hydroxy-cinnamic acid (CHCA) was used as matrix. Samples were prepared by dissolving the polymer in methanol at a concentration of 10 g/L. A 10 µL aliquot of this solution was added to 10 µL of a 10 g/L solution of the matrix and 1 µL of a solution of potassium trifluoroacetic acid (KTFA) (0.1M in methanol as cationization agent). A 1 µL aliquot of the mixture was applied to a multistage target, methanol evaporated and a thin matrix/analyte film was created.

DSC measurements were carried out using a Perkin-Elmer DSC 7 with a Perkin-Elmer thermal analysis controller TAC7/DX in the temperature range of -100 to 100 °C using heating rates of 20 and 10 K/min. The melting points of indium (T_m = 156.6 °C) and Millipore water (T_m = 0 °C) were used for calibration.

Polarized optical microscopy (POM) measurements were carried out at different temperatures using an Olympus BX-51 polarized optical microscope equipped with a digital camera. A small amount of the respective sample was placed on an object plate and covered with a thin glass slide.

Small angle X-ray scattering (SAXS) measurements were obtained with a system based on a conventional X-ray source for CuK_α radiation with a wavelength λ= 0.1542 nm, an X-ray mirror,

three pinholes to focus the beam and a two dimensional multi wire detector (Molecular metrology). This provides an accessible range of scattering vectors $q = 4\pi/(\lambda\sin(\theta))$ from $q = 0.013$ Å^{-1} to $q = 0.5$ Å^{-1}. Beam path and sample chamber were evacuated. Sample detector distance was 75 mm. The samples were put into a sandwich of three metal discs with central holes and kapton foil to keep the sample in place.

Reagents. All reagents and solvents were purchased from Acros and used as received, unless otherwise mentioned. Cholesterol was purchased from Fluka and stored at 4 °C. Dry solvents stored over molecular sieves were purchased from Fluka. Deuterated $CDCl_3$ and DMSO-d_6 were purchased from Deutero GmbH, dried and stored over molecular sieves.

Ethoxyethyl glyceryl ether (EEGE) was prepared as described in literature using glycidol and dried over CaH_2 directly before use.[24, 25, 27, 36] ^{1}H NMR (300 MHz, $CDCl_3$): δ (ppm) = 4.76 ($OCH(CH_3)O$), 3.35-3.90 (OCH_2CH_3 and $OCH_2C_2H_3O$), 3.15 (CH epoxide), 2.61-2.91 (CH_2 epoxide), 1.33 ($OCH(CH_3)O$), 1.19 (OCH_3).

Isopropylidene glyceryl glycidyl ether (IGG) was prepared as described in literature, dried over CaH_2 and freshly distilled before use.[33] ^{1}H NMR (300 MHz, CDCl3): δ (ppm) = 4.3 (CH acetal), 4.07 (CH acetal), 3.88-3.39 (OCH_2), 3.17 (CH epoxide), 2.81 (CH_2 epoxide), 1.44 (CH_3), 1.38 (CH_3).

Synthesis: Polymerization reactions. The synthesis of amphiphilic polyethers bearing one cholesterol-moiety was carried out following a general protocol reported previously.[23, 35]
Cholesterol was placed in a Schlenk flask, the appropriate amount of $CsOH{\cdot}H_2O$ (degree of deprotonation 90%) and benzene were added and the mixture was stirred for 30 min at 60 °C in argon atmosphere to generate the cesium alkoxide. The initiator was dried in vacuo at 90 °C and dry tetrahydrofurane (THF) was added via cryo transfer. Ethylene oxide was cryo-transferred first to a graduated ampoule and then to the Schlenk flask containing the initiator solution. The mixture was allowed to warm up to room-temperature, heated to 60 °C and polymerization was performed for 12 hours at 60 °C in vacuo. Subsequently, the flask was filled with argon, a sample was removed for NMR- and SEC-characterization, the appropriate amount of EEGE was added with a syringe and the reaction mixture was heated to 60 °C for additional 12 hours. After removal of another sample the acetal protecting groups of the PEEGE block were removed by addition of methanol, water and acidic ion-exchange resin, stirring for 12 hours at room-temperature. Filtration and subsequent precipitation in cold diethyl ether

resulted in the pure block copolymer that was dried in vacuo. Following the same synthetic approach cholesterol-PEG-*b*-PGG was obtained using IGG as the second monomer.

Cholesterol-poly(ethylene glycol)-block-polyglycerol: ^{1}H NMR (300 MHz, DMSO-d_6): δ (ppm) = 5.30 (C=CH cholesterol), 4.29 (br, OH), 3.76-3.22 (polyether backbone; CHO cholesterol), 2.28-0.82 (br, CH_2, CH cholesterol), 0.63 (br, CH_3 cholesterol).

The methylation of the block copolymers was carried out dissolving 500 mg of the respective polymer in water (2 mL), adding sodium hydroxide to yield a 1 n solution and benzene (2 mL). Methyl iodide (10 eq. of hydroxyl groups) was added slowly via syringe under vigorous stirring at room temperature. After additional 12 hours of stirring the reaction mixture was extracted with toluene, the organic phases dried over $MgSO_4$ and the solvents were removed to obtain the methylated product in yields of about 90%.

Cholesterol-poly(ethylene glycol)-block-polyglycerol (methylated): ^{1}H NMR (300 MHz, DMSO-d_6): δ (ppm) = 5.30 (C=CH cholesterol), 3.76-3.22 (polyether backbone; CHO cholesterol), 3.23 (OCH_3), 2.28-0.82 (br, CH_2, CH cholesterol), 0.63 (br, CH_3 cholesterol).

Results and discussion

The strong ordering effect of one cholesteryl unit on isotropic polyglyceryl chains has been studied recently by our group, however, cholesterol-poly(glyceryl glycidyl ether), the analogous structure with one branching point per monomer unit, was found to exhibit no LC behavior.[23] In the current work, the introduction of a short PEG spacer block into the polymer architectures was investigated with respect to its impact on the thermal behavior, particularly with respect to the formation of liquid crystalline phases.

Synthesis and characterization of cholesterol block copolymers. Liquid crystalline materials consisting of poly(ethylene glycol)-*block*-linear polyglycerol (PEG-*b*-*l*PG) and poly(ethylene glycol)-*block*-poly(glyceryl glycidyl ether) (PEG-*b*-PGG) have been synthesized using mesogenic cholesterol as an initiator and cesium hydroxide monohydrate as deprotonating agent for the ROP of ethylene oxide and ethoxyethyl glycidyl ether (EEGE) or isopropylidene glyceryl glycidyl ether (IGG). The use of commercially available cholesterol as an initiator permits not only the preparation of novel liquid crystalline materials, but simplifies the synthetic approach as no additional post polymerization derivatization step is required. Furthermore, the initiating

system led to good control over the molecular weights and over the degree of functionalization of both block copolymers presented in this study. Thus, narrow molecular weight distributions and low polydispersity indices (PDI = M_w/M_n < 1.2) were obtained.

The degree of polymerization for each block was determined via ^{1}H NMR spectroscopy integrating the methyl groups of cholesterol at a chemical shift of 0.63 ppm and the polyether backbone for PEG (3.76-3.22 ppm) and the acetal protecting groups (4.63 ppm for PEEGE or rather 4.14 ppm or respectively 3.96 ppm for PIGG). Comparison of the molecular weights determined via SEC in DMF (PEG standards) and the molecular weights calculated from ^{1}H NMR spectra revealed a general underestimation by SEC. Since elution times of the polyethers are strongly influenced by the cholesterol moiety and the polyglycerol block, molecular weights have been determined from ^{1}H NMR spectra.

Complete incorporation of the mesogen in every polymer chain, which is crucial for the LC behavior of the resulting material, has been evidenced via MALDI-ToF MS for all samples (Figure 2). Since the liquid crystalline behavior of the block copolymers is driven by the incorporation of one single mesogen moiety and related systems showed the formation of LC phases up to a degree of polymerization of 10-26,[3, 23] molecular weights were adjusted to be in the range of 1000-2400 g/mol. All of the amphiphilic block copolymers synthesized in this study (characterization data are summarized in Table 1) showed LC behavior in a wide temperature region, revealing the strong ordering effect of cholesterol.

Table 1. Characterization data of amphiphilic cholesterol-poly(ethylene)-*block*-linear polyglycerol and cholesterol-poly(ethylene)-*block*-poly(glyceryl glycidyl ether). [a] M_n determined via ^{1}H NMR spectroscopy. [b] M_n and M_w determined via SEC-RI in DMF with poly(ethylene glycol) standards. [c] M_n and M_w determined via SEC-RI in $CHCl_3$ with poly(styrene) standards. [d] Isotropic/liquid crystal transition temperature determined via POM.

#	polymer	M_n (th) g/mol	M_n[a] (NMR) g/mol	M_n (SEC) g/mol	PDI[b] (SEC)	T_g (DSC) °C	I/LC[d] (POM) °C	$T_{m, PEG}$ (DSC) °C	ΔH (DSC) kJ/mol
1	chol-PEG_7-*b*-lPG_5	860	1070	830[b]	1.11[b]	-46.2	150	-	-
2	chol-PEG_{10}-*b*-lPG_5	1000	1200	900[b]	1.10[b]	-47.5	100	16.3	18.6

3	chol-PEG_{15}-*b*-*l*-PG_5	1200	1420	1060 [b]	1.12 [b]	-46.5	90	22.9	37.5
4	chol-PEG_{21}-*b*-*l*-PG_5	1640	1680	1090 [b]	1.11 [b]	-47.1	60	24.4	35.2
5	chol-PEG_{36}-*b*-*l*-PG_5	2080	2340	1440 [b]	1.17 [b]	-47.8	55	32.5	59.5
6	chol-PEG_{46}-*b*-*l*-PG_5	2520	2780	1850 [b]	1.16 [b]	-55.7	(40)*	36.7	64.1
7	chol-PEG_5-*b*-PGG_7	1500	1650	990 [b]	1.13 [b]	-48.1	120	-	-
8	chol-PEG_{11}-*b*-PGG_5	1570	1610	1080 [b]	1.13 [b]	-42.7	115	-	-
9	chol-PEG_{15}-*b*-PGG_5	1790	1850	1160 [b]	1.21 [b]	-44.4	50	25.5	26.2
10	chol-PEG_{25}-*b*-PGG_5	2010	2230	1540 [b]	1.10 [b]	-48.2	60	26.7	45.8
11	chol-PEG_7-*b*-*l*-PG_5 (methylated)	1160	1160	780 [b] 900 [c]	1.20 [b] 1.38 [c]	-67.0	30	-	-
12	chol-PEG_{10}-*b*-*l*-PG_5 (methylated)	1280	1280	910 [b] 1070 [c]	1.12 [b] 1.49 [c]	-68.2	40	-	-
13	chol-PEG_{15}-*b*-*l*-PG_5 (methylated)	1500	1500	970 [b] 2050 [c]	1.14 [b] 1.21 [c]	-70.1	40	7.4	35.9
14	chol-PEG_{21}-*b*-*l*-PG_5 (methylated)	1770	1770	1310 [b] 2090 [c]	1.20 [b] 1.42 [c]	-71.1	45	16.5	51.5
15	chol-PEG_{36}-*b*-*l*-PG_5 (methylated)	2420	2420	1630 [b] 2200 [c]	1.12 [b] 1.18 [c]	-61.0	30	23.0	50.9
16	chol-PEG_{46}-*b*-*l*-PG_5 (methylated)	2860	2860	1950 [b] 3290 [c]	1.29 [b] 1.13 [c]	-71.1	35	23.5	50.5
17	chol-PEG_5-*b*-PGG_7 (methylated)	1860	1860	1050 [b] 1810 [c]	1.09 [b] 1.39 [c]	-70.6	-	-	-
18	chol-PEG_{11}-*b*-PGG_5 (methylated)	1760	1760	1050 [b] 2200 [c]	1.08 [b] 1.27 [c]	-70.2	-	-	-
19	chol-PEG_{15}-*b*-PGG_5 (methylated)	1940	1940	1150 [b] 2740 [c]	1.17 [b] 1.21 [c]	-80.3	-	8.2	19.2
20	chol-PEG_{25}-*b*-PGG_5 (methylated)	2380	2380	1190 [b] 3250 [c]	1.29 [b] 1.17 [c]	-73.0	-	16.2	42.4

* For block copolymers with a degree of polymerization exceeding 46, birefringence observed with the polarized optical microscope is explained by the formation of crystalline fractions.

Reflecting this, the macroscopic appearance of the amphiphilic cholesterol-PEG-*b*-*l*PG materials changes from honey-like liquids to solid materials with increasing chain length of the PEG block.

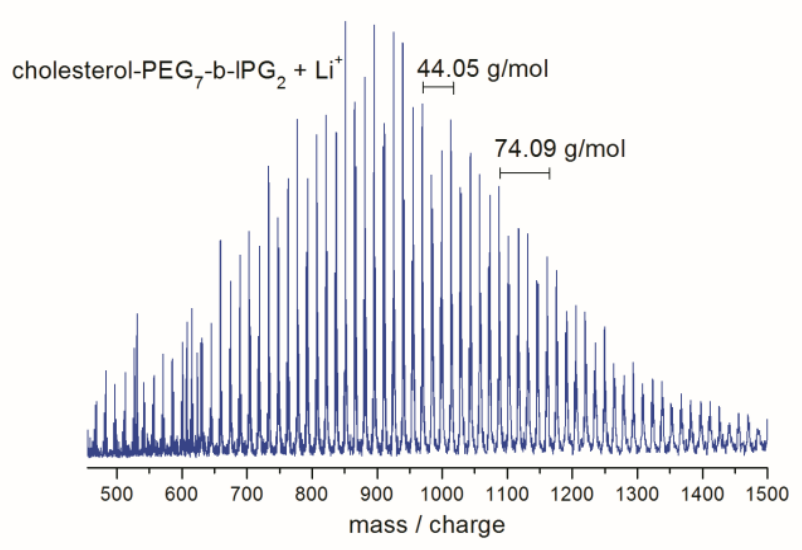

Figure 2. MALDI-ToF of linear poly(ethylene glycol)-*block*-polyglycerol (cf. compound 1, Table 1) initiated with cholesterol. The main distribution is obtained with lithium as a counter ion, the sub distribution is due to sodium as a counter ion.

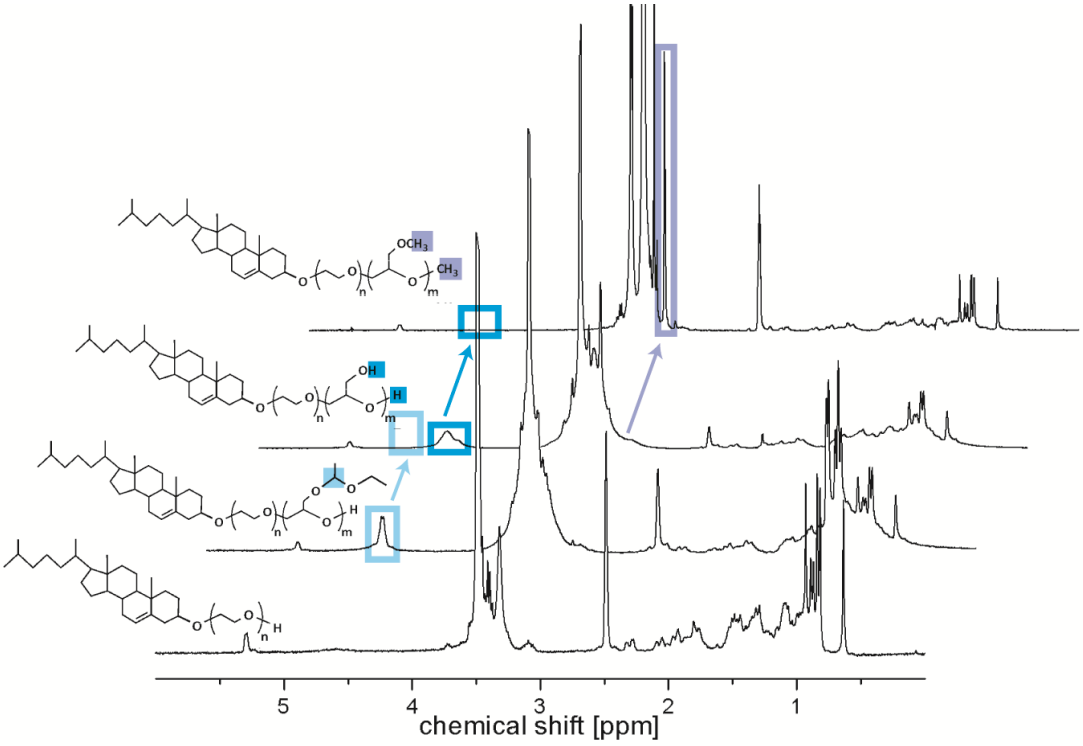

Figure 3. ^{1}H NMR spectra (300 MHz, DMSO-d_6) of cholesterol-*b*-PEG, cholesterol-PEG-*b*-PEEGE, cholesterol-PEG-*b*-*l*PG (cf. compound 3, Table 1) and methylated cholesterol-PEG-*b*-*l*PG-OMe (cf. compound 15, Table 1).

Thermal and optical characterization of cholesterol block copolymers. Previous studies revealed the strong ordering effect of a single cholesteryl unit on poly(ethylene glycol) or polyglycerol chains.[3, 23] This effect is limited in branched cholesterol-initiated poly(glyceryl glycidyl ether)s, which possessed no LC behavior. Via incorporation of a second PEG block into the polymer architectures the liquid crystalline order is clearly influenced due to the highly flexible poly(ethylene glycol) chain acting as a spacer between the rigid lipophilic mesogen and the branched hydrophilic PGG.

The series of cholesterol-initiated block copolymers has been varied on one hand in their molecular architecture by the use of ethoxyethyl glycidyl ether (EEGE) or isopropylidene glyceryl glycidyl ether (IGG) as comonomers. Thus, polymers with one hydroxyl group per monomer unit incorporated in the second block for the use of EEGE or respectively two adjacent hydroxyl groups for the use of IGG were synthesized. On the other hand the amphiphilicity of the polyethers has been varied by the preparation of different chain lengths as well as by the permethylation of the materials using methyl iodide, giving predominantly lipophilic materials (Table 1). The thermotropic liquid crystalline behavior of all polymers prepared in this study has been investigated via polarizing optical microscopy (POM), differential scanning calorimetry (DSC) and small angle X-ray scattering (SAXS). The glass transition temperatures (T_g) of the cholesterol-initiated polyethers determined by DSC measurements are located in a range of -50 to -40 °C for the amphiphilic block copolymers. Permethylation of the materials results in strongly decreased glass transition temperatures varying from -80 °C to -67 °C due to the elimination of hydroxyl groups along the polymer chain forming intermolecular hydrogen bonds.

Crystallization or melting of the PEG moiety has only been observed in compounds with PEG blocks of 10 units and higher for cholesterol-PEG-*b*-*l*PG, while PEG-*b*-PGG showed crystallization (or melting) in polymers containing 15 and more ethylene oxide units. In general, the crystallization temperature of the PEG moiety increases with increasing block length, varying from -15 °C to -30 °C. Full conversion of the hydroxyl groups along the second polymer block leads to reduced crystallization temperatures of the PEG block around -50 °C.

Investigation of the amphiphilic polymers with polarizing optical microscopy revealed the formation of liquid crystalline phases of all amphiphilic block copolymers presented in this study within a broad temperature range (Figure 4). Interestingly, also polymers containing branched PGG units in the second block showed LC ordering, while the corresponding

amphiphilic homopolymers (cholesterol-PGG) are incapable to self-assembly in LC structures.[23] Concerning these findings, the complex apolar-polar-polar block copolymers obviously exhibit higher tendencies to form ordered structures due to the linear PEG block, easily aligning in layers on one hand and forcing the amorphous PGG unit despite their one branching unit per monomer incorporated in the second block to array in the same LC arrangement.

Birefringence has been observed via POM between crossed polarizers at temperatures ranging from room temperature to 150 °C. In contrast to crystallization (or melting) temperatures of the PEG block, the temperatures for the liquid crystalline/isotropic transition decrease with increases chain length, varying from 150 °C for cholesterol-PEG_7-*b*-*l*PG_5, 100 °C for cholesterol-PEG_{10}-*b*-*l*PG_5, 90 °C for cholesterol-PEG_{15}-*b*-*l*PG_5 to 60 °C for cholesterol-PEG_{21}-*b*-*l*PG_5. The very same trend has been found in the series of PEG-PGG block copolymers (120 °C for cholesterol-PEG_5-*b*-PGG_7, 115 °C for cholesterol-PEG_{11}-*b*-PGG_5, 50 °C for cholesterol-PEG_{15}-*b*-PGG_5 and 60 °C for cholesterol-PEG_{25}-*b*-PGG_5. This phenomenon has been observed in related studies on the thermotropic LC behavior of cholesterol-PEGs presented by Xu et al.[37] Depending on the degree of polymerization of the PEG moiety, the final morphology of the amphiphilic material is determined by the dominant species. Thus, cholesterol-PEG_5 shows liquid crystalline behavior due to the amorphous PEG moiety and the LC cholesterol unit. With increasing chain length the PEG block becomes more dominant, so that LC and crystalline phases coexist in cholesterol-PEG_{10} and cholesterol-PEG_{15}. Further increase of the PEG chain length leads to mere crystalline materials owing to the dominant PEG moiety. Compared to these mesogen-modified PEGs, the formation of liquid crystalline phases in cholesterol-initiated PEG-*b*-*l*PG and PEG-*b*-PGG block copolymers can be found in materials up to a degree of polymerization of 36 units. By the incorporation of the amorphous polyglycerol or respectively poly(glyceryl glycidyl ether) block in the amphiphilic polymer, crystallization of the overall material due to the crystalline PEG block is suppressed resulting in a distinct formation of liquid crystalline structures of polymers with molar masses of above 2400 g/mol. Thus, emerging a facile synthetic strategy involving cholesterol-initiated ROP of different epoxide monomers, complex materials have been prepared that show the formation of liquid crystals over a wide range of temperatures and chain lengths. Following this approach the synthesis of polymeric LCs has been achieved that exceed molecular weights obtained for conventional liquid crystalline cholesterol-PEGs.

To draw conclusions from the optical textures revealed via POM on cooling from the isotropic melt of the amphiphilic cholesterol-initiated block copolymers presented in this study, the

existence of layered phases such as smectic A phases is assumed (Figure 4). This is in good accordance with results from related studies on the self-assembly of polyethers end-capped with cholesterol moieties.[5, 23, 38]

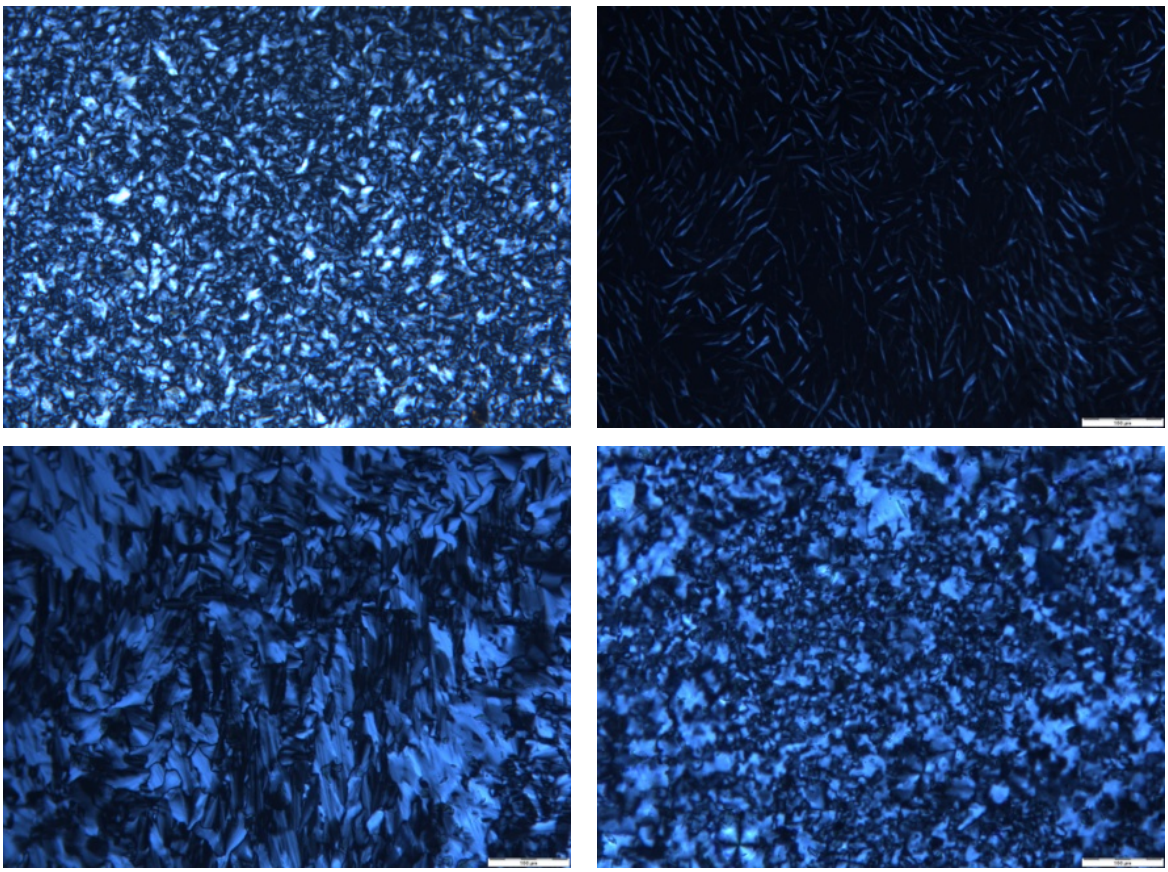

Figure 4. Optical textures of cholesterol-PEG-*b*-*l*PG observed under the polarizing microscope at different temperatures. POM micrographs of cholesterol-PEG_{15}-*b*-*l*PG_5 (cf. compound 3, Table 1) at 75 °C (top, left) and of cholesterol-PEG_5-*b*-PGG_7 (cf. compound 5, Table 1) at 120 °C straight after cooling from isotropic melt (top, right), at 120 °C in equilibrium state and at 40 °C (bottom, right).

Layered structures are favored in these amphiphilic materials due to microphase separation of the hydrophobic cholesterol and the hydrophilic polyether chains. In comparison to previous works on rod-coil structures with poly(ethylene oxide) (PEO) or poly(propylene oxide) (PPO) chains, the materials based on cholesterol-PEG-*b*-PG show lower tendency to crystallize due to the highly polar, isotropic structure of the PG block in contrast to the PPO moiety.[39, 40] Nevertheless, the presence of three different moieties, the mesogenic cholesterol, the crystallizable PEG block and the amorphous PG block results in complex phase behavior due to microphase separation between the lipophilic and hydrophilic segments as well as between the

crystallizable and amorphous polymer blocks. For block copolymers with a degree of polymerization above 46 no LC phases have been observed with POM. In these materials the crystalline PEG moiety determines the morphology, leading to mere crystalline structures, indicated by the formation of spherulites detected under cross polarizers. According to these findings, the macroscopic morphology of the cholesterol-PEG-*b*-*l*PGs with increased PEG chain lengths changes from honey-like materials for a degree of polymerization under 36 to predominantly solid materials for PEG moieties above 46 units.

The change in the amphiphilicity of the block copolymers induced by full methylation of the hydroxyl groups in the particular polyether polyol block (*l*PG or PGG) strongly affects the liquid crystalline behavior. Since the formation of LC in amphiphilic cholesterol-related compounds is mainly driven by the microphase separation of the incompatible lipophilic cholesterol and the hydrophilic moiety, the methylation of the polymer backbone of cholesterol-PEG-*b*-*l*PGs lead to reduced liquid crystalline ordering with lower I/LC transition temperatures of about 40 °C due the lack of hydrogen bonding interactions and lower T_gs of the methylated block copolymers. Nevertheless, the amphiphilicity caused by the residual hydrophilic PEG moiety is sufficient to force the formation of layered structures. In contrast, complete disappearance of the LC formation has been observed in the permethylated cholesterol-PEG-*b*-PGG compounds, which can be referred to the higher number of hydroxyl groups per comonomer incorporated in the second block. Full conversion of all these functionalities disturbs the former amphilicity of the system and increases the steric demand of the polyether chain to an extend which inhibits the formation of lamellar structures.

Small-angle X-ray scattering of cholesterol block copolymers. Detailed studies regarding the structure of the liquid crystalline phases were carried out using small angle X-ray scattering (SAXS). The at room temperature obtained intensity profiles for a series of cholesterol-PEG_n-*b*-*l*PG_5 and cholesterol-PEG_n-*b*-PGG_5 are shown in Figures 5 and 6 respectively. First and second order peaks of a lamellar structure, such as sematic A phases, are clearly observed only for cholesterol-PEG-*b*-*l*PG block copolymers composed of rather short PEG blocks wih a degree of polymerization of 7-15 EO units, see Figure 5. Layered structures are favored in these amphiphilic materials due to microphase separation of the hydrophobic cholesterol and the hydrophilic polyether chains. According to previous studies on double-hydrophilic PEG-*b*-PG

block copolymers, in this molecular weight range, the short crystallizable PEG moiety is miscible with the linear polyglycerol block.[25]

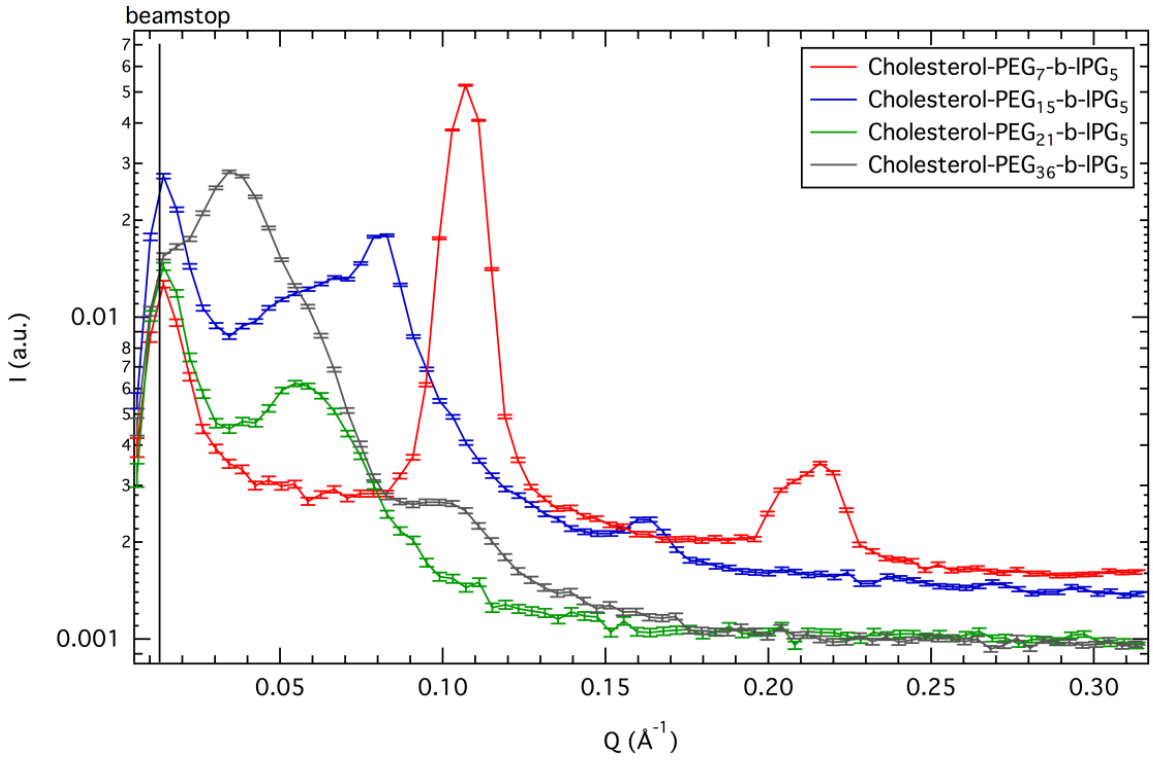

Figure 5. SAXS profiles of cholesterol-initiated PEG-*b*-*l*PG block copolymers measured at 22 °C.

The incorporation of longer PEG chains results in more complex phase behavior. In materials with PEG blocks with a degree of polymerization above 20 the formation of LC structures is influenced by an additional driving force, i.e., the crystallization-induced phase segregation of the hydrophilic PEG blocks. Thus, the resulting LC structure depends on the microphase separation between the lipophilic cholesterol and the hydrophilic polymer chains as well as on the separation of the PEG and PG blocks. The scattering profiles of cholesterol-PEG$_{21}$-*b*-*l*PG$_5$ and cholesterol-PEG$_{36}$-*b*-*l*PG$_5$ show complex reflections that cannot be explained with the existence of simple lamellar phases alone (Figure 5). In previous works on rod-coil structures with poly(propylene oxide) (PPO) chains, similar results have been presented.[20, 41] In this work, rod-coil molecules with 7 propylene oxide units showed layered smectic C and smectic A phases, while the respective mesogen with 12 PO units exhibits an optically isotropic cubic phase. Further investigations regarding the characterization of the structures present in the cholesterol-initiated block copolymers, i.e., PEG-*b*-*l*PG (Figure 5) and PEG-*b*-PGG (Figure 6) are in progress and will be reported in due course.

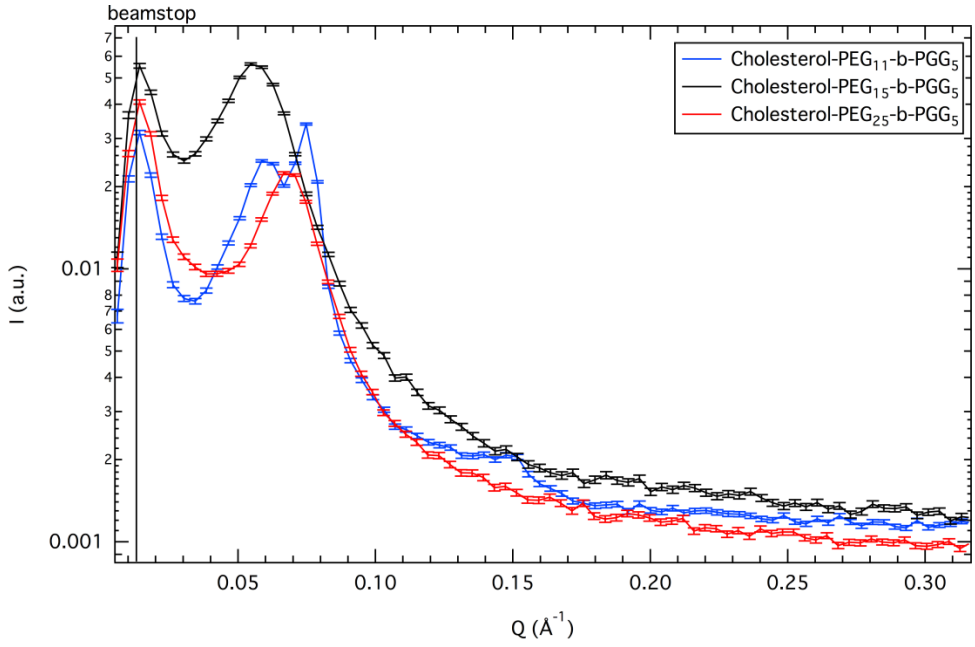

Figure 6. SAXS profiles of cholesterol-initiated PEG-*b*-*P*PG block copolymers measured at room temperature (22 °C).

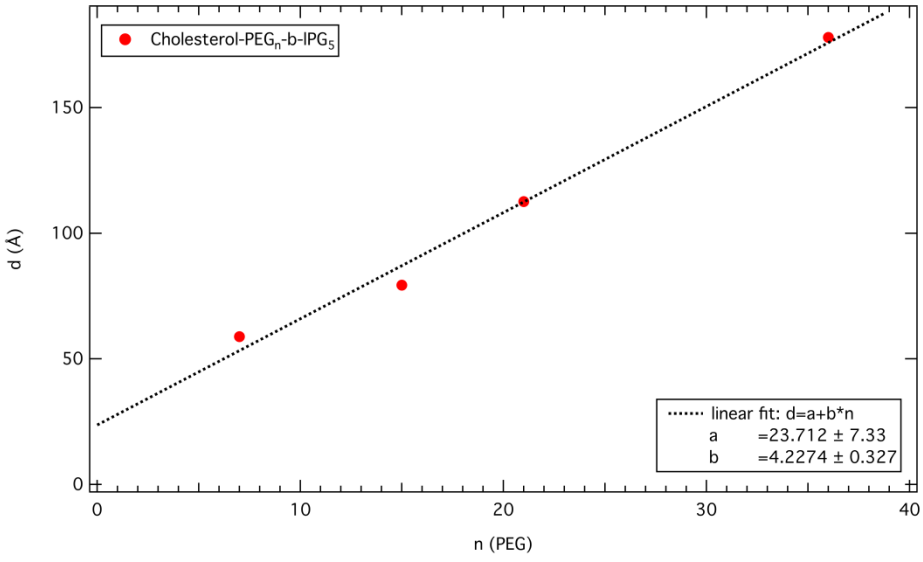

Figure 7. Layer thickness determined via SAXS measurements (peaks position) vs. degree of polymerization of the PEG block length of cholesterol-initiated PEG-*b*-*l*PGs.

The Q value of the first order reflection is directly related the the period of the structure $d = 2\pi/Q$. The position of the first peak was used to calculate the lamellar thickness d and a linear dependence on the degree of polymerization of the PEG-block can be deduced. Note that we have clear evidence for a lamellar structure (presence of a second order peak) only in the case of n=7 and n=15.

Conclusion

We have studied the liquid crystalline behavior of different complex double-hydrophilic polyether block copolymers based on ethylene glycol and glyceryl units, bearing a single mesogenic cholesterol moiety. The synthesis of poly(ethylene glycol)-*block*-polyglycerols (PEG-*b*-*l*PG) and of poly(ethylene glycol)-*block*-poly(glyceryl glycidyl ether) (PEG-*b*-PGG) was carried out via ring-opening oxyanionic polymerization (ROP) of ethylene oxide (EO) and ethoxyethyl glycidyl ether (EEGE) or isopropylidene glyceryl glycidyl ether (IGG). Direct use of the mesogenic cholesterol as an initiator for the polymerization allowed the investigation of the ordering effect of this single mesogen moiety.

Remarkably, the incorporation of a flexible PEG spacer in the amphiphilic structures resulted in the formation of LC order also in branched PGG-based materials, while cholesterol-PGG homopolymers exhibit no LC order. Furthermore, the materials based on cholesterol-PEG-*b*-PG and PEG-*b*-PGG show lower tendency to crystallize due to the highly polar, isotropic structure of the PG block in contrast to the PPO moiety investigated in previous studies on rod-coil structures with poly(ethylene oxide) (PEO) or poly(propylene oxide) (PPO) chains.[39, 40] Thus, the range of molecular weights capable of forming LC structures is increased in the block copolymers up to a degree of polymerization of 36.

Small-angle X-ray scattering demonstrated the existence of lamellar phases in compounds with relatively short PEG (7-15 EO units) due to microphase separation of the lipophilic cholesterol and the hydrophilic polyether chains. Since miscibility of the polar polymer blocks is possible in this molecular weight range, the formation of LC structures is determined clearly by the amphiphilicity of the material and the ordering effect introduced by the mesogenic, hydrophobic cholesterol. The incorporation of PEG blocks with a degree of polymerization above 20 results in more complex phase behavior. Additional driving forces, such as the crystallization-induced phase segregation of the hydrophilic blocks influence the resulting LC structures. Further characterization of the LC phase behavior of PEG-*b*-*l*PG and PEG-*b*-PGG is in progress and will be reported in due course.

Due to their facile preparation in a one-pot approach, their mere aliphatic polyether structure and their excellent solubility in aqueous systems the liquid crystalline PEG-*b*-PG and PEG-*b*-PGG block copolymers offer interesting properties for lyotropic LC hydrogels.

Acknowledgement

The authors thank Daniel Loeper and Eric Hoffmann for their valuable technical assistance. A. M. H. is a recipient of a fellowship of the Graduate School of Excellence MAINZ (Materials Science in Mainz) through funding of the Excellence Initiative (DFG/GSC 266).

References

(1) Reinitzer, F. *Monatsh. Chem.* **1888,** 9, 421-441.

(2) Zhou, Y.; Briand, V. A.; Sharma, N.; Ahn, S.-k.; Kasi, R. M. *Materials* **2009,** 2, 636-660.

(3) Xu, J.-T.; Xue, L.; Fan, Z.-Q. *Macromolecules* **2006,** 39, 2981-2988.

(4) Felekis, T.; Tziveleka, L.; Tsiourvas, D.; Paleos, C. M. *Macromolecules* **2005,** 38, 1705-1710.

(5) Lopez-Quintela, M. A.; Akahane, A.; Rodriguez, C.; Kunieda, H. *J. Colloid Interface Sci.* **2002,** 247, 186-192.

(6) Klok, H. A.; Hwang, J.; Iyer, S.; Stupp, S. *Macromolecules* **2002,** 35, 746-759.

(7) Yang, H.; Jia, L.; Zhu, C.; Di-Cicco, A.; Levy, D.; Albouy, P.-A.; Li, M.-H.; Keller, P. *Macromolecules* **2010,** 43, 10442-10451.

(8) Kaneko, T.; Nagasawa, H.; Gong, J. P.; Osada, Y. *Macromolecules* **2004,** 37, 187-191.

(9) Nagahama, K.; Ueda, Y.; Ouchi, T.; Ohya, Y. *Biomacromolecules* **2007**, 3938-3943.

(10) Tsiourvas, D.; Felekis, T.; Sideratou, Z.; Paleos, C. M. *Macromolecules* **2002,** 35, 6466-6469.

(11) Mouritsen, O. G.; Zuckermann, M. J. *Lipids* **2004,** 39, 1101-1113.

(12) Kurzchalia, T. V.; Ward, S. *Nat. Cell Biol.* **2003,** 5, 684-688.

(13) Tschierske, C. *Curr. Opin. Colloid Interface Sci.* **2002,** 7, 355-370.

(14) Tschierske, C. *J. Mater. Chem.* **1998,** 8, 1485-1508.

(15) Fischer, H.; Poser, S.; Arnold, M. *Liq. Cryst.* **1995,** 18, 503-508.

(16) Schneider, A.; Zanna, J. J.; Yamada, M.; Finkelmann, H.; Thomann, R. *Macromolecules* **2000,** 33, 649-651.

(17) Abeysekera, R.; Bushby, R. J.; Caillet, C.; Hamley, I. W.; Lozman, O. R.; Lu, Z. B.; Robards, A. W. *Macromolecules* **2003,** 36, 1526-1533.

(18) Ansari, I. A.; Castelletto, V.; Mykhaylyk, T.; Hamley, I. W.; Lu, Z. B.; Itoh, T.; Imrie, C. T. *Macromolecules* **2003,** 36, 8898-8901.

(19) Yi, Y.; Fan, X. H.; Wan, X. H.; Li, L.; Zhao, N.; Chen, X. F.; Xu, J.; Zhou, Q. F. *Macromolecules* **2004,** 37, 7610-7618.

(20) Lee, M.; Cho, B.-K.; Zin, W.-C. *Chem. Rev.* **2001,** 101, 3869-3892.

(21) Lee, M.; Oh, N.-K.; W.-C., Z. *Chem. Commun.* **1996**, 1787-1788.

(22) Lee, M.; Oh, N.-K. *J. Mater. Chem.* **1996,** 6, 1079-1086.

(23) Hofmann, A. M.; Wipf, R.; Stühn, B.; Frey, H. *Macromolecules* **2011,** 44, 6767-6775.

(24) Lapienis, G.; Penczek, S. *Biomacromolecules* **2005,** 6, 752-762.

(25) Wurm, F.; Nieberle, J.; Frey, H. *Macromolecules* **2008,** 41, 1184-1188.

(26) Dworak, A.; Baran, G.; Trzebicka, B.; Walach, W. *React. Funct. Polym.* **1999,** 42, 31-36.

(27) Dimitrov, P.; Utrata-Wesolek, A.; Rangelov, S.; Walach, W.; Trzebicka, B.; Dworak, A. *Polymer* **2006,** 47, 4905-4915.

(28) Hofmann, A. M.; Wurm, F.; Frey, H. *Macromolecules* **2011**.

29) Mangold, C.; Wurm, F.; Obermeier, B.; Frey, H. *Macromol. Rapid Commun.* **2010,** 31, 258-264.

(30) Eberich, M.; Keul, H.; Möller, M. *Macromolecules* **2007,** 40, 3070-3079.

(31) Halacheva, S.; Rangelov, S.; Tsvetanov, C. B. *Macromolecules* **2006,** 39, 6845-6852.

(32) Dimitrov, P.; Rangelov, S.; Dworak, A.; Haraguchi, N.; Hirao, A.; Tsvetanov, C. B. *Macromol. Symp.* **2004,** 215, 127-139.

(33) Wurm, F.; Nieberle, J.; Frey, H. *Macromolecules* **2008,** 41, 1909-1911.

(34) Mangold, C.; Wurm, F.; Obermeier, B.; Frey, H. *Macromolecules* **2010,** 43, 8511-8518.

(35) Hofmann, A. M.; Wurm, F.; Hühn, E.; Nawroth, T.; Langguth, P.; Frey, H. *Biomacromolecules* **2010**, 568-574.

(36) Dworak, A.; Baran, G.; Trzebicka, B.; Walach, W. *React. Funct. Polym.* **1999,** 42, 31-36.

(37) Xu, J.-T.; Xue, L.; Fan, Z.-Q.; Wu, Z.-H.; Kim, J. K. *Macromolecules* **2006,** 39, 2981-2988.

(38) Miao, J. J.; Xu, G. Q.; Zhu, L.; Tian, L.; Uhrich, K. E.; Avila-Orta, C. A.; Hsiao, B. S.; Utz, M. *Macromolecules* **2005,** 38, 7074.

(39) Lee, M.; B.-K., C.; Kim, H.; Zin, W.-C. *Angew. Chem., Int. Ed.* **1998,** 37, 638-640.

(40) Lee, M.; Cho, B.-K.; Kim, H.; Yoon, J.-Y.; Zin, W.-C. *J. Am. Chem. Soc.* **1998,** 120, 9168-9179.

(41) Lee, M.; Yoo, Y.-S. *J. Mater. Chem.* **2002,** 12, 2161-2168.

Conclusion and outlook

Conclusion and outlook

Polyether lipids based on poly(ethylene glycol) (PEG) and polyglycerol (PG) have been synthesized and their application for the formation of lipid vesicles, so-called “liposomes”, and the characterization of their physical behavior are presented.

During the last decades, PEG-modified lipids have attracted increased attention due to some exceptional characteristics, for instance their biocompatibility and their ability of self-assembly in various patterns. Especially in the field of biomedical research, amphiphilic polymers, such as PEG-conjugated phospholipids, have been investigated and applied for the preparation of drug carrier systems. Thus, PEG-coated liposomes show improved stabilities during storage in cell culture as well as in *in vivo* experiments and are approved for the encapsulation of cytostatica in different cancer therapies. A review about the basic science concerning liposomes, the employed polymeric systems and the approved medical formulations is given in the introducing part of this thesis.

The combination of linear and hyperbranched polymerization techniques for the ring-opening anionic polymerization of different epoxide monomers, such as ethylene oxide (EO), ethoxyethyl glycidyl ether (EEGE), isopropylidene glyceryl glycidyl ether (IGG) and glycidol using hydrophobic initiators allows the synthesis of multifunctional polyether lipids. Following this approach, a variety of amphiphilic stealth-type polymer lipids with systematically varied compositions (homopolymers, block copolymers and random copolymers) as well as structures (linear, branched and hyperbranched) have been obtained (Figure 1).

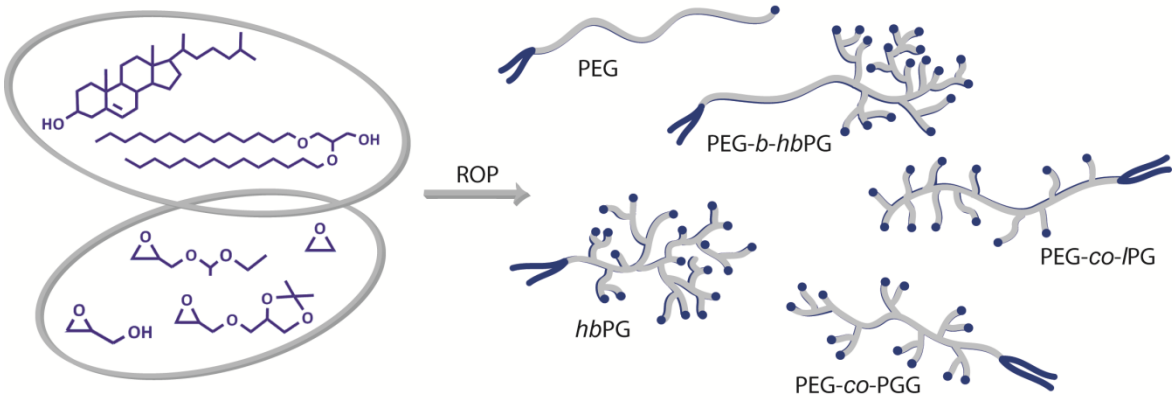

Figure 1. Structural variation of amphiphilic polyethers obtained via oxyanionic ring-opening polymerization of different epoxide monomers.

The resulting synthetic polyether lipids have been used for the preparation of functional liposomes and siRNA-loaded liposomes (cooperation Johannes Gutenberg-University Mainz, Prof. Langguth and Prof. Helm). The multiple functionality of the novel structures has been employed for the attachment of labeling moieties and specific targeting sites, exploiting the multivalent nature for active drug targeting.

Furthermore, the characterization of the physical behavior of these synthetic polyether lipids, for instance the self-assembly on the water-air interface in Langmuir and Langmuir-Blodgett films, are presented (cooperation Martin-Luther-University Halle, Prof. Kressler). Additionally, the strong interactions of cholesterol-initiated liner-hyperbranched PEG-PG block copolymers with monolayers of 1,2-dipalmitoyl-*sn*-glycero-3-phosphocholine, which are crucial for the anchoring of the polyether lipids in liposomal membranes, have been investigated.

Self-assembly in thermotropic phases has been long known for cholesterol-derived compounds. In fact, the first observation of liquid crystalline organization was made for cholesteryl benzoates and cholesteryl acetates. Unusual liquid crystalline polymers consisting of one single mesogenic cholesterol unit and linear polyglycerol (PG) as well as poly(ethylene glycol)-poly(glycerol) and poly(ethylene glycol)-poly(glyceryl glycidyl ether) block copolymer chains have been synthesized. The liquid crystalline behavior depends on the molecular weights and architecture of the polyether chains attached to the cholesterol moiety. Due to the strong ordering effect of cholesterol and the phase segregation between the apolar cholesterol and the highly polar polyether chains, LC phases are present over a broad temperature range and up to a high degree of polymerization (cooperation TU Darmstadt, Prof. Stühn). Cholesterol can thus be regarded as a valuable rod-type block for rod-coil block copolymers, exerting a strong ordering effect on the flexible, isotropic polyether chains.

Several projects directed at novel, complex polyether lipids in this thesis have motivated intensified studies in a number of related directions. Due to the broad nature of these fields, several issues could not be resolved in the limited context of this thesis, but present intriguing scientific topics for subsequent works.

In the field of liposome research further investigation of encapsulation efficiencies of PEG-PG-coated liposomes for siRNA as well as their stability during storage represents an ongoing project. Detailed studies regarding the cytotoxicity of these liposomal formulations and their transport properties are in progress. Furthermore, the specific targeting of the multifunctional

liposomes using folate-mediated endocytosis is studied, exploiting the multivalent nature of the polyether lipids for active drug targeting.

Intensified characterization of the liquid crystalline behavior of cholesterol-initiated PEG-PG and PEG-PGG block copolymers via small angle X-ray scattering is presently carried out and will be presented in the near future. In future projects, linear poly(glycerol) liquid crystals shall be functionalized with crosslinking moieties, such as methacrylates, in order to synthesize stable liquid crystalline hydrogels and networks.

Appendix

Macromolecular Chemistry and Physics

Macromolecular Journals

Full Paper

α,ω_n-Heterotelechelic Hyperbranched Polyethers Solubilize Carbon Nanotubes[a]

Frederik Wurm, Anna Maria Hofmann, Anja Thomas, Carsten Dingels, Holger Frey*

The synthesis of novel linear-hyperbranched (*linhb*) polyether block copolymers based on poly(ethylene oxide) and branched poly(glycerol), bearing a single pyrene or myristyl moiety at the α-position of the linear chain is described. The polymers exhibit low polydispersity ($\overline{M}_w/\overline{M}_n < 1.3$) and controlled molecular weights ($\overline{M}_n = 5\,000\ g \cdot mol^{-1}$). The mainly hydrophilic block copolymers with multiple hydroxyl end groups readily dissolve multiwalled carbon nanotubes (MWCNTs) in water by mixing and subsequent sonification, resulting in noncovalent attachment of the *linhb* hybrid structure to the carbon nanotubes (CNTs). Transmission electron microscopy (TEM) was employed to visualize the solubilized nanotubes; after sulfation of the multiple hydroxyl groups the polymer layer was detected in the TEM images.

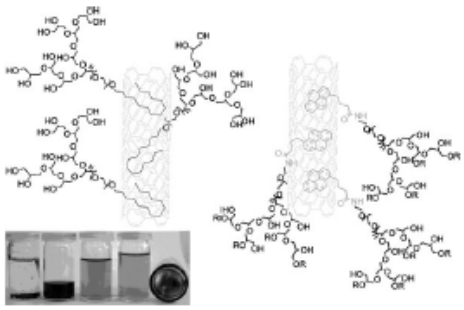

Introduction

Due to their unique physical, mechanical, and chemical properties, carbon nanotubes (CNTs) have attracted immense attention in recent years after their discovery in 1990.[1] However, their strong aggregation, resulting in insolubility in most common solvents is generally considered as a significant disadvantage for the use of CNTs. Particularly, their insolubility in water is one of the major concerns regarding their potential biomedical application[2] (e.g., for biosensors, drug delivery devices, and biomedical imaging).

F. Wurm, A. M. Hofmann, A. Thomas, C. Dingels, H. Frey
Institut für Organische Chemie, Makromolekulare Chemie, Johannes Gutenberg-Universität Mainz, Duesbergweg 10–14, D-55099 Mainz, Germany
E-mail: hfrey@uni-mainz.de

[a] Supporting information for this article is available at the bottom of the article's abstract page, which can be accessed from the journal's homepage at http://www.mcp-journal.de, or from the author.

In the last decade two main strategies have been developed to introduce (aqueous) solubility: covalent and noncovalent functionalization of CNTs. The covalent approach includes chemical modification[3] (e.g., halogenation, grafting of polymers, cycloaddition, etc.) to achieve sidewall functionalization, or defect site chemistry (e.g., oxidation[4]), allowing direct covalent attachment of substituents. Although chemical functionalization or modification provides a convenient opportunity for solubilizing CNTs, the major drawback is a shortening of the average tube length and surface destruction, resulting in a change in the electronic structure as well as product mixtures due to side reactions. The noncovalent functionalization is based on van der Waals (vdW) forces or π–π-stacking and thus offers the possibility of attaching solubilizing moieties without modification of the electronic structure of the tubes.[5] Several recent reports have shown that pyrene-carrying (linear) polymers,[6] oligothiophene-terminated poly(ethylene glycol) (PEG),[7] detergents,[8] or starch[9] can effectively solubilize CNTs in a supramolecular manner.

Only a few reports on the noncovalent attachment of hyperbranched (*hb*) polymers to nonmodified CNTs have

Macromol. Chem. Phys. **2010**, *211*, 932–939

InterScience

DOI: 10.1002/macp.200900652

been published very recently.[10] In the reported cases, hyperbranched materials of broad polydispersity with multiple interaction sites have been combined with the CNTs, achieving solubilization in organic solvents and water. However, to the best of our knowledge, there are no reports on the supramolecular attachment of specifically designed hyperbranched structures with a single, focal interaction moiety to multiwalled CNTs (MWCNTs). This is highly relevant, since the multifunctionality and compact globular structure of hyperbranched polymers give access to a wide range of modification reactions for further functionalization. Covalent grafting of *hb*-polyoxetanes and noncovalent adsorption of poly(phenylene vinylene)s on single-walled CNTs has also been reported.[11]

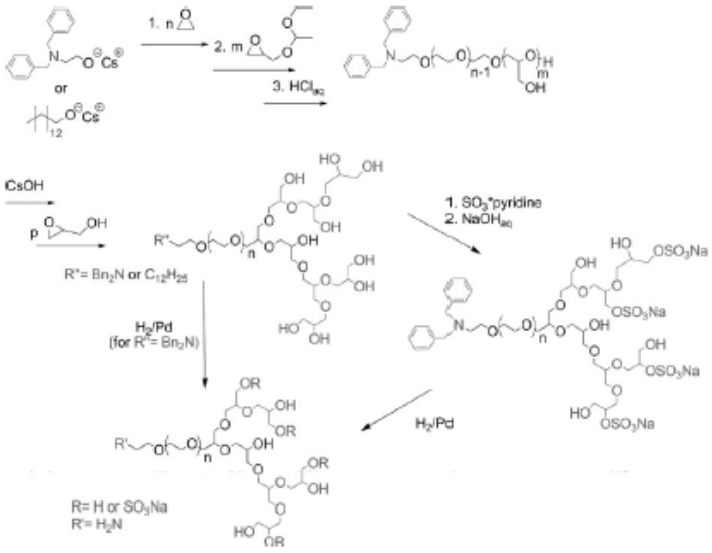

Scheme 1. Synthesis of α,ω_n-telechelics; a linear-hyperbranched polymer is obtained for $n > 1$, when omitting the polymerization of ethylene oxide ($n = 0$), a monoamino-hyperbranched polyglycerol homopolymer is formed.

Our group has investigated the ring-opening multibranching polymerization of glycidol that permits the controlled synthesis of *hb*-polyglycerol (*hb*PG) with polydispersities usually below 1.5 and adjustable molecular weights.[12] Polydispersity can be further reduced (<1.3) by using a two-step protocol for the synthesis of double-hydrophilic linear-hyperbranched (*linhb*) block copolymers based on PEG and *hb*PG that are merely built up from biocompatible segments avoiding any other linkages than aliphatic ethers.[13] In related works, amphiphilic derivatives with *hb*PG segments have also been developed.[14]

In order to obtain biocompatible conjugates of MWCNTs, PEG as one of the most important biocompatible, water-soluble polymers has been employed.[2,15] Its low toxicity, excellent solubility in aqueous solutions and extremely low immunogenicity and antigenicity as well as good pharmacokinetic and biodistribution behavior render PEG the polymer of choice for versatile biomedical applications.[15] The low intrinsic viscosity of *hb*PG and particularly its large number of derivatizable hydroxyl groups can provide advantages in pharmaceutical and medical fields compared to its linear analogs.[16] As expected from its structural similarity to PEG and polysaccharides, *hb*PG (at least up to $\overline{M}_n \approx 3\,000\ g \cdot mol^{-1}$) has been found to be as biocompatible as PEG.[16b]

In this paper we report different strategies for the supramolecular modification of MWCNTs with α,ω_n-heterotelechelic *linhb*-polyethers by (i) noncovalent pyrene-modified polymers in the α-position (π–π-stacking) or (ii) vdW interactions, based on myristyl alcohol as the respective initiator. In addition, first results of a novel covalent strategy relying on active esters attached to the CNTs are presented.

Experimental Part

Instrumentation

^1H, ^{13}C nuclear magnetic resonance spectra were recorded using a Bruker AC 300 or a Bruker AMX 400 spectrometer operated at 300 or 400 MHz for ^1H NMR, employing deuterated dimethylsulfoxide (DMSO) as a solvent. ^{13}C NMR spectra are referenced internally to solvent signals and were recorded at 100.15 MHz. FT-IR spectra were recorded on a Nicolet SDXC FT-IR spectrometer equipped with an ATR unit. SEC measurements in dimethylformamide (DMF) containing $0.25\ g \cdot L^{-1}$ of lithium bromide, an Agilent 1100 Series GPC Setup (gel permeation chromatography) was used as an integrated instrument, including a PSS HEMA column ($10^6/10^5/10^4\ g \cdot mol^{-1}$), a UV (254 nm), and RI detector. Calibration was carried out using poly(styrene) or poly(ethylene oxide) standards, provided by Polymer Standards Service. The eluent was used at 50 °C and at a flow rate of $1\ mL \cdot min^{-1}$. Matrix-assisted laser desorption and ionization time-of-flight (MALDI-TOF) measurements were performed on a Shimadzu Axima CFR MALDI-TOF mass spectrometer equipped with a nitrogen laser delivering 3 ns laser

pulses at 337 nm. α-Cyano-4-hydroxycinnamic acid was used as matrix. Samples were prepared by dissolving the polymer in methanol at a concentration of 10 g · L^{-1}. A 10 μL aliquot of this solution was added to 10 μL of a 10 g · L^{-1} solution of the matrix and 1 μL of a solution of KTFA (0.1 M in methanol as cationization agent). A 1 μL aliquot of the mixture was applied to a multistage target to evaporate $CHCl_3$ and create a thin matrix/analyte film. The samples were measured in positive ion and in reflection mode of the spectrometer.

Reagents

Diglyme (99%, Acros), glycidol (99%, Acros), ethanolamine (98%, Acros), pyridine (99%, Acros) were purified by distillation from CaH_2 directly prior to use. Ethoxyethyl glycidyl ether (EEGE) or isopropylidene(glyceryl glycidyl ether) (IGG) was prepared as described in literature,[23,27] dried over CaH_2, and freshly distilled before used. The procedure for introduction of sulfate groups into hyperbranched poly(glycerol) can be found elsewhere and was adopted.[18] Sulfur trioxide pyridine complex (99%), pentafluorophenol (99%), benzyl bromide (99%), 1-pyrene-butyric acid (97%), myristyl alcohol (99%) was purchased from Aldrich and used as-received. MWCNTs were purchased from Aldrich and used as-received (outer diameter: 10–15 nm, length: 0.1–10 μm, >90% AS MWCNT), and "short" MWCNT (compare Figure S17) were obtained from Aldrich ("bucky tubes," as produced cylinders 7.5% MWCNT content).

Cesium hydroxide monohydrate, palladium on activated charcoal, potassium carbonate, *N,N'*-dicyclohexylcarbodiimide (DCC) was purchased from Acros and used as-received. Deuterated DMSO-d_6 was purchased from Deutero GmbH, dried, and stored over molecular sieves. Methanol and other solvents and reagents were purchased from Acros and used as-received, if not otherwise mentioned.

N,N-Dibenzyl-2-aminoethanol

A mixture of 2-aminoethanol (30 g, 0.5 mol), benzyl bromide (171.3 g, 1 mol), K_2CO_3 (276 g, 2 mol), and water (900 mL) was refluxed and vigorously stirred for 5 h. The organic phase was diluted with diethyl ether and separated from the aqueous layer. The organic phase was washed two times with water (each 100 mL, dried over Na_2SO_4), and evaporated to give 105 g of crude product as a pale yellow oil. The product was crystallized from 9:1 mixture pentane/ethyl acetate and recrystallized twice to form white crystals mp. 38 °C, 60 g (50%) ^{1}H NMR ($CDCl_3$): δ = 7.31–7.32 (m, 10 H, Ar-H), 3.60 (s, 4 H, CH_2Ph), 3.57 (t, J = 5.7 Hz, 2H, CH_2OH), 2.65 (t, J = 5.4 Hz, 2H, CH_2CH_2OH). ^{13}C NMR ($CDCl_3$): δ = 54.7 (CH_2N), 58.4 ($C_6H_5CH_2N$), 58.5 (CH_2OH), 127.2, 128.4, 129.0, 138.7 (aromatic carbons).

1-Pyrene-butyric Acid Pentafluorophenyl Ester

1-Pyrene-butyric acid (1 g, 3.47 mmol) was dissolved in a mixture of dry dichloromethane:dry pyridine (50:50, ca. 25 mL) at 50 °C, cooled to room temperature, and then pentafluorophenol (645 mg, 3.5 mmol) was added. The reaction mixture was cooled with an ice bath, and DCC (714 mg, 3.5 mmol) in dry dichloromethane (5 mL) was added dropwise within 30 min. The mixture was allowed to warm up to room temperature overnight. The DCU formed was removed (filtration) and washed with dichloromethane (10 mL). The combined solutions were concentrated and kept at room temperature for 5 h. A small amount of residual DCU was removed by filtration, the solvent was evaporated, and the crude mixture was purified via flash chromatography with dichloromethane as eluent. Yield: 90% after column, yellow crystalline powder. ^{1}H NMR (300 MHz, $CDCl_3$): δ = 8.32–7.88 (m, aromat.), 3.50 (t, 2H), 4.31 (m, 1H, CHN methin.), 2.80 (t, 2H), 2.35 (q, 2H).

General Procedure for Anionic Polymerization

Linear Block Copolymers

N,N-Dibenzyl-2-aminoethanol or myristyl alcohol was dissolved in benzene in a Schlenk flask and a stoichiometric amount of cesium hydroxide monohydrate was added under argon. The mixture was stirred at 60 °C for 45 min and evacuated at 90 °C (10^{-2} mbar) for 2 h to remove benzene and water. The dry cesium alkoxide was dissolved in dry DMSO or toluene (20 wt.-%). In a separate setup, THF was cryo-transferred into a Schlenk flask from a dark purple colored sodium/benzophenon THF solution. Subsequently, ethylene oxide was first cryo-transferred to a graduated ampoule and then into the flask containing THF to produce a ca. 50 wt.-% solution. The solution was kept at 0 °C and the initiator was added via canula. The slightly yellow mixture was allowed to slowly warm up to room temperature and polymerization was performed for 1–2 d in vacuo at 40 °C. Subsequently the flask was filled with argon, the appropriate amount of EEGE or IGG was added with a syringe and temperature was raised to 80 °C for 12 h. The polymerization was terminated by addition of methanol and acidic ion exchange resin. Filtration and precipitation in cold diethyl ether resulted in the pure polymer. Yields: 95% quantitative.

For *N,N*-dibenzyl-2-aminoethanol as the respective initiator and EEGE as second monomer: ^{1}H NMR (300 MHz, $CDCl_3$): δ = 7.33 (m, C_6H_5), 4.69 (br, acetal-H), 3.86–3.37 (polyether backbone), 2.32 (br, NCH_2Ph), 1.28–1.15 (br, CH_3 acetal).

For myristyl alcohol as the respective initiator and IGG as second monomer: ^{1}H NMR (300 MHz, $CDCl_3$): δ = 4.3 (m, 1H, *CH* acetal), 4.07 (m, 1H), 3.86–3.37 (polyether backbone), 1.45 (br, CH_2 (initiator)), 1.44 (br, 3H, CH_3), 1.38 (br, 3H, CH_3), 1.23 (CH_2 (initiator)), 0.84 ppm (CH_3 (initiator)). 0.84 ppm and broad signals for the methylene groups at 1.23 and 1.45 ppm.

DPn of EEGE or IGG was determined by comparison of aromatic signals of the initiator and the methyl signals for PEEGE or PIGG block. Molecular weights were obtained by comparison of the aromatic protons with the polyether signals.

Deprotection to Linear Block Copolymers

The acetal protecting groups were removed by the addition of 1 M hydrochloric acid to a 20% solution of the polymer in ethanol and stirring for 30 min. Purification of the block copolymer was achieved by repetitive precipitation from a concentrated ethanolic solution in diethyl ether or by exhaustive dialysis in methanol using a dialysis tube with an MWCO of 1 000 g · mol^{-1}. Yields: 80–90%. The polymers with *N,N*-dibenzyl-2-aminoethanol as initiator are usually obtained as the respective ammonium chlorides; recovery of the free amine is achieved by addition of triethylamine during dialysis.

Macromol. Chem. Phys. **2010**, *211*, 932–939

Macromolecular Journals

DOI: 10.1002/macp.200900652

^{1}H NMR (300 MHz, DMSO-d_6): δ = 11.14 (br, Bn_2NH^+), 7.62, 7.40 (br, C_6H_5), 4.59 (br, OH), 3.59–3.27 (polyether backbone), 2.46 (br, NCH_2Ph).

Hypergrafting to Linear-Hyperbranched Block Copolymers

The linear macroinitiator was placed in a Schlenk flask and dissolved in benzene (20 wt.-%). Subsequently the appropriate amount of cesium hydroxide monohydrate was added to achieve 30% of deprotonation of the hydroxyl groups along the backbone. After heating to 60 °C for 30 min and evacuation (10^{-2} mbar) at 90 °C for 2 h dry diglyme was added to produce a 20 wt.-% solution and the flask was placed in an ultrasonic bath for 15 min to ensure complete suspension of the macroinitiator. The mixture was heated to 100 °C and a 20 wt.-% solution of glycidol in dry diglyme was added slowly with a syringe over a period of ca. 12 h. The reaction was terminated by addition of an excess of methanol and an acidic cation exchange resin. The products were filtrated, concentrated, and precipitated into cold diethyl ether. The resulting material was dried in vacuo for 2 d at 40 °C. Yields: quantitative.

^{1}H NMR for *N,N*-dibenzyl-2-aminoethanol as initiator (300 MHz, DMSO-d_6): δ = 7.62, 7.40 (br, C_6H_5), 4.79–4.42 (br, OH, different signals due to branched PG), 3.59–3.27 (polyether backbone), 2.46 (br, NCH_2Ph).

Hydrogenation of Linear-Hyperbranched Block Copolymers H_2N-Poly(ethylene oxide)-Block-Hyperbranched-poly(glycerol)

Under an argon atmosphere, 1 g *N,N*-dibenzyl-poly(ethylene oxide)-*block*-hyperbranched-poly(glycerol) was dissolved in methanol and palladium on activated charcoal (10%) was added. The vessel was flushed with hydrogen (8 bar) and the reaction was allowed to stir for 48–72 h at room temperature, completion of the reaction was monitored via ^{1}H NMR spectroscopy. The solution was filtered, concentrated, and precipitated into cold diethyl ether. Yields: quantitative.

^{1}H NMR (300 MHz, DMSO-d_6): δ = 4.79–4.42 (br, OH, different signals due to branched PG), 3.59–3.27 (polyether backbone).

Synthesis of Sulfates 2a and 2b

The sulfation of the polymers 2a and 2b was performed according to the method described by Haag and coworkers.[18] (a) To a stirred solution of 500 mg polymer Bn_2NhbPG_{47} (6.7 mmol OH-groups) in 2 mL DMF was added dropwise a solution of 1.07 g (6.7 mmol) SO_3/pyridine complex in 7 mL DMF at 60 °C under an argon atmosphere. The reaction mixture was further stirred at 60 °C overnight. Distilled water (5 mL) was added to the cooled solution and immediately 1 M NaOH was added to reach a pH of at least 11. After concentration in vacuo the crude product was further purified by dialysis in water. Evaporation of the solvent gave the product as a yellow solid. Yield: 380 mg. FT-IR (ν, cm^{-1}): 3 439 ($PG(OH)_n$ stretch), 2 872 ($-CH_2-$ stretch (polyether backbone)), 1 653 (–C=C– stretch, aromatic), 1 458 ($-CH_2-$ deform.), 1 348 (–C–N– stretch), 1 219 (–C–O–SO_3), 1 068 (–C–O–C– stretch), 1 001 (–C–O–C– stretch), 939, 776 (=C–H deform.), 578.

Deprotection of the Polymer Sulfates

Under an argon atmosphere, the polymer sulfates were dissolved in water and acetic acid and palladium on activated charcoal (10%) was added. The vessel was flushed with hydrogen and the reaction was allowed to stir for 5 d at room temperature. The solution was centrifuged, filtered, and the solvent evaporated to obtain the product as a solid. Yields: quantitative.

^{1}H NMR (300 MHz, D_2O): δ = 4.7–4.5 ($-CH_2OSO_3Na$), 4.35–3.35 (polyether backbone).

Coupling Reaction of α,ω_n-Heterotelechelic H_2N-Poly(ethylene oxide)-Block-Hyperbranched-poly(glycerol) with Pyrene

H_2N-poly(ethylene oxide)-*block*-hyperbranched-poly(glycerol) (0.2 g, $\overline{M}_n$ = 5 200 g·mol^{-1}, 0.038 mmol) was dissolved in 3 mL of degassed DMF and 50 µL of freshly distilled triethylamine was added under argon. Pyrenebutyric pentafluorophenol ester (32 mg, 0.071 mmol) was added and the reaction was allowed to stir for 24 h at room temperature. The excess PFP-ester was removed by repetitive precipitation from DMF into cold acetone or exhaustive dialysis in DMF (MWCO 1 000 g·mol^{-1}). Yield: 0.2 g (quantitative).

^{1}H NMR (300 MHz, DMF-d_7): δ = 8.4–7.9 (br, aromat.), 4.79–4.42 (br, OH, different signals due to branched PG), 3.59–3.27 (polyether backbone), 2.6–2.0 (br, CH_2).

Coupling Reaction of α,ω_n-Heterotelechelic Polymers with MWCNTs

Noncovalent

Pyrene-activated polymer (45 mg) and MWCNTs (2.8 mg) were suspended in 3 mL of water and mixed by sonification for 3 h. After sonification the deep black solution was filtered through a Kim-wipe filter to remove traces of undissolved material and evaporated to give the MWCNT–polymer conjugate in quantitative yield. Dialysis of the aqueous solution did not reduce the amount of conjugate, indicating complete adsorption of the block copolymers onto the tubes.

Covalent

Acid treated MWCNTs (200 mg) were heated in thionyl chloride (30 mL) to produce acyl chloride groups.[3] The MWCNT–acyl chloride was dissolved in anhydrous DMF, 0.6 g pentafluorophenol were added, and the resulting mixture was sonificated for 30 min and stirred at room temperature for additional 12 h. Filtration to remove the solvents and excess reagents gave the MWCNT-active-ester (MWCNT-PFP) as a black solid (Yield quantitative, degree of functionalization not determined) (Scheme 2).

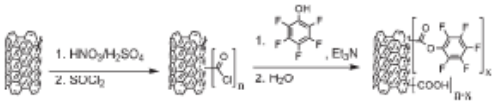

Scheme 2. Covalent modification of MWCNTs with PFP-active esters.

Covalent Coupling of Amino-terminated Poly(ether)s to MWNCT-PFP

MWCNT-PFP (3.7 mg) and H_2NhbPG (60 mg) ($\overline{M}_n = 6\,500\ g \cdot mol^{-1}$) were dissolved in anhydrous DMF and triethylamine was added to obtain the free amine. The mixture was sonicated for 5 h and stirred at room temperature for additional 12 h; the mixture was filtrated to obtain a black solution of MWCNT-CO-NH-PG in DMF. Evaporation gave the black solid product (Yield compared to polymer 70–90%).

FTIR (ν, cm^{-1}): 3 406 ($PG(OH)_n$ stretch), 2 878 ($-CH_2-$ stretch (polyether backbone)), 1 637 (C=O stretch), 1 458 ($-CH_2-$ deform.), 1 115 (–C–O–C– stretch).

Results and Discussion

The anionic polymerization of epoxides conveniently allows the incorporation of several (functional) initiators that can be selectively addressed subsequent to the polymerization of glycidol to introduce specific α-moieties (compare Scheme 1). The selective attachment of *linhb* block copolymers to generate such nanocomposites via a single, specific α-functionality opens the way for several further modifications in the *hb*-periphery, such as conjugation with drugs or electroactive moieties. In a first account of our group, noncovalent bioconjugation of avidin was found to be feasible via biotinylated *linhb*- and *hb*-polyethers.[19] Several polymers have been synthesized via the protocol summarized in Scheme 1 (detailed characterization data can be found in Table 1 and the Supporting Information).

As an example for selective modification of the hyperbranched polyglycerol block, the OH-groups can be converted into sulfates to enhance water solubility and to introduce specific biological properties. This reaction proceeds smoothly in DMF via the pyridine complex of sulfur trioxide.[18] The degrees of functionalization obtained for the sulfated samples was determined via ^{1}H NMR and were found to be similar as reported for nonfunctional *hb*PG homopolymers previously (i.e., 45% sulfate groups were targeted and achieved).

In the α-position of the *linhb* polyethers the dibenzyl-protective group can be removed conveniently via catalytic hydrogenation, liberating the primary amino group. Quantitative pyrene modification was achieved by the pentafluorophenyl (PFP) active ester of pyrene butyric acid and monitored via MALDI-ToF spectrometry (cf. Scheme 3 and Figure 1B, SEC traces and NMR spectrum can be found in the Supporting Information).

Table 1. Characterization data of linear-hyperbranched block copolymers and hyperbranched poly(glycerol) homopolymers.

#	Compound	$\overline{M}_n$ [a]	PDI [a]	$\overline{M}_n$ [b]
1	Bn_2NPEG_{25} *lin*PG_5	1 500	1.06	1400
2	Bn_2NPEG_{125} *lin*PG_{15}	6 300	1.05	6500
1a	Bn_2NPEG_{25} *hb*PG_{50}	4 700	1.23	5200
2a	Bn_2NPEG_{125} *hb*PG_{50}	8 400	1.19	9600
1a*	H_2NPEG_{25} *hb*PG_{50}	4 700	1.25	5200
2a*	H_2NPEG_{125} *hb*PG_{50}	8 200	1.18	9600
3	Bn_2N*lin*PG_{15}	1 200	1.17	1300
3a	Bn_2N*hb*PG_{80}	5 700	1.20	6300
3a*	H_2N*hb*PG_{80}	6 400	1.21	6300
4a	$C_{14}H_{29}O$-$PEG_{60}PGG_{15}$	4 800	1,08	5000
4b	$C_{14}H_{29}O$-PEG_{60} *hb*PG_{40}	5 200	1.19	5900

[a]Determined via size-exclusion chromatography in dimethylformamide versus polystyrene standards; [b]Determined via ^{1}H NMR spectroscopy in DMSO-d_6. *lin*PG: linear poly(glycerol), *hb*PG: hyperbranched poly(glycerol), PGG: poly(glyceryl glycidyl ether).

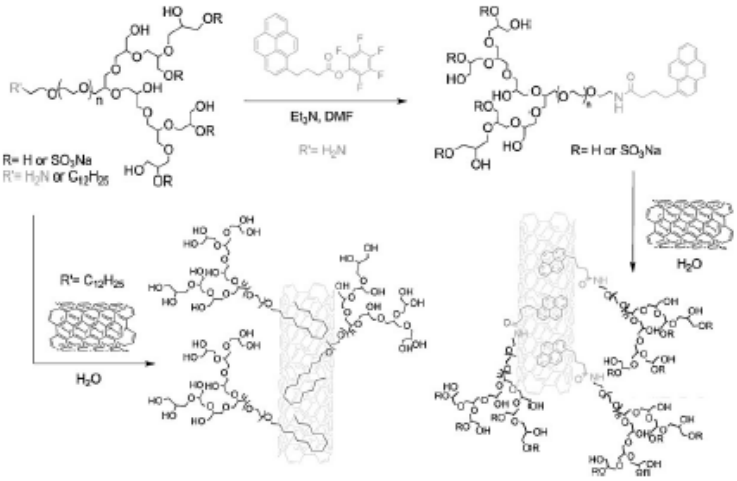

Scheme 3. Different strategies for noncovalent modification of MWCNT inducing water solubility. In α-position of the PEG-chains either a pyrene unit or a myristyl chain was attached.

Macromol. Chem. Phys. **2010**, *211*, 932–939

Macromolecular Journals

DOI: 10.1002/macp.200900652

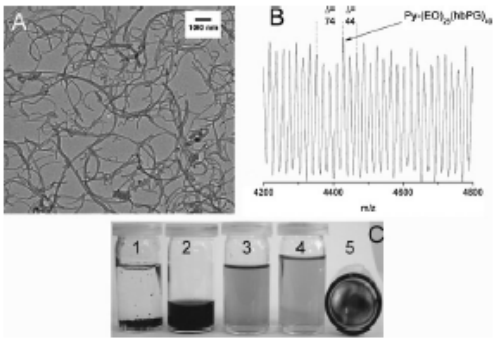

Figure 1. A: TEM image of an aqueous solution of pyrene-modified MWCNT. B: Section of MALDI-ToF of pyrene-modified PEG$_{25}$-*hb*PG$_{40}$. C: Images of aqueous MWCNT solutions: (1) Pristine MWCNT (not soluble), (2) myristyl-alcohol-modified PEG-*hb*PG (c = 10 g·L^{-1}), (3) pyrene-modified PEG$_{120}$-*hb*PG$_{50}$ (c = 0.3 g·L^{-1}, strongly diluted for UV measurements), (4) covalently modified MWCNT (c approx. 0.1 g·L^{-1}), and (5) film obtained after drying PEG$_{25}$-*hb*PG$_{40}$.

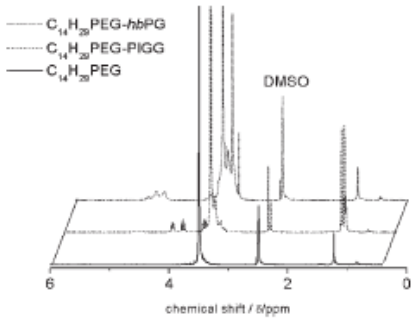

Figure 2. ^{1}H NMR spectra of myristyl alcohol-initiated PEG (bottom), C$_{14}$H$_{29}$PEG$_{60}$-PIGG$_{15}$ (middle), and the final product C$_{14}$H$_{29}$PEG$_{60}$-*hb*PG$_{40}$ (top).

With this strategy no side reactions or interferences with the multiple OH-groups were detected. The introduction of myristyl alcohol can be achieved directly by employing this compound as an initiator for the polymerization of ethylene oxide (the respective MALDI-ToF spectrum can be found in the Supporting Information). These polymers are amphiphilic and form micelles in water, but readily solubilize MWCNTs. It is worth mentioning that the synthetic protocol for the myristyl alcohol-modified PEG-*hb*PG is based on a novel strategy for an amphiphilic, branched polyether. Furthermore, it has to be emphasized that no further derivatization is necessary and polydispersities and molecular weights can easily be tailored, keeping the polydispersity low. For the solubilization experiments a polymer consisting of C$_{14}$H$_{29}$-PEG$_{60}$ *hb*PG$_{40}$ ($\overline{M}_n$ = 5 900 g·mol^{-1} PDI = 1.19) was applied. ^{1}H NMR spectra of different steps of the myristyl alcohol-based system are shown in Figure 2. The lower spectrum shows the first block "C$_{14}$H$_{29}$-PEG" with the respective broad signals for the initiator with a triplet for the methyl group at 0.84 ppm and broad signals for the methylene groups at 1.23 and 1.45 ppm. The middle spectrum is obtained from the protected linear precursor, here based on poly(isopropylidene(glyceryl glycidyl ether)), and the top spectrum was recorded for the final *linhb* block copolymer after hypergrafting with glycidol. The hyperbranched structure was confirmed via ^{13}C NMR analysis according to literature procedures[12] and is also visible in the ^{1}H NMR due to the different signals for the hydroxyl groups between 4 and 5 ppm.

Mixing of the pyrene-modified or myristyl alcohol-initiated block copolymers with MWCNT in water and subsequent sonification for approximately 3 h resulted in deep black solutions that were stable over months. The sulfated block copolymers gave dark solutions, *albeit* with lower CNT content; we assume this is due to interference of the polyanion with the pyrene adsorption. Interestingly, for the sulfated polymers, transmission electron microscopy (TEM) investigation directly revealed the polymer layer on the MWCNTs due to the enhanced contrast of sulfur. Predominantly rod-like polymer micelles have been detected (Figure 1 and Supporting Information).

UV/vis, TGA, and TEM studies confirmed efficient solubilization of MWCNTs in water by the polyhydroxyl-functional polymers. Figure 3A shows a typical TEM image of the supramolecular water-solubilized MWCNTs that are present as discrete nanotube structures (for additional images, see Supporting Information). ^{1}H NMR spectra of the CNT–polymer conjugates showed broad signals and the signals for myristyl alcohol or pyrene, respectively, can be hardly detected due to interaction with the nantotubes.

As an alternative to the supramolecular strategy presented here, a covalent approach for water-soluble MWCNTs relies on the oxidation of the tubes via HNO$_3$/H$_2$SO$_4$ introducing multiple carboxylic acid functionalities

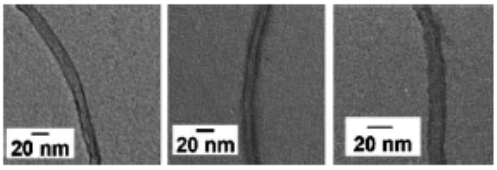

Figure 3. Transmission electron microscopy images of MWCNTs drop-cast from an aqueous solution (all samples were prepared with the same amount of MWCNTs). Left: C$_{14}$H$_{29}$O-PEG$_{60}$ *hb*PG$_{40}$(SO$_4$Na)$_n$, middle: C$_{14}$H$_{29}$O-PEG$_{60}$ *hb*PG$_{40}$, right: *hb*PG$_{80}$-@MWCNT (covalent).

that were reacted with thionyl chloride to form the acyl chlorides, and subsequently with pentafluorophenol to the respective active esters. The latter can react selectively with the polyethers carrying the amino group in the α-position in DMF. Also in this case stable, black aqueous solutions were formed after solvent exchange. This approach might be useful if the electronic properties of the tubes are not essential for a targeted application. However, the covalent approach is less controlled due to the harsh oxidation conditions (reaction scheme cf. Experimental Part). For this covalent solubilization approach shortened CNTs with a partly destroyed surface are detected via TEM, as expected. On the other hand, the novel covalent strategy relying on PFP-active esters may find useful application for other amine-containing polymers that will be investigated in the future.

How does the structure of the α,ω_n-block copolymers influence solubilization and surface coverage of the CNTs? TGA measurements show that by solubilizing CNTs with the *lin*hb systems introduced in this work the amount of solubilized CNTs can be further increased in comparison to the *hb*-homopolymer, probably due to steric effects. This can be supported by TGA measurements for different block ratios, indicating the lowest MWCNT-incorporation, when the *hb*PG$_{80}$ homopolymer ($\overline{M}_n = 6\,kg \cdot mol^{-1}$, PDI = 1.21) is used (Supporting Information).

Figure 3C shows images of the MWCNT solutions in water: (1) pristine MWCNT are insoluble in water; (2) myristyl alcohol-modified block copolymer solution ($c = 10\,g \cdot L^{-1}$); (3) pyrene-modified PEG$_{125}$-*hb*PG$_{50}$ ($\overline{M}_n = 6\,kg \cdot mol^{-1}$, PDI = 1.14) ($c = 0.3\,g \cdot L^{-1}$, strongly diluted for UV measurements); and (4) covalently modified MWCNT (c approx. $0.1\,g \cdot L^{-1}$) showing a clear and stable CNT solution. Interestingly, a homogeneous film was obtained after drying of the MWCNTs modified with PEG$_{25}$-*hb*PG$_{40}$ ($\overline{M}_n = 4.1\,kg \cdot mol^{-1}$, PDI = 1.25) due to the low T_g of *hb*PG (−30 °C) and suppression of the PEG melting point (Figure 3B-5).

Conclusion

We have presented a synthetic pathway for heterotelechelic *lin*hb block copolymers bearing a single pyrene moiety or aliphatic chain (myristyl alcohol) in the α-position, permitting supramolecular solubilization of MWCNTs in water. The block copolymers exhibit rather narrow molecular weight distributions with $\overline{M}_w/\overline{M}_n < 1.3$ in all cases; for myristyl alcohol as the respective initiator, this protocol allows the synthesis of complex amphiphiles in only two steps, which readily dissolve MWCNTs in water. The homogeneous aqueous solutions were stable over months. Additionally, partial functionalization of the OH-groups in *hb*PG into sulfates has been achieved and the first supramolecular solubilization of MWCNTs with an *hb*-polyelectrolyte was presented. Further studies concerning modification, drug loading, and circulation times are under investigation. Preliminary data for a versatile covalent approach relying on the selectivity of PFP-active esters to amines has also been presented.

Acknowledgements: H.F. acknowledges the *Fonds der Chemischen Industrie* (FCI) for valuable financial support. A.M.H. is grateful to the graduate class of excellence "*POLYMAT*" in the context of the graduate school of excellence MAINZ for funding. H.F. acknowledges the *SFB 625* and the *German Science Foundation* (DFG) for valuable support.

Received: November 21, 2009; Published online: February 1, 2010; DOI: 10.1002/macp.200900652

Keywords: carbon nanotubes; hyperbranched polymers; linear dendritic block copolymers; poly(ethylene glycol); polyglycerol

[1] S. Iijima, *Nature* **1991**, *354*, 56.
[2] Z. Liu, S. Tabakman, K. Welsher, H. Dai, *Nano Res.* **2009**, *2*, 85.
[3] D. Tasis, N. Tagmatarchis, A. Bianco, M. Prato, *Chem. Rev.* **2006**, *106*, 1105.
[4] [4a] I. D. Rosca, F. Watari, M. Uo, T. Akaska, *Carbon* **2005**, *43*, 3124; [4b] J. Liu, A. G. Rinzler, H. J. Dai, J. H. Hafner, R. K. Bradley, P. J. Boul, A. Lu, T. Iverson, K. Shelimov, C. B. Huffman, F. Rodriguez-Macias, Y. S. Shon, T. R. Lee, D. T. Colbert, R. E. Smalley, *Science* **1998**, *280*, 1253; [4c] A. V. Ellis, M. R. Waterland, J. Quinton, *Chem. Lett.* **2007**, *36*, 1172.
[5] [5a] S. Meuer, L. Braun, R. Zentel, *Chem. Commun.* **2008**, 3166, DOI: 10.1039/b803099e; [5b] D. Tasis, N. Tagmatarchis, V. Georgakilas, M. Prato, *Chem. Eur. J.* **2003**, *9*, 4000; [5c] G. Prencipe, S. M. Tabakman, K. Welsher, Z. Liu, A. P. Goodwin, L. Zhang, J. Henry, H. Dai, *J. Am. Chem. Soc.* **2009**, *131*, 4783.
[6] [6a] G. J. Bahun, C. Wang, A. Adronov, *J. Polym. Sci. Part A: Polym. Chem.* **2006**, *44*, 1941; [6b] C.-H. Xue, R.-J. Zhou, M.-M. Shi, Y. Gao, G. Wu, X.-B. Zhang, H.-Z. Chen, M. Wang, *Nanotechnology* **2008**, *19*, 215604.
[7] J. U. Lee, J. Huh, K. H. Kim, C. Park, W. H. Jo, *Carbon* **2007**, *45*, 1051.
[8] M. F. Islam, E. Rojas, D. M. Bergey, A. T. Johnson, A. G. Yodh, *Nano Lett.* **2003**, *3*, 269.
[9] A. Star, D. W. Steuerman, J. R. Heath, J. F. Stoddart, *Angew. Chem.* **2002**, *114*, 2618.
[10] [10a] T. Ogoshi, T. Saito, T. A. Yamagishi, Y. Nakamoto, *Carbon* **2009**, *47*, 117; [10b] W. Zhou, S. Lv, W. Shi, *Eur. Polym. J.* **2008**, *44*, 587.
[11] [11a] Y. Xu, C. Gao, H. Kong, D. Yan, Y. Z. Jin, P. C. P. Watts, *Macromolecules* **2004**, *37*, 8846; [11b] A. Star, F. Stoddart, *Macromolecules* **2002**, *35*, 7516; [11c] J. Zhang, Y. Zheng, P. Yu, S. Mo, R. Wang, *Polymer* **2009**, *50*, 2953.
[12] [12a] A. Sunder, R. Hanselmann, H. Frey, R. Mülhaupt, *Macromolecules* **1999**, *32*, 4240; [12b] D. Wilms, F. Wurm, J. Nieberle, P. Böhm, U. Kemmer-Jonas, H. Frey, *Macromolecules* **2009**, *42*, 3230; [12c] E. Barriau, L. Pastor-Pérez, E. Berger-Nicoletti, A. F.

DOI: 10.1002/macp.200900652

M. Kilbinger, J. Pérez-Prieto, H. Frey, S.-E. Stiriba, *J. Polym. Sci., Polym. Chem.* **2008**, *46*, 2049. [12d] D. Wilms, J. Nieberle, J. Klos, H. Löwe, H. Frey, *Chem. Eng. Technol.* **2007**, *30*, 1519; [12e] D. Wilms, S. E. Stiriba, H. Frey, *Acc. Chem. Res.* **2009**, DOI: 10.1021/ar900158p. [12f] M. Calderon, M. A. Quadir, S. Sharma, R. Haag, *Adv. Mater.* **2009**, *22*, 190.

[13] [13a] F. Wurm, J. Nieberle, H. Frey, *Macromolecules* **2008**, *41*, 1184; [13b] F. Wurm, U. Kemmer-Jonas, H. Frey, *Polym. Int.* **2009**, *58*, 989.

[14] [14a] V. Istratov, H. Kautz, Y.-K. Kim, R. Schubert, H. Frey, *Tetrahedron* **2003**, *59*, 4017; [14b] A. Sunder, T. Bauer, R. Mülhaupt, H. Frey, *Macromolecules* **2000**, *33*, 1330; [14c] T. Demina, I. Grozdova, O. Krylova, A. Zhirnov, V. Istratov, H. Frey, H. Kautz, N. Melik-Nubarov, *Biochemistry* **2005**, *44*, 4042.

[15] [15a] S. Zalipsky, *Adv. Drug Delivery Rev.* **1995**, *16*, 157; [15b] E. W. Merrill, *Poly(ethylene glycol) Chemistry: Biotechnical and Biomedical Applications*, J. M. Harris, Ed., Plenum Press, New York 1992; [15c] M. J. Roberts, M. D. Bentley, J. M. Harris, *Adv. Drug Delivery Rev.* **2002**, *54*, 459.

[16] [16a] R. K. Kainthan, D. E. Brooks, *Biomaterials* **2007**, *28*, 4779; [16b] R. K. Kainthan, S. R. Hester, E. Levin, D. V. Devine, D. E. Brooks, *Biomaterials* **2007**, *28*, 4581.

[17] F. Wurm, J. Nieberle, H. Frey, *Macromolecules* **2008**, *41*, 1909.

[18] H. Türk, R. Haag, S. Alban, *Bioconjugate Chem.* **2004**, *15*, 162.

[19] F. Wurm, J. Klos, H. Räder, H. Frey, *J. Am. Chem. Soc.* **2009**, *131*, 7954.

Supporting Information for *Macromol. Chem. Phys.*, DOI: 10.1002/macp.200900652.

α,ω_n-Heterotelechelic Hyperbranched Polyethers Solubilize Carbon Nanotubes

*Frederik Wurm, Anna Maria Hofmann, Anja Thomas, Carsten Dingels, and Holger Frey**

Institut für Organische Chemie – Makromolekulare Chemie, Johannes Gutenberg-Universität Mainz, Duesbergweg 10-14, 55099 Mainz, Germany,

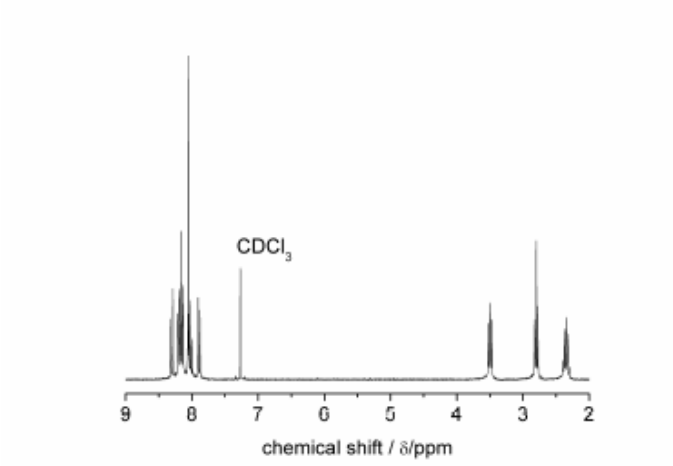

Figure S1: ^{1}H-NMR (300 MHz, $CDCl_3$) of pyrene-butyric acid pentafluorophenol-active ester.

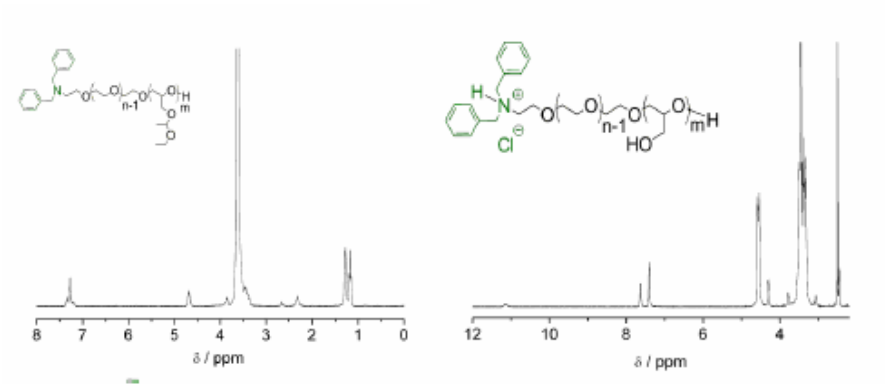

Figure S2: *left:* ^{1}H-NMR ($CDCl_3$) of Bn_2N-PEG_{120}-PEEGE$_{15}$. *right:* ^{1}H-NMR (DMSO-d_6) of HCl*Bn_2N-PEG_{20}-linPG$_{15}$.

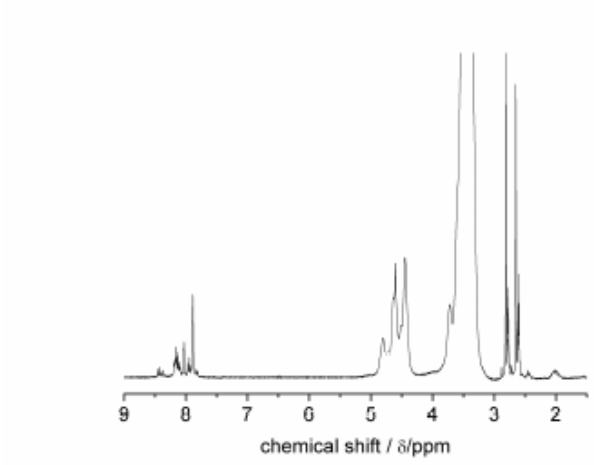

Figure S3: ^{1}H-NMR (DMF-d_7) of pyrene-butyric acid-NH-PEG_{20}-*hb*PG_{50}.

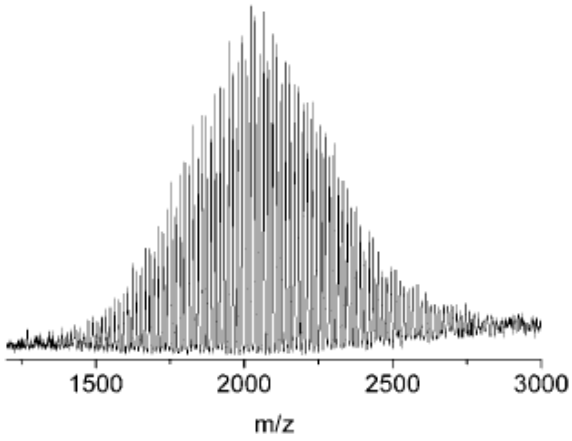

Figure S4: MALDI-ToF of Bn_2N-PEG_{25}-$hbPG_{20}$, evidencing quantitative functionalization.

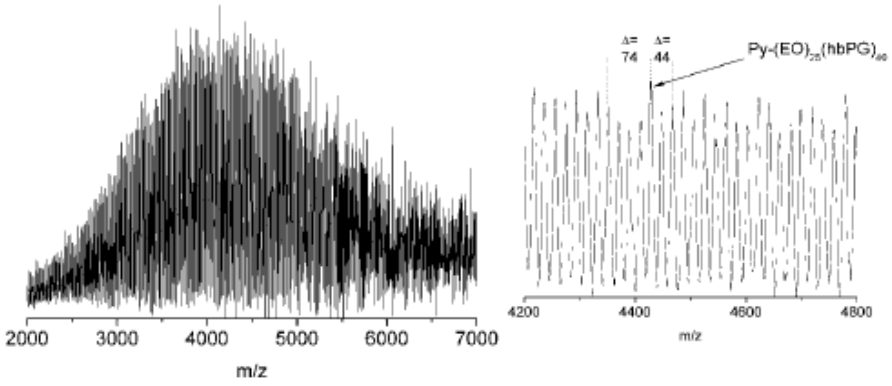

Figure S5: MALDI-ToF of pyrene-modified H_2N-PEG-hbPG supporting quantitative functionalization (right: zoom-in as shown in Figure 1, main manuscript).

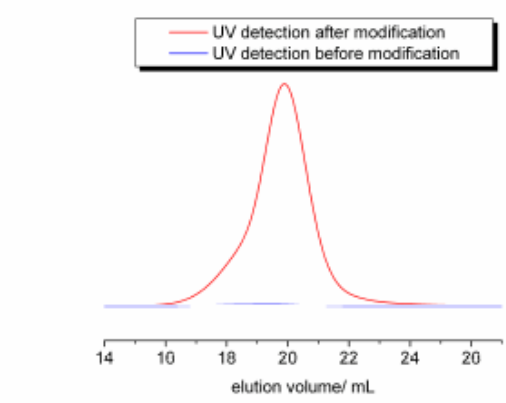

Figure S6: UV-detection during SEC-elugram of H_2N-PEG_{25}-*hb*PG_{50} (blue, no UV-active signal) and pyrene-modified PEG_{25}-*hb*PG_{50} (red, strong absorption).

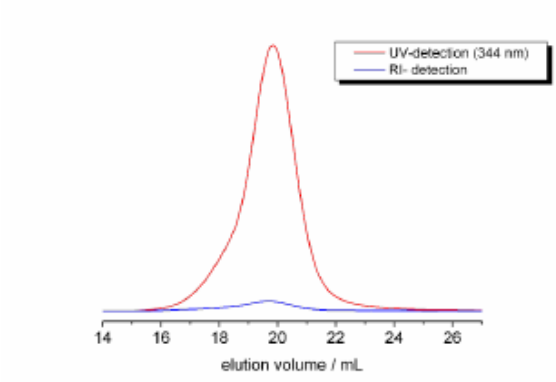

Figure S7: SEC-elugram of pyrene-modified PEG_{25}-*hb*PG_{50} with RI and UV-detection at 344 nm (strong signal).

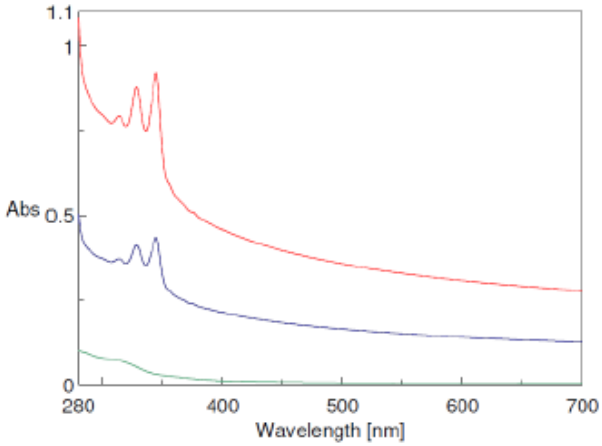

Figure S8: UV/vis-spectra of aqueous solution of MWCNTs in water via pyrene-modified PEG_{25}*hb*PG_{50} at different concentrations (blue, red) showing strong absorption at high wavelength due to presence of MWCNTs in the solution. For comparison, green: MWCNTs after sonification in water for 5 h and filtration – no signal detected due to insolubility of MWCNTs in water.

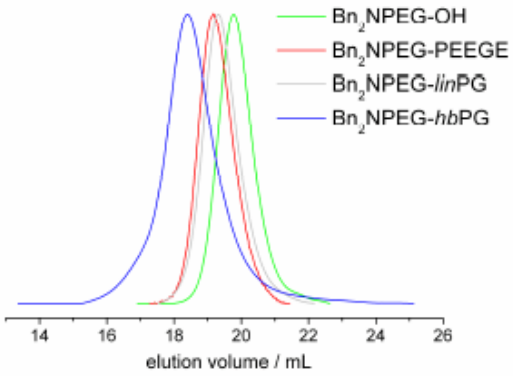

Figure S9: SEC elugrams in DMF of different polymers initiated with N,N-dibenzyl-2-aminoethanol.

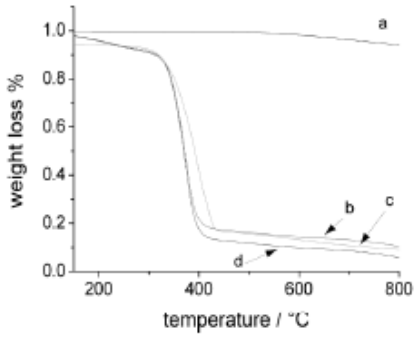

Figure S10: TGA curves of pyrene-modified MWCNT (a) pristine MWCNTs, b) 13% residue (pyr-PEG$_{25}$*hb*PG$_{50}$), c) 11% residue (pyr-PEG$_{125}$*hb*PG$_{50}$), d) 9% residue pyr-*hb*PG$_{80}$)).

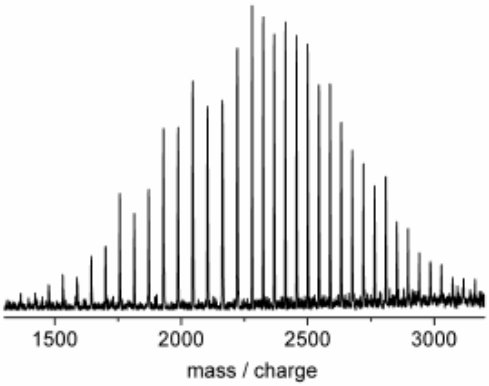

Figure S11: MALDI-ToF spectrum of $C_{14}H_{29}PEG_{50}$-OH evidencing complete incorporation of the initiator.

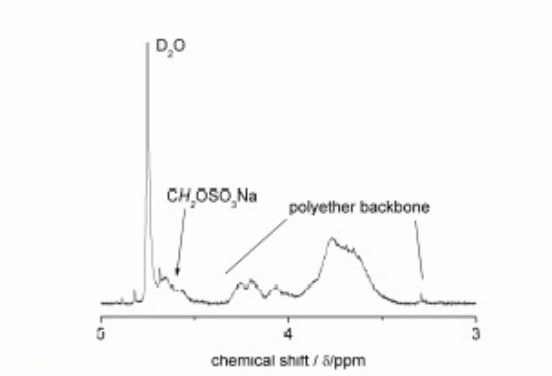

Figure S12: ^{1}H-NMR (D_2O) spectrum of H_2N-*hb*$PG_{40}(SO_3Na)_n$.

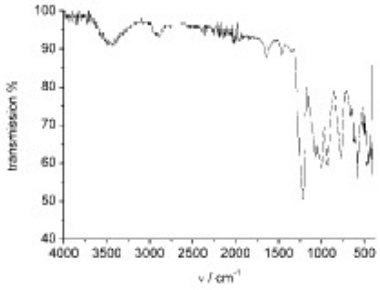

Figure S13: IR-spectrum of PEG_m-*hb*$PG_n(OSO_3Na)_x$, degree of modification 31% (NMR).

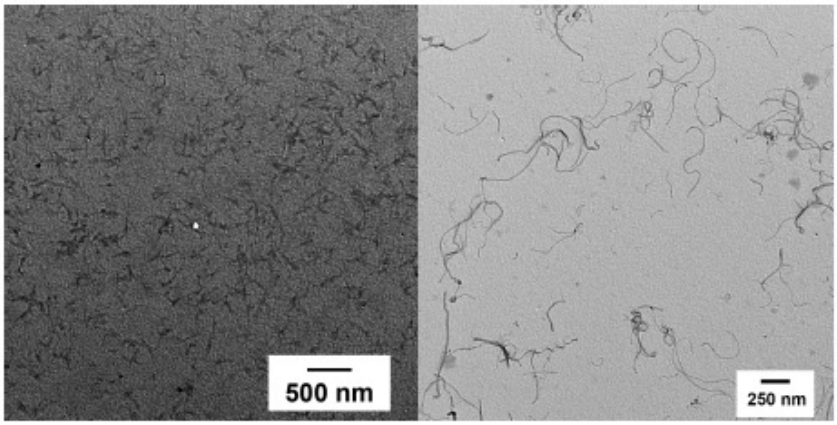

Figure S14: *left*: rodlike micelles formed by $C_{14}H_{29}PEG_{60}$*hb*$PG_{40}(SO_4Na)_n$, *right:* noncovalently solubilized MWCNTs by $C_{14}H_{29}PEG_{60}$*hb*$PG_{40}(SO_4Na)_n$.

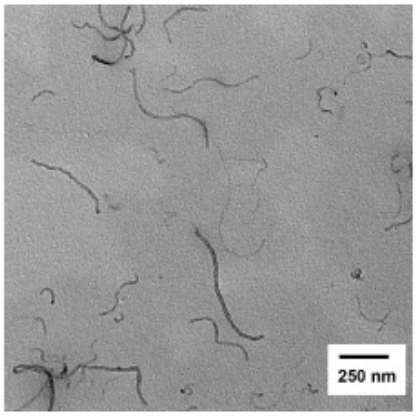

Figure S15: TEM image of an aqueous solution of solubilzed MWCNTs by $C_{14}H_{29}O$-$PEG_{60}PGG_{15}$.

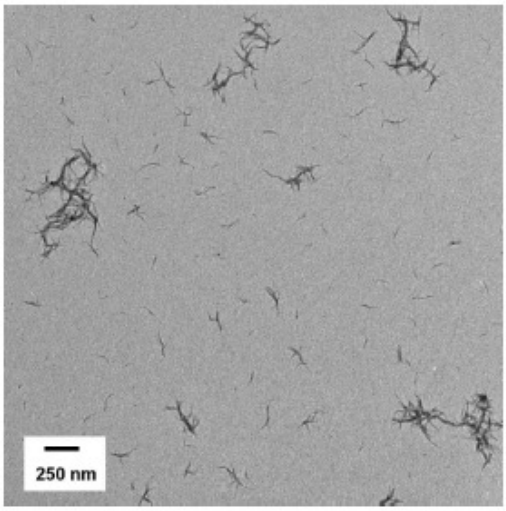

Figure S16: TEM image of short MWCNTs in water solubilized via pyrene-PEG_{25}-*hb*PG_{50}.

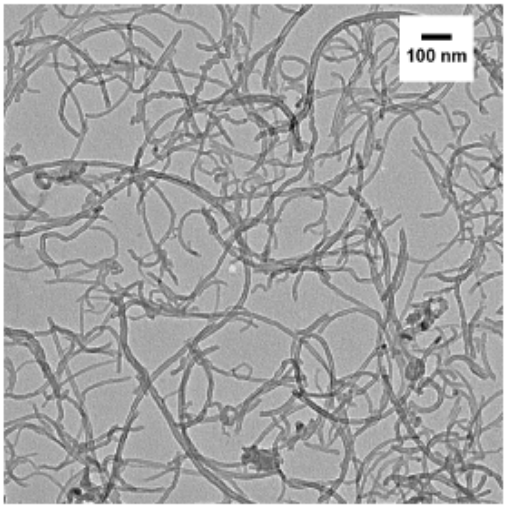

Figure S17: Enlarged TEM image of MWCNTs in water (compare main manuscript); solubilization via pyrene-PEG_{25}-*hb*PG_{50}.

3314 *Macromolecules* **2010**, *43*, 3314–3324
DOI: 10.1021/ma902844m

Macromolecules
ARTICLE

Poly(isoglycerol methacrylate)-*b*-poly(D or L-lactide) Copolymers: A Novel Hydrophilic Methacrylate as Building Block for Supramolecular Aggregates

Florian K. Wolf, Anna M. Hofmann, and Holger Frey*

Institut für Organische Chemie, Johannes Gutenberg-Universität Mainz, Duesbergweg 10-14, D-55099 Mainz, Germany

Received December 27, 2009; Revised Manuscript Received March 6, 2010

ABSTRACT: On the basis of a new acetal-protected glycerol monomethacrylate monomer (*cis*-1,3-benzylidene glycerol methacrylate/BGMA) a series of potentially biocompatible and partially biodegradable homo- and block copolymers were synthesized. ATRP polymerization of BGMA yielded well-defined polyacrylates with pendant benzylidene acetal groups and high glass transition temperatures (115−130 °C). This hydrophobic poly(*cis*-1,3-benzylidene glycerol methacrylate) could be readily transformed into the hydrophilic and water-soluble poly(1,3-dihydroxypropyl methacrylate), referred to as poly(isoglycerol methacrylate) (PIGMA). It exclusively contains primary hydroxyl groups and therefore differs significantly from the commonly known poly(glycerol methacrylate) (PGMA). Block copolymer systems based on poly(lactide) and BGMA were realized via two orthogonal living polymerization techniques starting from a bifunctional initiator, employing first atom transfer radical polymerization (ATRP) of BGMA and in the second step organo-base catalyzed polymerization of L- or D-lactide. This route provides well-defined block copolymers of low polydispersity (PDI 1.12−1.17) and molecular weights in the range of 7000 to 30000 g/mol (NMR). Rapid and highly selective acetal hydrolysis of the PBGMA block resulted in the release of the hydrophilic and water-soluble poly(1,3-dihydroxypropyl methacrylate) (poly(isoglycerol methacrylate), PIGMA). Acidic hydrolysis of the acetal protecting groups of poly(BGMA)-*b*-poly(lactide) copolymers proceeded smoothly to amphiphilic structures, notably without affecting the potentially labile polyester block. The novel PIGMA-*b*-PLLA copolymers are capable of supramolecular self-assembly to spherical aggregate structures in aqueous environment. The polymers generally exhibited low aggregation constants (CAC: 8−20 mg/L). Because of the unique feature of stereocomplex formation of poly(lactide), the corresponding aggregate morphology could be adjusted by mixing two nearly identical PIGMA-*b*-PLA copolymers with enantiomeric poly(lactide blocks) in a 1:1 ratio. In this case the uniformly shaped micelles (20 nm) changed to large vesicles with diameters ranging from 600 to 1400 nm. These features render this new type of amphiphilic block copolymers promising for drug delivery applications.

Introduction

Biodegradable polyesters are among the best established, but also most promising materials in current Polymer Science for the design of "smart" biomedical devices, such as drug delivery and controlled release systems in the form of nanoparticles,[1] micelles and polymersomes.[2] Amphiphilic block copolymers are currently subject of intense research with respect to their potential application as encapsulation devices of therapeutic agents exhibiting triggered release.[3] Linear aliphatic polyesters represent excellent building blocks for the formation of hydrophobic domains because of their established *in vivo* degradability and nontoxicity. Poly(lactide) (PLA) has been successfully combined with poly(ethylene glycol) (PEG) and other hydrophilic blocks.[4] Among biocompatible and biodegradable polyesters, poly(lactide) exhibits the unusual feature of stereocomplex-formation of enantiomeric, homochiral chains. This is not only accompanied by a strong increase of the melting temperature by approximately 50 °C, but can also be exploited for the kinetic and thermodynamic stabilization of block copolymer aggregates in aqueous environment.[5] Hedrick and co-workers have shown in elegant recent work that stereocomplex-driven association between PEG-*b*-PDLA and PNIPAM-*b*-PLLA leads to the formation of mixed micelles.[6] Generally, copolymers of PEG and PLA have been in the focus of interest in the aggregate-promoted application as drug delivery vehicles.[7] This is at least partially attributed to their facile synthesis, which relies on commercially available monomethyl ether PEGs. Nevertheless, PEG-based systems show some disadvantages, such as the lack of further functionality and toxicity of the gaseous monomer ethylene oxide. In less academic circles, the ill-founded fear of product contamination by trace amounts of ethylene oxide in PEG-based products is currently developing a market pull for suitable alternatives.

In this context, we have directed our focus on poly(methacrylate)-based polymers, which possess a functional moiety that can easily be adjusted by simple esterification reaction of the respective alcohol with methacrylic acid. In general, poly(methacrylate)s provide access to non degradable, but readily tunable systems in terms of e.g., hydrophilicity,[10] pH- and temperature-induced phase behavior[11] as well as loading with therapeutic agents[12] by simple variation of the substituent, as demonstrated in Scheme 1. Via ATRP single and multiheaded initiators can be conveniently obtained and introduced in polymers with low synthetic effort.[13−15] Block copolymers are accessible by an acrylate- or lactone-first[16−22] strategy or even by simultaneous

*Corresponding author. E-mail: hfrey@uni-mainz.de.

 Published on Web 03/19/2010

Scheme 1. The New Poly(isoglycerol methacrylate) (PIGMA) Can Be Classed in a Family of Hydrophilic Methacrylates/Methacrylamides Representing Suitable Building Blocks for Biomedical Application[a]

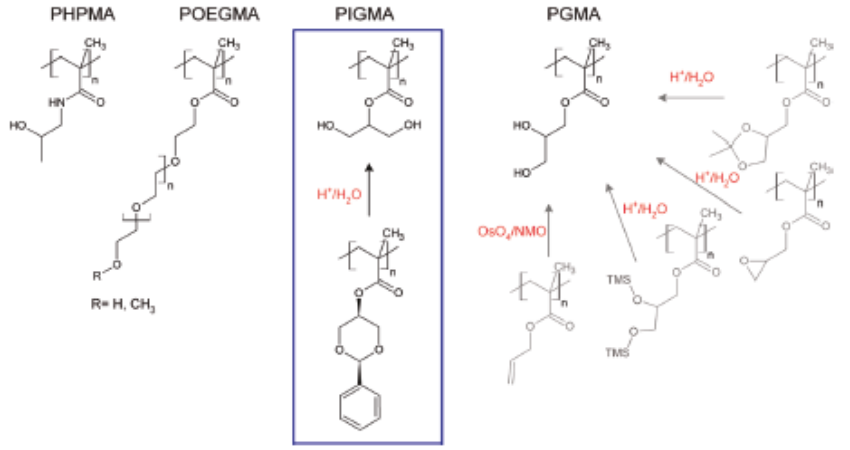

[a] Abbreviations: PHPMA (poly(2-hydroxypropyl methacrylamide)),[8] POEGMA (poly(oligoethylene glycol methacrylate)),[9] and PGMA (poly(glycerol methacrylate)).[22,32,33,35]

growth of the two blocks under optimized conditions.[23] Very recently, Trimaille et al. have succeeded in combining NMP of *n*-butyl acrylate and the ROP of ε-caprolactone in a one step procedure, starting from a bifunctional, SG1nitroxide functionalized initiator, yielding well-defined block copolymers.[34] In a previous work, we have introduced a straightforward one-pot procedure to poly(lactide)-*b*-poly(HEMA) copolymers.[25] This system represents one of only few examples describing the combination of a hydrophobic, aliphatic polyester with a hydrophilic poly(acrylate), carrying pendant hydroxyl groups.[26−28] Although these block copolymers could be prepared without additional protective groups from plain HEMA, they were not capable of aggregation into stable polymeric aggregates in aqueous solution due to the insufficient water solubility of the poly(HEMA) block.[29] Structurally similar methacrylate monomers are well-known and provide similar (2-hydroxypropyl methacrylate) and superior (glycerol methacrylate, 2-hydroxypropyl methacrylamide) hydrophilicity in their respective polymeric forms.[30,31] An obvious approach to enhance the hydrophilicity of HEMA relies on the increase of the number of hydroxyl groups per repeating unit. To date, this has been realized by poly(2,3-dihydroxypropyl methacrylate), which is commonly known under the name poly(glycerol methacrylate) (PGMA). The synthesis of PGMA is often based on its ketal-protected form: solketyl methacrylate (2,3-isopropylidene glycerol methacrylate), which was first realized in 1990.[32] The PGMA block can either be deprotected in an additional pre- or in a post polymerization step by acid-catalyzed hydrolysis.[33] Nevertheless, alternative pathways have been subject of past and current research. Borsali and co-workers recently employed silylated glycerol monomethacrylate (2,3-bistrimethylsilyloxypropyl methacrylate) to yield amphiphilic block copolymers with poly(ε-caprolactone) block after deprotection.[26] Ruckenstein et al. used the postpolymerization osmylation-reaction for the oxidative introduction of PGMA's bis(hydroxyl) group in poly(styrene)-*b*-poly(allyl methacrylate)s, which was obtained by successive carbanionic polymerization.[34] Davis and co-workers recently obtained poly(glyceryl methacrylate)-*block*-poly(pentafluorostyrene) by hydrolysis of the less polar poly(glycidyl methacrylate) precursor after RAFT polymerization.[35] The increased hydrophilicity and functionality of PGMA[36] and its suitability for drug delivery systems,[37−39] hydrogels for soft contact lenses[40] or antifouling coatings[41] lead to an increasing commercial interest in this kind of polymer.

Considering glycerol methacrylate (GMA), the synthetic methods published to date only offer access to the 2,3-dihydroxypropyl isomer, which provides a primary and a secondary hydroxyl functionality. Depending on the purity of the employed solketal, the methacrylate synthesized in this manner may contain impurities of up to 8% of the 2,3-isopropylidene glycerol isomer of GMA. This results in random incorporation of 1,3-dihydroxyisopropyl methacrylate in the polymer backbone in the respective ratio after polymerization and deprotection.[29] However, poly(1,3-dihydroxyisopropyl methacrylate).[56] has not been obtained in its pure form yet. In this work, we describe the synthesis and ATRP-polymerization of a new methacrylate monomer (2), granting access to the 1,3- dihydroxy form of poly(glycerol monomethacrylate) (3) (Scheme 2). Furthermore, we present a series of well-defined block copolymers of poly(isoglycerol methacrylate) and poly(lactide) segments and describe their aggregation behavior in aqueous solution with respect to the stereochemistry of the PLA blocks employed.

Experimental Part

Instrumentation. NMR investigation: All ^{1}H and ^{13}C nuclear magnetic resonance (NMR) spectra were recorded at 25 °C, using a Bruker AMX 400 (400.1/100.67 MHz) spectrometer. The spectra were measured in $CDCl_3$ and THF-d_8, and the chemical shifts are assigned by internal calibration on the solvents residual peaks. (^{1}H proton NMR signal, 1.73 ppm for THF-d_8 and 7.26 ppm for $CDCl_3$; ^{13}C carbon NMR signal, 25.37 ppm for THF-d_8 and 77.00 ppm for $CDCl_3$). Size exclusion chromatography (SEC) was performed with an instrument consisting of a Waters 717 plus autosampler, a TSP Spectra Series P 100 pump, and a set of three PSS-SDV 5A columns with 100, 1000, and 10 000 Å porosity. THF was used as an eluent at 30 °C and at a flow rate of 1 mL/min. UV absorptions were detected by a SpectraSYSTEM UV2000. The specific refractive index increment (dn/dc) was measured at 30 °C, using an Optilab DSP interferometric refractometer (also RI detector) and determined with the Wyatt ASTRA IV software (Version 4.90.08). Calibration was carried out using poly(styrene) standards provided by Polymer Standards Service and performing a third

Scheme 2. Synthesis of Benzylidene Glycerol Methacrylate (BGMA, 2) in Two Steps

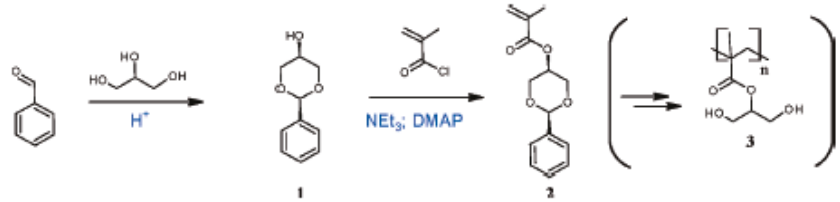

order polynomial fit. MALDI−ToF MS measurements of poly(lactide) macroinitiators were performed on a Shimadzu Axima CFR MALDI−ToF MS mass spectrometer, equipped with a nitrogen laser delivering 3 ns laser pulses at 337 nm. Dithranol (1,8-dihydroxy-9(10*H*)-anthracetone, Aldrich 97%), was used as a matrix. Potassium triflate (Aldrich, 98%) was added for ion formation. Good results were obtained for samples prepared from THF solution by mixing matrix (10 mg/mL), polymer (10 mg/mL), and salt (0.1 N solution) in a ratio of 5:1:1. A volume of 0.9 μL sample solution was deposited on the MALDI target and allowed to dry at room temperature for 2 h prior to the measurement.

Differential scanning calorimetry (DSC) measurements were carried out on a Perkin-Elmer 7 Series Thermal Analysis System with auto sampler in the temperature range of 0 to 200 °C at a heating rate of 20 K/min. The melting points of indium (T_m = 156.6 °C) and Millipore water (T_m = 0 °C) were used for calibration. In order to visualize the X-ray diffraction information obtained for BGMA we used the basic version of Mercury Crystal Structure Visualization and Exploration software (version 2.2) available free of charge at http://www.ccdc.cam.ac.uk/mercury.

Materials. All solvents were of analytical grade and purchased from Acros Organics. Methylene chloride was refluxed over phosphorus pentoxide and distilled immediately prior to use. 1,8-Diazabicyclo[5.4.0]undec-7-ene (DBU) was obtained from Acros Organics (98%) and distilled from CaH_2 prior to use. Glycerol (25 kg; 99.5%) of plant origin was kindly donated by Caldic (Germany). Deuterated chloroform-d_1 and THF-d_8 were purchased from Deutero GmbH, dried and stored over molecular sieves. Dilactide was purchased from Purac (Gorinchem, NL), recrystallized 3 times from dry toluene and stored under vacuum prior to use. 2-Hydroxyethyl 2-bromo-2-methylpropanoate (HBMP) was synthesized as described previously.[25] 5-Hydroxy-2-phenyl-1,3-dioxane was prepared with a standard rotary evaporator and isolated from cold diethyl ether on a multi 100 g scale according to a procedure adapted from Aasbø et al.[42]

Dialysis of the micellar solution was performed with Cellu SepH1 membranes (Membrane Filtration Products, Inc.) with a molecular weight cutoff of 1000 g/mol.

Monomer Preparation: 2-Phenyl-1,3-dioxan-5yl Methacrylate (BGMA). A 32 g (0.18 mol) sample of 5-hydroxy-2-phenyl-1,3-dioxane, 21 g (0.21 mol, 28.5 mL) of triethylamine, and 50 mg of *N,N*-(dimethylamino)pyridine were dissolved in 400 mL of dry dichloromethane in a 1 L flask equipped with a 250 mL dropping funnel and an argon balloon. Subsequently a solution of 20 g (0.19 mol) of methacryloyl chloride in 150 mL of dry dichloromethane was added dropwise under constant cooling (0−5 °C) over a period of 2 h. The solution was slowly allowed to warm to room temperature and stirred for an additional 72 h. The solution was extracted twice with water and twice with saturated potassium carbonate solution (50 mL each). The organic phase was dried over a 1/10 mixture of anhydrous potassium carbonate and magnesium sulfate. After evaporation of the solvents, the crude product was taken up in 20 mL of THF and poured into 200 mL of a 1:1 mixture of diethyl ether and hexanes. The product crystallized in colorless needles upon standing at −25 °C for 48 h (34.8 g/78%). ^{1}H NMR ($CDCl_3$, 400 MHz) δ (ppm): 2.01 (s, 3H, CCH_3); 4.18−4.35 (m, $CHCH_2O$); 4.77 (s, 1H, $-OCHH(CH_2O)_2$); 5.58 (s, 1H; $-OCHHO$); 5.65 (s, 1H, $C=CH_2$ (*E*)), 6.30 (s, 1H, $C=CH_2$ (*Z*)); 7.36−7.53 (m, 5H−, aromat.). ^{13}C NMR ($CDCl_3$, 100 MHz) δ (ppm): 18.23 (CCH_3); 66.10 ($-OCH(CH_2O)_2-$); 69.00 ($-OCH(CH_2O)_2-$); 101.30 (CH_2O_{cycl}); 126.05 (CH_{aromat} 2 + 6); 126.54 (CCH_2); 128.31 (CH_{aromat} 3 + 5); 129.12 (CH_{aromat} 4); 137.93 (C_{aromat} 1); 167.16 ($CCOOCH$).

General Procedures for the Synthesis of the First Block: ATRP of BGMA. This was exemplarified for PBGMA-MI (4) with a monomer/alkyl halide/copper/ligand ratio of [100]:[1]:[1]:[1]) A 2:1 mixture of benzene and methanol was predegassed by three freeze−pump−thaw cycles. Monomer and initiator were charged into an argon-flushed Schlenk-tube, dissolved in a benzene/methanol mixture and degassed in three freeze pump thaw cycles. The ligand, hexamethyl triethylenetetramine (HMTETA) (2-fold excess) was charged in a separate Schlenk tube, dissolved in 10 mL of benzene/methanol 2:1 and degassed as described above. Then 5 mL of the ligand solution were injected into a pre-evacuated Schlenk-tube, containing the desired amount of CuCl. The tube was flushed with argon and sonicated for 10 min, upon which a nearly colorless solution of the copper complex formed. Polymerization was initiated upon injecting the copper/HMTETA complex to the monomer/initiator solution, preheated to the reaction temperature of 80 °C. Polymerization was quenched after 5 h by removal of the reaction vial from the oil bath followed by exposure to air. A sample was harvested for conversion analysis. Since the block copolymer partially precipitated from the reaction mixture upon cooling, benzene was added and the solution was left to stand to evaporate excess methanol. The less polar environment facilitated catalyst removal via filtration over a short column filled with neutral aluminum oxide (10 mL/g polymer). Further work-up including complete removal of residual monomer was achieved by precipitation in excess methanol (150 mL/g polymer). After filtration, the block copolymer was obtained as a white powder in a yield reflecting the respective conversion.

^{1}H NMR ($CDCl_3$, 400 MHz) δ (ppm): 0.94−1.46 (m, $C(CH_3)$-$(COOCH(CH_2O-)_2)$; 1.80−2.34 (m, $-CH_2C(CH_3)(COOCH$-$(CH_2O-)_2)$; 3.56−4.33 ($COOCH(CH_2OH)_2$); 4.20−4.57 ($COOCH(CH_2O-)_2$); 5.27−5.49 ($COOCH(CH_2O-)_2CHC_6H_5$); 7.16−7.54 ($COOCH(CH_2O-)_2CHC_6H_5$).

Polymerization of Lactide. The ω-hydroxyl-PBGMA macroinitiator and lactide of the respective D- or L-configuration were charged into a Schlenk-tube at predetermined molar ratios (Table 2). The tube was sealed with a rubber septum and repeatedly flushed with argon after evacuation. Freshly distilled dichloromethane (4 mL/g lactide) was added via a syringe. Polymerization was initiated after 2 min by injecting a 10% (weight) solution of DBU corresponding to 1 mol % of the monomer. Polymerization was quenched after 20 min by injecting 1 mL of methanol. A small sample was removed for conversion analysis prior to precipitation in an excess of methanol. The polymer was collected by filtration.

^{1}H NMR ($CDCl_3$, 400 MHz) δ (ppm): 0.94−1.46 (m, $C(CH_3)$-$(COOCH(CH_2O-)_2)$; 1.57 (d, ^3J = 7.0 Hz $CHCH_3$, poly(lactide)), 1.80−2.34 (m, $-CH_2C(CH_3)(COOCH(CH_2O-)_2)$; 3.56−4.33

(COOCH(CH_2OH)$_2$); 4.20−4.57 (COOC*H*(CH_2O−)$_2$); 5,15 (q, ^3J = 7.0 Hz C*H*(CH_3), poy(lactide)); 5.27−5.49 (COOCH-(CH_2O−)$_2$C*H*C$_6$H$_5$); 7.16−7.54 (COOCH(CH_2O−)$_2$CHC$_6$*H*$_5$).

Acetal Cleavage: Kinetics via ^{1}H NMR. First, 20 mg of the block copolymer were dissolved in 0.82 mL of deuterated THF and charged into a standard NMR tube. The probe head was preheated to 37 °C prior to injection of 0.15 mL of a 1 N HCl/DCl solution. Spectra were measured in intervals of 15 min with four scans each (approximately 30 s/experiment), the first scan 1 min after the injection. ^{1}H NMR (first spectrum obtained)-(82% THF-d_8, 18% 1 N HCl/DCl; 400 MHz) δ ppm: 0.90−1.22 (m, C(C*H*$_3$)(COOCH(CH_2OH)$_2$); 1.46 (d, ^3J = 7.0 Hz OCH(C*H*$_3$), poly(lactide)); 1.85−2.20 (m, −C*H*$_2$C(CH$_3$)(COO-CH(CH_2OH)$_2$); 3.69−3.81 (COOCH(C*H*$_2$OH)$_2$); 4.65−4.77 (−COOC*H*(CH_2OH)$_2$); 5.15 (q, ^3J = 7.0 Hz C*H*(CH$_3$); poy-(lactide)); 5.48 (d, ^3J = 6.0 Hz *H*OCH(CH$_3$), poly(lactide) *term. unit*).

Micelle Preparation. 10−15 mg of the block copolymer were dissolved in 2.7 mL of THF and 0.5 mL of 1 N hydrochloric acid were added. The vial was sealed with a rubber septum and the content stirred at 37 °C for 8 h. Subsequently 10 mL of water were added dropwise under vigorous stirring over a period of 4 h. Samples were dialyzed against 3 × 1 L of water for a total of 48 h. The first dialysis solution was buffered with 0.1 mg of sodium acetate. The aggregate morphologies were studied using a transmission electron microscope (TEM). The TEM samples were prepared by drop casting the above-mentioned aggregate solution (c = 1−1.5 mg/mL) on a plasma treated carbon coated copper grid. The samples were allowed to dry at room temperature under a slight nitrogen flux for at least 16 h prior to examination.

Fluorescence Measurements. The extremely hydrophobic pyrene is preferentially solubilized in the hydrophobic interior of the aggregate. This can be readily observed in the fluorescence excitation spectra of the probe at an emission wavelength of 372 nm.[43] In the concentration range of aqueous micellar solutions, a shift of the excitation band in the 335 nm region toward higher wavelength is observed for the employed block copolymers. The ratio of the fluorescence intensities at 339 and 335 nm was used to validate the shift of the broad excitation band. The critical aggregation concentrations (CAC) were determined from the crossover point in the low concentration range. Pyrene-containing samples were prepared by continuous dilution of the aggregate solution with a saturated pyrene stock solution. The mixtures were allowed to equilibrate for 48 to 64 h prior to investigation by fluorescence spectroscopy.

Results and Discussion

Monomer Synthesis. The synthetic strategy for benzylidene glycerol methacrylate (BGMA) is shown in Scheme 1. The monomer was readily obtained on a multigram scale via a two-step route, starting from the acetal formed by glycerol and benzaldehyde with subsequent esterification of the secondary hydroxyl group with methacryloyl chloride.

In comparison to ketones, as employed in solketyl methacrylate synthesis, benzaldehyde and its derivates show a strong preference for the formation of six-membered cyclic acetals due to the energetically favored equatorial position in the chair conformation of the ring. This acetal protecting group provides excellent stability in neutral and basic environment and is conveniently cleaved under slightly acidic conditions. The isolation of 2-phenyl-5-hydroxyphenyl-1,3-dioxane (**1**) relies on a crystallization step, which exclusively yields the *cis*-isomer of the compound in very high purity (Figure 1). The coupling reaction with methacryloyl chloride was conducted in dichloromethane in the presence of stoichiometric amounts of triethylamine (TEA) and catalytic amounts of dimethylaminopyridine (DMAP). The novel

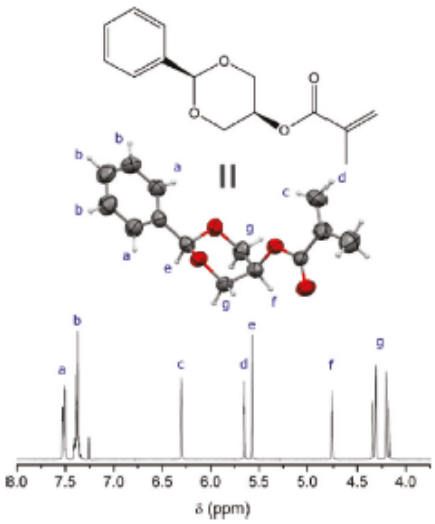

Figure 1. ^{1}H NMR analysis and crystal structure derived from the X-ray diffraction pattern of BGMA.

monomer (**2**) could be readily obtained in 78% yield by crystallization from THF/diethyl ether/hexanes (1:10:10), and the white crystals exhibited a melting point of 65.7 °C. This methacrylate significantly differs from 2-phenyl-(1,3-dioxane-4-yl)methyl methacrylate, which was previously described and obtained by an elaborate synthesis from solketyl methacrylate via 2,3-dihydroxypropyl methacrylate and subsequent reprotection as benzylidene acetal.[44]

Considering the bifunctional initiator used for the synthesis of the targeted block copolymers and the quantitative protection of the hydroxyl groups of the monomer, two different synthetic routes appeared to be viable: (A) synthesis of a poly(lactide) macroinitiator and subsequent chain extension with poly(lactide), or (B) preparation in reverse manner, that is, ATRP of BGMA with subsequent chain extension by ROP of lactide (cf. Scheme 3). Both pathways have been tested. To ensure fast initiation, ATRP was conducted with the mixed halide exchange technique,[45] starting from highly reactive isobutyryl-bromide, using copper(I) chloride in combination with stoichiometric amounts of HMTETA. A suitable solvent system providing good polymerization control for the ATRP of BGMA, while offering sufficient solubility for BGMA and lactide based homopolymers, was found with a 1:2 mixture of methanol and benzene. The low polarity of the PBGMA based polymers also ensures convenient removal of the Cu complex after polymerization. Column filtration over neutral aluminum oxide with a low polarity solvent (e.g., benzene) permitted excellent retention of the colored Cu species. Furthermore, PBGMA and poly(L-lactide) as well as their block copolymers of arbitrary composition ratios can be readily purified by (a single) precipitation in their common nonsolvent methanol. A change in block copolymer composition was not observed in this step. Residual monomer and catalyst (DBU−benzoate salt as well as Cu complex) were removed by this procedure. Generally speaking, the benzylidene acetal of BGMA not only contributes to an increase in the monomer and polymer solubility in commonly employed, apolar organic media, but also gives access to

other controlled polymerization methods (e.g., living anionic polymerization), which show far less tolerance toward the presence of functional groups than ATRP. Obviously, block copolymer synthesis involving two or more orthogonal polymerization methods, employing monomers of different functionality and/or polarity necessitates masking of their functional groups.

ATRP of BMGA. ATRP was the obvious method of choice for the preparation of a narrow polydispersity block of the novel monomer. The semilogarithmic plot of the kinetic polymerization data derived from ^{1}H NMR shows a nearly linear correlation throughout the major part of the polymerization, with a small decrease toward high conversion. Hence, the reaction can be considered living with a close to constant radical concentration during the polymerization. The slight flattening of the plot can be explained by traces of oxygen, which might have been introduced during sample harvesting, although all syringes were carefully purged with argon prior to the process. The kinetically evaluated sample reached a conversion of only 66%. The characterization data are shown in Table 1.

The evolution of molar mass correlated linearly with conversion (Figure 2). The monodisperse SEC-traces observed revealed narrow molecular weight distributions (PDI 1.18−1.30), characteristic for well-controlled CRP/ATRP processes. The decrease in PDI was very pronounced during the earlier stages of the polymerization and became significant after 60 min. We assume that this point is indicative of complete consumption of the initiator, followed by exclusive propagation with constant chain growth. This goes along with the appearance of a nonzero extrapolation of the linear fit and can be explained by the use of the mixed halide exchange technique and hence a significantly faster initiation than propagation reaction, which results in slightly faster monomer consumption at the onset of the polymerization. First DSC studies showed a rather high T_g of the PBGMA homopolymer (115−130 °C depending on M_n), which is due to the high rotational barrier introduced by the bulky benzylidene acetal substituents at the methacrylate polymer chain. We will report in detail on the interesting thermal properties of PBGMA-based polymers in a subsequent publication.

Chain Extension with Poly(lactide). Since the poly(isoglycerol methacrylate) hydroxyl groups are fully protected, the lactide chain growth commences from the single hydroxyl moiety of the bifunctional macroinitiator. Ring-opening polymerization was conducted under organo-base catalysis with DBU (1,8-diazabicyclo[5.4.0]undec-7-ene), which has proven to work excellent for lactide ring-opening[46] on a laboratory or semibatch scale. It provides superb end group-fidelity, good polymerization control and fast kinetics, even at room temperature. The polymerization time for the samples prepared was kept between 15 and 45 min, depending on the monomer/initiator ratio and resulted in conversion ranging from 85 to 99% (1.5 mol % catalyst loading).

While route B (cf. Scheme 3) resulted in well-defined block copolymers (Table 2), the pathway A led to the formation of less defined structures, presumably composed of a mixture of homo and block copolymers. This was indicated by a change in composition (depletion of the lactide block, sometimes even complete disappearance) after precipitation in a non-solvent for both blocks and broader molecular weight distributions. This is astonishing, since the polylactide macroinitiators were completely functionalized (single distribution

Scheme 3. Two Alternative Synthetic Pathways to Poly(isoglycerol (mono)methacrylate)-*b*-poly(lactide) Block Copolymers: (A) Lactide First; (B) BGMA First[a]

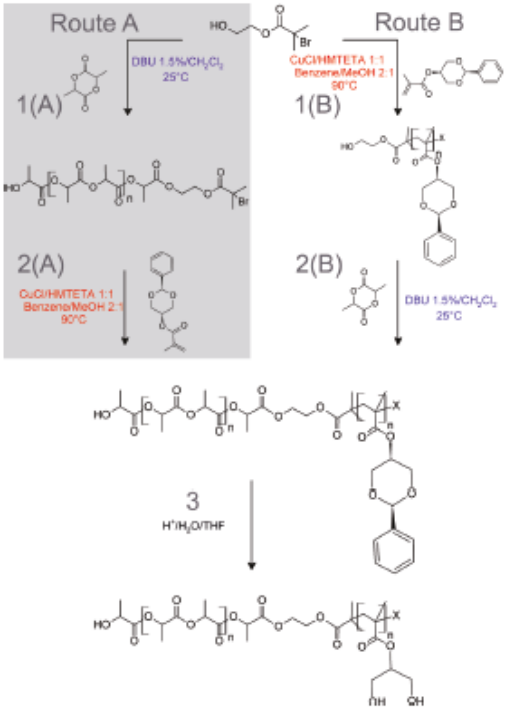

[a] While route B resulted in well-defined block copolymers, route A showed inefficient block formation and was not further pursued.

Table 1. Molecular Characterization Data for the Preparation of PBGMA Macroinitiators[a]

	Polymer	Initiator	Monomer	M/I	M_n theo. (100% conv.)	M_n (NMR)	Time (min)	Conv. (NMR)	M_n (SEC)	PDI	Composition (NMR)
1. ATRP of BGMA	PBGMA-MI 1	2-HBMP	**BIGMA**	25	6400	5480	300	0.85	3830	1.23	$PBGMA_{21}$
	PBGMA-MI 2	2-HBMP	**BIGMA**	40	9900	9520	300	0.96	5700	1.26	$PBGMA_{38}$
	PBGMA-MI 3	2-HBMP	**BIGMA**	55	13600	11700	300	0.86	6300	1.30	$PBGMA_{47}$
	PBGMA-MI 4	2-HBMP	**BIGMA**	100	24800	20200	300	0.80	11700	1.20	$PBGMA_{80}$
	PBGMA-MI 5	2-HBMP	**BIGMA**	110	27500	22400	300	0.81	11900	1.18	$PBGMA_{89}$
	PBGMA-MI 6	2-HBMP	**BIGMA**	200	49700	35800	300	0.72	18700	1.15	$PBGMA_{144}$
	PBGMA-MI 7	2-HBMP	**BIGMA**	400	99300	65900	360	0.66	24400	1.24	$PBGMA_{266}$

[a] SEC in THF, evaluation with polystyrene standards.

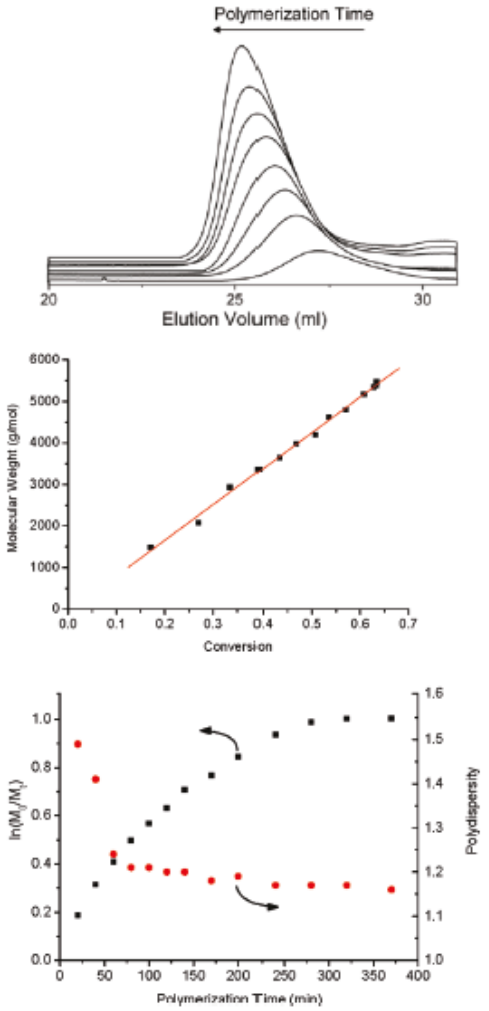

Figure 2. Kinetics of the polymerization of BGMA: SEC traces (top, plotted for 20−170 min reaction time) show a clean shift toward lower elution volumes in the course of the polymerization; middle, linear correlation of molecular weights (SEC_{THF} data), derived from PS standards with conversion; bottom, $\ln(M_0/M_t)$ vs polymerization time.

in MALDI−ToF spectra) and chain extension of these macroinitiators via ATRP has already been conducted successfully with HEMA (in DMSO with CuCl/bipyridyl), as recently described by the authors.[25] However, route B results in the formation of well-defined block copolymers and is slightly more practical, since diversification of the macroinitiator is possible, using the synthetically more convenient ROP of L-lactide (polymerization at room temperature, polymerization time < 15 min, no oxygen free environment necessary). In this case, all samples were monomodal and their block ratios remained unchanged during the purification process (filtration, precipitation), as was verified by ^{1}H NMR and SEC (Figure 3).

For the chain extension with poly(lactide) the respective degrees of polymerization were targeted by adjusting the monomer/initiator molar ratio, affording hydroxyl-functional PBGMA homopolymer precursors of varying chain lengths. Because of pronounced underestimation of molecular weight by SEC (PS standards) absolute molecular weights were estimated from the monomer/initiator ratio, considering the specific conversion of the sample calculated from NMR in the case of the PBGMA-macroinitiator. This underestimation is explained by the bulkiness of the substituents along the polymethacrylate backbone. In general, the use of the bifunctional initiator made post polymerization reactions redundant and the completely functionalized macroinitiators allowed quantitative chain extension with lactide.

Cleavage of the Acetal Protecting Group. The formation of the hydrophilic PIGMA from its protected precursor PBGMA was investigated via ^{1}H NMR. We observed that the rate of the acetal hydrolysis depends significantly on the reaction temperature. Screening of suitable time/temperature deprotection conditions was conducted by exposing the initial test sample to 3 different temperatures (A) 19 °C for 23 h (24%), (B) 4 °C for 12 h (6%) and (C) 27 °C, 12 h (100%). The first reaction mixture was composed of 90% THF and 9% D_2O and 1% 10 n HCl (0.1 mol/L). Upon completion of the acetal cleavage during the last deprotection sequence, the polymer precipitated from the reaction mixture and was redissolved by increasing the water/HCl content of the mixture to 18%. These results indicate that acetal cleavage at slightly increased (30−40 °C) temperatures should result in shorter reaction times, which are still tolerable for the polyester backbone of the second block.[47] This was confirmed and monitored via NMR analysis in THF-d_8/1 N DCl in the respective ratio (Figure 4).

As expected, the pronounced amphiphilic nature of the block copolymers did not permit SEC measurements in THF after deprotection. Nevertheless, DMF offers sufficient solubility for homo- and block copolymers of the employed components before as well as after acetal hydrolysis. In Figure 5 monomodal SEC traces with DMF as an eluent reveal narrow monomodal molecular weight distributions and illustrate the successful 3-step process to the amphiphilic block copolymers, free of detrimental side reactions. Remarkably, the block copolymers exhibit a significantly decreased elution volume after deprotection (Table 3). This is in good agreement with the observed underestimation in molecular weight for polymers consisting of PBGMA by evaluation with calibration standards like PEG, PS, and PMMA, which were at hand. PBGMA homopolymers were cleavable under the same conditions and could be redissolved in water (D_2O) after solvent evaporation.

The shelf life of the block copolymers under the acidic conditions of the deprotection reaction was found to be remarkable. Even for times representing a multitude of those required for complete acetal cleavage, no degradation of polylactide or isomerization of the poly(isoglycerol methacrylate) could be observed. This is supported both by ^{1}H NMR and by the constant ratio of lactide and cleaved benzaldehyde-related signals (Figure 6). Furthermore, SEC traces measured 24 and 96 h after deprotection strongly resemble each other.

Aggregate Formation of the PIGMA−PLLA Block Copolymers. Using the so-called indirect dissolution method with subsequent dialysis, well-defined micelles were formed upon self-organization of PIGMA-*b*-PLA. The acetal protecting groups of the double hydrophobic PBGMA-*b*-PLA copolymers were cleaved prior to the aggregation studies without isolation from solution, as described in the previous section. First of all the critical aggregation concentration (CAC) has

Table 2. Molecular Charachterization Data for the Chain Extension of the PBGMA Macroinitiators with Lactide[a]

	Polymer	Initiator	M#	M/I	M_N theo. (100%conv.)	M_N NMR	Time (min)	Conv. (NMR)	M_N (SEC*)	Composition (NMR)
2. ROP of Lactide	PBGMA-PLA 1	$PBGMA_{69}$ (MI 5)	L-LA	35	27400	26100	20	0.74	15200	$PBGMA_{69}$-$PLLA_{27}$
	PBGMA-PLA 2	$PBGMA_{69}$ (MI 5)	D-LA	35	38300	29500	20	0.45	13600	$PBGMA_{69}$-$PDLA_{16}$
	PBGMA-PLA 3	$PBGMA_{47}$ (MI 3)	L-LA	30	16000	15400	45	0.86	9770	$PBGMA_{47}$-$PLLA_{26}$
	PBGMA-PLA 4	$PBGMA_{47}$ (MI 3)	D-LA	30	16000	15700	45	0.92	9970	$PBGMA_{47}$-$PDLA_{28}$
	PBGMA-PLA 5	$PBGMA_{21}$ (MI 1)	L-LA	15	7600	7550	20	0.96	6100	$PBGMA_{21}$-$PLLA_{14}$
	PBGMA-PLA 6	$PBGMA_{21}$ (MI 1)	D-LA	15	7600	7550	20	0.96	6270	$PBGMA_{21}$-$PDLA_{14}$
	PBGMA-PLA 7	$PBGMA_{60}$ (MI 4)	D-LA	46	28600	27900	30	0.88	16900	$PBGMA_{60}$-$PDLA_{40}$

[a] The asterisk indicates SEC in THF; evaluation with polystyrene standards. The # indicates M = monomer (L-/D-LA = L-/D-lactide).

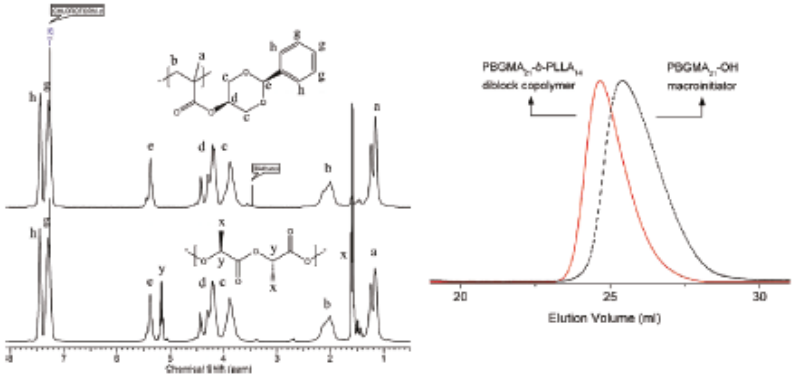

Figure 3. Chain extension of the PBGMA−macroinitiator with poly(lactide) depicted in the form pre/post NMR (left) and SEC (right) measurements. Although the sample chosen is composed of few lactide repeating units (i.e., DP = 14), it shows clean chain extension. This fact is attributed to the high initiating potential of the primary hydroxyl group of the PBGMA prepolymer.

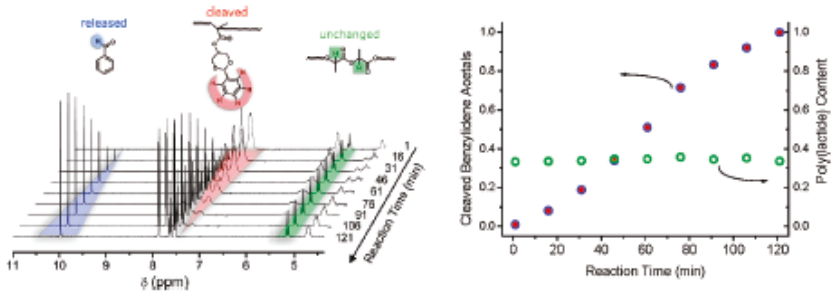

Figure 4. Deprotection of the benzylidene−acetal groups of the diblock copolymer, monitored by ^{1}H NMR in THF-d_8. While the poly(lactide) backbone remains unaffected, the benzylidene protecting groups of the polymer are fully cleaved within only 2 h at 37 °C.

been examined. Fluorescence measurements with pyrene as fluorescent probe are an excellent method to obtain information concerning aggregate formation. The ratio of the fluorescence intensities at 339 and 335 nm was used to evaluate the shift of the excitation spectra. The ratio remained constant below a certain concentration but changed substantially above a critical concentration, reflecting the partitioning of pyrene between the aqueous solution and aggregated phases. It has to be emphasized that the micellar aggregates formed by enantiomerically pure PLA block copolymers already possess high thermodynamic stability in aqueous solution and may perform as favorable drug carriers themselves.[48] Nevertheless, the special stereochemistry of poly(lactide) provides access to non covalent stabilization via stereocomplexation of two isotactic and enantiomeric poly(lactide) chains. This was achieved by dissolving equal amounts of two block copolymers of similar composition with enantiomeric poly(lactide) blocks prior to hydrolysis of the acetal goups.

From the set of synthesized polymers we focused on those with an approximate block ratio of 2:1. (i.e., $PIGMA_{47}$-*b*-$PLLA_{26}$ and $PIGMA_{47}$-*b*-$PDLA_{28}$). Since it is known that crystallization occurs in enantiomeric (1:1) blends at PLA chain lengths shorter than their isotactic counterparts, we aimed at keeping the PLA block length below the critical limit of 30 repeating units. At this chain length (and even below), stabilization by crystalline stereocomplexes in amphiphilic block copolymers based on poly(lactide) is possible.[49] They generally crystallize in a triclinic unit cell, in which the chains exhibit a characteristic 3_1 helical conformation. Figure 7 shows the apparent CAC values obtained for the different amphiphilic block copolymers. The CAC lies in the same order of magnitude—being approximately twice as high for the $PIGMA_{47}$-*b*-$PLLA_{26}$ block copolymer compared to the PEG_{123}-*b*-$PLLA_{29}$ sample (from ref 5). This indicates an increase in hydrophilicity and hence stabilization potential of PIGMA compared to PEG in aqueous solution. Therefore, an increase of the PIGMA chain length at nearly constant PLLA chain lengths resulted in an increase of the CAC by a factor of approximately 2 ($PIGMA_{47}$-*b*-$PLLA_{26}$ to $PIGMA_{89}$-*b*-$PLLA_{27}$). Generally speaking, the low CAC permits application of the block copolymers in highly dilute systems, such as the blood plasma.

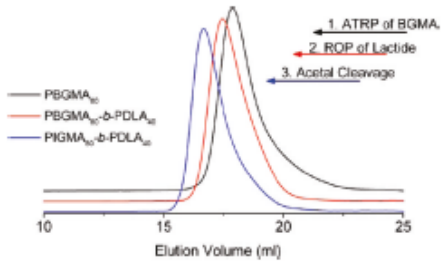

Figure 5. SEC traces (DMF): (1) $PBGMA_{80}$ (right); (2) $PBGMA_{80}$-*b*-$PDLA_{40}$; (3) $PIGMA_{80}$-*b*-$PDLA_{40}$.

The influence of the assumed stereocomplexation (mixture of $PIGMA_{47}$-*b*-$PLLA_{26}$ and $PIGMA_{47}$-*b*-$PDLA_{28}$) on the CAC was small, confirming results obtained by Leroux et al.[5] for PEG−PLA block copolymers. Intriguingly, the diastereomeric mixing of two block copolymers of very similar composition has a strong influence on the aggregates' morphology. As pointed out, the chosen block lengths had a positive hydrophilic to hydrophobic ratio between 3.5 and 2 (e.g., $PIGMA_{47}$-*b*-$PLLA_{26}$), which clearly explains the formation of spherical micelles with an approximate diameter of 20−30 nm (Figure 8, top).

Although block copolymers with a crystallizable hydrophobic block show a tendency toward the formation of nonspherical wormlike micelles—a fact that can be attributed to the lamellar packing of the crystallizable chains—X-ray diffraction studies of PEG−PLLA-based polymeric micelles performed by Leroux et al.[5] showed that the stereoregular poly(lactide) does not crystallize, if the block length remains below 30 repeating units. In the case of mixtures of similar PIGMA-*b*-PLA block ratios with enantiomeric poly(lactide) blocks an entirely different morphology was found. Surprisingly, TEM images of the aggregates prepared from mixed solutions (1/1 mixture) of the diasteromeric block

Table 3. Comparison of SEC Data for the PBGMA−PLA Based Block Copolymers before and after Deprotection[a]

before deprotection				*after deprotection*			
Composition (NMR)	M_N theo.	M_N (SEC)	PDI	M_N (theo)	M_N (SEC)	PDI	Composition
$PBGMA_{21}$	5480	3800	1.15	3330	5800	1.22	$PIGMA_{21}$
$PBGMA_{89}$	22400	11500	1.18	14300	18300	1.25	$PIGMA_{89}$
$PBGMA_{89}$-*b*-$PLLA_{27}$	26100	8400	1.17	18100	13900	1.27	$PIGMA_{89}$-*b*-$PLLA_{27}$
$PBGMA_{47}$-*b*-$PLLA_{26}$	15400	8200	1.17	11300	11900	1.26	$PIGMA_{47}$-*b*-$PLLA_{26}$
$PBGMA_{47}$-*b*-$PDLA_{28}$	15700	8500	1.16	11600	11800	1.27	$PIGMA_{47}$-*b*-$PDLA_{28}$
$PBGMA_{47}$-*b*-$PLLA_{26}$ + $PBGMA_{47}$-$PDLA_{28}$	s.a.[b]	s.a.[b]	s.a.[b]	11400	12500	1.31	$PIGMA_{47}$-*b*-$PLLA_{26}$ + $PIGMA_{47}$-*b*-$PDLA_{28}$
$PBGMA_{21}$-*b*-$PLLA_{14}$	7550	5300	1.12	5400	7450	1.24	$PIGMA_{21}$-*b*-$PLLA_{14}$
$PBGMA_{60}$-*b*-$PDLA_{40}$	27900	13700	1.17	18900	20700	1.18	$PIGMA_{60}$-*b*-$PDLA_{40}$

[a] The apparent increase in molecular weight after hydrolysis is noticeable, despite a nominal weight loss of 40% for the transformation of PBGMA to PIGMA (SEC in DMF; evaluation was achieved with poly(ethylene glycol) standards). [b] See above.

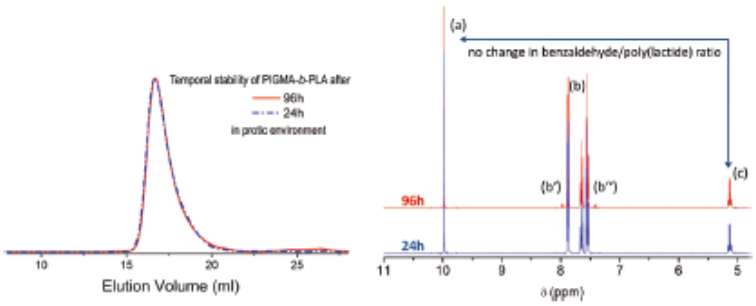

Figure 6. Stability of the amphiphilic PIGMA-*b*-PLA copolymer in acidic environment beyond the time frame required for deprotection of the acetal as indicated by consistent elugrams (left) and unchanged signal ratios in ^{1}H NMR.

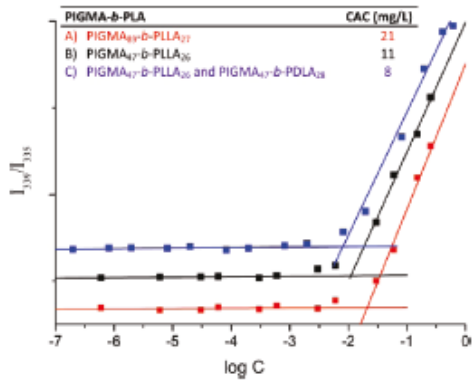

Figure 7. CAC measurements using pyrene fluorescence excitation spectra at an emission wavelength of 372 nm: (A) (red) $PIGMA_{49}$-*b*-$PLLA_{27}$; (B) (black) $PIGMA_{47(7500)}$-$PLLA_{26(3800)}$; (C) (blue) $PIGMA_{47(7500)}$-$PLLA_{26(3800)}$ and $PIGMA_{47(7500)}$-$PDLA_{28(4000)}$ (1:1).

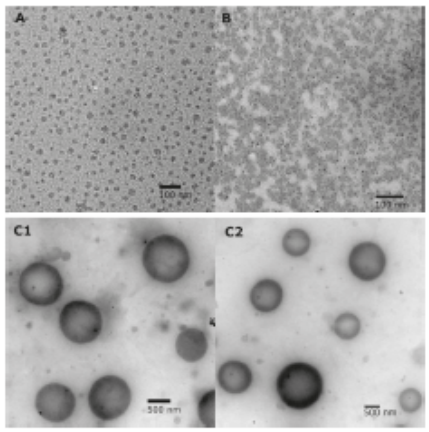

Figure 8. TEM image of (A) $PIGMA_{47}$-*b*-$PLLA_{26}$ and (B) $PIGMA_{47}$-*b*-$PDLA_{28}$[57] micellar aggregates with an average diameter of 20 to 30 nm. Sample preparation was carried out under identical conditions with a 1:1 mixture of $PIGMA_{47}$-*b*-$PLLA_{26}$ and $PIGMA_{47}$-*b*-$PLLA_{28}$ afforded large polymersomes (C1 and C2) with a diameter between 600 and 1400 nm (bottom).

copolymers showed the formation of vesicular aggregates, i.e., "polymersomes" with average diameters between 600 and 1400 nm (Figure 8, bottom). For the hydrophilic to hydrophobic volume ratio chosen, spherical micelles or cylindrical aggregates would have been expected from a conventional point of view—especially since it is known that crystalline domains in the hydrophobic block of an aggregate can promote the formation of cylinders with a small length/width aspect ratio.[50] Since our block copolymers show a significantly increased hydrophilic to hydrophobic ratio, polymersome formation[7] is unlikely and indeed not observed for aggregate solutions with a single homochiral PLA component (Figure 8, top). Since all other parameters remained unchanged during aggregate preparation, stereocomplexation can be considered to be a very likely cause for the change in the aggregate morphology. Here, the question arises, how bilayer formation, as a prerequisite for polymersome formation, is triggered. Since the thermodynamic parameters are not known for this new block copolymer system, we can only argue with the sum of poly(lactide)s' known characteristics[51] to put forward a conclusive explanation. Because of its stereoregular methyl substituent in alpha-position, poly(D/L-lactide) represents a rather stiff hydrophobic part of the block copolymer with a low conformational degree of freedom, resulting in a rather high T_g, i.e., 30−40 K above room temperature. This stiffness is generally known to promote the formation of planar bilayer structures. Although this behavior is obviously not sufficiently pronounced for non crystalline poly(L-lactide), as expected for the employed average number of repeating units (26 and 28), the formation of stereocomplex-induced crystallization appears to be important for the mixed block copolymers. Antonietti and Förster concluded that "*planar assemblies are spontaneously formed in a much broader range in phase space, if there is a tendency of the tecton* (in this case a block copolymer) *to exhibit at least nematic order*".[52] The additional 3-dimensional positional order of the 3_1 helical conformation in the β-form, in which the stereocomplexed poly(lactide) "tecton" is packed in a parallel fashion[53] is based on noncovalent secondary valences and most likely promotes the formation of planar assemblies and hence represents the reason for the formation of polymersome-type structures. We believe that the preparation technique employed via the indirect dissolution[54] from THF with water is an important factor to obtain the defined aggregates we observed. THF is a good solvent for stereoregular PLA of moderate molecular weight and a poor solvent for crystalline, stereocomplexed PLA. This ensured sufficient chain mobility upon aggregate formation, while not endangering the formation of stable crystalline domains, which are not formed unless a controlled amount of water as poor solvent for the inner PLA-block is added.

This is further supported by SEC examination (DMF, from THF/HCl solution) of the freshly prepared 1:1 mixture of $PIGMA_{47}$-*b*-$PLLA_{26}$ and $PIGMA_{47}$-*b*-$PDLA_{28}$ prior to selective dissolution. Intriguingly, the SEC trace of this mixture was monomodal and showed no aggregate formation. Evaluation with PS-standards provided a sample of similar molecular weight and polydispersity resembling those obtained for their homopolymers (Table 3). A more detailed report on the intriguing topic of stereocomplex-induced changes in block copolymer aggregate morphology in solution will be the subject of a forthcoming publication.

An additional interesting feature of the prepared aggregates is the high number of primary hydroxyl groups at their periphery. This provides interesting potential for the block copolymer in targeted drug delivery, since the abundance of hydroxyl groups at the corona allows attachment of (multiple) distinct piloting/targeting functions to the micelle corona by straightforward chemistry. Stereocomplex-induced crystallization knowingly contributes to an enhanced kinetic and thermodynamic stability of aggregates. In their potential application as sustained release devices, stereocomplexation could thus increase plasma circulation time of PIGMA-*b*-PLA copolymers, facilitating their accumulation at the target site.

Conclusion

This work presents the first synthesis of poly(*cis*-benzylidene isoglycerol methacrylate) (PBGMA), a polymer which exhibits interesting materials properties and can easily be transformed into poly(isoglycerol methacrylate (PIGMA), which exclusively contains primary hydroxyl groups along the backbone. This was realized by selective acetal protecting chemistry in form of the new

glycerol based methacrylate monomer BGMA (benzylidene glycerol methacrylate). The monomer is suitable for the preparation of polyester-based block copolymers with a bifunctional initiator via (i) ATRP and (ii) ring-opening polymerization of lactide. Selective acetal cleavage of the benzylidene groups yielding the amphiphilic poly(isoglycerol methacrylate)-*b*-(poly(L-lactide)), which was capable of self-assembly in micellar solution. Structural similarity is obvious for the recently investigated poly(glyceryl glycerol), which is accessible from oxyanionic polymerization, employing either osmylation chemistry or release from its acetonide protecting group.[55]

Illustrating the aggregation potential of the block copolymers, we have been able to demonstrate that PIGMA is a potential alternative for PEG as hydrophilic component in biocompatible block copolymers with promising attributes for drug delivery systems. In combination with poly(lactide), micelles with low CAC could be obtained. Their morphology could be adjusted from micellar to polymersome type aggregates by changing the physiochemical cross-linking with enantiomeric poly(lactide) blocks via stereocomplexation. With this work, we aim at further exploration of the field of amphiphilic polyester/polyacrylate-based block copolymers suitable for biomedical purposes.

Acknowledgment. Special thanks go to Annika Hörberger and Saskia Mulhjadi for valuable support in the lab. F.K.W. acknowledges the IMPRS of the Max Planck Society for continuous support. A.M.H. is grateful to the graduate class of excellence "POLYMAT" in the context of MAINZ for valuable financial support.

References and Notes

(1) Jacobson, G. B.; Shinde, R.; Contag, Ch. H.; Zare, R. N. *Angew. Chem.* **2008**, *120*, 7998–8000.
(2) Meng, F.; Zhong, Z.; Feijen, J. *Biomacromolecules* **2009**, *10*, 197–209.
(3) Liu, S.; Maheshwari, R.; Kiick, K. L. *Macromolecules* **2009**, *42*, 3–13.
(4) Meng, F.; Hiemstra, Ch.; Engbers, G. H. M.; Feijen, J. *Macromolecules* **2003**, *36*, 3004–3006.
(5) Kang, N.; Perron, M.-E.; Prud'homme, R. E.; Zhang, Y.; Gaucher, G.; Leroux, J.-C. *Nano Lett.* **2005**, *5*, 315–319.
(6) Kim, S. H.; Tan, J. P. K.; Nederberg, F.; Fukushima, K.; Yang, Y. Y.; Waymouth, R. M.; Hedrick, J. L. *Macromolecules* **2009**, *42*, 25–29.
(7) Yin, H.; Kang, S.-W.; Bae, Y. H. *Macromolecules* **2009**, *42*, 7456–7464.
(8) Kopeček, J.; Bažilová, H. *Eur. Polym. J.* **1973**, *9*, 7–14.
(9) Robinson, K. L.; de Paz-Bánēz, M. V.; Wang, X. S.; Armes, S. P. *Macromolecules* **2001**, *34*, 5799–5805.
(10) Save, M.; Weaver, J. V. M.; Armes, S. P.; McKenna, P. *Macromolecules* **2002**, *35*, 1152–1159.
(11) Feil, H.; Bae, Y. H.; Feijen, J.; Kim, S. W. *Macromolecules* **1993**, *26*, 2496–2500.
(12) Barz, M.; Tarantola, M.; Fischer, K.; Schmidt, M.; Luxenhofer, R.; Janshoff, A.; Theato, P.; Zentel, R. *Biomacromolecules* **2008**, *9*, 3114–3118.
(13) Hu, F.; Neoh, K. G.; Kang, E.-T. *Macromol. Rapid Commun.* **2009**, *30*, 609–614.
(14) Hawker, C. J.; Hedrick, J. L.; Malmström, E. E.; Trollsas, M.; Mecerreyes, D.; Moineau, G.; Dubois, Ph.; Jérôme, R. *Macromolecules* **1998**, *31*, 213–219.
(15) Mecerreyes, D.; Moineau, G.; Dubois, Ph.; Jérôme, R.; Hawker, C. J.; Malmström, E. E.; Trollsas, M. *Angew. Chem., Int. Ed.* **1998**, *37*, 1274–1276.
(16) Chen, Y. M.; Wulff, G. *Macromol. Rapid Commun.* **2002**, *23*, 59–63.
(17) Jakubowski, W.; Lutz, J. F.; Slomkowski, S.; Matyjaszewski, K. *J. Polym. Sci. A: Polym. Chem* **2005**, *43*, 1498–1510.
(18) Schappacher, M.; Fur, N.; Guillaume, S. M. *Macromolecules* **2007**, *40*, 8887–8896.
(19) Jakubowski, W.; Matyjaszewski, K. *Macromol. Symp.* **2006**, *240*, 213–223.
(20) Messman, J. M.; Scheuer, A. D.; Storey, R. F. *Polymer* **2005**, *46*, 3628–3638.
(21) Hales, M.; Barner-Kowollik, Ch.; Davis, Th. P.; Stenzel, M. H. *Langmuir* **2004**, *20*, 10809–10817.
(22) Spasova, M.; Mespouille, L.; Coulembier, O.; Paneva, D.; Manolova, N.; Rashkov, I.; Dubois, Ph. *Biomacromolecules* **2009**, *10*, 1217–1223.
(23) Jakubowski, W.; Matyjaszewski, K. *Macromol. Symp.* **2006**, *240*, 213–223.
(24) Chagneux, N.; Trimaille, Th.; Rollet, M.; Beaudoin, E.; Gerard, P.; Bertin, D.; Gigmes, D. *Macromolecules* **2009**, *42*, 9435–9442.
(25) Wolf, F.; Friedemann, N.; Frey, H. *Macromolecules* **2009**, *42*, 5622–5628.
(26) Giacomelli., C.; Borsali, R. *Macromol. Rapid Commun.* **2008**, *29*, 573–579.
(27) Bougard, F.; Giacomelli, C.; Mespouille, L.; Borsali, R.; Dubois, Ph.; Lazzaroni, R. *Langmuir* **2008**, *24*, 8272–8279.
(28) Clément, B.; Trimaille, T.; Alluin, O.; Gigmes, D.; Mabrouk, K.; Féron, F.; Decherchi, P.; Marqueste, T.; Bertin, D. *Biomacromolecules* **2009**, *10*, 1436–1445.
(29) Weaver, J. V. M.; Bannister, I.; Robinson, K. L.; Bories-Azeau, X.; Smallridge, M.; McKenna, P.; Armes, S. P. *Macromolecules* **2004**, *37*, 2395–2403.
(30) Save, M.; Weaver, J. V. M.; McKenna, P.; Armes, S. P. *Macromolecules* **2002**, *35*, 1152–1159.
(31) Ishizone, T.; Han, S.; Okuyama, S.; Nakahama, S. *Macromolecules* **2003**, *36*, 42–49.
(32) (a) Oguchi, K.; Sanui, K.; Ogata, N. *Polym. Eng. Sci.* **1990**, *30*, 449–452. (b) Mori, H.; Hirao, A.; Nakahama, S. *Macromolecules* **1994**, *27*, 35–39.
(33) Pilon, L. N.; Armes, S. P.; Findlay, P.; Rannard, S. P. *Langmuir* **2005**, *21*, 3808–3813.
(34) Zhang, H.; Ruckenstein, E. *Macromolecules* **2000**, *33*, 4738–4744.
(35) Gudipati, Ch.S.; Tan, M. B. H.; He, Ch.; Davis, T. P. *Macromol. Rapid Commun.* **2008**, *29*, 1902–1907.
(36) Amado, E.; Augsten, Ch.; Mäder, D.; Blume, A.; Kressler, J. *Macromolecules* **2006**, *39*, 9486–9496.
(37) Giacomelli, C.; Schmidt, V.; Borsali, R. *Langmuir* **2007**, *23*, 6947–6955.
(38) Jones, M.-Ch; Gao, H.; Leroux, J.-Ch *J. Contr. Rel.* **2008**, *132*, 208–215.
(39) Giacomelli, C.; Schmidt, V.; Borsali, R. *Macromolecules* **2007**, *40*, 2148–2157.
(40) Mequanint, K.; Patel, A.; Bezuidenhout, D. *Biomacromolecules* **2006**, *7*, 883–891.
(41) Patrucco, E.; Ouasti, S.; Vo, C. D.; De Leonardis, P.; Pollicino, A.; Armes, S. P.; Scandola, M.; Tirelli, N. *Biomacromolecules* **2009**, *10*, 3130–3140.
(42) Carlsen, P. H. J.; Sørbeye, K.; Ulven, T.; Aasbø, K. *Acta Chem. Scand.* **1996**, *50*, 185–187.
(43) Wilhelm., M.; Zhao, C.-L.; Wang, Y.; Xu, R.; Winnik, M. A.; Mura, J.-L.; Riess, G.; Croucher, M. D. *Macromolecules* **1991**, *24*, 1033–1040.
(44) Coskun, M.; Ilter, Z.; Ozdemir, E.; Demirelli, K.; Ahmedzade, M. *Polym. Degrad. Stab.* **1998**, *60*, 185–193.
(45) Matyjaszewski, K.; Shipp, D. A.; Wang, J. L.; Grimaud, T.; Patten, T. E. *Macromolecules* **1998**, *31*, 6836–6840.
(46) (a) Dove, A. P.; Pratt, R. C.; Lohmeijer, B. G. G.; Waymouth, R. M.; Hedrick, J. L. *J. Am. Chem. Soc.* **2005**, *127*, 13798–13799. (b) Pratt, R. C.; Lohmeijer, B. G. G.; Long, D. A.; Lundberg, P. N. P.; Dove, A. P.; Li, H. B.; Wade, C. G.; Waymouth, R. M.; Hedrick, J. L. *Macromolecules* **2006**, *39*, 7863–7871.
(47) Sosnowski, S. *J. Polym. Sci., Part A: Polym. Chem.* **2008**, *46*, 6978–6982.
(48) Zhang, J.; Wang, L.-Q.; Wang, H.; Tu, K. *Biomacromolecules* **2006**, *7*, 2492–2500.
(49) Kim, S. H.; Tan, J. P. K.; Nederberg, F.; Fukushima, K.; Yang, Y. Y.; Waymouth, R. M.; Hedrick, J. L. *Macromolecules* **2009**, *42*, 25–29.
(50) Lazzari, M.; López-Quintela, M. A. *Macromol. Rapid Commun.* **2009**, *31*, 1785–1791.
(51) Slager, J.; Domb, A. J. *Adv. Drug Delivery Rev.* **2003**, *55*, 549–583.
(52) Antonietti, A.; Förster, S. *Adv. Mater.* **2003**, *15*, 1323–1333.
(53) Okihara, T.; Tsuji, M.; Kawaguchi, A.; Katayama, K.; Tsuji, H.; Hyon, S.-H.; Ikada, Y. *J. Macromol. Sci.-Phys.* **1991**, *B30*, 119–140.
(54) Zhang, L.; Eisenberg, A. *Science* **1995**, *268*, 1728–1731.
(55) Wurm, F.; Nieberle, J.; Frey, H. *Macromolecules* **2008**, *41*, 1909–1911.

(56) For reasons of simplicity and clarity, the new poly(1,3-dihydroxyisopropyl methacrylate) will be referred to as poly(isoglycerol (mono)methacrylate) (PIGMA), which exhibits two primary hydroxyl-groups in contrast to the commonly employed isomer poly(glycerol methacrylate) (PGMA).

(57) In the case of sample preparation of the $PIGMA_{47}$-*b*-$PDLA_{28}$, the copper grids were not hydrophilized by argon/oxygen plasma treatment because of an equipment failure. This fact impaired the spreading of the sample on the grid and thus caused higher local aggregate concentrations.

List of publications

Journal articles

1) α,ω_n-Heterotelechelic hyperbranched polyethers solubilize carbon nanotubes
F. Wurm, A. M. Hofmann, A. Thomas, C. Dingels, H. Frey *Macromol. Chem. Phys.* **2010**, 211, 932-939.

2) Hyperbranched polyglycerol-based lipids via oxyanionic polymerization: Toward multifunctional stealth liposomes
A. M. Hofmann, F. Wurm, E. Hühn, T. Nawroth, P. Langguth, H. Frey *Biomacromolecules* **2010**, 568-574.

3) Poly(isoglycerol methacrylate)-*b*-poly(D or L-lactide) copolymers: A novel hydrophilic methacrylate as building block for supramolecular aggregates
F. K. Wolf, A. M. Hofmann, H. Frey *Macromolecules* **2010**, 43, 3314-3324.

4) Langmuir and Langmuir-Blodgett films of multifunctional, amphiphilic polyethers with cholesterol moieties
S. Reuter, A. M. Hofmann, K. Busse, H. Frey, J. Kressler *Langmuir* **2011**, *27*, 1978-1989.

5) Rapid access to polyfunctional lipids with complex architecture via anionic ring-opening polymerization
A. M. Hofmann, F. Wurm, H. Frey *Macromolecules* **2011**, 44, 4648-4657.

6) Mesogen-initiated linear polyglycerol isomers: The ordering effect of a single cholesterol unit on “sticky” isotropic chains
A. M. Hofmann, R. Wipf, B. Stühn, H. Frey *Macromolecules* **2011**, 44, 6767-6775.

7) Strong interactions between DPPC and a cholesteryl moiety covalently bound to a linear-hyperbranched polyether-based diblock copolymer
X. Peng, A. M. Hofmann, Sascha Reuter, H. Frey, J. Kressler, *submitted.*

8) Introduction of a PEG-spacer block in amphiphilic polyether-polyol block copolymers permits formation of ordered structures
A. M. Hofmann, T. Spehr, B. Stühn, H. Frey, *in preparation*.

9) Preparation of PEG-PG liposomes via dual asymmetric centrifugation for efficient encapsulation and targeted delivery of siRNA
M. Hirsch, A. M. Hofmann, H. Frey, M. Helm, *in preparation*.

Conference contributions

1) Hyperbranched polyglycerol-based liposomes via oxyanionic polymerization: A novel type of stealth structure?
19th IUPAC International Symposium on Ionic Polymerization, Krakow, Poland (poster)

2) Liposomes with hyperbranched polyglycerol anchor groups: Synthesis and characterization of novel stealth architectures
8th Conference on Advanced Polymers via Macromolecular Engineering, Dresden, Germany (poster)

3) Architectural variation of polyether-modified lipids
239th ACS National Meeting, San Francisco, USA
Polym. Prepr. (Am. Chem. Soc., Div. Polym. Chem.) 2010, 51, 128.

4) Liquid crystalline polyethers via cholesterol-initiated oxyanionic ring-opening polymerization
241st ACS National Meeting, Anaheim, USA
Polym. Prepr. (Am. Chem. Soc., Div. Polym. Chem.) 2011, 368.